NANOSTRUCTURED POLYTHIOPHENE MATERIALS FOR ELECTROCHROMIC APPLICATIONS

TIAGO ANDRÉ SEMEDO MOREIRA

Master in BioOrganic Chemistry

DOCTORATE IN CHEMISTRY

NOVA University Lisbon

September, 2022

NANOSTRUCTURED POLYTHIOPHENE MATERIALS FOR ELECTROCHROMIC APPLICATIONS

TIAGO ANDRÉ SEMEDO MOREIRA

Master in BioOrganic Chemistry

DOCTORATE IN CHEMISTRY

NOVA University Lisbon

September, 2022

NANOSTRUCTURED POLYTHIOPHENE MATERIALS FOR ELECTROCHROMIC APPLICATIONS

TIAGO ANDRÉ SEMEDO MOREIRA

Master in BioOrganic Chemistry

Adviser:	César António Tonicha Laia
	Assistant Professor, NOVA School of Science and Technology
Co-adviser:	António Jorge Dias Parola
	Associate Professor with Habilitation, NOVA School of Science and Technology

Examination Committee:

Chair:	Ana Isabel Nobre Martins Aguiar de Oliveira Ricardo,
	Full Professor, NOVA School of Science and Technology
Rapporteurs:	Luís Miguel Nunes Pereira,
	Associate Professor, NOVA School of Science and Technology
	Clara Isabel Barbosa Rodrigues Pereira,
	Assistant Researcher, Porto University
Adviser:	César António Tonicha Laia,
	Assistant Professor, NOVA School of Science and Technology
Members:	Francesca Di Maria,
	Researcher, CNR-ISOF, Italy
	Samuel Jacques André Guieu,
	Assistant Researcher, Aveiro University
	Ana Isabel Nobre Martins Aguiar de Oliveira Ricardo,
	Full Professor, NOVA School of Science and Technology

DOCTORATE IN CHEMISTRY

NOVA University Lisbon
September, 2022

Nanostructured Polythiophene Materials for Electrochromic Applications

ACKNOWLEDGMENTS

First of all, I would like to express my gratitude to the Cultural Heritage and Responsive Materials group for providing me unconditional support to develop my PhD thesis and to always make me feel at home.

A deep and special thanks to my supervisor, Professor César Laia for believing in me through all these years and for always pointing me to the right directions on my scientific and personal decisions. I would also like to thank my co-supervisor Professor Jorge Parola for all the help throughout these years, for always being available and comprehensive, and for the trust expressed in me. I would like to thank Professor João Carlos Lima for his crucial contribution throughout all the time I was in the CHARM group, for his advice, feedback and for always being available to guide me to a better direction.

For all the Professors mentioned above, thank you for being my mentors, for believing in me and keeping me motivated. My work and development as a person would not have been the same without your contribution. Obrigado!

I would also like to thank the people involved in this PhD thesis that are external from NOVA School of Science and Technology. First of all, a sincere thanks to Dra. Francesca Di Maria, Dr. Mattia Zangoli and Dra. Giovanna Barbarella for the warm way they welcomed me through the 6 months I worked at Mediteknology, in Bologna. I really felt I was at home, I learned a lot as a researcher and as a person, and I feel a sincere and true gratitude towards you. To Dr. Antoine Stopin, thank you for your lessons, for always helping me to keep focused and on the right track, and for your sincere friendship! I would also like to thank Dr. Cosimo Anichini for his collaboration and contribution for the work developed in my PhD thesis. From Ynvisible, I would like to thank Dr. Carlos Pinheiro, Aida Branco, Lucia Gomes and Soraia Assunção for all the help on building my first electrochromic devices and for always being available to share feedback and ideas.

To the people mentioned above and all those involved in the European projects running during the time of my PhD (INFUSION and DECOCHROM), thank you for your crucial contributions throughout all the work and development of my PhD.

To all individual members of the CHARM group, thank you all for being part of this journey in my life, for helping me to avoid that small problems could turn into big problems. The CHARM group is full of empathy and companionship, it seems that being a good person is a requisite to become a member of the CHARM group, and I finish this journey with all of you in my heart. A special recognition to current and old members of the CHARM group, Pedro Mateus, Joana Martins, André Seco, Ana Lúcia, Catarina Viola, Mani Outis, Andreia Ruivo, Nuno Trindade, Alfonso Alejo, Ana Pinheiro, Johan Mendoza, Miguel Santos, Nuno Basilio, Patrícia Máximo, Paula Nabais, Vanessa Otero and many others. Thanks to all of you, for sharing, helping, teaching and for your generosity towards me through all these years.

A special thanks to Artur Moro and João Avó. Words cannot describe my love and friendship for you, but I end this journey and take you as my friends for life. Wine is on me.

To my friends, João Ricardo, Beatriz Santos, André Gutierres, Hugo Monteiro, João Matos, Rodrigo Duarte, Sandro Casaleiro, Paula Domingues, Diogo Rodrigues, Fábio Júlio, João Jesus, Pedro Bastos thank you all for all the support and friendship.

To my family, Matilde, Tatiana, Pai, Mãe and Ricardo, thank you for being such strong pillars in my life, it was impossible to accomplish this without your love and support, you are always there no matter what. This was a long path, and it was much easier with all of you present in my life.

Muito Obrigado.

ABSTRACT

The development of semiconductor polythiophenes for optoelectronic applications requires tailored design and synthetic strategies to obtain materials with tunable optical and electronic properties and morphology in order to enhance their properties. To achieve this goal, the design, synthesis, and characterization of new nanostructured polythiophene materials was studied and tested in terms of processability, performance and stability through the assembly of solid-state electrochromic devices (ECDs). The use of films with poly(3-hexylthiophene-2,5-diyl) nanoparticles (P3HT-NPs) is reported, prepared by the nanoprecipitation method using water-based solutions with enhanced electrochromic properties. Additionally, it is reported the synthesis of a new class of thiophene-based electrochromic polymers using a repeated unit of the same linear thienyl-phenyl-thienyl-thienyl backbone. The tuning of the optoelectronic properties was achieved by introducing alkyl or alkoxy substituents in the thiophene unit and/or the presence of either -CH=CH- or -CH$_2$-CH$_2$- linkers, connecting the repeated units and acting as conjugation modulators. The design of the newly synthesized polymers was optimized to obtain a yellow-colored polymer with low redox potentials and demonstrate that the use of nanoparticle films deposited from water solutions, significantly improves their electrochromic performance.

In a different approach, stable dispersions of carbon nanotubes (CNTs) were developed, through the establishment of π-π stacking interactions between the CNTs and a newly synthesized pyrene-appended polythiophene. Hybrid thin-film composites were produced, and their electrochromic performance was evaluated through the assembly of solid-state ECDs. Lastly, the use of copper-nanowire/reduced-graphene-oxide (CuNWs-rGO) hybrid coatings was explored as transparent and conductive material for flexible electronic applications, through their use as electrodes in indium-tin-oxide (ITO)-free electrochromic displays.

Keywords: Electrochromism, Electrochromic Devices, Polythiophenes, Nanoparticles, Carbon Nanotubes, Copper Nanowires, Graphene Oxide

Resumo

O desenvolvimento de politiofenos semicondutores para aplicações optoelectrónicas requerem um planeamento e estratégias sintéticas elaboradas de maneira a obter materiais com propriedades e morfologias ajustáveis para melhorar as suas propriedades. Para atingir este objetivo, foram feitos o planeamento, síntese e caracterização de novos materiais nano-estruturados de politiofenos que foram testados no que diz respeito a processabilidade, desempenho e estabilidade através da montagem de dispositivos electrocrómicos no estado sólido (ECDs). O uso de filmes com nanopartículas de poli(3-hexiltiofeno-2,5-diilo) (P3HT-NPs) é reportado, preparados pelo método de nano-precipitação usando soluções à base de água com propriedades electrocrómicas melhoradas. Adicionalmente, é também reportada a síntese de uma nova classe de polímeros baseados em tiofeno utilizando a mesma estrutura base linear de tienil-fenil-tienil-tienil. A modelação das propriedades optoelectrónicas foi alcançada através da introdução de substituintes alquil ou alquiloxi na unidade de tiofeno e/ou a presença de espaçadores -CH=CH- ou -CH$_2$-CH$_2$-, conectando as unidades repetidas e atuando como moduladores de conjugação. O planeamento da síntese de novos politiofenos foi otimizado de maneira a obter um polímero de coloração amarela com um baixo potencial redox e demonstrar que, o uso de filmes com nanopartículas depositados através de soluções baseadas em água melhora significativamente o seu desempenho electrocrómico.

Numa abordagem diferente, dispersões estáveis de nanotubos de carbono (CNTs) foram desenvolvidas, baseadas em interações π-π entre nanotubos de carbono e um novo politiofeno sintetizado com uma unidade de pireno incorporada. Filmes finos de compósitos híbridos foram produzidos, e o seu desempenho electrocrómico foi avaliado através da montagem de dispositivos electrocrómicos no estado sólido. Por último, o uso de uma camada híbrida de nanofios de cobre/óxido de grafeno reduzido (CuNWs-rGO) foi explorada como material transparente e condutor para aplicações eletrónicas flexíveis, através do seu uso como elétrodos em dispositivos electrocrómicos sem óxido de estanho e índio (ITO).

Palavras-Chave: Electrocromismo, Dispositivos Electrocrómicos, Politiofenos, Nanopartículas, Nanotubos de Carbono, Nanofios de Cobre, Óxido de Grafeno

CONTENTS

LIST OF FIGURES

LIST OF TABLES

LIST OF SCHEMES

ACRONYMS

A/Abs	Absorbance
AFM	Atomic force microscopy
CE	Coloration efficiency
CHARM	Cultural Heritage and Responsive Materials
CIE	International Commission of Illumination
CNTs	Carbon nanotubes
CR	Contrast ratio
CT	Charge transfer
CuNWs	Copper nanowires
CV	Cyclic voltammetry
CVD	Chemical vapor deposition
DFT	Density functional theory
DLS	Dynamic light scattering
DMF	*N,N*-Dimethylformamide
EC	Electrochromic
ECDs	Electrochromic devices
EDOT	3,4-ethylenedioxythiophene
EIS	Electrical impedance spectroscopy
FETs	Field effect transistors
FTO	Fluorine-tin-oxide

GIWAXS	Grazing-incidence wide-angle X-ray scattering
GO	Graphene oxide
GPC	Gel permeation chromatography
HOMO	Highest occupied molecular orbital
ITO	Indium-tin-oxide
LCDs	Liquid-crystal displays
LEDs	Light-emitting diodes
LUMO	Lowest unoccupied molecular orbital
MWCNTs	Multi-walled carbon nanotubes
NIR	Near infrared
NMR	Nuclear magnetic resonance
NPs	Nanoparticles
OLEDs	Organic light-emitting diodes
OPV	Organic photovoltaic
P3HT	Poly(3-hexyxlthiophene-2,5-diyl)
PDI	Polydispersity index
PEDOT	Poly(3,4-ethylenedioxythiophene)
PEGMA	Poly(ethyleneglycol)methacrylate
PEN	Poly(ethylene-2,6-naphtalene)
PET	Polyethylene terephthalate
PLEDs	Polymer light-emitting diodes
PMMA	Poly(methyl methacrylate)
PSS	Polystyrene sulfonate
PTs	Polythiophenes
PTP	Polythiophene copolymer with a pyrene-appended unit

PVD	Photovoltaic devices
Q	Consumed charge
QY	Quantum yield
R	Reflectance
R&D	Research and development
R2R	Roll-2-roll
RE	Reference electrode
rGO	Reduced graphene oxide
SDS	Sodium dodecyl sulfate
SEM	Scanning electron microscopy
ST	Switching time
STM	Scanning tunneling microscopy
SWCNTs	Single-walled carbon nanotubes
T%	Transmittance
T^{70}	Time for 70% of total transmittance
T^{90}	Time for 90% of total transmittance
TCEs	Transparent conductor electrodes
TEM	Transmission electron microscopy
THF	Tetrahydrofuran
TMs	Thiophene-based materials
UV	Ultra-violet
Vis	Visible
WE	Working electrode
XRD	X-ray diffraction
Ynv.El.	Ynvisible's patented electrolyte

$\Big|$ 1

INTRODUCTION

1.1 Motivation and Aim of the Dissertation

1.1.1 Motivation

Electrochromism is defined as a phenomenon in which a color of material can be changed upon voltage application, leading to distinct colored states at different redox states. In an increasingly connected world full of smart objects and devices, electrochromic materials-based systems have the potential to become the most practical and widely deployable human interfaces for ambient intelligence. By bringing graphics and surfaces to life on consumer products and throughout our everyday living environments, electrochromic materials printed, coated as thin-films and further processed into end-products, create immensely diverse opportunities for the creative industries and the design and manufacture of new added-value applications for electrochromic materials.

Recently, electrochromic devices (ECDs) have been exploited for their use in smart consumer items or environmental areas including labels, lifestyle, wearables, security and design, displaying valuable information for users.[1–9] As an example, *Ynvisible®* company has been developing within the market of smart labels for packaging, safety tags, health monitorization, embedding ECDs on everyday products promoting an ubiquitous presence of these displays as non-intrusive forms of communication, using electrochromism as a technology.[9] Such displays present advantages like their flexibility, low power consumption and a vast number of possible solutions for an intelligent environment.

In the last years, polythiophene-based materials have been highly studied and developed for electrochromic applications due to their remarkable electrochromic properties in terms of the color palette, color contrast and simple processability. In particular, Reynolds's group has offered a large contribution in the past years, exploring a large range of chemical structures and electrochromic properties of polythiophene materials.[10–14] Yet, their implementation at an industrial scale, except for the well-known poly(3,4-ethylenedioxythiophene) (PEDOT), is still hampered by stability issues. Indeed, during my almost 3 years' experience working in *Ynvisible®* as an early-stage researcher, developing and producing electrochromic materials and devices, I was directly in contact with the limitations of polythiophenes that despite the vast color palette, still do not present viable long-term processability and stability to be used in ECDs for practical applications. Similarly, to other type of semiconducting problems, polythiophene materials lack on solubility except for toxic organic solvents such as chloroform or toluene, resulting in simple, but limited processability. Additionally, polythiophene materials present low electrical conductivity, poor chemical stability and cycling stability that limit their use in electrochromic devices for a higher number of applications.[15] The limited use, processability and stability of polythiophene materials for solid-state ECDs, increases the motivation on developing solutions to take advantage of the remarkable properties of these materials such as their opto-electronic properties and vast color pallet for electrochromic applications. Additionally, one of the key components of electrochromic devices is the conductive layer that, in the majority of the displays, is constituted by indium-tin-oxide (ITO) coatings. Due to the global raw materials consumption issues, indium low availability and high production cost of materials like ITO, the necessity of a green and viable solution for transparent and conductive electrodes also emerges.

1.1.2 Aim

The aim of this work is to develop new nanostructured polythiophene-based electrochromic materials and assemble solid-state ECDs towards an enhancement of the current state-of-the-art on electrochromism. The work here produced and presented is focused on the production of nanostructured polythiophene materials through the design, synthesis, and characterization of new electrochromic polymers as well as their nanostructuration using two different strategies.

Firstly, *via* a direct nanostructuration of a well-known polythiophene like poly(3-hexyxlthiophene-2,5-diyl) (P3HT) through the formation of water-dispersible nanoparticles

using the nanoprecipitation method. The nanostructuration of polythiophene materials is further studied on a new class of polymers designed and synthesized, focused on the yellow coloration. Secondly, through the formation of hybrid nanostructured thin film composites using nanotemplates such as carbon nanotubes (CNTs) or copper nanowires (CuNWs).

Despite the unquestionable advantages that polythiophene-based materials can offer such as their low bandgap (which generates intrinsic semiconductive characteristics), easily tunable opto-electronic properties through simple synthetic procedures, increased color pallet for electrochromic applications and simple processability; the solid-state morphology of these materials in electrochromic displays, their limited processability and their poor chemical stability tightens their use in electrochromic applications through solid-state ECDs.

Furthermore, the purpose of this work aspires to an improvement of polythiophene-based materials through an optimization and comprehensive study on the impact of:
- The overall performance of solid-state electrochromic devices using polythiophene nanoparticles (switching time, color contrast, durability) while using processable water-based solutions;
- The design and synthesis of a new class of compounds targeting yellow colored polythiophenes with low redox potential;
- The use of organic-inorganic hybrid materials as thin films to enhance electrochromic performances and;
- The use of new alternatives to ITO as transparent and conductive electrodes for electrochromic applications.

Each point addressed above will be important to reach the goal by optimization of the design and synthesis, as well as the employment of each new developed system on solid-state electrochromic devices, to achieve enhanced electrochromic performances which represent a real improvement on the current state-of-the-art on electrochromic applications.

1.1.3 Framework

The work presented in this thesis was developed during the period where two European projects were running, simultaneously. The collaborations coming from those two European projects allowed the author to establish several connections and create a framework that offered a crucial contribution to the work. At the same time, the continuous collaboration between the CHARM (Cultural Heritage and Responsive Materials) group at NOVA School of Science and Technology[16] and *Ynvisible*® [17] was present throughout the time of this dissertation by kindly

providing materials, feedback, and know-how on the assembly of solid-state electrochromic devices.

The synthesis and formation of water-dispersible nanoparticles is investigated, through a collaboration between the CHARM group and *Mediteknology*® located at the CNR-ISOF in Bologna,[18] Italy, on the scope of an EU H2020-MSCA-RISE 2020 project with reference 734834 – INFUSION.[19] *Mediteknology*® possesses a vast know-how on the synthesis, characterization of polythiophene-based materials and their nanostructuration in water-dispersible nanoparticles for different applications.[20]

The development of hybrid nanostructured thin film composites using nanotemplates is disclosed through a collaboration with the *Bonifazi Group* in the University of Vienna,[21] Austria led by professor Davide Bonifazi and the *Nanochemistry Laboratory* in the University of Strasbourg,[22] France, led by Professor Paolo Samori on the scope of an EU H2020 programme reference nº760973 – DECOCHROM.[23] With the expertise of *Bonifazi Group* on the use of carbon-based materials and the knowledge of the *Nanochemistry Laboratory* on multicomponent nanostructures and networks for optoelectronic applications; the design and development of a system capable of enhancing the electrochromic properties of polythiophene materials in solid-state devices and the development of a viable alternative for indium-tin-oxide (ITO) as transparent and conductive layer for ECDs are investigated.

1.2 Thesis Layout

The layout of this thesis starts with an introductory chapter divided in three main sections. One first section (1.3) includes a brief description on the concept of electrochromism and its state-of-the-art regarding materials and applications. A second section (1.4) describes the different electrochromic materials focusing mainly on polythiophenes, polythiophene nanoparticles and hybrid materials. The third section (1.5) presents a detailed description of electrochromic devices functionality, components, and performance evaluation. Before the work chapters, a brief description of the main achievements is presented.

Chapters 2 to 5 involve the results and discussion of the work developed towards the achievement of the objectives proposed in this thesis. Chapter 2 describes the synthesis of poly(3-hexyxlthiophene-2,5-diyl) (P3HT) nanoparticles in water-based dispersions and their employment in solid-state ECDs. Furthermore, the electrochromic performance evaluation of the nanoparticles in solid-state displays is investigated. Chapter 3 describes the development

of a new synthetic method to produce electrochromic polymers with tailored optical and electronic properties focusing on the yellow color. Furthermore, the polymer nanostructuration using water-based dispersions and their electrochromic performance in solid-state displays is evaluated. Chapter 4 involves a different approach to increase the electrochromic performance of thiophen-based polymers. The high electronic density characteristic of the CNTs is exploited through the formation of π-π stacking interactions with a newly synthesized pyrene-appended polymer, hybrid blends of polymer-CNTs are developed and used for the assembly of fast switching and long-lasting ECDs. Finally, chapter 5 exploits the use of copper nanowires (CuNWs) with reduced graphene oxide (rGO) as transparent and conductive electrodes for the assembly of ITO-free electrochromic devices.

Furthermore, the structure of each individual chapter from 2 to 5 is written with a publication type format, containing a brief introduction to the work, the discussion of the results and the dedicated experimental section, since chapters 2 and 3 are based on published publications in peer-reviewed journals, while chapters 4 and 5 are based on manuscripts under submission.

In chapter 6 the main achievements and conclusions of this thesis are highlighted, as well as future perspectives of this research.

Finally, chapter 7 presents the list of publications produced during the time of the dissertation. Additionally, a list of oral and poster communications presented in scientific conferences focused on the work of this thesis is presented.

1.3 Electrochromism

Electrochromism can be defined as a reversible color change, associated to an electrochemical induced redox reaction. Electron-transfer reactions are at the core of chemistry, leading to changes in the redox states of molecules and the properties of materials. There are many examples in Nature, some of them triggered by light such as photosynthesis. However, the so-called redox reactions were applied in a systematic way to produce color changes by Deb in a pioneering work in the late 1960's.[24] The concept of electrochromism was born through the assembly of the first electrochromic device, soon becoming one of the most promising research areas for the development of "smart-windows".[25–28] The basic concept is to reversibly change color using redox reactions, enabling the user to fine management of the perceived light coming out of the window. Electrochromism is, therefore, one of the processes to control color transitions, along with *e.g.*, photochromism, thermochromism, piezochromism and many others.[28–30] The fact that the user can adjust color with electrical energy gives a much higher level of human control since this is a chromism that is adjusted by users according to their desires. The development of electrochromic devices (ECDs) occurs in parallel with the development of, *e.g.*, lithium batteries, photovoltaic devices (PVD) and light-emitting devices. ECDs, batteries, PVDs and LEDs, which have very similar architectures, stacking different layers of materials with different functions to ensure a proper flux of electrons to the electrodes, emerging the functionality of the electrochromic materials.

1.3.1 State-of-the-art

The first conceptual proposal for this type of materials appeared in 1961 by J.R. Platt,[31] developed using the pioneer work of Deb that presented the first examples of ECDs where metal oxides were used as electrochromic material,[24] controlled by a well-known reaction involving redox reactions of tungsten oxide (WO_3) species that changed color from blue to uncolored,[32] further studied in Germany in the 1940s and 1950s.[33,34] His observations appeared from his work on amorphous and crystalline metal oxides, particularly the semiconductor WO_3, at the American Cyanamid Corporation in the USA, during the 1960s, being published for the first time in seminal papers on electrophotography in 1969 using WO_3 films,[24] and in 1973 explaining the basic properties of these films.[35,36]

The studies of Deb demonstrating the reversible and electrically induced coloration of metal oxides in thin films, from uncolored state to deep blue colored between 1690s and 1970s,

gave rise to the interest and development of electrochromic materials and devices for applications such as displays, mirrors and windows.[32,37,38] Thus, electrochromic mirrors were the first commercially available application of electrochromism,[39] since car rearview mirrors based in electrochromic displays appear as a pertinent area for the industry which was pioneered by Schott Company in Germany starting in 1977,[32,40–42] setting the use of metal oxide based devices. Later in 1994, Gentex[43] exploited the bypyridium salt (or viologens) solutions in a new design of rearview mirrors, following the footsteps originally suggested by Platt.[31] Viologens also develop deep blue colors and were described earlier in the 1970s,[44,45] soon after the work of Deb. Gentex, along with Schott, were the pioneers of applications of electrochromic devices in the automobile industry which still constitutes a major player in the field, including electrochromic windows in aircraft (see Figure 1.1). Later, Donnelly Corporation (now Magna Donnelly Corp) followed and presented their own version of the rearviewmirror.[46]

Figure 1.1. A - Gentex self-darkening rearview mirror.[47] B - Electrochromic window of Boeing 787 Dreamliner aircraft.[48]

In the first half of 1980s, this technology was found as being important for energy efficient fenestration and, therefore, the term *"smart window"* was devised in 1985 by Svensson and Granqvist to describe windows that electrochemically change in transmittance and thus allowing the user to control the amount of light and heat that enters in the room, accordingly to user wishes.[39,49,50] Windows prototypes for buildings based on inorganic metal oxides started to be developed, followed by the presentation of the first commercial electrochromic smart window by Pilkington in 1998 produced using glass substrates.[51] Sage Electrochromics Inc. (currently Saint-Gobain group) developed an electrochromically switchable window named SageGlass (see Figure 1.2).[28,51–53]
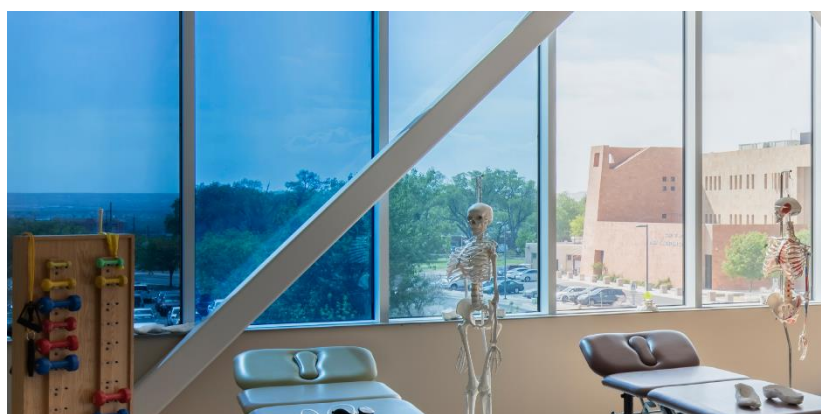
Figure 1.2. SageGlass smart window, from full colored to clear state.[54]

These developments were crucial for the establishment of electrochromism as a technology through promising applications. Mainly in the 70s and early 80s, where the findings of Deb served as inspiration and increased the number of published patents during those two decades (see Figure 1.3), especially due to developments of electrochromic mirrors and windows. Nevertheless, these applications were achieved using deposition techniques such as sputtering or chemical vapor deposition, which are not printing techniques (like screen or ink-jet printing, spray-coating or roll-to-roll) and contributed to a decrease on the number of published patents on the late 80s. True printed electrochromics would have to wait for the development of processable ink formulations and wet methods since, in the case of metal oxides or Prussian blue, the use of colloidal nanoparticles would be crucial. Additionally, there was an enormous limitation in terms of available color palette, so the field had to wait for the development of semiconductor polymers.

The rise of semiconductive polymers in electrochromism, started to emerge in the early 1990s, and quickly became an area of interest in electrochromism, mainly due to the appearance of poly(3,4-ethylenedioxythiophene) (PEDOT), causing a significant increase of research papers published during that decade (see Figure 1.3). The appearance of PEDOT and the most recent developments of polythiophene (PT) derivatives has been contributing to an escalated number of patents and publications since the decade of 2010.
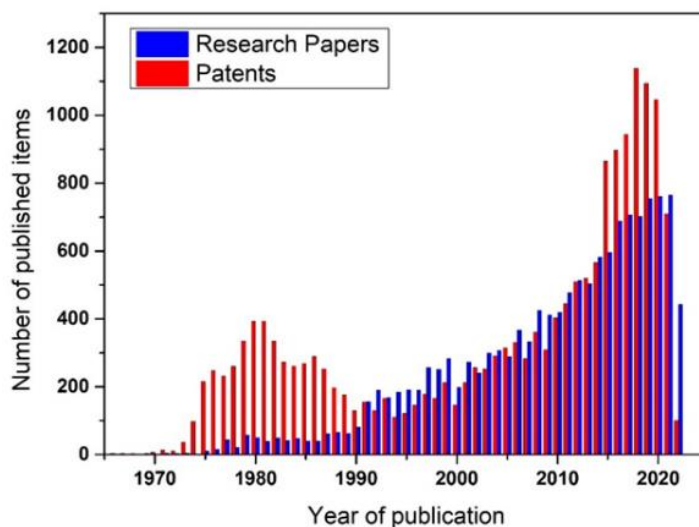
Figure 1.3. Number of published patents and research papers throughout the years, in electrochromism (Search from *Espacenet* (patents) and *Web of Science* (papers), made on August 10th, 2022, using "electrochromic" OR "electrochromism" as query keywords).

1.4 Electrochromic Materials

The different classes of electrochromic compounds can be divided in four distinct groups:[55]

i) Small molecules, such as viologens[56,57] or perylenes,[58] which undergo strong color changes between different redox states. These molecules are typically used in solution-based devices or cells.

ii) Metal oxides, such as WO_3, which are semiconductors where their optical bandgap is controlled by the amount of positive or negative charges doping the material.[59–62] These materials are in the form of a thin-film deposited on the top of the electrode.

iii) Miscellaneous compounds, such as the popular Prussian Blue,[63] metal coordination compounds,[64] organic/inorganic hybrid compounds[65–67] etc.

iv) And Semiconductor polymers that were discovered in the 70s,[68,69] with unique optical properties. Among them are polythiophenes or polyaniline including the popular PEDOT.[70–73] This class appeared in the 90s and quickly became very popular due to the rise of an expanded color palette through simple synthetic modifications and offer many advantages in terms of processability.

There are advantages and drawbacks in all these types of compounds. Generally, metal oxides are better for outdoor applications (such as windows) because they are more resistant to photochemical degradation caused by UV-light and may be deposited in large areas via

sputtering. Examples such as the SageGlass products, which provide smart-windows for optimal comfort inside buildings with minimal electric consumption.[74] Small molecules like viologens have very deep color changes, and may be used in applications such as rearview mirrors,[57] which led to very successful applications by Gentex Corporation products.[75]

The growing demand for consumer electronics such as smart cards, flexible displays, electronic paper, smart packaging, etc., has increased the interest in fully printed electrochromic devices made of cheap and widely accessible components in order to develop more efficient human machine interfaces.[1,76] *Ynvisible®* company operates with the market of smart labels for packaging, safety tags, health monitorization, embedding printed electronics on everyday products for an ubiquitous presence of electrochromism as a technology.[9] In this sense, electrochromic materials based on conjugated semiconducting polymers have quickly become a topic of enormous interest as they can exhibit low switching kinetics, good contrasts, and low power consumption.[77] Additionally, with the rise of printed electronics, the necessity of an extended color palette for different electrochromic applications also increased, along with a required high processability. Therefore, the appearance of semiconductive polymers offered new prospects for electrochromism with special attention given to polythiophene-based materials.

1.4.1 The Rise of Semiconducting Polymers

Hideki Shirakawa, Alan MacDiarmid and Alan Heeger between 1974 and 1978[78–81] made a landmark by describing extensively the electric conduction properties of doped polyacetylenes and as result, a new class of materials emerged: semiconductor organic polymers.

The electric conductivity of semiconductive conjugated polymers can be controlled by means of p- or n-doping. In the case of p-doping, electrons are removed from the occupied orbitals of the polymer, giving rise to positive charges, or holes, while n-type doping represents the addition of electrons into the unoccupied orbitals of the conjugated polymer. Thus, the semiconductive polymers are typically defined as p-type (hole transport) or n-type (electron transport) materials.

During the 1980s, the majority of the monomers required for the production of conducting polymers used nowadays were synthesized,[82] and among them would be polythiophenes.[83–88] Soon their electric conductivity, simple processing, electrical, magnetic and optical features similar to metals or semiconductors, interesting thermoelectric, photovoltaic and lighting properties, chemical diversity, as well as their low cost of solution and processability

were described.[89–92] These characteristics allowed their application in sensors, electrochromic devices, solar cells, batteries, photovoltaics, among others.[71,93,94]

1.4.1.1 Polythiophenes

A sub-class of semiconductive polymers quickly started to urge and became the most explored material for electrochromic applications, polythiophenes. Compared to the previously mentioned electrochromic materials, polythiophenes are potential candidates for the next-generation electrochromic (EC) materials since: *i)* they can be easily synthesized *via* different procedures, *ii)* their opto-electronic properties can be simply tuned through structural modification, and *iii)* can be efficiently processed by different low-cost techniques such as spin coating, spray casting, or ink-jet-printing facilitating large-area film formation.[10,95–97]

Their optical and charge storage properties were earlier described by Heeger,[68,69] highlighted by the observation that the polymers doped with positive charge had a different light absorption spectroscopy. The neutral state is characterized by π,π^* electronic transitions in the visible region, but positive holes lead to polaronic states with light absorption in the Near-Infra Red region but short in the visible range presenting, therefore, intrinsic electrochromic properties. Later Bayer AG in Germany developed poly(3,4-ethylenedioxythiophene) (PEDOT) in 1988.[73,89,98] Despite its excellent electric properties, its solubility in common solvents was extremely low hindering promising industrial applications. The low solubility problem was transposed using a soluble polyelectrolyte, poly(styrene sulfonate) (PSS), during the polymerization process. This compound is hydrophilic due to the presence of $-SO_3H$ groups, and thus the mixture PEDOT:PSS (see Figure 1.4), fully dispersible in water was achieved, and developed again by Bayer researchers in 1990.[99] This aqueous dispersion of PEDOT:PSS, presenting a deep blue color in the reduced state, was firstly commercialized under the name BAYTRON® P (where P stands for polymer).[73,100,101] Soon afterwards, the electrochromism of polythiophenes[102] including PEDOT[103,104] were described, making them a new class of electrochromic materials (along with other semiconductor polymers such as polyanilines[105]).

11
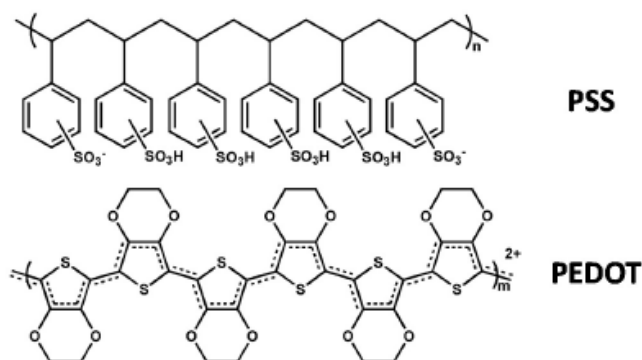
Figure 1.4. Schematic representation of the structure of PEDOT:PSS.[101]

PEDOT:PSS is an interesting material due to its easy synthesis, soft nature, high transparency and ductility, mixed electronic and ionic conductivity, electrochemical stability, easily tunable viscosity, printability and low production cost, which allows its use in several applications, such as solar cells, sensors, smart windows, electronic papers, batteries, organic light-emitting diodes (OLEDs), among others.[90,92,106] Moreover, PEDOT:PSS presents excellent electrochromic features, being cathodically electrochromic since it presents a strong blue color when reduced and a very high transmissive state, when oxidized.[38,107] Additionally, PEDOT:PSS aqueous dispersions are used for the development of inks used in facile printing techniques such as spray deposition, screen and ink-jet printing, among others, where PEDOT-based inks represent the majority of the commercially available inks.[100,107]

As referred before, electrochromic conductive and semi conductive polymers are very attractive due to their intrinsic properties such as: transparency, stability, low band-gap and low redox potentials.[108] Specifically, when it comes to electrochromic applications, thiophene-based polymers have one feature that stands out; the possibility to obtain an extensive color palette, spread all across the visible region.[11,95] This feature is crucial for industrial electrochromic applications since gives an extremely large space of possibilities in terms of color tunability by careful and subtle synthetic modifications of the polymeric backbone (see Figure 1.5).[13,109,110]
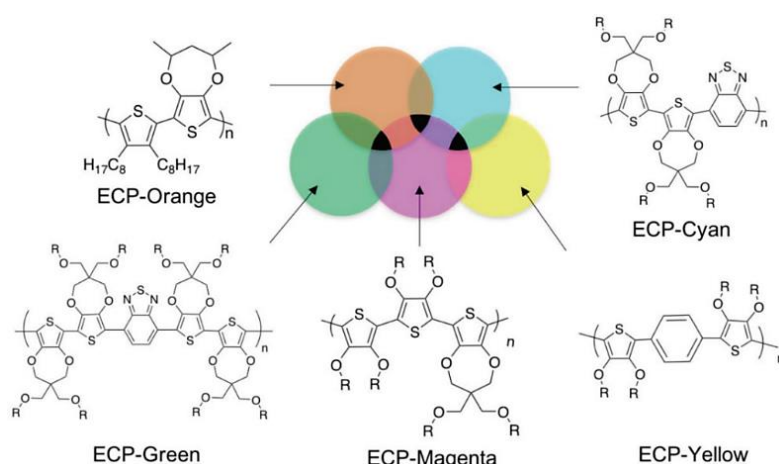
Figure 1.5. Representation of the color palette using polythiophenes reported by Savagian *et al*.[110]

In particular, Reynolds group made a large contribution in the last 20 years, exploring a large range of chemical structures and electrochromic properties.[8,10,117–124,108,110–116] To achieve the desired polymer, two main routes can be explored: electrochemical synthesis and chemical synthesis. Electrochemical synthesis, in this case, is not very attractive since a lack of solution processability limits their application as depositing homogeneous films in large area electrodes for ECDs is hard and expensive to achieve. Therefore, chemical synthesis is a route that offers more flexibility to obtain different colors while controlling solubility and solution processability for homogeneous and processable inks. The usual practice to improve the solubility of semiconducting polymers is through the introduction of long alkyl or alkyloxy side chains in an aromatic unit, like thiophene. Reynolds and Beaujuge reviewed the vast number of possibilities to achieve different colors by chemical manipulation of thiophene monomers and posteriorly an oxidative polymerization, typically using iron(III) chloride ($FeCl_3$) as a Lewis acid (see Figure 1.6).[10]
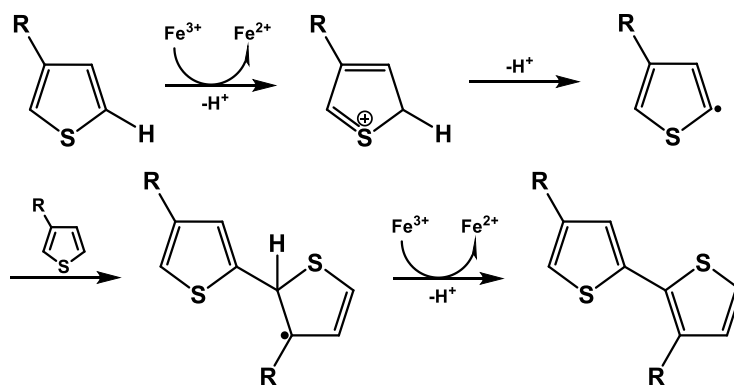
Figure 1.6. Schematic representation of the mechanism of oxidative polymerization using Iron(III) Chloride, in polythiophenes.

The control of polythiophene properties can be performed, based on the donor-acceptor concept or strategy; by adding alkyloxy chains to the core structure of a monomer lowers the oxidation potential, while adding alkyl sidechains induces solubility and steric distortion to the neutral polymer backbone, shortening or lengthen conjugations that gives rise to different colored polymers and offer low or higher solubilities. Reynolds *et al.* explored the addition of alkyloxy chains while obtaining orange and red to transmissive states.[11] Thus, the optimization of the backbone structure allows the accurate control of the optical properties, modulation of redox potentials, optical contrast, switching kinetics and, through functionalization with side chains, the improvement of solution processability,[77] enabling their implementation, in a large-extent, to electrochromic applications.[8,110,125,126] The prevalence of thiophene in electrochromic materials is due to the fact that: thiophene-based materials are readily available, and the chemistry of thiophene is well developed and understood, facilitating the functionalization of the thiophene-ring to synthesize new polymers and/or classes of polymers.

On a different and straightforward approach, mixing two or more polymers with complementary colors was also explored as an additional possibility in order to obtain different colors. The advantage of this strategy is to use already known and characterized polymers in order to obtain the desired color, as reported by Österholm *et al.,* where different shades of the same color (brown) were achieved by mixing different proportions of the same polythiophene materials (see Figure 1.7).[8]
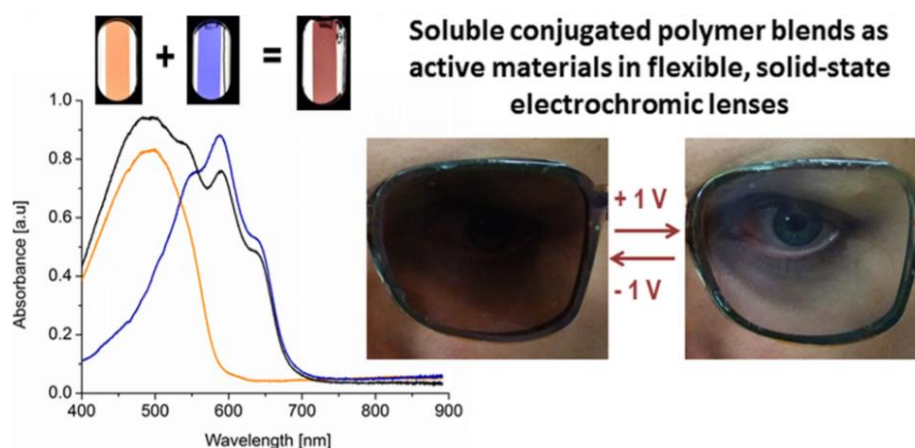
Figure 1.7. Brown color obtained by mixing different polythiophenes.[8]

However, the solid-state morphology of a material also affects the electrochromic properties, since the surface area may determine different interactions with the electrolyte, thus influencing the diffusion and migration of ions, mainly in the Stern layer.[127] Polythiophene

electrochromic materials present very good performances in liquid state.[10,122] On the other hand, these performances are suppressed when a solid-state ECD is assembled. Despite the undeniable advantages that polythiophene materials offer, in solid-state displays organic conjugated polymers such as polythiophenes present low electrical conductivities and poor chemical and cycling stability that hamper their use, in a larger extent, in electrochromic applications through solid-state electrochromic devices.[10,15,128] Additionally, and similarly to other type of conductive polymers, the main drawback of polythiophenes is their lack of solubility except for solvents such as chloroform or toluene, due to their strong interchain interactions, that results in limited processability in a short list of toxic organic solvents. This is also one of the reasons why PEDOT was so successful, due to its ability to disperse in more polar solvents like water or ethanol, when conjugated with PSS.

In this regard, the use of conductive preorganized thiophene-based nanostructures appears to be an attractive strategy for the integration of organic materials into ECDs, providing further opportunities to enhance their performance.[129–132]

Indeed, in analogy with inorganic materials, the nanostructures of organic materials can favor for instance, more efficient charge transfers (CT), taking into account the increase of the contact area between the electrodes and the electrolyte and, consequently, influence important parameters such as color contrast and response time and durability.[59,133] Additionally, the use of water-based dispersions would avoid the presence of toxic organic solvents during the preparation of electrochromic inks or displays representing a major advantage for R&D and industry, in the area of electrochromism.

1.4.1.2 Polythiophene Nanoparticles

Nanostructuration of polythiophenes, such as polythiophene colloidal nanoparticles can be deposited on large areas, from inexpensive and environment friendly solvents at ambient temperature, by employing high throughput printing techniques.[96,131] These techniques avoid the use of hazardous chlorinated solvents, such as chloroform, toluene, etc., generally used for the deposition of thin-film polymers, as referred before. Recently, poly(3-hexyxlthiophene-2,5-diyl) nanoparticles (P3HT-NPs) have been applied as the active layer in field-effect transistors, photovoltaic cells, and electrochromic devices.[134–136] Nanoparticles can be considered as uniform systems in terms of composition, supramolecular arrangement, dimension and can be prepared as water suspensions following two main methods:

nanoprecipitation/reprecipitation and miniemulsion. Figure 1.8 illustrates the two different preparation methods of P3HT-NPs.
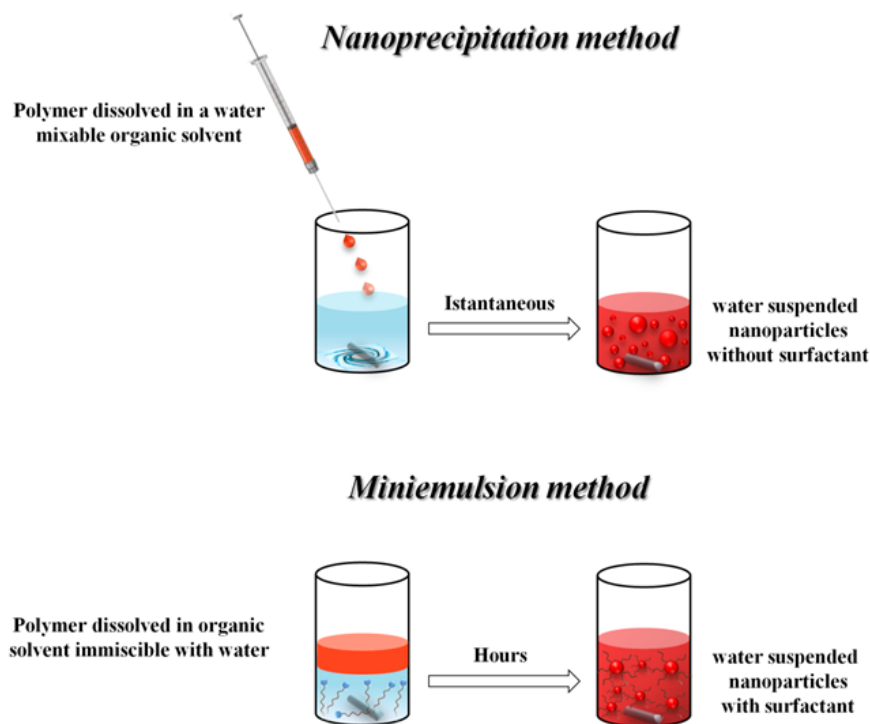
Figure 1.8. Preparation of water suspensions of P3HT-NPs using the nanoprecipitation and miniemulsion methods.

In the nanoprecipitation method, a few milligrams of the polymer are dissolved in an organic solvent miscible with water, like tetrahydrofuran (THF). Then, the solution is slowly dropped into deionized water under stirring or sonication.[137–139] As soon as the polymer meets water, hydrophobic and π-π interactions come into play leading to the self-aggregation of the polymer which excludes water molecules while minimizing its contact area. It has been observed that with this method, the final dimensions of the nanoparticles and the polydispersity of the samples depend on a series of factors: concentration, and regioregularity of the polymer, solvent volume, dripping time, stirring speed, and temperature. By controlling these parameters, it becomes possible to obtain a good reproducibility of the samples. P3HT colloidal suspensions are rather stable and do not require the use of any surfactant dissolved in the aqueous medium. However, in some cases, the preparation of thiophene-based nanoparticles can also be carried out in the presence of surfactants, such as sodium dodecyl sulfate (SDS) or Triton X-100, in order to stabilize the resulting colloidal suspension.[136] After the preparation of the nanoparticles, the traces of organic solvent must be removed from the solution, since they

could decrease the stability of the NPs and alter the surface of the NPs leading to partial dissolution. The organic solvent can be either evaporated under reduced pressure by increasing the temperature or removed by dialyzing the nanoparticles suspension with a dialysis membrane. However, in the latter case, the process is slower and the particles may grow in size.[136] Differently, nanoparticles obtained by mini emulsion methods are prepared starting from polymers dissolved in an organic solvent which is immiscible in water in the presence of a surfactant. P3HT is generally dissolved in chloroform, toluene, or cyclohexane (2 mg mL^{-1}), which represent the organic phase of the emulsion. A surfactant is added to water, generally SDS, poly(ethylene glycol methyl methacrylate (PEGMA), and so on, in a concentration higher than its critical micellar concentration. The aqueous and organic phases are combined (in 3:1 ratio) and kept under stirring, or sonication, overnight to obtain the nano-/microemulsion. The organic solvent is usually removed by vacuum evaporation leaving a suspension of water dispersed polymer nanoparticles while the surfactant is removed by dialysis. It has been demonstrated that the stirring method employed to mix the aqueous and organic phases, the concentration of surfactant, the emulsion temperature, the selected organic solvent, etc., have a significant effect on the aggregation of the P3HT macromolecules with consequent marked photophysical and morphological differences of the resulting nanoparticles.[140,141] For instance, it was found that P3HT-NPs prepared using a mixture of organic solvents, *e.g.,* chloroform/toluene, displayed a higher structural order compared to those prepared using only chloroform.[140] In addition, the nature of the surfactant employed and the conditions selected to prepare the dispersion allow to drastically change the molecular aggregation, leading to *H-* or *J-*like behavior.[141] One of the main problems encountered in these preparation methods is that not all the nanoparticles produced have the same dimensions, *i.e.,* the samples are highly polydisperse. For example, P3HT-NPs prepared by nanoprecipitation method exhibit a wide range of sizes from 100 nm to 1 μm. However, through differential centrifugation, it is possible to isolate, within a sample, different fractions having more homogeneous dimensions.[142] As shown in Figure 1.9, NP suspension is centrifuged several times while the revolutions per minute (rpm) are diminished, thus lowering centrifugal force at each step. By separating the supernatant from the precipitate, which is in turn resuspended and subjected to another run of centrifugation at a lower speed, it is possible to fractionate the NPs according to their dimension.
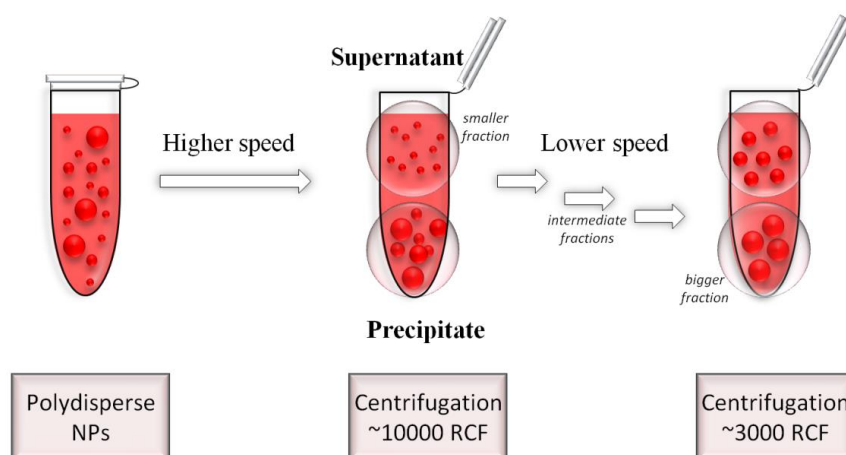
Figure 1.9. Differential centrifugation of a polydisperse sample of P3HT-NPs.

The size, size dispersity, and morphology of thiophene-based nanoparticles are commonly determined by combining dynamic light scattering (DLS) and microscopic techniques such as scanning electron microscopy (SEM) and transmission electron microscopy (TEM). From DLS measurements, both the average size and polydispersity index (PDI) of the sample are easily obtained. In addition, DLS allows determining another key parameter: the Z-potential, which is indicative of the surface charge of the nanoparticle and is related to the stability of the suspension. For instance, P3HT-NPs obtained by nanoprecipitation show a high degree of PDI (>0.2) and an average size of 300 nm.[143] However, thanks to differential centrifugation, it is possible to isolate samples with a desired size and, at the same time, to reduce the polydispersity of the sample (<0.02). The Z-potential values of these different-sized suspensions indicate a high degree of stability, with values in the range between 30 mV and 40 mV. Moreover, P3HT nanoparticles show structured absorption and emission spectra. While the absorption spectrum is influenced by the size of the nanoparticles—indeed, a redshift is observed by increasing the NP size— the fluorescence spectrum is notably less affected. Stokes shifts of about 0.54 and 0.34 eV are observed for the smallest and the largest NPs.[143] Recently, it has been demonstrated that water dispersed thiophene-based nanoparticles prepared with the miniemulsion method, using both poly [2,3-bis-(3-octyloxyphenyl) quinoxaline-5,8-diyl-alt-thiophene-2,5-diyl]) (TQ1) and P3HT, can be introduced into electrochromic polymer electrodes using the spray-coating technique.[131] In both cases, the nanoparticle electrode exhibits a much faster switching speed and better coloration efficiency (CE) than the compacted electrode, in which the polymer is simply deposited as a homogeneous thin-film. The superior switching response of the NP films could be attributed to a more efficient counter-ion diffusion, i.e., the insertion

and extraction of the anion (ClO$_4^-$) between the electrolyte and the NP films determined by an increase of the effective contact area.

In addition to the direct nanostructuration of polythiophene materials emerging as an attractive strategy for integration in electrochromic devices with enhanced performances, it is also reported in the current state-of-the-art the use of organic-inorganic materials, taking advantage of the synergetic properties of the resulting hybrid materials.

1.4.2 Hybrid Materials

Hybrid materials in electrochromism can combine the functionality of the organic polymers and the chemical stability and additional properties of the inorganic materials generating thus, enhanced performances or characteristics of the electrochromic materials.

In addition, the use of a cooperative win-win strategy through the use of hybrid materials can solve practical issues, especially when a single organic material cannot meet the requirements desired for electrochromic applications enabling the effect "*1 + 1 > 2*".[144] To enhance the desired properties of the organic and inorganic units in a hybrid material, while decreasing the limitation of one (or both) components individually, the major goal is to develop a design and system strong enough so that the organic and inorganic material can work efficiently, taking advantage from the properties of the components (or the interaction of both).

Recently, there has been an increase of the research interest combining conjugated polymers with inorganic materials to form nanostructured hybrid electrochromic materials. Despite the development and improved stability of semiconducting polymers using the donor-acceptor approach[10,11] the durability and performance still remains an obstacle when using of these organic materials in solid-state devices, due to their low electrical conductivities and poor chemical and cycling stability, as it was referred before. In literature a wide variety of components were tested to enhance the properties of semiconducting polymers such as metal oxides like WO$_3$ or TiO$_2$ and conductive materials like silver, gold, graphene and carbon nanotubes.[65,145–151]

1.4.2.1 Carbon nanotubes

Carbon nanotubes (CNTs)[152] (see Figure 1.10) are an especially attractive material due to their low electrical percolation threshold, high mechanical resistance and semiconducting characteristics, due to a high density of delocalized electrons.[152–155] Specifically, multiwalled carbon nanotubes (MWCNTs) are commercially available at a lower price when compared with

single-walled carbon nanotubes (SWCNTs), due to the facilitated bulk preparation of MWCNTs. Additionally, it was reported by Byrne *et al.* that MWCNTs present increased mechanical strength due to the sp^3 interwall bonding and higher purities, when compared with SWCNTs.[156]

SWCNT   MWCNT
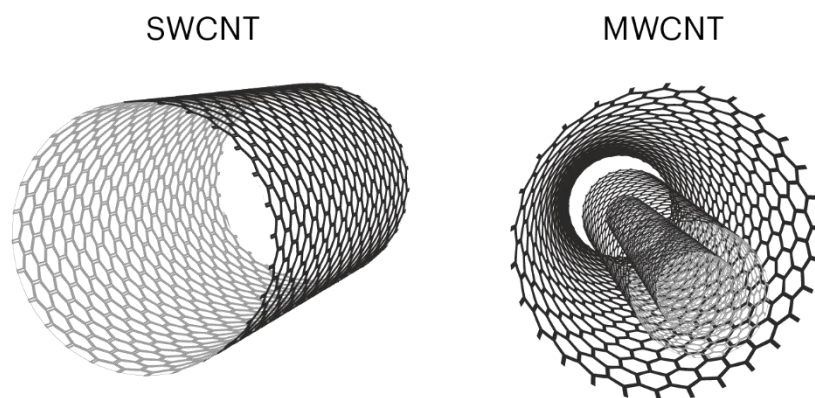
Figure 1.10. Schematic representation of a single-walled carbon nanotube (SWCNT) and a multi-walled carbon nanotube (MWCNT).

Since semiconducting polymers like polythiophenes lack in high electrical conductivities and cycling stability thus, producing hybrid materials using polythiophenes with high electron density materials such as CNTs seems a fitting approach. Hence, carbon materials exploitation for the production of hybrid electrochromic materials is a growing topic in research, including their use with semiconducting polymers.[157–161]

As it was referred before, for a hybrid system to work efficiently, the design and development of a hybrid system needs to be strong enough to take advantage of the desired properties from the organic and inorganic units. When referring to CNTs, the high density of delocalized electrons can be manipulated to enable π-π stacking interactions in an external electron rich unit such as pyrene. This interaction has already been explored through the assembly of hybrid materials with enhanced properties in fluorescence microscopy,[162,163] biology,[164,165] catalysis,[166] sensors,[167,168] and opto-electronic applications,[169,170] including electrochromism.[171]

Therefore, combining the electrochromic properties of polythiophene materials with the high electron density and mechanical robustness characteristics of CNTs can be explored to produce highly conductive hybrid thin films for electrochromism, generating high performance ECDs or acting as possible alternatives as conductive electrodes for electrochromic displays.

With the rising number of different electrochromic applications, the production of more cost-effective electrochromic devices seems inevitable, starting by replacing the most expensive component in the ECDs, indium-tin-oxide (ITO), which is the most widely used material as transparent and conductive electrode (detailed description in section 1.5.3). ITO's hard processability and the scarce of indium turns ITO a very expensive material to produce ECDs, in a large scale. Here, CNTs can also have an important role since it also has been reported their use as conductive materials for ITO replacement in electrochromic devices[172–175] as reported by Kim *et al.* with the production of carbon-based electrodes for electrochromic displays with improved electrochemical and mechanical stability.[176]

1.4.2.1.1 Alternative Materials as Conductive Electrodes

ITO replacement for optoelectronic applications and the development of highly transparent electrodes (TCEs) is essential to the future of flexible electronics since is a key component for such displays: liquid crystal displays (LCDs), solar cells, light emitting diodes (LEDs), organic emitting diodes (OLEDs) and touch screens. The development of several alternatives for TCEs is progressing with the research on materials like the referred CNTs, conducting polymers (*e.g.*, PEDOT),[177] metal nanowires and graphene.[178]

Recently, metallic copper nanowires (CuNWs) gained substantial attention due to their high electrical conductivity and optical transmittance comparable with ITO.[179] Indeed, alternatives to ITO require a green and sustainable approach that represents advantages for industrial applications from its easy processability and scale-up, where copper fulfils those requirements.

1.5 Electrochromic Devices

Electrochromic devices (ECDs) work like normal electrochemical cells (*e.g.*, commonly used batteries) therefore, the basic principle of an ECD contains two electrodes separated using an ion-based electrolyte. Since the ECDs performance is based in color and optical change, ECD structures demand transparent components using one or more transparent conductive electrodes (TCEs). ECDs activation requires external voltage application, either by manipulation of current or potential. Indeed, since an ECD uses a two electrode system, potentiostatic control is more common.[180]

The classic structure of an electrochromic device involves three main layers: *i)* **Conductive substrate**; usually transparent to enable color change observation, also acting as a protective layer for the electrochromic material. *ii)* **Electrochromic layer**, also defined as the active layer where the electrochromic material is deposited using one (or more) different deposition techniques (described in section 1.5.5) and offers the desired color changes upon redox reactions and *iii)* **Electrolytic layer**; this layer is normally of high ionic conductivity (with a salt in its composition) and offers the balance and neutrality to the ECD as a whole during oxidation or reduction of the electrochromic layer.

1.5.1 Architectures

When assembling solid-state ECDs, there are two main architectures that can be approached namely, vertical, and co-planar architectures.

The *vertical* stack architecture is a sandwich-type design, and it is the most widely used laminated configuration where the Substrate/Electrode/Electrochromic layers are closed together with an electrolytic layer between (see Scheme 1.1) while using an inert adhesive to separate both electrodes.[181]
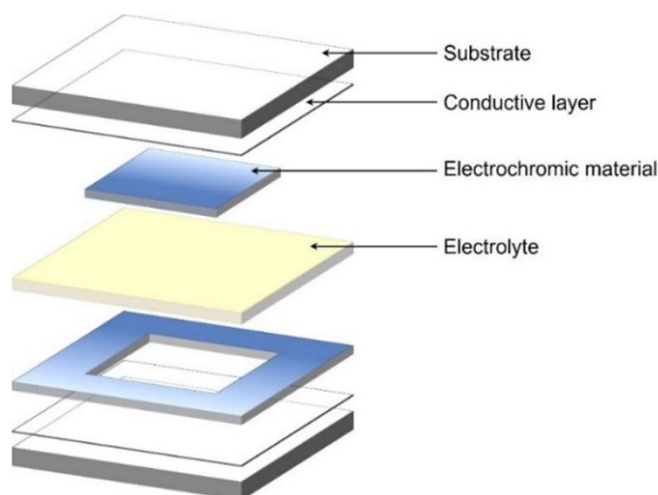
Scheme 1.1. Schematic representation of an electrochromic device using a vertical architecture.

Other possibility for solid-state ECD assembly is using the co-planar architecture.[182,183] This architecture can also be denominated as side-by-side or lateral design where the color change of the oxidized and reduced state occurs simultaneously, in the same substrate (see Scheme 1.2). This architecture is advantageous to produce more cost-effective ECDs since only one conductive substrate is required (segmented, creating two different electrodes in the same substrate), while the second substrate can be transparent but non-conductive. However, the

limitation of this architecture requires intrinsically conductive electrochromic materials for a fast switch of the colored material (*e.g.,* PEDOT) since the ion migration between the two segmented electrodes travels a longer path when compared to the vertical stack architecture. This architecture is employed usually while assembling ECDs bearing opaque substrates (*e.g.,* paper), since only the top substrate is required to be transparent for color change observation.[184,185]
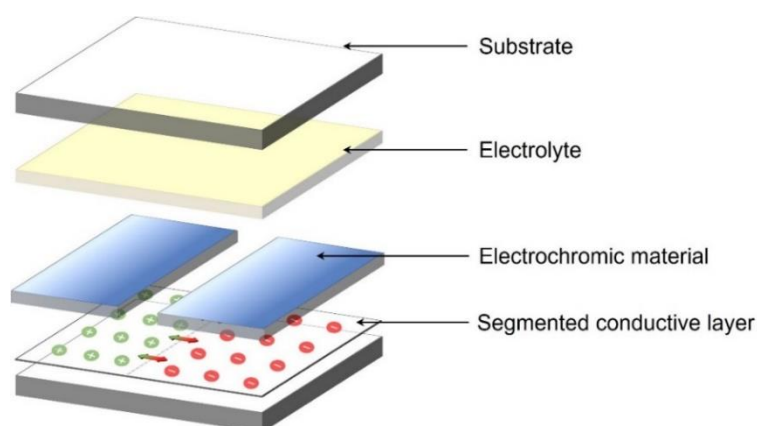
Scheme 1.2. Schematic representation of an electrochromic device using a co-planar architecture.

1.5.2 Substrates

Substrates define most of the optical properties of the electrochromic device. The substrates used for an ECD assembly are usually transparent (*i.e.,* light is capable of passing through, working in a *transmissive mode*) or opaque substrates (i.e., that reflects incident light, working in *reflection mode*). This protective layer can also be defined in terms of their mechanical properties, such as rigid substrates (*e.g.,* glass) or flexible substrates (*e.g.,* plastic, paper, textiles). The use of rigid or flexible substrates depends ,mainly, on the type of application that is desired for the assembled electrochromic device, however, there are some deposition methods that require high temperatures (*e.g.,* sputtering or vapor deposition) narrowing substrate selection to glass. The use of flexible substrates offers a more versatile range of applications such as smart packaging, smart cards, electronic paper, etc.

One of the most demanding characteristics for substrates in solid-state ECDs is their transparency. Specifically, a transparent substrate should have the following characteristics: *i)* High optical quality, with a high visible light transmittance and preferentially uncolored; *ii)* Low-cost and recyclable; *iii)* Versatility and *iv)* High chemical, thermal and photochemical stability.

There are no physical restrictions on the use of a material as substrate for an electro-chromic device if the deposition of the different layers is possible. However, some materials offer considerable advantages in terms of availability, sustainability, and scalability for differ-ent electrochromic applications therefore, glass and plastic are the most commonly used ma-terials for solid-state ECDs. Quantitatively, glass substrates are still the most common used material since they present high availability, mechanical durability, and it can be produced at low-cost, especially for the production of smart windows. However, in more recent years an increased attention has been given to flexible displays, increasing the use of plastic substrates. Plastic offers an increased flexibility to solid-state displays and can also be easily functional-ized with conductive layers for ECDs, inducing an increased exploration of flexible ECDs for daily-based applications, including wearables.[2–4,6,7] Polyethylene terephthalate (PET) and poly(ethylene-2.6-naphtalene) (PEN) are the most commonly used plastic materials in printed electronics and electrochromic applications, especially in roll-to-roll processing and as compo-nents for touch screens, smart windows and solar cells.[77,186–188]

Plastic substrates, alike glass, present very high values of visible light transmittance (see Figure 1.11) as it was described by Guillén *et al.* even when coated with ITO proving their suitability for employment in electrochromic devices.[189]
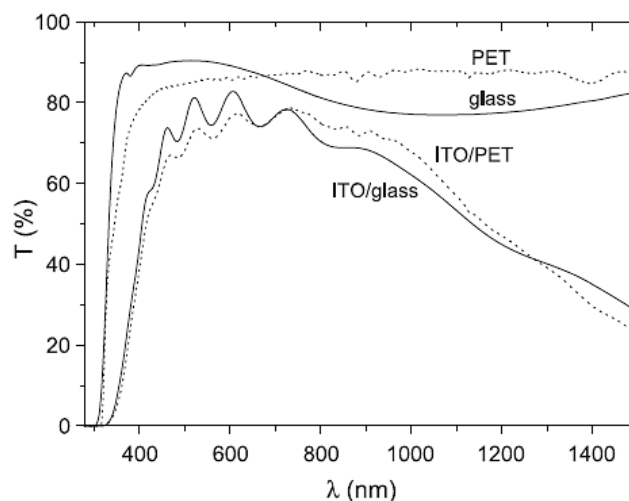
Figure 1.11. Optical transmittance of PET/Glass substrates be-fore and after the grown of ITO thin-films.[189]

1.5.3 Conductive layers

Conductive layers can be denominated as transparent conductive electrodes (TCE) and they are key components for the functionality of an electrochromic device, usually formed as a thin layer applied on the surface of substrates such as glass or PET, in order to induce charge transfer into the electrochromic layer.

As referred before, optical transparency of the materials is one crucial characteristic to be employed as conductive layer for solid-state electrochromic devices as well as their electrical conductivity. Additionally, TCEs require parameters such as roughness and electrochemical stability that strongly influence the electron injection onto the electrochromic layer and thus, the solid-state device performance. Furthermore, the mechanical properties of the TCE like their processability, deposition method, cost and environmental impact are key factors when comparing different materials used for the production of the TCEs.

The most commonly used TCE for optoelectronic applications, including electrochromism, is ITO as metal oxide thin-films deposited into glass or PET as well as fluorine-doped tin oxide (FTO), in a smaller scale. ITOs high conductivity and transparency have been commonly achieved through physical or chemical vapor deposition (PVD, CVD) techniques with sputtering on a commercial scale.[190] Vapor deposition techniques offers the TCE films dense structures and benchmark properties of resistivity around 20 Ωsq and transparency with transmittances > 85% for 100-200nm thick films, suitable optoelectronic applications.

Unfortunately, the requirements of high vacuum specifications and sophisticated equipment associated with vapor deposition techniques and the scarcity of indium on Earth turns ITO thin-film processing very expensive, increasing the research interests in creating ITO alternatives.[190,191]

Indeed, with the recently breakthroughs in optoelectronic displays, the development of new, low-cost, and large area transparent electrodes is one major challenge in materials science in order to produce cost-effective conductive electrodes for optoelectronic applications, including electrochromism.[177,178,192,193] Other type of materials have also been developed as opaque metallic conductive electrodes such as platinum-based alloys,[40,41] copper,[66,194] carbon/carbon-based materials[174,175] and graphite[195].

1.5.4 Electrolytes

The electrolytic layer embedded in the displays is located between the two electrochromic layers on the structure of a solid-state electrochromic device. In parallel to a battery or an electrochemical cell, the electrolyte has the function of providing ionic exchange and connection between the two electrodes, while physically separating them, avoiding direct contact and electron transfer from both conductive electrodes, thus avoiding short circuits in the displays. Therefore, the electrolytic layer should be a good ionic conductor and an electronic insulator at the same time.[55] The ionic conductivity is provided by the presence of one or more salts that dissociate providing cations and anions.

Electrolytes can be presented in the liquid, semisolid (gel), or solid form. Liquid electrolytes are consisted mostly by a salt dissolved in a liquid solvent, however, liquid electrolytes for solid-state ECDs are not suitable since there is always a risk of leakage or solvent evaporation in between the different layers. Nevertheless, ionic liquids have been previously reported as electrolytes for electrochromism.[196–198]

In the literature, there is a number of published papers describing different types of electrolytes for electrochemical applications especially in the area of lithium-ion batteries, fuel cells and supercapacitors. The literature reports their advantages and disadvantages, the techniques used for the processing of the materials, structures and thermal or ion transport characterizations for the different electrolytes. In this section, the focus is directed to the group of polymeric electrolytes for electrochromic applications. Indeed, polymer electrolytes have been linked to be the electrolytes of choice for the development of ECDs.[199]

For electrochromic devices, the polymer electrolyte formulation is very important for the performance and durability of the display,[200–202] while taking advantage of the properties of the electrochromic material (*e.g.*, dried solvents) since, the interface between the electrolyte and the electrochromic layer controls the overall performance of the display.[203]

Therefore, for the successful employment of polymer electrolytes in electrochromic displays, they should have the following characteristics:[204]

- *High ionic conductivity:* Polymeric electrolytes should be good ionic conductors ($\sigma_e < 10^{-12}$ S.cm^{-1}) and electronic insulators so that ion exchange can be facilitated, and self-discharge minimized (possible short circuits in order to achieve similar performances of liquid electrolyte-based systems. High ionic conductivities facilitate the movement of the ions in and out of the electrochromic layer to induce color change.

- *High optical transmittance:* in ECDs, higher transparencies allow a higher transmittance of the final displays in order to increase color contrast between the bleached and reduced states.
- *A wide electric potential window:* no redox reactions on the electrolyte should occur in the range of potentials used for an electrochromic material.
- *Chemical and electrochemical stability:* the electrolyte and its components should not be reactive towards the electrochromic material and electrodes in the operational potential range.
- *Thermal stability and robustness:* the switch of a solid-state ECD can produce heat and the display can be exposed to elevated temperatures, as it may occur in smart windows. Additionally, the electrolyte should also be mechanically robust for a long-term use, even under UV exposure.
- *Low cost and environmental sustainability:* The components of the electrolyte should be cost-effective, easily available, and harmless for health and environment for commercialization and implementation of electrochromic devices.

Polymer electrolytes are composed of a salt dispersed in a neutral polymer matrix (usually lithium-based salts), where the salt is capable of being dissociated in anions and cations within this polymeric matrix.[204] Depending on the composition of the matrix, electrolytes can present good mechanical strength, good interface contact with the active material, flexibility and processability.

Polymer electrolytes for electrochromic applications can be essentially classified in solid or semisolid polymer electrolytes. Solid or semisolid electrolytes present higher advantages when compared to liquid-based electrolytes, such as: they are usually safer and less reactive, higher range of working temperature, less prompt for leakage, can act as a physical separator between the different ECD layers (preventing the risk of short-circuit in the display), and providing an increased mechanical strength to the ECD.

Solid polymer electrolytes are defined due to its solvent free system characteristics with an ionic conducting phase formed by their dissolved salts in a polar polymeric matrix.[205,206] This type of electrolytes presents several advantages from the referred before, such as chemical and electrochemical stability, flexibility, mechanical robustness and easy processing in large-area displays. However, ionic conduction mechanism is based on the free movement of ions in the electrolytic layer therefore, ionic conductivity of these systems is typically low, at room temperature.

Semisolid or gel polymer electrolytes are usually produced by integrating a suitable solvent or solvents to the polymeric matrix that are capable of forming a stable gel with the polymer main structure. Due to their unique network structure, gel-based electrolyte can simultaneously possess the cohesive properties of a solid with the high ionic conductivity of liquid-based electrolytes. Therefore, a compromise needs to be achieved between the increase of ionic conductivity and the decrease of mechanical strength of the formulated gel, where the polymer acts as a solidifier for the added solvents and the salt acts as the conduction medium. Gel-based electrolytes are the most widely type of electrolytes used for electrochromic applications since, the most recent research and industrial electrochromic applications require the production of flexible displays with higher performances.

In 2014, *Ynvisible®* developed an UV-curable Li^+-based gel electrolyte (patent n°20140361211A1)[207] that is deposited between both electrochromic layers and, after exposure to UV radiation becomes more rigid, maintaining high ionic conductivity while providing increased mechanical strength to the assembled electrochromic device. This electrolyte is used in all assembled solid-state ECDs presented in this thesis.

1.5.5 The Rise of Printed Electronics and Printing Techniques

In this growing era of disposable, flexible and high-performance displays used on a daily basis, the low-cost manufacturing production that meets the necessary requirements becomes more challenging. Thus, solid-state ECDs have to combine mechanical flexibility and high color contrasts using processable electrochromic materials.

The previously described organic polymers offer the required color contrasts for electrochromic features upon electric current application. Additionally, their high processability (in toxic or non-toxic solvents) fits perfectly into the development of different ink formulations, to explore the use of different printing techniques, depending on the printing requirements.

In recent years, the development of organic and hybrid semiconductors has enabled a new paradigm for manufacturing electronics, in the form of printable electronics.[208] Printable electronics revolutionized the modern world, by providing low-cost, clean solutions, large area printability, smart packaging and cheap displays through adaptable device architectures, highly customizable materials and a wide variety of printing-based manufacturing techniques. Therefore, printed electronics are emerging in the last decades due to the possibility of being applicable in everyday life, for instance, in packaging, buildings and construction, labels, sensors, photovoltaic cells, batteries, OLEDs, textiles, among others, by introducing electronic

devices on common substrates, such as plastic, paper or metals.[59,209–211] The main goal of printed electronics consists in building electronic devices and components where transistors, light-emitting or electrochromic devices can be integrated by roll-to-roll (R2R) printing methods and thus allowing the production of these devices at industrial scale.[59,63]

In a preliminary phase, the printing optimization for each material is performed at a smaller research scale, using printing techniques more accessible to common users. The most common printing techniques used to assemble ECDs goes from simple drop casting techniques, through screen and ink-jet-printing and spray-coating.

1.5.5.1 Drop-Casting

While drop-casting is not a real printing technique, it can be very useful for testing new synthesized materials. Actually, while developing new electrochromic materials, it should be the first "electrochromic test" to be performed. Drop-casting involves simply a solubilization or dispersion of the newly obtained material and cast it dropwise into a conductive substrate, evaporate the used solvent and assemble a display. The biggest advantage of drop-casting is its simplicity and quick assessment if a material is electrochromic or not. On the other hand, the low homogeneity of the casted drops can also mislead about the true performance of the material.

1.5.5.2 Screen-Printing

Screen-printing is a more matured technique that can be applied in planar-based systems, being the more widely used printing method in industry with low costs[211–213] and it has been largely used in printed electronics.[7] Screen-printing also represents the transition from a smaller laboratory scale, to industrial scale, when the electrochromic materials are stable enough for this printing method. Screen-printing (see Figure 1.12) uses a screen mesh with open and closed areas that define a fixed printing area, in direct contact with the substrate.[211,214] The movement of the blade (or squeegee) spreads the ink, fills the mesh of the screen and thus, while in contact with the substrate, defines the final printed image onto the substrate.

In electrochromics, this printing technique is widely used for commercially available inks, especially with PEDOT (*e.g.*, Heraeus Clevios). Screen-printing is a technique that requires ink formulations with high viscosities that are controlled by the addition of binders or surfactants. In addition to the complexity of the ink formulation, the addition of these additives can suppress the electrochromic activity of the material, turning screen-printing a viable printing-technique only for very highly developed and stable ink formulations.
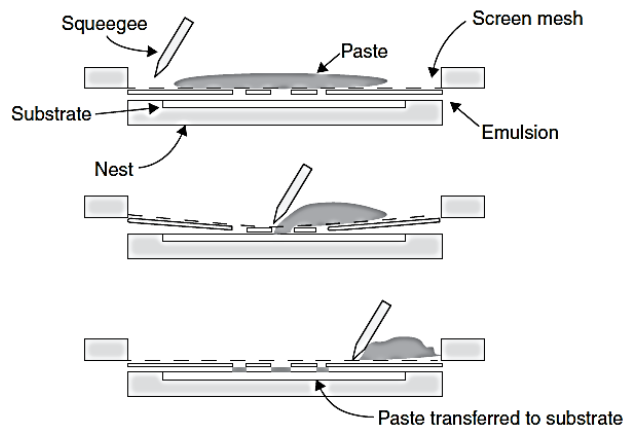
Figure 1.12. Principles of screen-printing deposition technique.[213]

1.5.5.3   Ink-jet Printing

Ink-jet-printing is a recognized and efficient method from its ability to print any graphical image by loading small drops in a substrate. Different types of ink-jet printing machines can be found, from low-cost, quick, and conventional type ink-jet printers for small consumers, to very large professional machines used in an industrial scale for a wide range of applications. Due to its high adaptability, ink-jet printing is nowadays used in large scale for the production of sensors,[215,216] LEDs,[217,218] transistors,[219,220] and displays such as, electrochromic devices[59,221,222] taking advantage of its high-quality coatings[17] and fast prototyping capabilty.

This technique involves the release of small ink drops through a printhead, controled by the ink-jet-printer itself. This printhead contains a series of nozzles, which allows the ink drops to be realeased onto the substrate (at specific temperatures), with controlled size and speed. (see Figure 1.13).
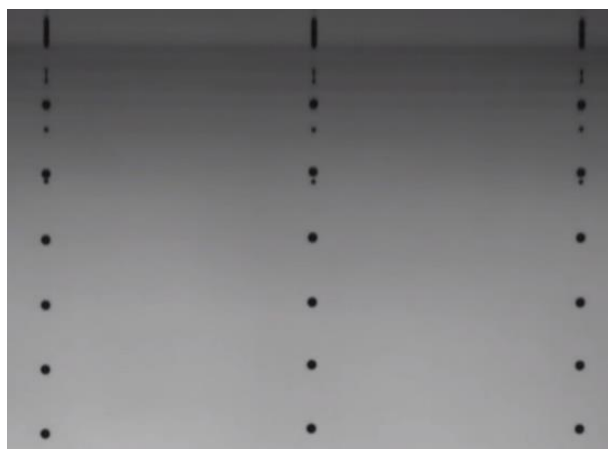
Figure 1.13. Droplets released from an ink-jet printer Dimatix Fujifilm®.

30

Comparably to the screen-printing technique, ink formulations for ink-jet also have specific parameters and requirements, depending on the type of printer that is being used. This feature makes the preparation of inks for ink-jet printing quite challenging, specifically, ink formulations for ink-jet have to obey to certain rheological parameters such as viscosity or surface tension. These rheological parameters are controlled by the presence of additives, surfactants or solvents, optimizing the viscosity of the final ink. Usually, the viscosity required for ink-jet printing is rather low (about 20 cP), indeed, water-based solutions or dispersions present suitable viscosities for the use of this printing technique. Since ink-jet printing technique has been evolving for the past 10 years, the number of compatible ink-jet printers for water-based solutions have been evolving, making the production of electrochromic displays using water-based inks more promising for eco-friendly and high-performance coatings.

1.5.5.4 Spray-Casting

Spray coating (or spray casting) technique is a very straightforward deposition method, since it does not require the development of ink formulations bearing additives, binders, or surfactants.

This technique is also very convenient for processing in a research laboratory scale since it enables a fast and simple coating in any substrate, while sparing the time required to produce ink formulations and their optimization.[8,11,223,224] Additionally, the direct solubilization/dispersion of the electrochromic material without additives ensures that, after coating and drying, only the deposited electrochromic material is being evaluated through its performance on a final solid-state ECD.

Although most optoelectronic applications of π-conjugated polymers, including PLEDs and OPVs, require dense coatings for strong interchain interactions, that is not the case for electrochromism. Indeed, due to the necessity of thiophene-based polymers to be entangled in electrolytic solutions (or gels) to enable efficient contact of the films with electrolyte ions, thin-film production is desired.[224]

To assure the homogeneity of the coated films, the spray-coating needs to be performed at a constant spraying rate and distance from the substrate, certifying that only the aerosol part of the sprayed solution is deposited into the substrate (see Figure 1.14).

Figure 1.14. Representation of the spray-casting technique. Highlighted the aerosol part of the sprayed solution.

Additionally, the coated substrate is required to be at a specific temperature, depending on the solvent or mixtures of solvents that are being deposited. As an example, if a chloroform solution is being spray-casted in a glass substrate it is required for the glass to be at ≈60°C, promoting a fast evaporation of the solvent, to avoid coffee-stain effects in the deposited films.

1.5.5.4.1 Coffee-Stain Effect

The coffee-stain effect phenomenon is related to the deposition of most of the material along the perimeter of the drop after the solvent evaporates. The coffee-stain effect appears when the evaporation of the deposited drop is faster at the edges than that at the center, and a ring-like structure is formed.

Coffee-stain effects can emerge while using printing techniques such as ink-jet printing or spray casting, since they are non-contact deposition methods. Thus, this phenomenon needs to be taken into account during drop formation and drying processes when producing thin-films for electrochromic applications since heterogeneous films can lead to poor electrochromic performances, due to particle aggregation.[225]

Mampallil *et al.*[226] described, in 2018, that the coffee-stain effect can be suppressed through three physical strategies: preventing the pinning of the contact line, disturbing the capillary flow toward the contact line and preventing the particles being transported to the edge of the drop. In the specific case of electrochromic displays, since the depositions are performed in a specific substrate (paper, plastic, or glass), the coffee-stain effect should be avoided

by preventing the particles being transported to the edge of the drop, while controlling the temperature of the plate.

Different evaporation rates can also decrease the coffee-stain effect as Li *et al*.[227] described in 2016. Concluding that controlled drying processes using different evaporation kinetics allowed a decrease of coffee stain while increasing thickness at different temperatures (see Figure 1.15).
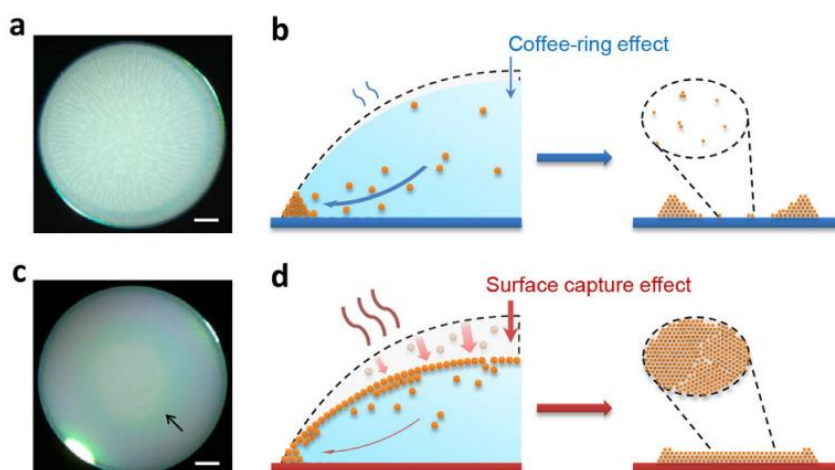
Figure 1.15. Drop drying process controlled by different evaporation rates. (a,b – T=30°C and c,d – T=70°C) described by Li *et al*.[227]

Mixing solvents[226,228] or adding surfactants[226,229–231] were reported as interesting tools to avoid the coffee-stain effect however, in electrochromism, additives and/or surfactants are not always an advantage. Some additives (like resins) can delay or completely suppress the electrochromic activity, mainly through loss of electrical conductivity of the thin film. Therefore, upon testing the electrochromic materials, the absence of additives and surfactants is recommended, while the mixture of pure solvents like water-ethanol can be an interesting alternative in order to avoid coffee-stain effect as reported by Zhong *et al*.[232]

1.5.6 Optical Properties

As referred before, an electrochromic device is constituted by different stacked layers, where each one will interact differently with light.[233] Each layer will have a specific refraction index (n), a wavelength dependent light absorption coefficient (ε), thickness and light scattering.[234] These factors add up, decreasing the light transmission and/or light reflection that impose limits to the optical properties of an electrochromic device. When using transparent substrates,

the color assessment of the devices is made in the *Transmissive Mode* (*e.g.,* smart windows) or for opaque substrates displays will work in the *Reflection Mode* (*e.g.,* paper), in each case the position of the observer is different.[15] The performance of the electrochromic device is therefore usually defined in terms of standard conditions in order to lead to reproducibility of results. An electrochromic system should work in the visible range of the light spectrum (see Figure 1.16), although other spectral regions such as the near-infrared range may be considered for electrochromic applications.
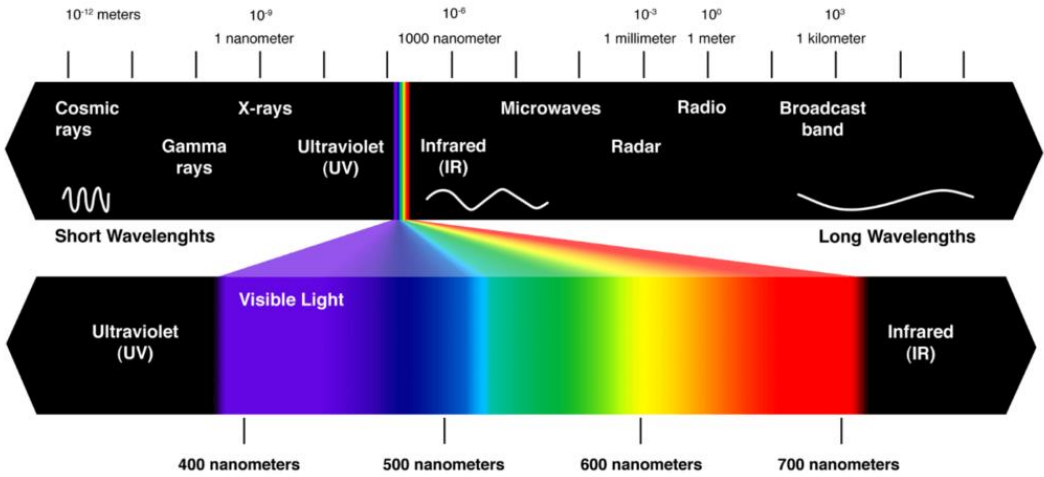
Figure 1.16. Complete spectrum of electromagnetic radiation with visible light expanded.

In electrochromism, the optical properties are usually determined in transmittance (*T*) or Absorbance (*Abs*). T and Abs reflect the true spectroscopic changes of the electrochromic material, without the interference of the baseline (or background). The use of transmittance or absorbance values depends on the scope of the study, as an example, the interpretation of the optical properties of smart windows should be carried out in transmittance values because what is being evaluated is the amount of light that passes through the window, and not the amount of absorbed light.

For a given system, the wavelength (λ) dependent light transmission (*T*) can be evaluated according to the equation below:[235]

$$T(\lambda) = \frac{I_{trans}(\lambda)}{I_0(\lambda)} = 1 - R(\lambda) - A(\lambda) - S(\lambda) \qquad\qquad \text{equation 1}$$

Where *R* is the amount of reflected light, *A* is the amount of absorbed light and *S* is the amount of scattered light. Figure 1.17 represents the amount of scattered, reflected, absorbed, and transmitted light upon incident light on a solid-state electrochromic device.
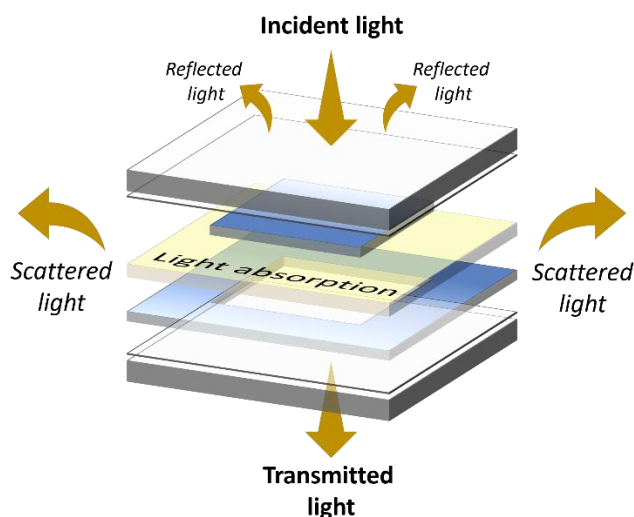
Figure 1.17. Scattered, reflected, absorbed, and transmitted light upon incident light on an assembled electrochromic device.

During the color switch in an electrochromic device, upon incident light, there is an amount of scattered light in all directions where, only a small negligible part will contribute to the transmitted light, which means that T(λ) is always smaller than 100%.

To achieve a modulation of T(λ) it is important to reduce as much as possible R(λ) and S(λ) by using materials that do not absorb light in the visible region. A(λ) represents the quantity of light absorbed and will depend on the redox state of the electrochromic material. This will reflect in the overall perception of the color that also depends on the film thickness, concentration, and extinction coefficient of the material (ε), accordingly to the Lambert-Beer law.

1.5.7 Performance Evaluation of Electrochromic Devices

In order to evaluate different electrochromic materials and devices, it is important to use standard procedures to assess their performance. Since electrochromism is a way to control color, usually the main goal is to achieve maximum color contrast on a solid-state ECD with a very small energy consumption and fast switching times between the reduced and oxidized states.

Cyclic voltammetry (CV) is one of the procedures to obtain qualitative and quantitative information regarding the electrochemical processes of an electrochromic material. CV measurements are usually performed in solution, previously to the assembly of an ECD and involve

the application of a potential window with a specific scanrate (*e.g.*, 20mV/s). This characterization in solution is usually carried out by using a thin-film of the electrochromic material deposited in PET-ITO substrates used as the working electrode (WE) in a three-electrode cell system. Working electrode, reference electrode (RE) and counter-electrode (CE) are dipped in an electrolytic solution usually containing $LiClO_4$ as a salt with a 0.1M to 1M concentration.

For a quick and accurate performance evaluation of a solid-state electrochromic display, some commonly used and important performance indexes including optical contrast, switching time, consumed charge, coloration efficiency and durability will be described.

1.5.7.1 Optical Contrast

Optical contrast is the primary parameter that represents the color-switching ability of an electrochromic material or display. This parameter is defined as the difference in absorbance (A) or transmittance (T) at a specific wavelength (λ) before and after the redox switch (see equation 2).

$$\Delta T_{\lambda} = T_{bleached} - T_{colored} \ \ or \ \ \Delta A_{\lambda} = A_{colored} - A_{bleached} \hspace{2cm} \text{equation 2}$$

Where, ΔT and ΔA represent the optical modulation. $T_{bleached}$, $T_{colored}$, $A_{colored}$ and $A_{bleached}$ represent the transmittance in bleached and colored states, absorbance in the colored and bleached states, respectively. For a device working in reflection mode, the difference in reflection of the colored and bleached states can also be used to define their optical modulation.

The contrast ratio (CR) is also commonly used to evaluate the color switch ability of an electrochromic material or device, as shown in equation 3 where the CR can refer either to a specific wavelength or the overall color contrast, in absorbance (A) or transmittance (T).

$$CR_T = T_{bleached} / T_{colored} \ \ or \ \ CR_A = A_{colored} / A_{bleached} \hspace{2cm} \text{equation 3}$$

These parameters are usually obtained through spectroelectrochemical measurements where, an electrochromic device is switched between the colored and the bleached state using a wide range of potentials, before transmittance/absorbance spectra acquisition.

Besides light intensity calculated through the amount of light transmitted or absorbed, coloration also plays a major role in ECDs, due to the vast color pallet of electrochromic materials embedded in solid-state displays.

The perception of color occurs in the cone receptors in the eye retina and, usually the receptors are active in the blue, green, and red region of the visible spectra, rising to the primary colors and the RGB color mode. However, RGB mode does not consider light intensity thus, in 1976, the International Commission in Illumination (CIE) defined the CIELAB color space, also referred as L*a*b* coordinates, expresses color as three values: L* for perceptual lightness and a* and b* for the four colors that the human eye can percept: red, green, blue, and yellow. The CIELAB space is three-dimensional and covers the entire range of the human eye color can perceive and defining it color numerically, making L*a*b* coordinates often used in industrial applications, including electrochromism. L*a*b* are defined as a three-axis system X, Y and Z representing L*, a* and b* respectively (see Figure 1.18).[236]
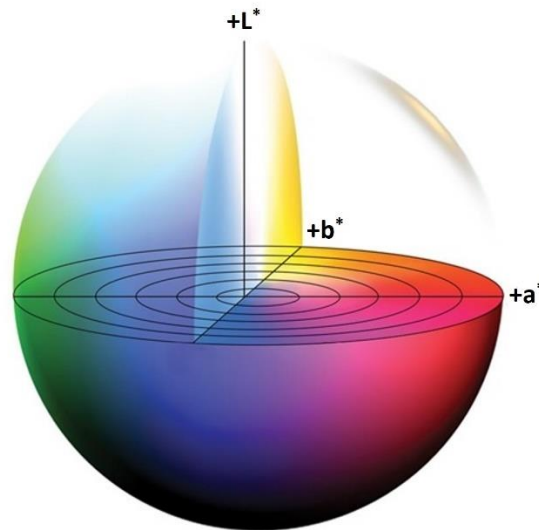
Figure 1.18. Spherical representation of the three-axis system that define L*, a* and b* color coordinates.

Thus, when defining color contrast using L*a*b* coordinates for two given colors within the CIELAB color space (L_1^*, a_1^*, b_1^*) and (L_2^*, a_2^*, b_2^*), the parameter ΔE* is calculated. Definition made by the CIELAB system in 1976 using the following formula described in equation 4.

$$\Delta E^* = \sqrt{(L_1^* - L_2^*)^2 + (a_1^* - a_2^*)^2 + (b_1^* - b_2^*)^2} \qquad \text{equation 4}$$

Additionally, when a color contrast is calculated with ΔE<2.3 it is considered *just noticeable difference*, which means that contrasts values below 2.3 cannot be perceptible by human eye.[237]

1.5.7.2   Switching Time

One of the most important characteristics of electrochromic devices is the switching time (ST) required to perform a color switch between the oxidized and reduced states. The switching time can be defined as the time required of an electrochromic material to color from its bleached state and *vice versa*, usually, for an ECD to reach 90% (t_{90}) of its full optical modulation. For the case of ECDs with a high optical density, full optical modulation of 70% (t_{70}) can also be considered.[202,238]

Recently, Hassab *et al.* proposed a model to simultaneously calculate optical modulation (ΔT) and switching times using the following equation:[239]

$$\Delta T = \Delta T_{max}\left(1 - e^{-\frac{t}{\tau}}\right) \hspace{4cm} \text{equation 5}$$

Where, from the exponential fitting of the experimental data it can be obtained simultaneously the maximum of ΔT and the switching time (τ). From τ it can be calculated the switching time for 90% (t_{90}) or 95% (t_{95}) of optical modulation:

$$t_{90} = 2.3\tau \hspace{1cm} \text{and} \hspace{1cm} t_{95} = 3\tau \hspace{3cm} \text{equation 6}$$

The switching time of an electrochromic material is highly dependent on the ionic conductivity of the electrolyte, ion diffusion to the coated thin films, the applied potential to the ECD, film thickness and the morphology of the films.[204] In this thesis, the experimental procedure to obtain the switching times of the ECDs was the following: application of a pre-treatment of 15 cycles using a 10 second cycle, (usually between -1.5 to 1.5V) for the electrochemical stabilization of the ECD. Afterwards, 3 full cycles of 60 seconds at each potential were performed for qualitative assessment of the ECD. The experimental setup involved a potentiostat coupled to a spectrophotometer where the optical experimental data (from the spectrophotometer) and the data of the consumed charge (from the potentiostat) were used to calculate switching times (τ), consumed charge (Q) and coloration efficiency (CE).

1.5.7.3   Coloration Efficiency

Coloration efficiency (CE) is considered the most important parameter when evaluating the performance of electrochromic displays. CE (or η)[233] is calculated from the ratio of color change obtained for a certain amount of injected charge per unit area (Q) at a specific wavelength as shown in equation 7 (assuming no side electrochemical reactions), usually in mC/cm² units.

$$CE(\lambda) = \frac{\Delta Abs(\lambda_{max})}{Q} \ (C^{-1}.cm^2) \qquad\qquad \text{equation 7}$$

CE is used to compare the efficiency of the electrochromic displays using a classic efficiency index where, higher optical modulations can be achieved by ECDs with higher CEs under the same amount of injected charge. In other words, an ECD with a higher CE requires less charge to achieve the same optical modulation. The values of CE are calculated at specific points of the switching, normally at 90% when the total change of optical modulation is obtained.

1.5.7.4   Durability

Durability refers to the repeatedly cycling of the electrochromic device between its color and bleached state, resulting from the application of oxidation and reduction potentials (usually 1.5 and -1.5V). Display failure will eventually occur, resulting from physical changes in the different layers or from chemical side reactions where, external environmental conditions like temperature, humidity or photodegradation might occur.[204]

Thus, the durability of ECDs is evaluated by performing cycling measurements to the display applying a certain number of cycles or, enable the device to switch continuously until optical contrast is no longer perceptible, in a controlled environment. This parameter is of great importance to evaluate if a certain electrochromic material or device is suitable for a specific electrochromic application, depending on the number of cycles required. For applications that require a long lifetime (*e.g.,* smart windows or labels), the electro-optical switching capacity of an ECD should be maintained after a higher number of coloring-bleaching cycles.

The cycling measurements are performed taking into account the previously calculated switching times for the electrochromic material, when assembled in a solid-state ECD. The switching times calculated, and the purpose of the cycling experiment will determine how the cycling will be performed. As an example, for short-term cycling (*e.g.,* 1000 cycles) the cycling experiment can be made in transmittance/absorbance mode using a spectrophotometer coupled to a potentiostat, applying the desired voltage during a specific time. For long-term cycling, since the experiment can be active for days/weeks, a system was developed by *Ynvisible®* that involves a *cycling box* in which a function generator is attached (see Figure 1.19). The function generator applies the desired potential using a squared wave function using a controlled time (*e.g.,* 1 cycle = 10 seconds with 5 seconds at -1.5V and 5 seconds at 1.5V, for an indetermined period). Inside the box is located a digital camera under diffused light that takes a certain number of pictures, during a certain period of time (these parameters are used defined). The pictures are analyzed using MATLAB functions that convert RGB coordinates into L*a*b*

coordinates thus, calculating the ΔE* of the ECDs during the cycling experiment, using a Col-orChecker® as reference.
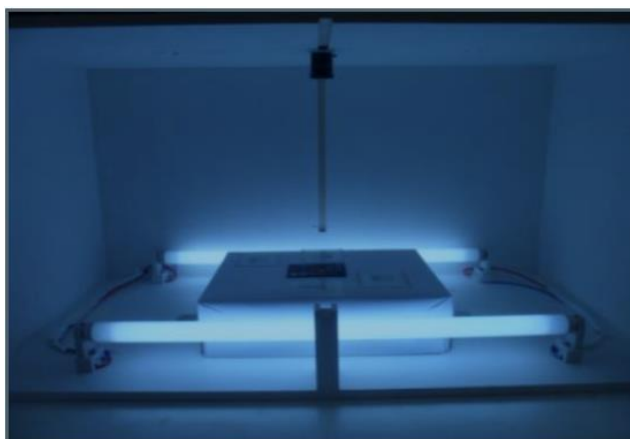
Figure 1.19. Cycling box system developed by *Ynvisible®* to perform cycling measurements using a ColorChecker® as reference.

1.6 Achievements of the Research Chapters

In this section, an overview of the work developed and presented in the research chapters, will be described.

With the goal of developing new nanostructured polythiophene-based electrochromic materials and devices, which represent an enhancement on the current state-of-the-art, the work started by the synthesis and optimization of water-dispersible nanoparticles, using polythiophene materials. This work followed a logic and comprehensive study that began with the nanostructuration of a well-known polythiophene such as P3HT. The expertise and know-how of *Mediteknology®* on the synthesis and characterization of P3HT nanoparticles allowed the author to learn and establish a very optimized method to synthesize and characterize polythiophene nanoparticles with controlled dimensions. Using the synthesized P3HT nanoparticles, solid-state electrochromic devices (ECDs) were assembled and characterized. Not only the absence of toxic organic solvents is essential for a safer and healthier environment, the P3HT nanoparticles, when assembled in ECDs, presented enhanced performances of switching time, color contrast and durability, as described in chapter 2.

With the obtained results, the author was prompt to give one step further in this study and test the nanostructuration of polythiophene-based materials in newly synthesized compounds. The following step was to produce a yellow colored polythiophene with low redox

potential, capable of forming water-dispersible nanoparticles. The yellow color is rare in solid-state ECDs and the production of water-dispersible solutions with enhanced performances was an additional driving force to synthesize these materials. So, again in collaboration with *Mediteknology®*, a new class of polythiophene materials was synthesized, using the same backbone of same π-conjugated thienyl-phenyl-thienyl-thienyl (Th-Ph-Th-TH) fragment with two *β*-alkyl/alkoxy substituents in the thiophene using the donor-acceptor approach as described in section 1.4.1.1. Additionally, with either -CH=CH- or -CH$_2$-CH$_2$- units added to the backbone of the polymers were used as conjugation modulators, and a yellow polymer with low redox potential was obtained. Furthermore, the polymer was used to form water-dispersible nanoparticles, also presenting enhanced performances in solid-state ECDs, when compared with the pristine polymer, as described in chapter 3.

In a different approach, however with the same goal of enhancing electrochromic performances, the formation of organic-inorganic hybrid thin-film composites using polythiophenes and CNTs, was developed and optimized using a newly synthesized pyrene-appended polythiophene capable on engaging in π-π stack interactions with the highly delocalized electrons present in the CNTs. This interaction between the organic and the inorganic material allowed the formation of very stable dispersions of the carbon material in chloroform:toluene solvent mixtures, the hybrid dispersions were used to assemble solid-state ECDs, and a remarkable enhancement of the switching time and durability of the polymer was achieved, when using CNTs, as described in chapter 4.

Finally, the use of copper nanowires and reduced graphene oxide (CuNWs-rGO) coatings as transparent and conductive electrodes was explored for the assemble of ITO-free electrochromic devices. ITO-free ECDs were assembled and characterized using PEDOT:PSS, and presented very similar performances when comparing with displays using ITO as conductive electrode, including color contrast, switching time, and durability, as described in chapter 5.

POLY-3-HEXYLTHIOPHENE (P3HT) NANOPARTICLES DEPOSITED FROM WATER-BASED SOLUTIONS ON FLEXIBLE PET-ITO SUBSTRATES

This chapter is based on the published paper "Moreira, T. *et al.*, Semicrystalline Polythiophene-Based Nanoparticles Deposited from Water on Flexible PET/ITO Substrates as a Sustainable Approach toward Long-Lasting Solid-State Electrochromic Devices, ACS *Appl. Polym. Mater.* (2020), **2**, 8, 3301-3309".

The author contributed to the planning and was the main responsible on the execution of all the experiments presented in this paper, including synthesis, optical and structural characterization of the materials (except for GIWAXS measurements, performed at APE reaserch in Trieste, Italy), assembly of solid-state electrochromic displays and their characterization. The author was also the main responsible for the interpretation and discussion of all the results, and contributed to the preparation of the manuscript.

Since the pioneering work of Deb in 1967,[24] the use of different redox states to control color became crucial for the development of intelligent windows for energy and light management of buildings or transportation (*e.g.*, rearview mirrors).[55,235,240] Metal oxides (*e.g.*, WO_3) and organic molecules such as methyl viologens are at the core of the commercial use of this technology. In the meantime, semiconductor polymers were discovered in 1979,[68,69] which prompted a wave of research about their optical properties. Heeger and co-workers discussed this, with special attention given to polythiophenes due to their relatively low toxicity and relatively simple synthesis. However, only in 1994 was a first electrochromic effect reported for PEDOT,[104,241,242] which is still today the most used polymer in electrochromic devices (ECDs. This was followed by a strong synthetic effort to tune polythiophene optical properties and solubility. Yet, while metal oxides could be deposited in a variety of ways including nanopatterning[37] to ensure faster kinetics and efficiencies for utilization in smart windows, only the mixture of PEDOT and PSS is a true commercial alternative to inorganic materials.[73] This is because PEDOT/PSS is water dispersible and their thin-films have a high electrical conductivity.

Currently, there is great interest in flexible ECDs and their numerous applications spanning innovative fields such as *adaptive camouflage, wearable and deformable electronics*, to the more futuristic *information signage* and *electronic skin*.[126,243] In parallel, expectations are increasing for green approaches to film formation in solid-state devices that would not require expensive optimization of deposition techniques, search for non-toxic solvents or additives addition. Very recently, application of nanostructures of semiconductor polymers in ECDs started to emerge and various methods of fabricating conducting polymer nanopatterned electrodes were described.[130–132] Nanostructures are expected to favor, for example, charge transport by virtue of the increase in contact area between the electrodes and the electrolyte and consequently to affect important parameters such as color contrast or response time.[59,133] In this framework, electrochromism based on semiconducting conjugated polymers plays a very important role. Most commercial applications of electrochromism are indeed focused on π-conjugated organic polythiophenes such as the widely studied poly-3,4-alkyldioxythiophenes[117,124] displaying electrochemical stability, electrical conductivity and chemical versatility towards the extension of color palette through structural modifications. Other polythiophenes have also been explored, such as poly-3-hexylthiophene-2,5-diyl, P3HT - one of the most studied conjugated polymers as a case polymer for the study of optoelectric properties on, *e.g.*, electrochromic devices and optically switchable transistors.[244–246] P3HT is soluble in organic solvents such as chloroform but not in water, the most environmentally friendly of all

solvents. However, the polymer can be prepared in the form of nanoparticles (NPs) as a stable aqueous suspension and deposited as thin film from an aqueous-phase.[131,134]

Here it is shown that P3HT prepared as stable aqueous suspensions of NPs through the surfactant-free reprecipitation method[138] behaves as an ink that can be easily deposited on flexible PET-ITO electrodes via spray-casting. It is proved that NPs with size of 100 nm present enhanced properties when compared to similar ECDs with larger NPs and thin films deposited from chloroform.

2.1 P3HT-NPs: Optical Properties, Morphology, and Devices

Table 2.1 shows the optical properties of P3HT-NPs in water dispersions. For comparison, Table 2.1 also presents the absorption and emission properties of P3HT in a chloroform solution. While P3HT in chloroform shows a broad unstructured absorption band, assigned to a π-π^* transition peaking at about 430 nm, the P3HT-NPs in water show structured absorption spectra (Figure 2.1A) that shift to the red with increasing NPs size. Furthermore, the increase of the NPs size induces a change in the vibronic progression resulting in an enhancement of the low energy shoulder, which is indicative of increased intermolecular interactions between P3HT chains.[247] Fluorescence spectra of the NPs resemble those previously reported for P3HT thin-film (Figure 2.1A),[248] however, they are not dependent on NPs size suggesting similar emitting regions in the nanostructures regardless of their sizes. According to Spano *et al*., the modifications observed both in absorption and emission spectra support the formation of aggregates with H-type arrangement, i.e. face to face orientation of the P3HT chains.[249] Notably, the absorption and emission spectra of the pre-aggregate structure remain preserved when processed into thin films (Figure 2.1B), thus allowing the fabrication of active layers with defined/reproducible optoelectronic properties independently of the processing steps.

Table 2.1. Optical properties of P3HT-NPs in water dispersions.

P3HT	λ_{Abs}^{max} (nm)	λ_{em}^{max} (nm)	Stokes Shift (eV)	Eg (eV)	ϕf (%)
CHCl$_3$	430	577	0.73	2.33	21.8
NPs 100 nm	499	722	0.77	1.92	0.45
NPs 200 nm	516	721	0.68	1.88	0.57
NPs 400 nm	541	721	0.57	1.80	— (a)

(a) High scattering dispersion.
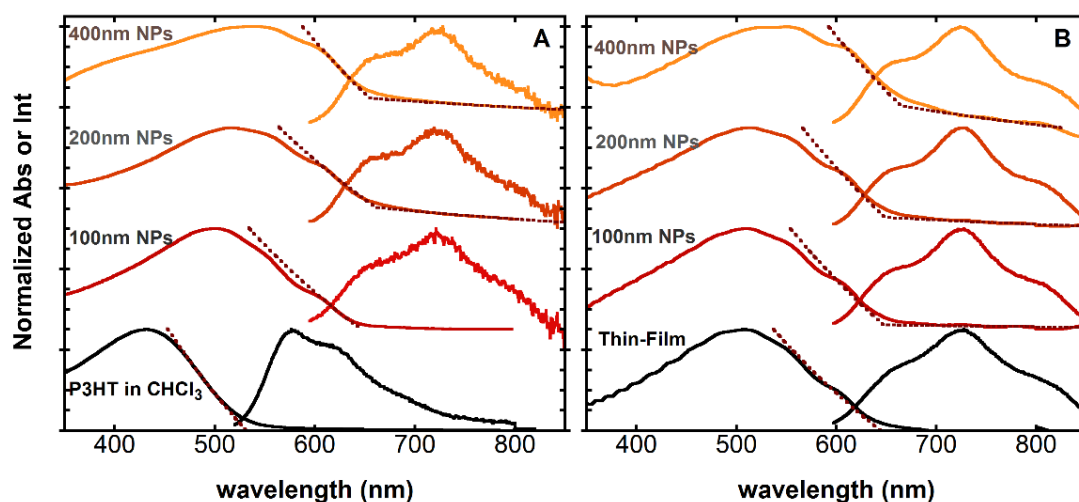
Figure 2.1. (A) Absorption and emission spectra of P3HT in chloroform solution (black) and of 100 nm (red), 200 nm (orange) and 400 nm (light orange) P3HT-NPs as water dispersions. (B) In situ absorption and emission spectra of P3HT as film in assembled ECD, where the film was prepared from P3HT chloroform solution (black); 100 nm (red), 200 nm (orange) and 400 nm (light orange) P3HT-NPs as water dispersions. Emission spectra obtained with excitation wavelength at 550 nm for all devices. Dashed lines represent linear extrapolation to obtain the polymer bandgap.

The presence of large crystalline domains in the NPs is confirmed by Grazing-Incidence Wide-Angle X-ray Scattering (GIWAXS) measurements of different sized P3HT-NPs spray-coated on silicon support.
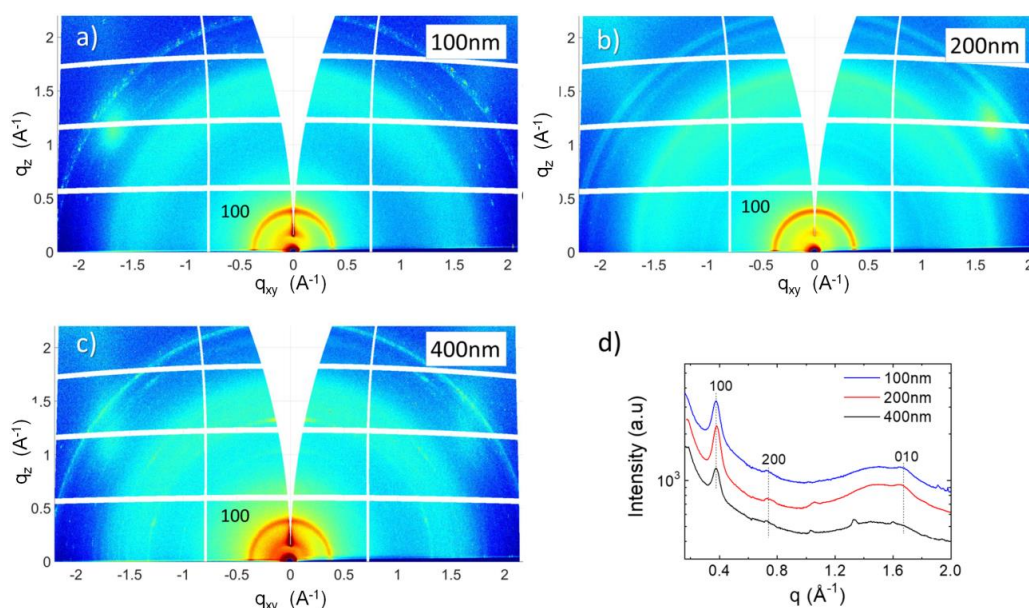
Figure 2.2. 2D-GIXRD images of different-sized P3HT NPs spray-coated on silicon support (a-c) and radially integrated intensity of the corresponding GIWAXS images (d). Credits to APE Research.

The GIWAXS technique, indeed, allows the characterization of thin films structure determining the presence or absence of crystalline structures and probing the orientation of crystalline domains. 2D-GIWAXS images, collected for NPs of 100, 200, and 400 nm size, are reported in Figure 2.2 a-c. They show several rings indicating the presence of crystalline domains randomly oriented, regardless of the NPs size. The radially integrated intensity curves, extracted from the corresponding images, point out the characteristic (100) and (010) reflections coming from the lamellar and π-π stacking (Figure 2.2d). Noteworthy, the presence of the (010) reflection confirms the presence of *H*-type aggregates, in agreement with optical measurements.

The dimension of the crystalline domains (L) has been evaluated from the (100) peak width, using the Scherrer-formula[250] and taking into account the beam footprint.[251] L slightly increases from 12 nm to 14.6 nm when NPs size increases from 100 nm to 400 nm. Moreover, a broad peak is also detectable in the range of 1.2-1.7 Å^{-1}, indicating the presence of amorphous regions too. Figure A.3.1 (see appendix) compares the specular XRD scans collected for thin film of P3HT spray-coated on silicon and for a film obtained from spray-coating P3HT NPs of 100 nm size. It highlights that the P3HT thin-film is more crystalline than the P3HT NPs film.

Several electrochromic devices were assembled using different P3HT-NPs batches. A comparison was always made with films that were cast by spray-drying from P3HT solutions in chloroform (hereafter called "*thin films*") and films cast by spray-drying from P3HT-NPs suspensions in water (hereafter called "*NPs films*"). The film's thickness were estimated by measuring the absorption spectra and calculating it from the Abs value at 550 nm using the reported value of the extinction coefficient.[252] The performance was evaluated through spectroelectrochemistry measurements and CIE L*a*b* color coordinates.[59,66,67,133,253] From the user point-of-view, the difference from using chloroform or water-based inks is enormous in terms of health safety. Special care is necessary for the depositions from organic solvents in order to ensure not breathing toxic vapors in the process, while water dispersions completely avoid organic solvent vapors, also making this process much more comfortable. This is an important requirement for future applications, especially for do-it-yourself electrochromic kits designed for users without any pre-determined skills, while using eco-friendly materials with low environmental impact.
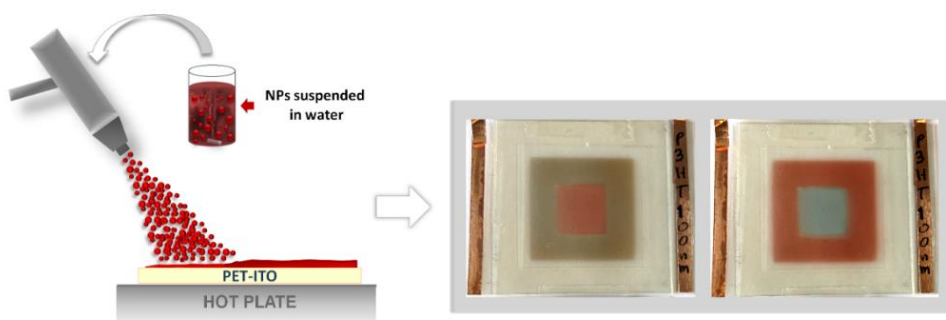
Figure 2.3. Electrochromic device with spray-coated 100 nm P3HT-NPs at different redox states. Inner square Reduced (Left) and Oxidized (Right). See video in Supporting Information.

Optical spectroscopy of the films cast from P3HT-NPs water dispersion in the ECD shows the same features as in the dispersion itself (Figure 2.1B). There are slight shifts in the absorption maxima, but with a magnitude close to experimental error (Table 2.2). The largest difference, as expected, is between P3HT in CHCl$_3$ solution and the thin-films obtained from that solution. The absorption spectra acquire vibrational structure and becomes similar to the NPs films with a bandgap of about 1.92 eV (as comparison, 1.89 eV was obtained for regioregular P3HT films[248]). Fluorescence spectra are similar in all films, with almost no shifts observed, and matching those obtained for the NPs dispersed in solution. Emitting states seem to be the same regardless of if we have NPs or films inside the ECDs. The matching of the optical properties of the NPs is also a strong indication that their shape remains after deposition and assembly of the ECD. In Table 2.2, it is also reported the oxidation onset potentials and HOMO–LUMO energy levels (see also Figure A.4.1 in appendix). In solution, the E_{HOMO} for P3HT was previously measured (-5.41 eV[254]) so the films clearly show a slight increase in the HOMO energy level and only a slight increase in the LUMO level.

Table 2.2. Optical and redox properties of P3HT materials spray-cast in PET/ITO substrates.

Sample	λ_{Abs}^{max} (nm)	λ_{em}^{max} (nm)	Stokes Shift (eV)	Eg (eV)	E^{onset}_{ox} (V) [(c)]	E_{HOMO} (eV)	E_{LUMO} (eV)
Thin-film(a)	510	731	0.74	1.92	0.53	-4.93	-3.02
100nm NPs (b)	511	731	0.73	1.91	0.50	-4.90	-3.00
200nm NPs (b)	514	731	0.72	1.90	0.50	-4.90	-2.99
400nm NPs (b)	551	727	0.54	1.86	0.52	-4.92	-3.06

(a) Deposition of P3HT from CHCl$_3$ solutions.

(b) Deposition of P3HT NPs from water dispersions.

(c) *vs*. Ag/AgCl, thin-films measured in acetonitrile solutions. The P3HT redox potentials of the thin-film matches with previous observations.[255,256]

The P3HT ECDs show color transitions between red and light blue (see pictures in Figure 2.3). All devices made from P3HT-NPs or P3HT solutions in chloroform are capable of reversible electrochromic transitions by applying -1.5/1.5 V, with general properties resembling those previously reported for P3HT when deposited via other methods (such as electropolymerization). Here, however, the deposition is *via* a facile and safe method which in the future may be validated for, *e.g.,* ink-jet printing.
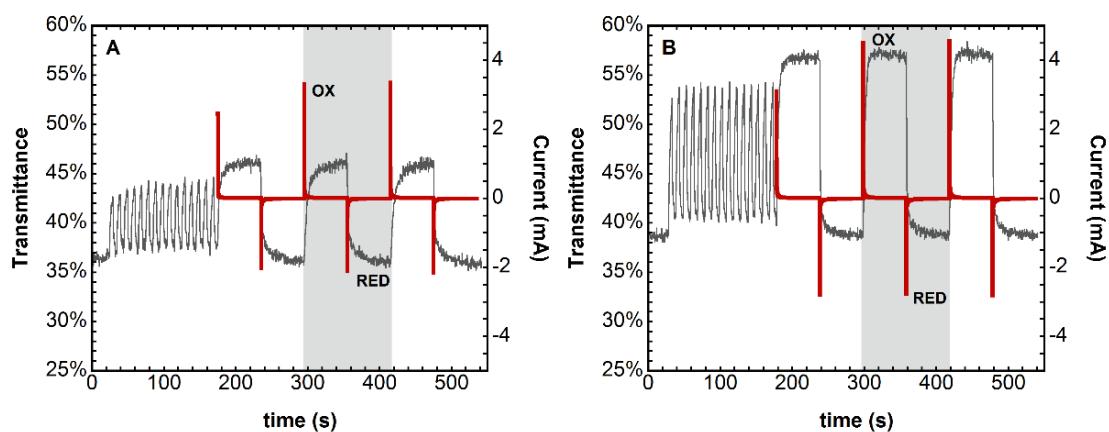
Figure 2.4. (A, B) Transmittance (black) and current (red) data obtained from the characterization of the device using P3HT as thin-film and NPs of 100 nm, respectively.

Absorption and electric current measurements were performed for all assembled devices. Figure 2.4 shows an experimental example, where the shadowed region is the selected data for further analysis (calculations of switching times and coloration efficiency).

Spectroelectrochemistry reveals that upon oxidation bands in the Near Infra-Red appear (NIR, Figure 2.5) which are assigned to the presence of polarons as described by Patil *et al.*[69] This is synchronized with the decrease of intensity of the π,π^* transition in the visible region for voltages above 0 V. The insertion of positive holes leads to polaronic states that evolve with the positive doping. Bands *circa* 750 nm appear and gradually become predominant with some blue shift for higher voltages. These features were observed in all devices, regardless of the NPs size or if P3HT was spray-cast from chloroform solutions.
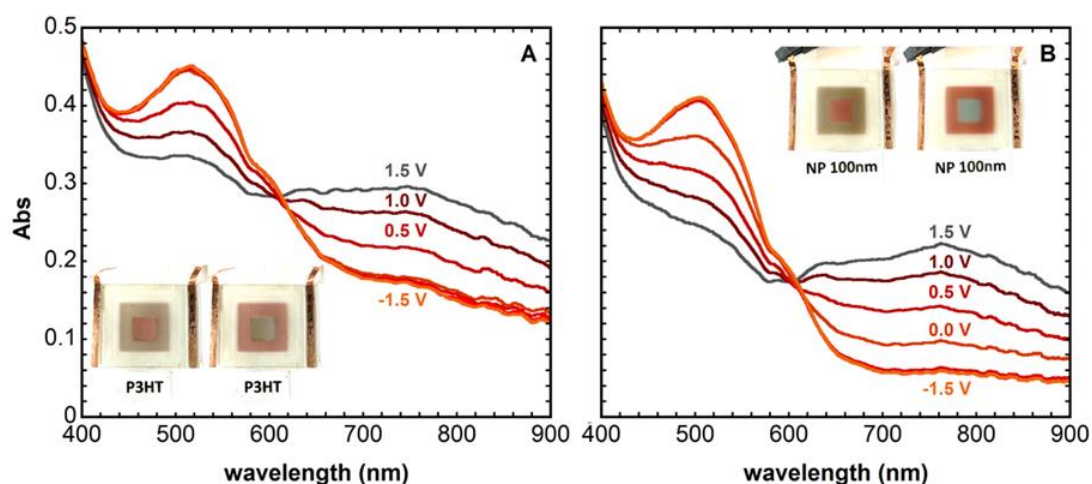
Figure 2.5. (A, B) Spectroelectrochemistry measurement performed on the device using P3HT as thin-film spray-coated from chloroform and as NPs of 100 nm, respectively. Both experiments were per-formed using 1.5, 1, 0.5, 0, -0.5, -1 and -1.5V with 1 min stabilization of the device at each potential before spectral acquisition.

Switching cycles show sharp electrochromic transitions for all devices as recorded by changes in the absorption spectra. Figures of merit were calculated (as described in section 1.5.7) from all experimental data to evaluate ECD performance (Figure 2.6 and Table 2.3).[233]

Table 2.3. Transmittance (T_{Red}, T_{Ox}), optical contrast ($\Delta T/T_{Ox}$), charge consumption (Q_{Red}, Q_{Ox}), switching time (t_{90}^{Red}, t_{90}^{Ox}) and coloration efficiency (**CE**) values calculated for the Thin-film and 100 nm NPs de-vices as prepared and after 1000 cycles using -1.5V.

ECD	$T_{Red}^{(a)}$ (%)	$T_{Ox}^{(a)}$ (%)	$\Delta E^{*\,(b)}$	Q_{Red} (mC)	Q_{Ox} (mC)	t_{90}^{Red} (s)	t_{90}^{Ox} (s)	$CE^{(a)}$ (C^{-1}.cm^2)
As prepared								
Thin-film	36.3±0.1	46.6±0.2	12.0±0.7	-0.76±0.02	0.87±0.03	13.4±0.9	11.4±3.1	124±3
100nm NPs	38.7±0.1	57.8±0.1	17.9±0.3	-0.81±0.02	1.18±0.01	4.4±0.6	6.0±0.2	180±2
After 1000 cycles								
Thin-film	33.2±0.4	49.3±1.2	17.0±1.0	-0.82±0.03	0.94±0.03	9.2±1.0	9.7±1.4	162±3
100nm NPs	33.6±1.5	67.3±2.0	25.7±0.6	-1.35±0.04	1.41±0.03	3.8±0.4	4.2±0.3	161±3

(a) λabs=510 nm

(b) Color contrast between oxidized ("uncolored") and reduced ("colored") states.

These values were obtained for a specific wavelength that, in this case, the chosen wavelength is 510 nm where optical contrast is stronger for P3HT. The t_{90} is calculated using the method recently described by Hassab et al[239] and the CE is calculated at t_{90}^{Red} as $\Delta Abs/Q$ at that specific time. All values on Table 2.3 are averages of the 3 cycles (see Figure 2.4) and the errors are one standard deviation.
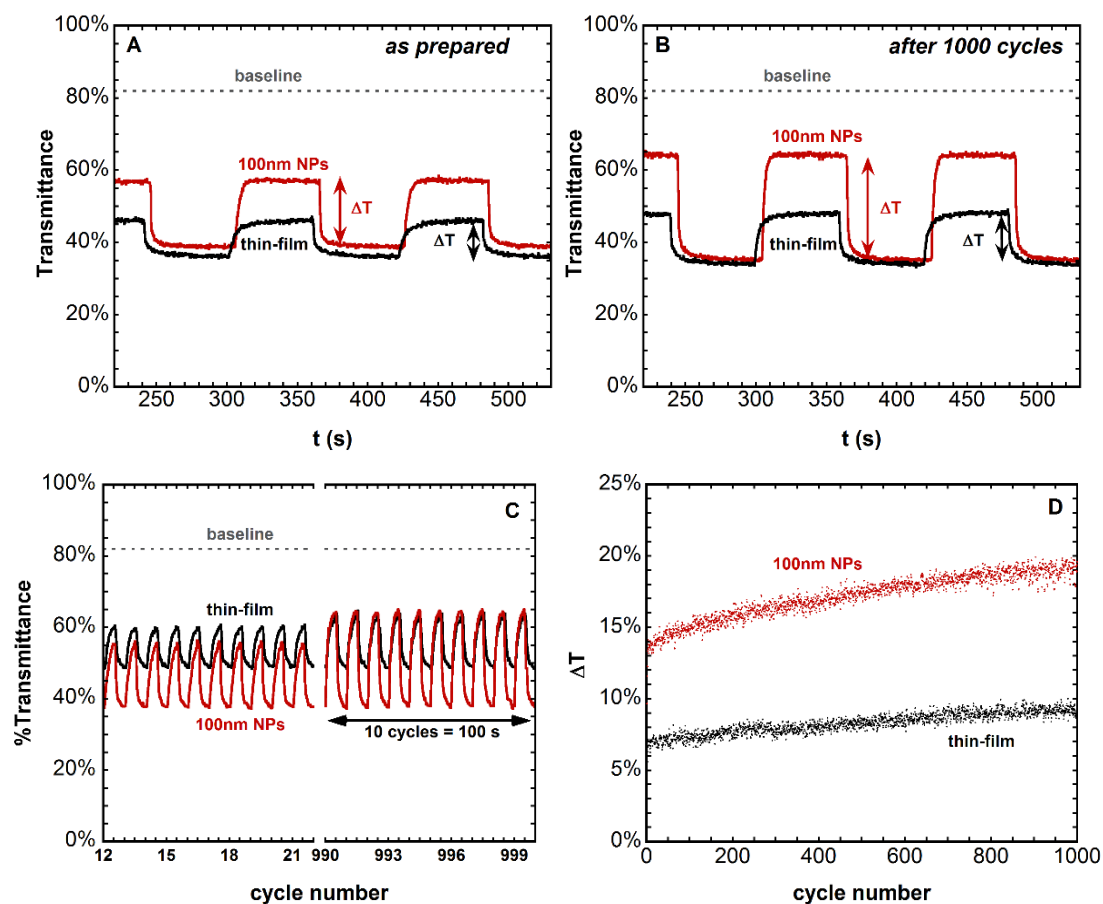
Figure 2.6. (A, B) Comparison, in transmittance of the devices using P3HT thin-film and P3HT-NPs (100 nm), as prepared and after 1000 cycles, respectively. (C) Changes in transmittance of P3HT thin-film and P3HT 100 nm NPs devices during the cycling measurement and (D) Optical contrast evolution (in ΔT) of the P3HT thin-film and P3HT 100 nm NPs devices during the 1000 cycles performed. In all measurements, 1.5V was used for Oxidation and -1.5V was used for reduction (1cycle=10s).

For the freshly prepared devices, CE values are higher for the device prepared with P3HT-NPs of 100 nm. P3HT thin-films cast from chloroform solution show a normal value for P3HT (about 124±3 $C^{-1}cm^2$) but the P3HT films from water-dispersions of 100 nm NPs it is much higher (180±2 $C^{-1}cm^2$). As a comparison, the best reported value is 293.5 cm^2C^{-1} using glass/ITO as substrate in a liquid state electrochemical cell.[244] In this case, it is a completely sealed solid-

state device without any annealing using PET/ITO as substrate (which has poor optical properties compared with glass/ITO).

Switching times and optical contrast are even more striking, a reduction switching of 4.4±0.6 s is reached. In the thin-film this value is much higher (13.4±0.9 s), indicating hindered kinetics for the thin-films. A full oxidation state is not reached in the thin-films, where the π,π^* band is still intense at -1.5 V (see Figure 2.4 and Figure 2.5). Therefore, the use of NPs facilitates a full oxidation of P3HT reducing the intensity of the π,π^* band. This is crucial to obtain a higher color contrast and better switching times.

Durability tests were performed by measuring absorption changes upon 10 s oxidation/reduction cycles (1.5/-1.5V) for 1000 cycles where 1cycle = 10 seconds. At that stage, the performance of the devices was measured again. Durability depends on several factors, such as the substrate used, the electrolyte and deposition method. A direct comparison with literature is not easy because of the number of variables that are in play, but for P3HT electrochromism values of about 1000 cycles are reported.[245] In the present case no degradation was observed after 1000 cycles for both samples (Figure 2.5A), in fact, an increase of ΔAbs appears. This points out to an electrochemical annealing of the films, where conformational changes give rise to better performances.

After 1000 cycles, the figures of merit were again calculated. The conclusions are the same, since the device with 100 nm NPs has a much better performance in terms of optical contrast (reaching almost 50%) and 4s switching times (Table 2.3). The thin-film also performs better, but still does not reach these values. CE at this stage is, interestingly, the same within experimental error.

Additionally, the durability of different sized P3HT-NPs was tested in electrochromic devices, 100 nm, 200 nm, and 400 nm in order to compare with P3HT spray-coated from chloroform solutions. In Figure 2.7 are presented the cycling measurements (in L*a*b* coordinates), showing a trend in which larger sized P3HT-NPs present lower durability. 400 nm P3HT-NPs have a strong decay, when the ECD stopped working around 3000 cycles, 200 nm nanoparticles present cyclability very similar to the thin-film ECDs prepared while the 100 nm NPs device presented longer durability with very poor electrochromic activity only around 15000 cycles. This result is very promising in terms of durability when P3HT is transformed in lower sized NPs. Thus, durabilities over 10000 cycles are presented that, for optoelectronic applications is very interesting, comparing with previous durability tests made with the same polymer.[245]
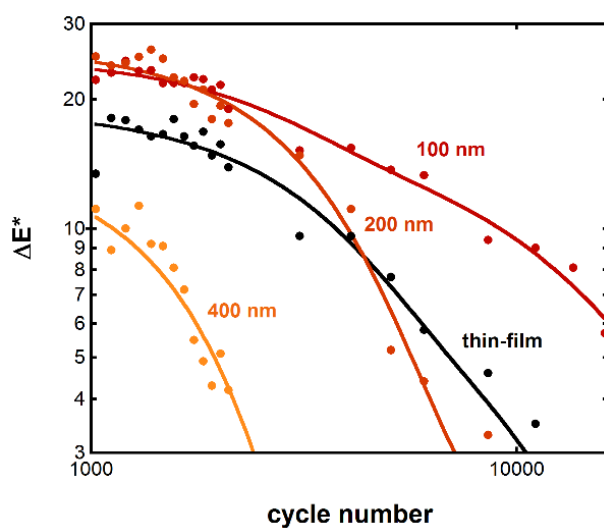
Figure 2.7. Durability measurements performed in ECDs using P3HT thin-film, and different sized NPs (100 nm, 200 nm and 400 nm). The results are presented in L*a*b* coordinates calculated using a ColorChecker® as reference.

2.2 Conclusions

Using standard procedures currently employed in industrial applications ECD prototypes were developed from water dispersions of a classic polythiophene (P3HT), an approach that may be extended to different polythiophenes. Our approach offers very important advantages:

i) Avoiding toxic organic solvents, such as chloroform during the deposition of the electrochromic layer, ensuring the health safety of the user and reducing the environmental impact. This is particularly important for Do-It-Yourself kits,[257] in which anyone will be able to fabricate an electrochromic device at home.

ii) Observing enhanced performances with NPs ECDs. This enhancement confers faster switching times and shows a clear trend on higher durability. This is an extra and welcomed feature, which is crucial for industrial applications.

PEDOT formulations with PSS as water suspensions developed by Bayer in the later 1990's enabled their application in commercial products in the field of printed-electrochromics.[73] It is believed that this approach will trigger a new progress in the industry by allowing a strong dissemination among designers and artists[3,258–261] with the appearance of new-colors otherwise difficult to reach with metal oxides. Metal oxides are still the best option for smart windows and outdoors, but polymers allow a wider range of deposition techniques and color palette. Very beautiful colors were created in the last 20 years by researchers such as Reynold's group,[8,10,73,114,116,121–123] but processability and stability was always an issue towards their

commercialization. This new approach should finally give a boost for electrochromic applications, definitely putting it in the roadmap of the internet-of-things that will develop in the incoming years.
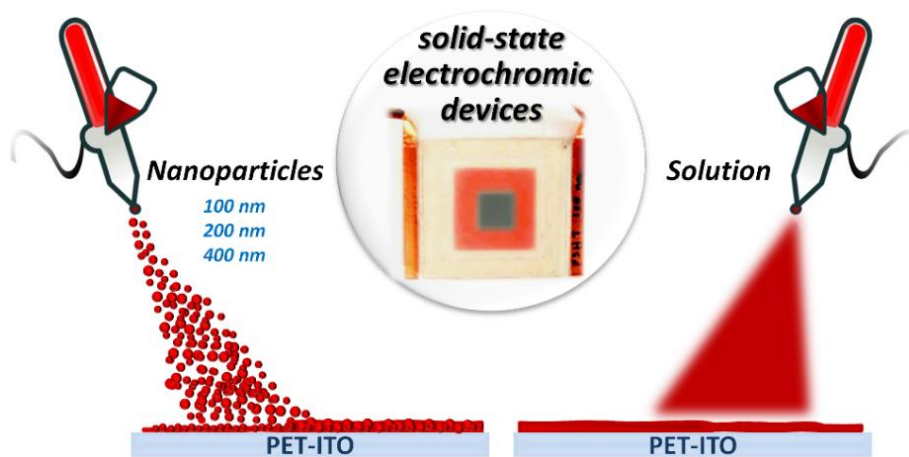
Figure 2.8. Graphical abstract from the published paper in *ACS Appl. Polym. Mater.*
(2020), **2**, 8, 3301-3309.

2.3 Experimental Section

2.3.1 Synthesis of P3HT
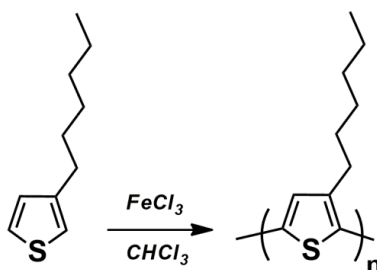
Scheme 2.1. Synthesis of P3HT.

Poly(3-hexylthiophene-2,5-diyl), P3HT, was synthesized by oxidative polymerization, as already reported.[143]

The excess of iron (III) ion in the polymers was completely removed by washing with 2% aq. HCl solution until negative essay with NH4SCN. The resulting polymer was further purified by removing the shorter fractions soluble in methanol and acetone. Yield 50%. Dark red solid. Mn= 25800 gmol^{-1}, MW= 48000 gmol^{-1}, PDI = 1.87. ^{1}H NMR (400 MHz, CDCl$_3$, TMS/ppm): δ 7.02 (s), 7.00 (s), 6.98 (s), 6.95 (s), 2.82-2.73 (m), 2.58-2.48 (m), 1.72-1.50 (m), 1.44-1.20 (m), 0.91-0.81 (m) (see figure A.1.1 in appendix).

2.3.2 Synthesis of P3HT-NPs

Colloidal solutions of P3HT nanoparticles P3HT-NPs have already been described.[131,134] To avoid the presence of any surfactant, P3HT NPs are prepared by the reprecipitation method[138], using a small portion of P3HT dissolved in pure THF which was added dropwise to miliQ water under vigorous stirring (see Scheme 2.2).
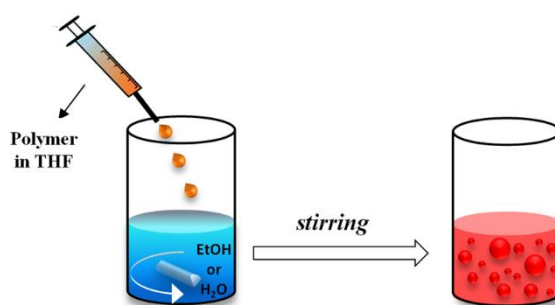
Scheme 2.2. Scheme of nanoparticles formation by nanoprecipitation method.

The size of the final NPs was selected by differential centrifugation[138]. Dynamic Light Scattering (DLS) was performed in order to characterize the size of the NPs (see table A.2.1 in appendix).

The P3HT polymer as well as the corresponding NPs were deposited on the PET-ITO electrodes by the spray-casting method. The PET-ITO substrates were placed over a heating plate at 60 °C (P3HT polymer dissolved in $CHCl_3$) or 90 °C (P3HT-NPs dispersed in miliQ water). The P3HT formulations were then spray-casted on the electrodes and dried in the heating plate for 1 minute between each layer. The P3HT printed solutions had a 5mg/ml concentration, in chloroform, while the NPs dispersion concentration varied depending on their size (1mg/7ml to 5mg/7ml, in miliQ water). Grazing Incidence X-ray Diffraction measurements (GIXRD) were performed on P3HT NPs deposited on silicon wafer. The 2D-GIXRD images were recorded at the XRD1 beamline at the Elettra synchrotron facility at Trieste (Italy) using a monochromatic beam with a wavelength of 1 Å. The incident angle of the X-ray beam, α_i, was chosen 0.15°, in order to probe the crystal structure of the whole sample. The scattering patterns were recorded using a 2D camera (Pilatus detector) placed normal to the incident beam direction.

The produced ECDs were assembled using the following structure: PET-ITO / Polymer or NPs / Electrolyte / Polymer or NPs / ITO-PET. The assembly of these ECDs was performed by producing the two substrates of PET-ITO with the material deposited and then closing them together face-to-face using a double-taped adhesive in order to avoid short-circuits between the two PET-ITO substrates. The electrolyte was deposited by hand filling the "pool" using the amount calculated accordingly to the volume needed to fill the final ECD. The electrolyte used was an Li+ based UV curable electrolyte denominated *Ynv.El.®* property of *Ynvisible®* with the patent nº 20140361211. The absorption spectra of the ECD's (at different potentials) were run in a Cary 5000 UV-Vis-NIR spectrophotometer coupled to an Autolab PGSTAT 100N potentiostat. The range of potentials used varied from -1.5V for reduction and 1.5V for oxidation. Switching time measurement involves a pre-treatment of 15 cycles with 5 seconds at each potential, followed by 3 cycles with 60 seconds for oxidation and reduction while the charge consumed by the ECD's was calculated from the current (in Amperes) developed during the switching time of the experiment. The consumed charge is used to calculate the coloration efficiency (CE) according to the change of color (in absorbance) using the CE equation.[55] The cycling experiments of the devices were made in a cycling box. Attached to this cycling box is a function generator to apply the desired potential, -1.5V / 1.5V in a squared function.

The L*a*b* coordinates are generated by MATLAB functions created by the company *Ydreams®* from conversion of RGB coordinates using a *ColorChecker®*, as reference.

<div style="text-align: right">

3

</div>

Processable Thiophene-based Polymers with Tailored Electronic Properties and their Application In Solid-State Electrochromic devices using Nanoparticle Films

This chapter is based on the published paper "Moreira, T. *et al.*, Processable Thiophene-Based Polymers with Tailored Electronic Properties and their Application in Solid-State Electrochromic Devices using Nanoparticle Films, *Adv. Electron. Mater.* (2021),**7**, 2100166".

The author contributed to the planning and was the main responsible on the execution of all the experiments presented in this paper, including synthesis, optical and structural characterization of the materials (except for DFT calculations performed at the Institute of Microelectronics and Microsystems in Lecce, Italy), assembly of solid-state electrochromic displays and their characterization. The author was also the main responsible for the interpretation and discussion of all the results, and contributed to the preparation of the manuscript.

It is well known that conjugated thiophene-based oligomers and polymers are among the most investigated organic materials for application in organic electronics, in particular in a variety of devices including field-effect transistors (FETs), light-emitting diodes (LEDs), photovoltaic cells (PVDs) and, to a lesser extent, electrochromic devices (ECDs).[262–265] Over the last few years, much progress has been made in device optimization and many studies have been devoted to the attempt of elucidating the relationship between molecular structure, solid-state organization, and device performance. Nevertheless, there is still a great demand to address key points to solve the problems that should make the devices ready for the market. Among them, the engineering of molecular structures capable to spontaneously achieve the desired solid-state aggregation leading to the optimum device.[266]

Electrochromic materials and devices are currently investigated for smart windows, mirrors, eyewear and for other numerous applications such as electronic paper, displays, camouflage, wearable devices where a switchable color change with high optical contrast and low operating external voltage is required.[267–269] Several classes of materials have been analyzed: from transition metal oxides[270] to small organic molecules[271] and conjugated polymers,[272,273] metal-organic complexes,[274] electrochromic gels,[275–277] and plasmonic materials[274]. Among conjugated polymers, thiophene-based materials (TMs) have emerged as one of the most promising classes of organic electrochromic materials.[96,225,278] A key advantage of TMs stems from the wide possibility of controlling their structure and manipulating their morphology, which allows modifying *ad hoc* their chemical-physical properties, resulting in a fine-tuning of polymer's bandgap and color.[12,224,254,279–284] Although most works reported in the literature focus on the effects of structural changes on the electrochromic properties of materials, less attention has been paid to describing the effect of their nanostructuration in solid-state EC devices. In this respect, it has been recently reported that the use of films obtained from water-suspended colloidal NPs of poly(3-hexyxlthiophene-2,5-diyl) (P3HT) deposited onto flexible polyethylene terephthalate – indium tin oxide (PET-ITO) electrodes via spray-casting, allows the fabrication of devices with improved properties compared to those obtained using cast films from organic solvents such as chloroform.[131,285] Furthermore, this methodology avoids toxic organic solvents during the deposition of the electrochromic layer, which is a remarkable advantage for users and the environment.

With the aim of expanding the toolbox of thiophene based electrochromic materials, a new class of polymers was developed coupling a simple structure, facile synthesis, tunable electrochromic properties, and nanostructuration ability that is expected to enhance the

organic material's response and improve its switching dynamics.[131,285,286] The synthesis was planned in order to be easy, flexible, and scalable. The tuning of the optoelectronic properties is achieved by introducing alkyl or alkoxy substituents in the thiophene moiety and/or by the presence of either –CH=CH– or –CH₂–CH₂– linkers connecting the repeat units and acting as conjugation modulators. Density functional theory (DFT) and T-DFT calculations were employed to elucidate the relationship between changes in single structural elements and changes in polymer electrochromic properties. The calculations account for changes in conformation, π-delocalization following minor structural changes, and, more importantly, charge redistribution occurring upon removal of one electron (oxidation). All polymers, which are processable in common organic solvents, can be easily obtained as stable suspensions of NPs in water by using the reprecipitation method.[20,286] Our results demonstrate that these engineered nanostructures can be employed as active elements in flexible solid-state ECDs. Indeed, it is shown that the use of NPs films spray-coated from water dispersions instead of cast films from chloroform solutions leads to the enhancement of the final ECDs performance in terms of switching time (ST), charge consumption (Q), optical contrast (ΔT) and improved durability (Cycling).

3.1 Results and Discussion

The molecular structures of the newly synthesized polymers described in this study are shown in Scheme 3.1.
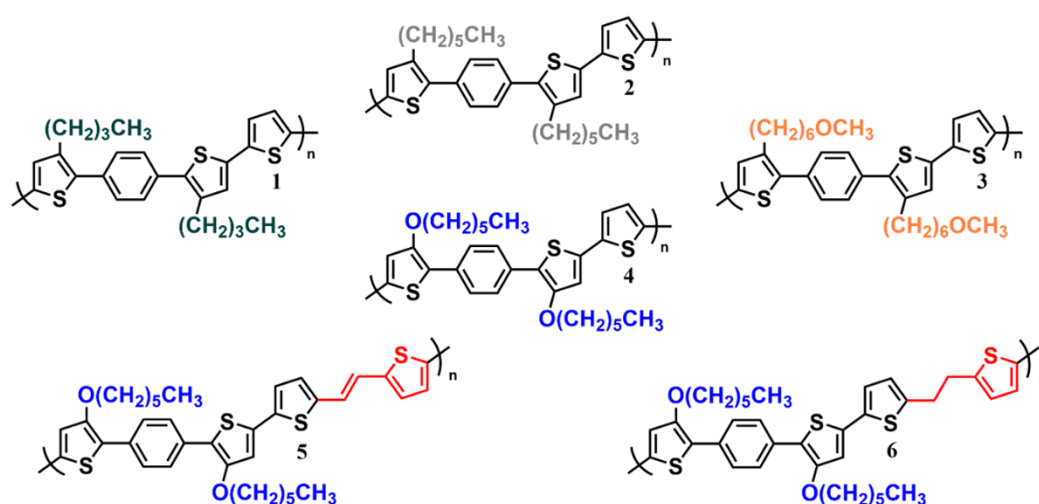
Scheme 3.1. Molecular structure of the polymers discussed in this study. In black, the repeated unit common to all compounds.

All polymers have the repeat unit made of the same π-conjugated thienyl-phenyl-thienyl-thienyl fragment (Th-Ph-Th-Th, see Scheme 3.1) with two *β*-alkyl/alkoxy substituents in thiophenes next to phenyl and the presence of one linker, either –CH=CH–Th or –CH₂–CH₂–Th, connecting the different units. Thiophene substituents are expected to hinder the rotation around the C-C bond connecting phenyl with thiophenes thus preventing the planarization of the repeat units on passing from solution to the solid-state. The linkers and the presence of an alkoxy chain with oxygen directly bound to thiophene (**5-6**) or at the end of the alkyl chain (**3**) are expected to act as conjugation modulators.
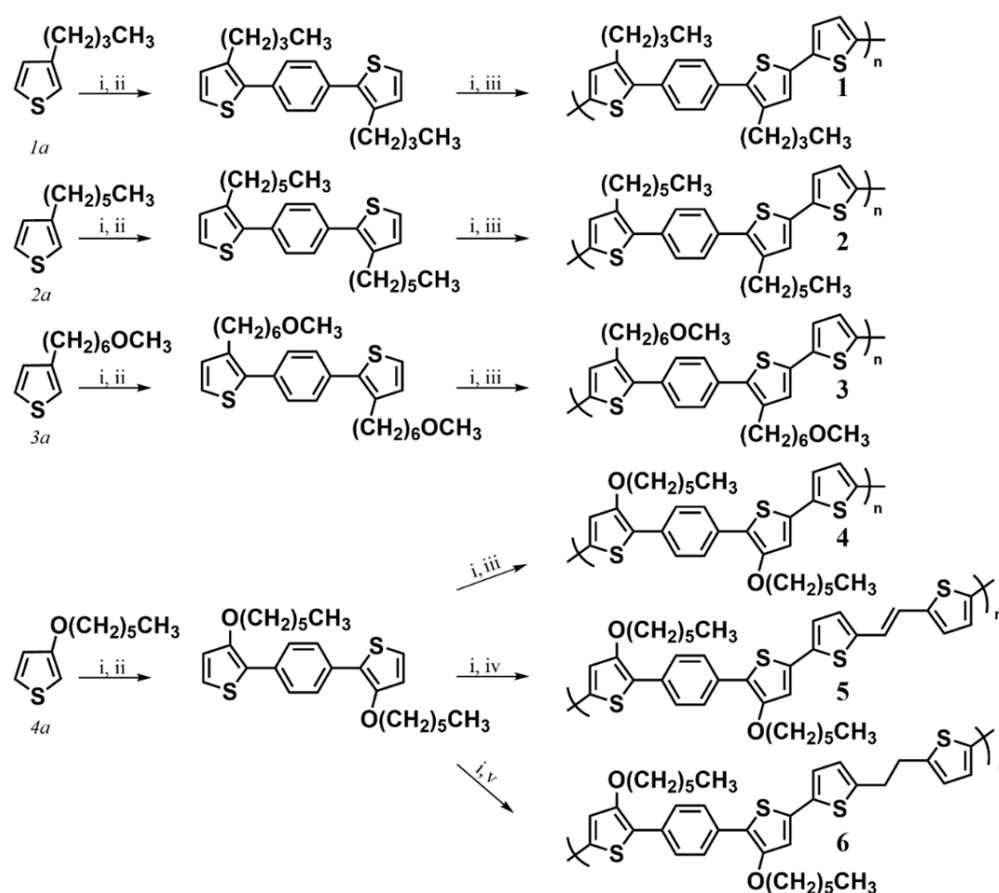
Scheme 3.2. Synthetic pattern for the synthesis of polymers 1-6. *i)* NBS, CH2Cl2, 25°C; *ii)* 1,4-benzenediboronic acid dipinacol ester, NaHCO₃, Pd(dppf)Cl2, THF/H2O, 80°C, MW; *iii)* 2,5-bis(tributylstannyl)thiophene, Pd(PPh3)4, toluene, 110°C; *iv)* 1,2-bis(5-(trimethylstannyl)thiophen-2-yl)ethene, Pd(PPh₃)₄, toluene, 110°C. *v)* 1,2-bis(5-(trimethylstannyl)thiophen-2-yl)ethane, Pd(PPh₃)₄, toluene, 110°C.

3.1.1 Synthesis of Polymers

The synthesis was developed in two steps (see Scheme 3.2). Firstly, a series of polythiophenes – **1**-**3** and **4** – were synthesized with the same aromatic backbone and assessed the effect of alkyl/alkoxy thiophene substituents on their optical properties. Secondly, polymers **5** and **6**, were synthesized where the aromatic backbone with the $–OC_6H_{13}$ substituent was modified by further addition of $–CH_2–CH_2–Th–$ or $–CH=CH–Th–$ linkers. The polythiophenes were synthesized through sequential bromination / stannylation / Stille or Suzuki coupling steps exploiting ultrasound assistance for all bromination steps and microwave assistance for Stille and Suzuki couplings.[287,288]

3.1.2 Optical and Redox Properties of Polymers 1-6

Figure 3.1 shows the absorption and emission spectra of the polymers in chloroform solutions while Table 3.1 displays the corresponding maximum wavelengths together with fluorescence quantum yields calculated using the comparative method, as described in the experimental section.
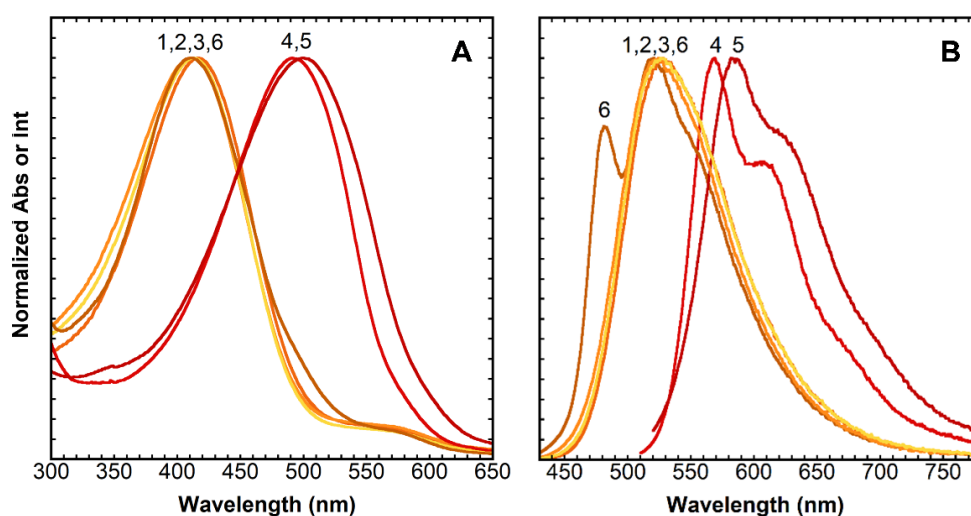
Figure 3.1. Absorption (A) and emission (B) spectra of the synthesized polymers in chloroform solution. Emission spectra were obtained using as excitation wavelength the maximum of absorbance for all polymers.

Table 3.1. Optical properties of the newly synthesized polymers in chloroform.

Polymer	λ_{abs} (nm)	λ_{em} (nm)	Stokes Shift (eV)	E_g (eV)	ϕ_f (%)
1	417	528	0.62	2.49	35.4
2	410	524	0.65	2.52	21.0
3	413	526	0.64	2.52	10.5
4	491	569	0.35	2.16	27.9
5	499	582	0.35	2.06	12.2
6	411	521	0.64	2.46	9.20

The unstructured absorption bands of the UV-Vis spectra of Figure 3.1– that in thiophene-based compounds are generally related to π-π* transitions[289] – are separated in two groups: one pertaining to polymers **1**-**3** and **6** (417, 413, 410, and 411 nm, respectively) and the second pertaining to polymers **4** and **5** (491 and 499 nm, respectively). The large red shift in absorbance of the second group of polymers compared to the first one is caused by the presence of the $-OC_6H_{13}$ substituents with the oxygen atoms directly attached to the thiophene ring and exerting an electron-releasing mesomeric effect. Therefore, of the six polymers reported, four have a rather high energy gap (in the range 2.46-2.52 eV), typical of yellow-orange electrochromic polymers, and two have a smaller energy gap (in the range 2.06-2.16 eV) typical of red electrochromic systems (see figure B.3.1 in appendix).[77] It is worth noting that polymers **5** and **6** have the same chemical structure except for the presence of the unsaturated –CH=CH– linker between repeat units in the former and the saturated $-CH_2-CH_2-$ group in the latter. Owing to the saturated linker, in **6** the conjugation between the repeat units is completely broken and in consequence, the polymer has optical properties similar to those of yellow electrochromic polymers with the advantage of having a lower oxidation potential due to the presence of $-OC_6H_{13}$ substituents.[290] On the contrary, in **5** there is no conjugation breaking and the polymer belongs to the group of red electrochromic polymers. As is generally the case for thiophene oligomers and polymers, all polymers are characterized by large Stokes shifts indicative of the transition from a distorted ground state to a planar excited state.[10] All polymers also display quite sizeable fluorescence quantum yields, from the lowest value (9.2%) of **6** to the highest (35.4%) of **1**. The newly synthesized polymers were spray-casted from chloroform solutions on PET-ITO substrates in order to characterize the different colors obtained in the solid state (see Figure B.2.1 for the L*a*b* coordinates for reduced and oxidized states) and their electronic properties.

The redox properties of the polymers were studied by cyclic voltammetry (CV) performed using Ag/AgCl as the reference electrode, a platinum wire as the counter electrode, working electrode the PET-ITO substrate with the material deposited on top, and an electrolytic solution of $LiClO_4$ (0.1M) in acetonitrile. Figure 3.2 shows the voltammograms of compounds **1**-**6** deposited on PET-ITO and the switching color of the films from yellow/red to blue/gray passing from the neutral and oxidized state, respectively (See insets on Figure 3.2). The optical bandgap of the polymers were calculated from spectroelectrochemistry measurements (Figure 3.4C; Figure B.9.1, in appendix) and the voltammograms in Figure 3.2, respectively. Furthermore, according to the method described by Cardona *et al.*,[291] from cyclic voltammetry measurements and optical spectroscopy data of the films deposited on PET-ITO, was possible to calculate the HOMO and LUMO levels of the polymers (Table 3.2; Figure B.3.1, in appendix). For comparison, the table also reports the DFT calculated HOMO values for the model dimers of polymers **2**-**6**, which are in very good agreement with those obtained from CV data. The HOMO energy of polymers **1** and **2** is 5.3 eV, the lowest observed for the investigated materials, in agreement with their oxidation potentials which are the highest observed. In polymer **3** the HOMO energy reaches -5 eV, this can be ascribed to the inductive effect of the oxygen atoms linked at the end of the alkyl side chains. On the other hand, in polymers **4**-**6**, where the oxygen atoms are directly linked to the thiophene backbone, a further increase of the HOMO energy is observed (-4.9 eV). This is probably due to the additional mesomeric effect of the oxygen lone pairs, in clear agreement with the electronic distribution observed in DFT calculations (Figure 3.3). Furthermore, as reported in Table 3.2, polymer **6** shows a higher energy gap with respect to polymers **4** and **5**, which is related to an increase of the LUMO energy (from -3 eV to -2.8 eV) reflecting a decreased conjugation caused by the $-CH_2-CH_2-$ moiety.
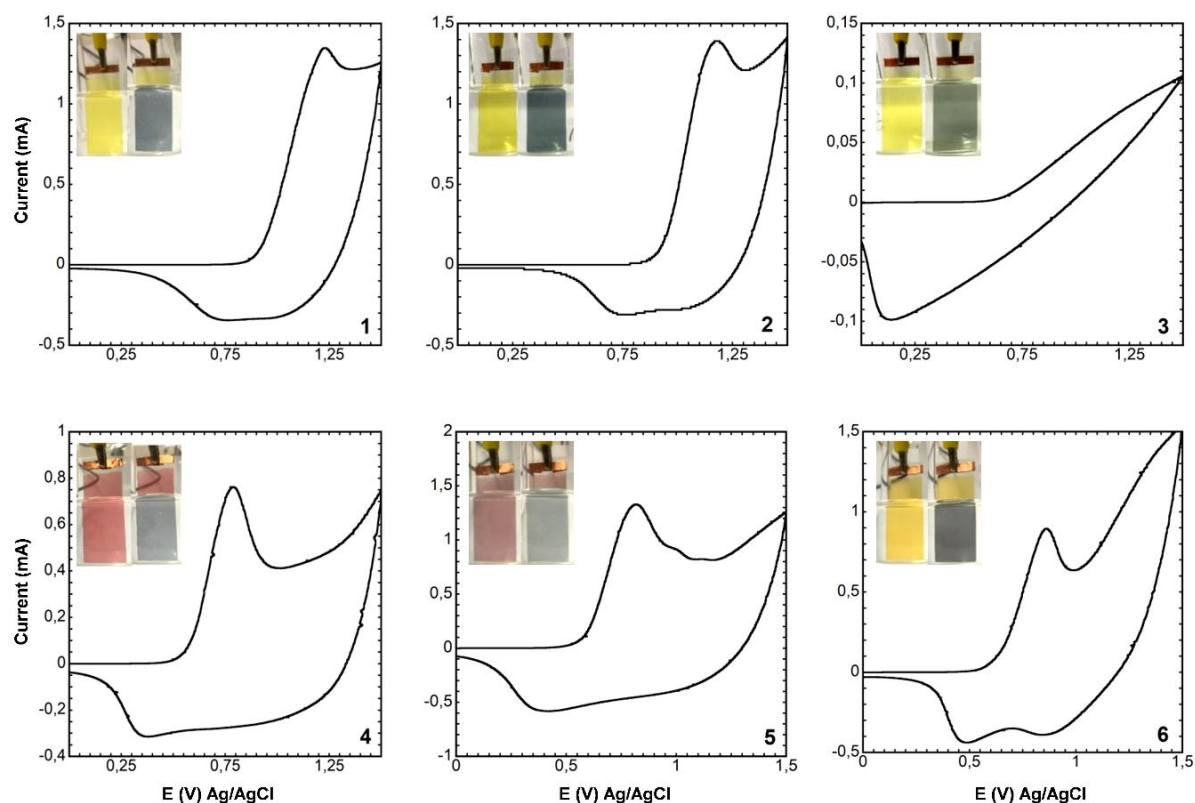
Figure 3.2. Cyclic voltammograms of polymers 1-3 and 4-6 deposited on PET-ITO from chloroform solutions and used as the working electrode. The yellow and red colorations were obtained at 0V while the blue/grey colorations were obtained on the peak of the oxidation process (See photos on the inset of the figures) using a scan rate of 20mV/s. An Ag/AgCl electrode was used as the reference, a platinum wire as counter-electrode, and an electrolytic solution of LiClO$_4$ (0.1M) in ACN.

Table 3.2. Optical and redox properties of the polymers spray casted in PET/ITO substrates.

Polymer [a]	λ_{abs}^{max} (nm)	λ_{em}^{max} (nm)	Stokes Shift (eV)	E_g (eV)	E^{onset}_{ox} (V) [a]	E_{HOMO} (eV)	E_{HOMO} (eV) [c]	E_{LUMO} (eV)
1	412	575	0.85	2.30	0.92	-5.32	—	-3.02
2	422	563	0.74	2.35	0.92	-5.32	-5.47	-2.97
3	421	535	0.63	2.36	0.65	-5.05	-5.24	-2.69
4	512	(b)	—	2.00	0.57	-4.97	-4.96	-2.97
5	501	(b)	—	1.90	0.59	-4.99	-4.91	-3.09
6	406	482	0.48	2.18	0.63	-5.03	-5.04	-2.85

(a) *vs.* Ag/AgCl, thin films measured using LiClO$_4$ (0.1M) in an ACN electrolytic solution.

(b) Non-emissive in the solid-state.

(c) Theoretical DFT values obtained from neutral-oxidized total energy differences.

3.1.3 DFT Calculations

Several model structures have been studied at the DFT and TD-DFT level of theory to investigate the charge distribution in the polymers, especially upon oxidation, and the nature of excitations. The calculations were carried out on dimers of the repeat units as models for polymers **1-6**, with the objective, in particular, of evaluating the effect of the oxygenated substituents and of the groups linking the different repeat units on the electronic structure. Figure B.4.1 shows the geometry optimization of the model structures in the neutral and oxidized states. The figure reveals that in the neutral (reduced) ground state the polymers with the oxygen directly linked to the thiophene ring (**4-6**) display a moderate torsion along the molecular backbone due to steric interaction of different units. This torsion is less prominent in the oxidized ground state because the oxidation reduces the charge on the more electronegative atoms, thus reducing steric repulsion. For a similar reason, removing the oxygen atom from the side chain, as in the case of polymer 1-2, or moving it to the terminal position, as for polymer 3, causes an increased distortion of the molecule, especially in the terminal rings.

The density distribution in the various systems can be deduced by inspecting the electrostatic potential of each molecule, as reported in Figure 3.3. In polymers **4-6**, in the neutral ground state the charge is quite uniform along the molecular backbone due to π-conjugation. However, a small excess of electrons (red areas) is observed in correspondence with the Th-Ph-Th moieties; this is due to the oxygen atoms attracting electrons from the side alkyl chains (blue areas) and share them with the aromatic moieties. As shown, this effect is rather independent of the type of linker considered (–CH$_2$–CH$_2$–, –CH=CH–). On the other hand, in polymers **1-3**, the absence of electronegative oxygen atoms in direct conjugation with the thiophene unit partially hinders the transfer of electrons from the alkyl side chains to the Th-Ph-Th backbone thus reducing the excess of electrons.
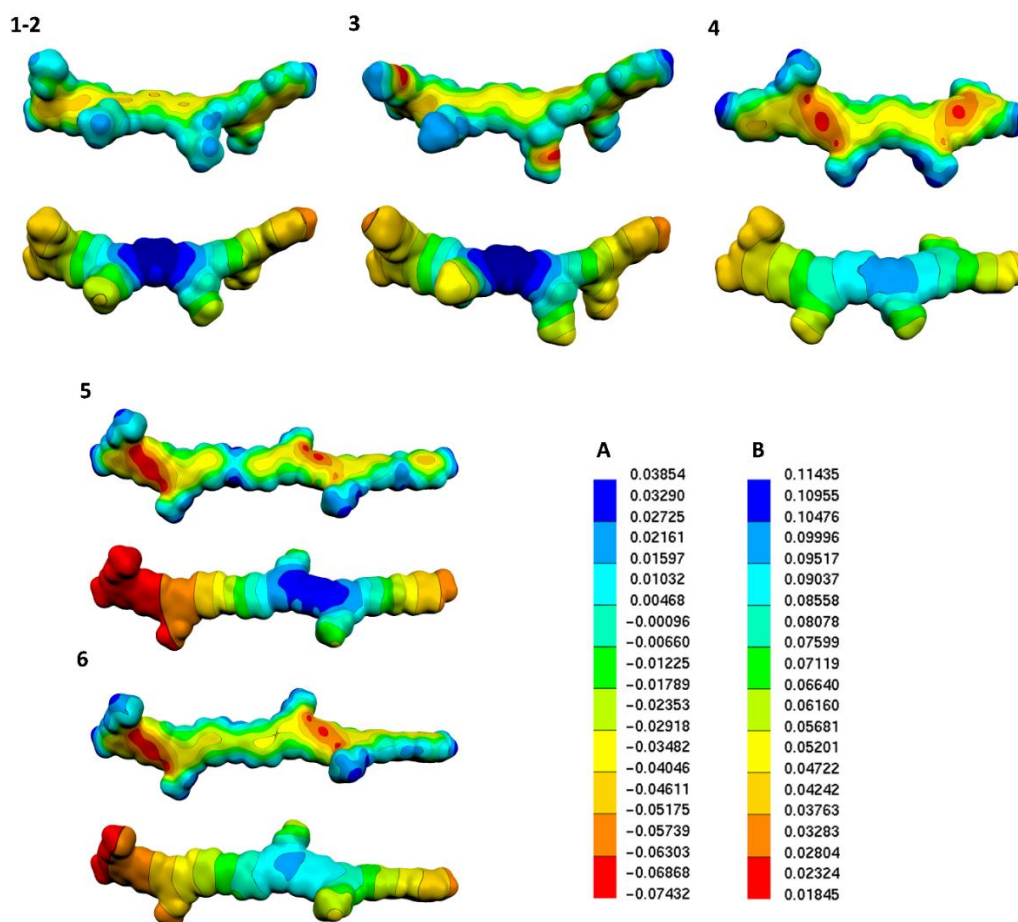
Figure 3.3. From top to bottom: structure, electrostatic potential in the neutral state, and oxidized-neutral variation in the electrostatic potential due to oxidation for the dimers taken as models for polymers 1-6. Legends for the electrostatic potential (A) and variation (B).

As can be seen in Figure 3.3, after oxidation, charge distribution is not influenced by the presence of oxygen atoms on the side alkyl chains but, on the contrary, by the nature of the linker which plays a fundamental role. In fact, it is evident that in all cases the charge hole (blue area) is localized in the thiophene, and phenyl units close to the linker region and a relevant polarization is observed. In particular, the –CH$_2$–CH$_2$– linker (**6**) is producing a stronger localization, whereas the –CH=CH– linker (**5**) has a smaller effect, similarly with the case where no linker is present (**4**). Thus, in this respect, polymers **1-3** behave similarly to polymer **4**.

It is noticed that the localization of the charge hole and the corresponding polarization of the oxidized compound is very important for the electrochromic behavior of the material since the charge separation is a crucial factor to promote CT excitations. Thus, the possibility to control the localization of charge allows to possibly tune the CT excitations in the oxidized species and therefore to modulate the color of the material upon application of the external

potential. The computed excitation energies for the various compounds are reported in Figure 3.4, together with the simulated absorption spectra and the iso-density plots of the density change upon photoexcitation.
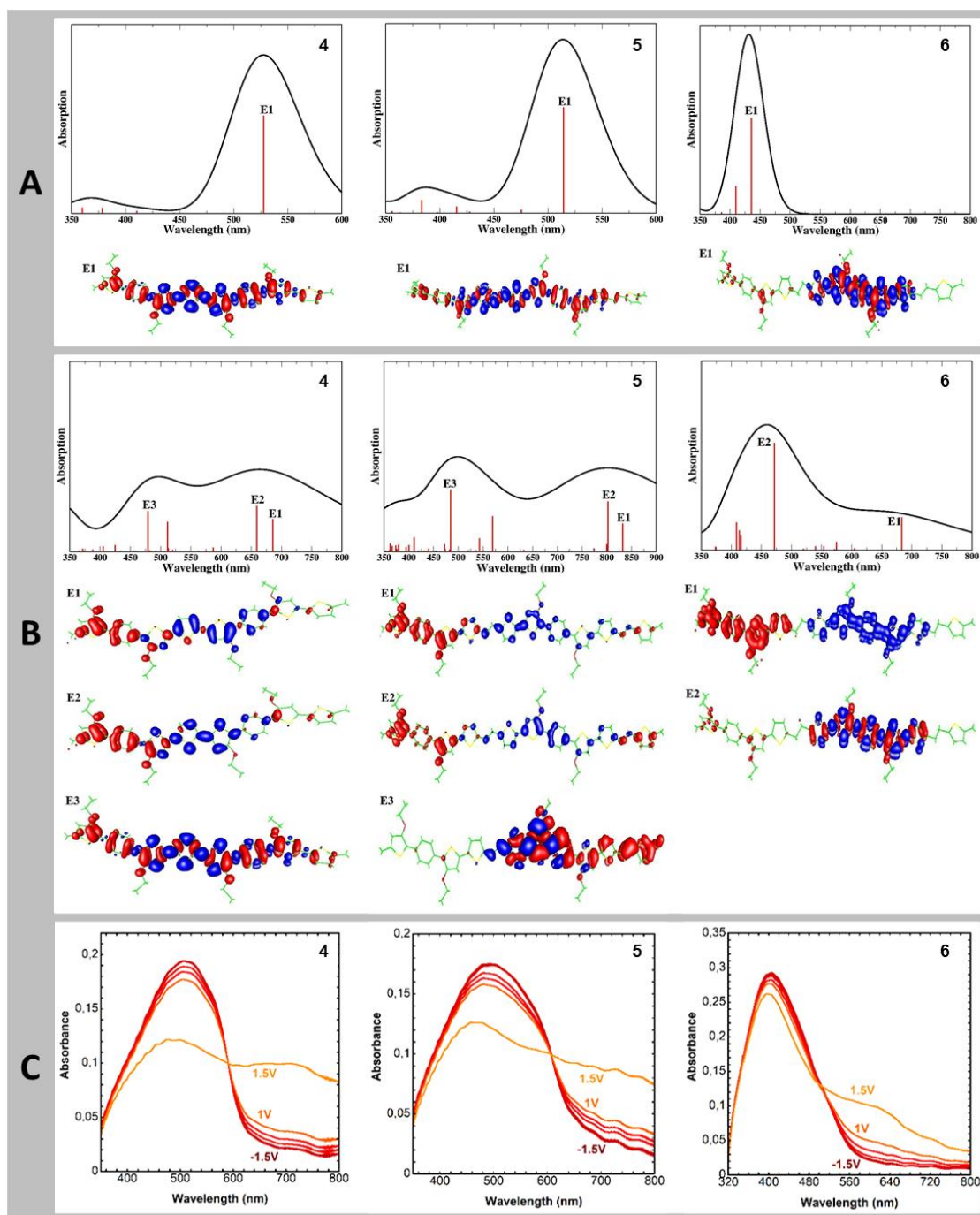
Figure 3.4. TD-DFT calculated absorption spectra of neutral (A) and oxidized (B) of the dimers simulating polymers 4-6. Vertical lines denote the computed excitation energies. Photoinduced density variations are also shown. (C) Spectroelectrochemistry spectra of polymers 4-6.

Inspection of the figure shows that for all systems in the neutral state the absorption is dominated by a π-π* transition. This excitation occurs at about 500 nm for the dimers models of **4** and **5**, while it is computed to be at about 450 nm for the dimer model of **6**. This difference traces back, as discussed before, to the stronger localization of charge in the latter system. The same π-π* excitations, having roughly the same energy, appear also in the absorption spectra of the charged species; in this case, however, they are accompanied by lower energy CT excitations, with energies around 700-800 nm. These CT states are related to the photoinduced transfer of an electron from the edge of the molecule to the charge hole region located at the thiophene and phenyl units next to the linker region. The CT excitations are thus fundamentally related to the polarization of the oxidized species described in Figure 3.4, similar to the polaronic transitions observed in polythiophene materials.[68] Figure 3.4C reports the spectroelectrochemistry of polymers **4**-**6** and shows a remarkable similarity between the calculated excited state spectra of the model dimers and the spectra of the real polymers under voltage application.

3.1.4 Nanostructuration of Polymers 1-6

All polymers can be nanostructured into nanospheres by the reprecipitation method which does not require the use of surfactants (Figure B.5.1).[285,286] Dynamic light scattering (DLS) characterizations indicate that the dimensions of NPs are in the range of ≈160-430 nm (Table B.6.1) and Scanning Electron Microscopy (SEM) analysis confirm the spherical morphology of the nanostructure (Figure B.7.1 and B.7.2). As shown, NPs formed starting from polymers having $-OC_6H_{13}$ substituents (4-6) are smaller in size compared to the others, suggesting that the mesomeric effect of the oxygen atom directly linked to the thiophene ring impacts not only the electronic properties of the materials but also inter- and intramolecular interactions during particle formation. In agreement, a smaller scattering in their absorption spectra is also observed (Figure B.6.1).[285]
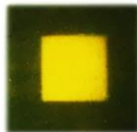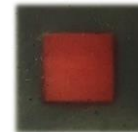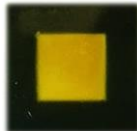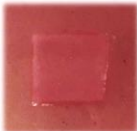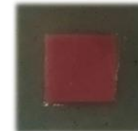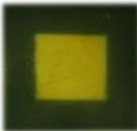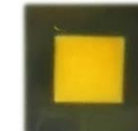
As reported in appendix B.6, all absorption and emission spectra of water-suspended NPs are red shifted with respect to the corresponding polymers in chloroform solution due to a higher degree of intra- and interchain order (Figure B.6.1). Furthermore, compared to the solution, the Stokes shift of the NPs is larger particularly for NPs of 4-6 in which the presence of oxygen probably results in more twisted conformations. Among the NPs with $-OC_6H_{13}$ substituents, 6-NPs exhibit the largest stokes shift (0.81 eV) suggesting that the concomitant presence of the oxygen atom and the $-CH_2-CH_2-$ linker can lead to an even larger distortion of the

polymer backbone in the NPs (Table B.6.2). Nanostructuration of the materials into NPs showed to induce only a small decrease of the oxidation potential, which results only in a negligible decrease of the ionization potential (see Figure B.9.1 and Table B.9.1).

3.1.5 Electrochromic Devices

Polymers **1-6** were spray-coated on PET-ITO substrates from chloroform solutions with a concentration of 5mg/mL. Subsequently, the devices were assembled and characterized (see the experimental part for details). Table 3.3 pictures the assembled displays in the neutral state and after the application of a specific potential range required to obtain maximum color contrast in solid-state ECDs.

Table 3.3. ECDs of the synthesized polymers and respective colors in neutral, reduced (inner square) and oxi-dized (outside square) and the redox potentials employed in PET-ITO solid-state ECDs.

Polymer	Neutral	Active	Redox Potential	Polymer	Neutral	Active	Redox Potential
1			-2.0/2.0V	4			1.5/1.5V
2			-1.8/1.8V	5			1.5/1.5V
3			-1.7/1.7V	6			1.5/1.5V

As shown, polymers **4-6** can be fully reduced and oxidized using -1.5/1.5V, whereas polymers **1**, **2**, and **3** require a higher potential to achieve full color contrast: -2.0/2.0V-1.8/1.8V-1.7/1.7V, respectively. The potentials needed to oxidize and reduce the different polymers in solid-state ECDs, reflect the oxidation potentials measured in solution (Table 3.2), where polymers **4-6** require lower voltages due to the presence of alkyloxy chains which allow lowering the oxidation potential.[11] On the other hand, polymers **1-3** require a higher potential range to be fully oxidized due to the absence of the strong electron-donor effect of the oxygen atom directly attached to the thiophene unit, and in which the alkyl groups induce steric distortion of the polymer backbone. Concerning polymers **1**-**3** which contain alkyl chains directly attached to

thiophene, the redox potentials prove to be higher as the side-chain goes shorter. However, adding a methoxy group at the end of a hexyl chain appears to be an interesting strategy to lower the oxidation potentials, since polymer **3** requires a lower potential to switch color comparing with **1** and **2**. In polymer **4**, with an alkyloxy chain linked to thiophene, there is a significant reduction of the oxidation potential, down to 1.5V, in solid-state. Polymer **6** was synthesized taking into consideration the donor effect of the oxygen while adding a –CH$_2$–CH$_2$– spacer to the backbone of the polymer, resulting in a conjugation break that rises a final yellow polymer with low redox potential (±1.5V). In polymer **5**, it was introduced a double bonded –CH=CH– spacer which restored the conjugation, giving back the red coloration on the final polymer with low redox potential.

The nanostructuration of the polymers in NPs does not change the redox potential required to obtain the maximum color contrast (Table B.8.1).[131,285] The comparison between cast films from chloroform and NPs films from water was performed only for polymers 4-6, since at higher potentials, as required for polymers 1-3, it is visible in the absorption spectra the degradation and color change of PET-ITO itself.[292]

The performance of the ECDs assembled using the thin-films produced from chloroform solutions and the ECDs produced using their respective NPs dispersed in water was evaluated through spectroelectrochemistry, switching time (ST), charge consumption (Q), optical contrast (ΔT) and durability (Cycling). As observed from SEM images reported in Figure B.7.2, the NPs of polymers **4-6** deposited in thin-film from water give a homogenous coverage of the substrate forming a closely packed multilayer structure, and the NPs dimensions are in line with those observed by DLS (see Table B.6.1).

All the assembled ECDs are capable of reversible electrochromic transitions by applying ±1.5V (for 60s at each potential). Furthermore, switching cycles show clear electrochromic transitions for the produced devices as recorded by changes in the absorption spectra. Figures of merit from all experimental data were calculated to evaluate ECD performance (as described in section 1.5.7) and presented in Table 3.4.[233]

These values were obtained for specific wavelengths in which the optical contrast on the solid-state ECD is strongest. The t$_{90}$ is calculated using the method recently described by Hassab *et al*[239] and the qualitative characterization of all polymers and NPs devices were performed both before and after cycling (1000 cycles) by recording absorption changes upon 5 seconds of oxidation/reduction cycles (±1.5V) where 1 cycle = 10 seconds (See Table 3.4 and Figure 3.5).

Table 3.4. Transmittance (ΔT), optical contrast ($\Delta T/T_{Ox}$), switching time (t_{90}^{Red}, t_{90}^{Ox}) charge consumption (Q_{Red}, Q_{Ox}) and coloration efficiency (**CE**) values calculated using polymer **4**, **5** and **6** and **4**-NPs, **5**-NPs and **6**-NPs devices, as prepared and after 1000 cycles, when applicable (Values calculated using 60s at each potential).

ECD	$\Delta T^{(a)}$ (%)	$\Delta T/TO_x$ (%)	T_{Red} (%)	t_{90}^{Red} (s)	t_{90}^{Ox} (s)	Q_{Red} (mC.cm^{-2})	Q_{Ox} (mC.cm^{-2})	CE (C^{-1}.cm^2)
As prepared								
4[(a)]	19.9	41.6	28.0	0.9	5.6	-1.3	1.7	159
4-NPs[(a)]	15.9	42.0	22.0	1.5	11.0	-1.6	1.9	128
After 1000 cycles								
4[(a)]	21.0	44.6	26.2	1.0	3.0	-1.2	1.8	190
4-NPs[(a)]	18.8	51.6	17.6	1.3	6.0	-1.4	2.0	195
As prepared								
5[(b)]	13.4	20.7	51.3	4.4	20	-2.0	3.6	54
5-NPs[(b)]	15.7	36.8	27.0	0.7	11	-2.9	5.2	101
As prepared								
6[(c)]	2.5	10.4	20.9	7.5	28	-6.7	5.3	11
6-NPs[(c)]	8.9	19.6	35.6	3.0	8.1	-4.8	3.2	23
After 1000 cycles								
6[(c)]	2.3	11.5	17.1	3.6	11	-4.6	3.5	14
6-NPs[(c)]	8.5	22.4	28.7	2.2	1.7	-3.4	2.4	40

(a) λ_{abs}=510 nm; (b) λ_{abs}=520 nm; (c) λ_{abs}=410 nm.
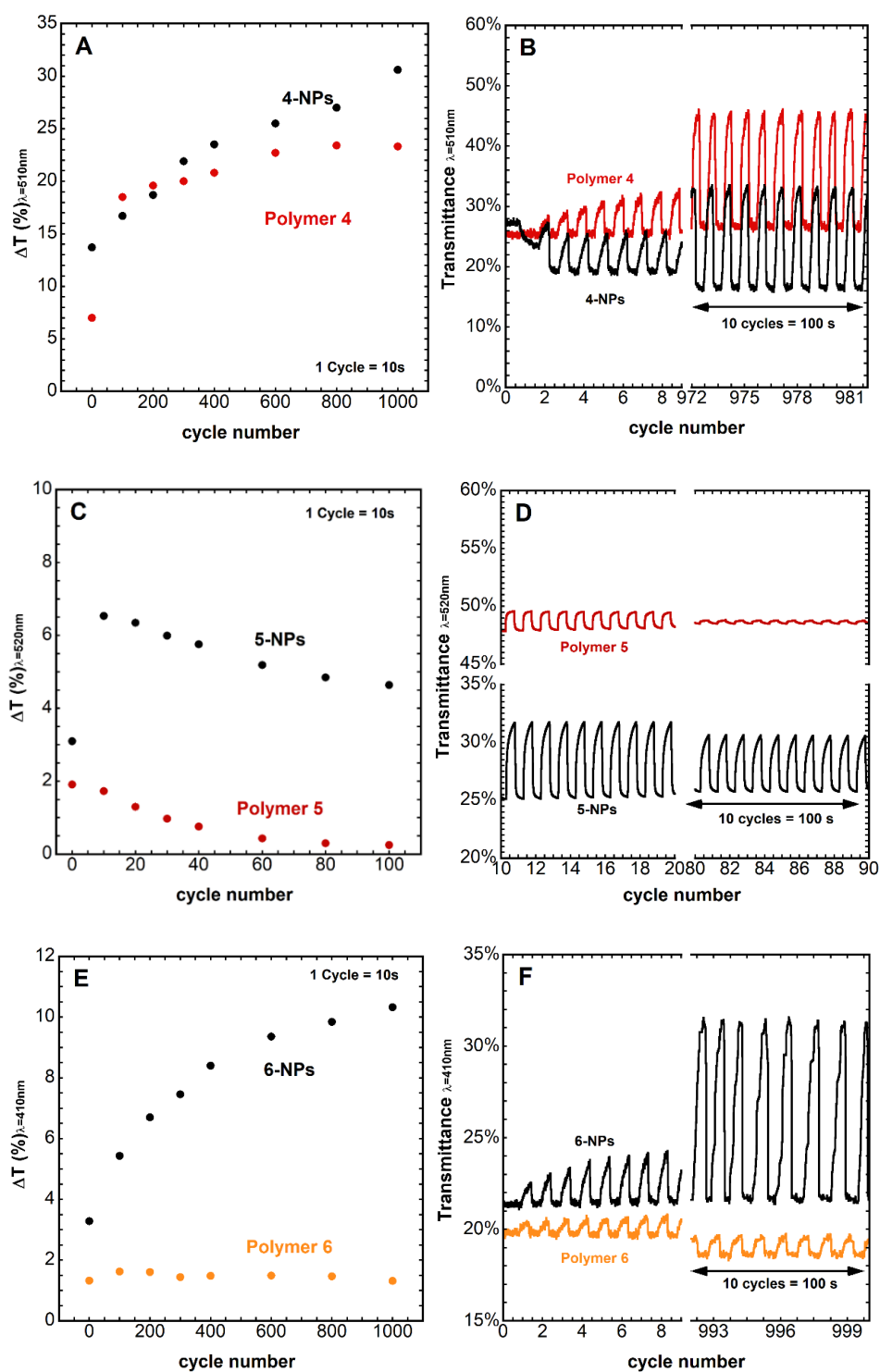
Figure 3.5. (A, C, E) Evolution of transmittance during the cycling experiment using polymer **4** vs **4**-NPs, **5** vs **5**-NPs and **6** vs **6**-NPs ECDs, respectively. (B, D, F) Changes in transmittance of polymer **4** vs **4**-NPs, **5** vs **5**-NPs and **6** vs **6**-NPs ECDs, respectively during the cycling experiment. In all measurements, 1.5V was used for oxidation and -1.5V was used for reduction (1cycle = 10 s).

From Table 3.4 and Figure 3.5 it is possible to evaluate the improvement in the performance of ECDs using NPs compared to thin-films spray-casted from chloroform. Regarding polymer **4**, the final ECDs presents fast switching times (t_{90}^{Red}=0.9s for **4** and t_{90}^{Red}=1.5s for **4**-NPs), as expected for a fully conjugated thiophene-based polymer with alkyloxy chains.[10] However, **4**-NPs ECD presents an improvement of the final optical contrast after 1000cycles (Figure 3.5A), with a drastic decrease of oxidation switching times (11.0 *vs* 6.0). In the case of polymer **5**, it was found a more evident increase in performance when comparing the casted polymer from chloroform with the NPs. The t_{90}^{Red} for the **5**-NPs ECD is < 1s while t_{90}^{Red} for polymer 5 is >4s, additionally, the oxidation step for **5**-NPs ECD required half of the time compared to polymer **5** ECD (11s *vs* 20s).

The durability of these devices was assessed over 100 cycles, while the **5**-NPs ECD was still performing with ΔT±5% (See Figure 3.5D), the polymer **5** in cast-film did not present anymore a significant color contrast. Concerning polymer **6**, ECDs made with NPs achieved a markedly increase in performance as observed by an improvement of color contrast (in %T), switching times in oxidation and reduction (t_{90}^{Red} and t_{90}^{Ox}) as well as a lower charge consumption after 60s of ±1.5V application. After 1000 cycles both ECDs, based on polymer **6** and **6**-**NPs**, did not show sign of degradation. More importantly, an increase of ΔT is observed in the case of NPs (Figure 3.5E), reflecting electrochemical annealing of the films where conformational changes facilitate full oxidation of the polymer giving rise to better electrochemical performance. Furthermore, the characterization of the ECD using **6-NPs** after 1000 cycles presented switching times 7-fold faster (1.7s vs 11s) with respect to the device using the cast polymer (**6**). From Figure 3.5F the ΔT can be evaluated comparing the initial color contrast, in transmittance, of the polymer **6** and **6-NPs** in the first and last 10 cycles of the cycling experiment. The CE values obtained for fully conjugated polymers and their NPs (**4** and **4-NPs**) are comparable with values reported on the literature.[285,286]

In polymers with conjugation stoppers (5 and 6) the CE values are lower although they increase going to the NPs. Nevertheless, the calculation of all CE's was performed at one specific wavelength (see Table 3.4), while color transitions observed are a result of the sum of all spectral transitions between the oxidized and reduced state. Spectroelectrochemistry measurements for ECDs of all polymers, deposited from chloroform and as NPs, before and after cycle experiments are reported in appendix B (Figures B.9.2-B.9.5).

In **4-6 NPs** devices, no degradation was observed in the performance of the device after the cycling measurements, with an increase of color contrast (up to 22%) in the **6**-**NPs** device that was not observed in the cast polymer ECD (see Figure B.10.1).

Furthermore, as reported in appendix (Figure B.11.1), flexible displays made from NPs present stable electrochromism while bending, a most appealing characteristic for their implementation in deformable electronics such as adaptive camouflage, wearable displays, fashion and so on.[243,293]

3.2 Conclusions

Newly synthesized and cost-effective polymers processable in common organic solvents and as nanoparticles in water colloidal solutions are described. Their easy chemistry allows straightforward structural modifications to tune absorption and emission profiles, energy levels and performance in electrochemical devices. The electrochromic properties of the polymers were tuned: *i)* by changing the steric effects of the alkyl substituents, *ii)* by introducing an oxygen atom in the side chain which when directly bound to thiophene allows rising low redox potentials, and *iii)* by adding spacers, *i.e.*, single and double C-C bonds, affecting the conjugation and, consequently, generating different ECDs colors using the same backbone. In particular, the strategy of synthesizing a polymer having the concomitant presence of strong electron donor substituents ($-OC_6H_{13}$) and a single bond spacer ($-CH_2-CH_2-$) was successful in obtaining a yellow ECD material switching at a very low potential value (-1.5V).

The dark blue oxidized state of the devices has been analyzed by DFT and T-DFT calculations and the different calculated absorption peaks have been associated with specific molecular fragments. In this way, it will be possible to rationally design an improved set of the reported polymers for the fabrication of devices displaying a wider palette of colors in the neutral and oxidized state and also being highly transmissive in the bleached state. It is demonstrated that all polymers form stable colloidal suspensions with particles sizes ranging from ≈160-430 nm.

Finally, it is shown that by using spray-casting colloidal NPs of the electrochromic polymer dispersed in water in flexible PET-ITO substrates instead of chloroform solutions of the polymer, a double objective can be attained: on one side, the nanostructuration of the active material leads to better performance - in terms of switching time, charge consumption, optical contrast and durability - and, on the other, the use of a safe solvent such as water.

It is worth noting that the considerable attention currently devoted to the field of electrochromism is not only concerned with its fascinating futuristic applications - from electronic skin to camouflage, most still at the research level - but also to applications such as Do-It-Yourself kits[257] designed for common users, needing the largest variety of colors. On the other hand, a large choice of easy-to-handle low-cost materials will also allow exploring innovative device structures with the possibility to integrate ECDs with other organic devices such as field-effect transistors, solar cells, or light-emitting diodes.
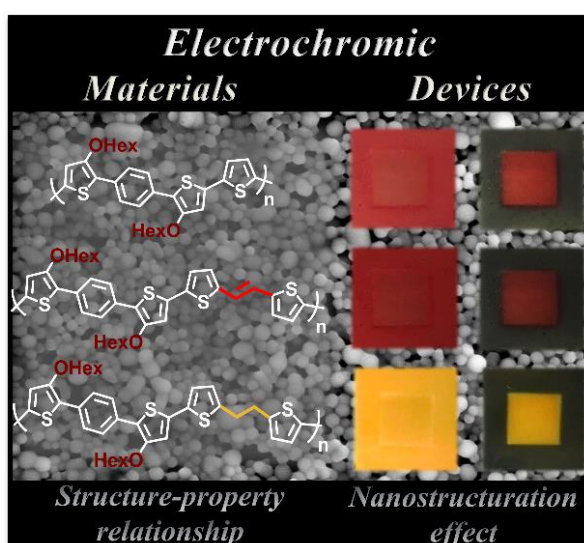
Figure 3.6. Graphical abstract from the published paper in Adv. Electron. Mater. (2021), 2100166.

3.3 Experimental Section

3.3.1 Synthesis of Polymers 1-6
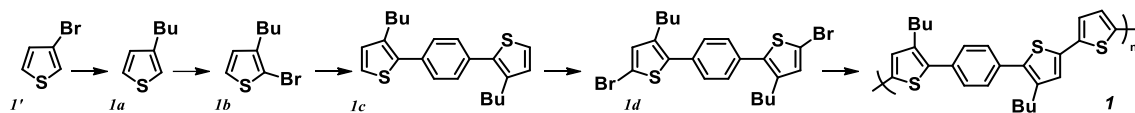
Scheme 3.3. Synthesis of Polymer **1**.

3-butylthiophene (1a) → To a suspension of magnesium turnings (1,5 mmol) in diethyl ether$_{(dry)}$ (≈ 4 M) a solution of 1-bromobutane (1,5 mmol) in diethyl ether$_{(dry)}$ (≈ 4 M) was added dropwise at 0°C and under N$_2$ atmosphere. The resulting solution was stirred for 1 hour and then transferred dropwise by a syringe to a solution of 3-bromothiophene (**1′**) (1 mmol) and [1,3-bis(diphenylphosphino)propane]nickel(II)chloride (0,001 mmol) in diethyl ether$_{(dry)}$ (≈ 2,5 M) at 0°C and under N$_2$ atmosphere. The reaction mixture was stirred overnight at room temperature and then quenched with water. The resulting aqueous mixture was extracted with diethyl ether, the organic layers were combined and evaporated under reduced pressure. The residue was purified by flash chromatography (Cyclohexane 100%). Colorless oil. Yield: 90%. EI-MS *m/z* 140(M$^+$). ^{1}H NMR (400 MHz, CDCl$_3$, TMS/ppm): δ 7.26 (m, 1H), 6.96-6.94 (m, 2H), 2.66 (t, 2H), 1.66–1.60 (m, 2H), 1.42–1.37 (m, 2H), 0.95 (t, 3H). ^{13}C NMR (100 MHz, CDCl$_3$, TMS/ppm): δ 143.2, 128.3, 125.0, 119.7, 32.7, 29.9, 22.4, 13.9.

2-bromo-3-butylthiophene (1b) → The compound was prepared following the general procedure for bromination starting from **1a** (1 mmol) using 1 mmol of NBS. The residue was isolated by flash chromatography (Cyclohexane). Colorless oil. Yield: 95%. EI-MS *m/z* 220(M$^+$). ^{1}H NMR (400 MHz, CDCl$_3$, TMS/ppm): δ 7.18 (d, ^3J =6.0, 1H), 6.79 (d, ^3J =6.0, 1H), 2.58 (t, 2H), 1.61–1.53 (m, 2H), 1.41–1.34 (m, 2H), 0.94 (t, 3H). ^{13}C NMR (100 MHz, CDCl$_3$, TMS/ppm): δ 141.9, 128.3, 125.1, 108.8, 31.9, 29.1, 22.3, 13.9.

1,4-bis(3-butylthiophen-2-yl)benzene (1c) → The compound was prepared following the general procedure for Suzuki Cross-coupling starting from **1b** (2 mmol) and 1,4-benzenediboronic acid dipinacol ester (1 mmol). The residue was isolated by flash chromatography (Cyclohexane/CH$_2$Cl$_2$, 95:5). Pale yellow solid. Yield: 75%. EI-MS *m/z* 354(M$^+$). ^{1}H NMR (400 MHz, CDCl$_3$, TMS/ppm): δ 7.48 (s, 4H), 7.24 (d, ^3J =5.2, 2H), 7.00 (d, ^3J =5.2, 2H), 2.71 (t, 4H), 1.64–1.59 (m, 4H), 1.41–1.33 (m, 4H), 0.91 (t, 6H). ^{13}C NMR (100 MHz, CDCl$_3$, TMS/ppm): δ 138.8, 137.3, 133.4, 129.8, 129.6, 129.3, 123.7, 33.2, 28.4, 22.6, 13.9.

1,4-bis(5-bromo-3-butylthiophen-2-yl)benzene (1d) → The compound was prepared following the general procedure for bromination starting from **1c**. The residue was isolated by flash chromatography (Cyclohexane/CH$_2$Cl$_2$, 95:5). Dark yellow semi-solid. Yield: 95%. EI-MS *m/z* 512(M$^+$). ^{1}H NMR (400 MHz, CDCl$_3$, TMS/ppm): δ 7.39 (s, 4H), 6.95 (s, 2H), 2.62 (t, 4H), 1.61–1.54 (m, 4H), 1.36–1.30 (m, 4H), 0.89 (t, 6H). ^{13}C NMR (100 MHz, CDCl$_3$, TMS/ppm): δ 139.6, 138.7, 133.1, 132.3, 129.3, 128.5, 110.6, 32.9, 28.3, 22.5, 13.8.

Polymer 1→ The compound was prepared following the general procedure for Stille Cross-coupling starting from **1d** and 2,5-bis(tributylstannyl)thiophene. The crude product was filtered, suspended in MeOH and centrifuged three times. Yellow solid. Yield: 65%. ^{1}H NMR (400 MHz, CDCl$_3$, TMS/ppm): δ 7.53–7.45 (m), 7.12–7.05 (m), 2.75–2.63 (m), 1.73–1.54 (m), 1.45–1.25 (m), 0.97–0.85 (m). Mw=4600, Mn=2000, PD=2.3.
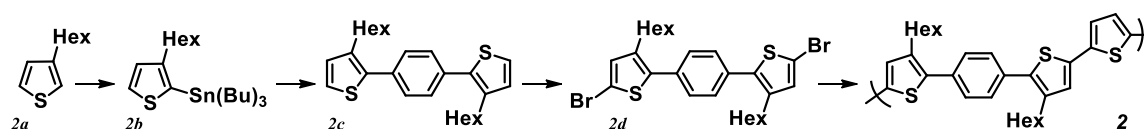
Scheme 3.4. Synthesis of Polymer **2**.

(3-hexylthiophenen-2-yl)tributylstannane (2b) → The compound was prepared following the general procedure for stannylation starting from **2a**. The crude product was used without further purifications. Brown oil. Yield: 95%. EI-MS *m/z* 458(M$^+$). ^{1}H NMR (400 MHz, CDCl$_3$, TMS/ppm): δ 7.53 (d, ^3J =4.8, 1H), 7.10 (d, ^3J =4.8, 1H), 2.60(t, 2H), 1.65–1.50 (m, 8H), 1.39–1.29 (m, 12H), 1.14-1.09 (m, 6H), 0.90 (t, 12H). ^{13}C NMR (100 MHz, CDCl$_3$, TMS/ppm): 150.7, 130.8, 130.6, 32.9, 32.2, 31.8, 29.4, 29.0, 27.3, 22.6, 14.0, 13.6, 10.8.

1,4-bis(3-hexylthiophen-2-yl)benzene (2c) → The compound was prepared following the general procedure for Stille Cross-coupling starting from **2b** (2 mmol) and 1,4-dibromobenzene (1 mmol). The residue was isolated by flash chromatography (Cyclohexane/CH$_2$Cl$_2$, 95:5). Pale yellow solid. Yield: 70%. EI-MS *m/z* 410(M$^+$). ^{1}H NMR (400 MHz, CDCl$_3$, TMS/ppm): δ 7.48 (s, 4H), 7.25 (d, ^3J =5.2, 2H), 7.01 (d, ^3J =5.2, 2H), 2.71 (t, 4H), 1.69–1.58 (m, 4H), 1.37–1.25 (m, 12H), 0.90–0.84 (m, 6H). ^{13}C NMR (100 MHz, CDCl$_3$, TMS/ppm): δ 138.9, 137.4, 133.8, 129.6, 129.3, 125.7, 123.8, 31.6, 31.0, 29.2, 28.8, 22.6, 14.0.

1,4-bis(5-bromo-3-hexylthiophen-2-yl)benzene (2d) → The compound was prepared following the general procedure for bromination starting from **2c** (1 mmol) using 2 mmol of NBS. The residue was isolated by flash chromatography (Cyclohexane/CH$_2$Cl$_2$, 95:5). Dark yellow semi-solid. Yield: 95%. EI-MS *m/z* 568(M$^+$). ^{1}H NMR (400 MHz, CDCl$_3$, TMS/ppm): δ 7.40 (s,

4H), 6.95 (d, 2H), 2.62 (t, 4H), 1.62–1.52 (m, 4H), 1.34–1.21 (m, 12H), 0.88 (t, 6H). ^{13}C NMR (100 MHz, CDCl$_3$, TMS/ppm): δ 139.6, 138.7, 133.1, 132.3, 129.3, 128.6, 110.6, 31.6, 30.8, 29.0, 28.6, 22.6, 14.1.

Polymer 2→ The compound was prepared following the general procedure for Stille Cross-coupling starting from **2d** and 2,5-bis(tributylstannyl)thiophene. The crude product was filtered, suspended in MeOH and centrifuged three times. Yellow solid. Yield: 75%. ^{1}H NMR (400 MHz, CDCl$_3$, TMS/ppm): δ 7.51–7.47 (m), 7.10–7.06 (m), 2.74–2.65 (m), 1.72–1.56 (m), 1.41–1.23 (m), 0.96–0.83 (m). Mw=2900, Mn=1400, PD=2.1.
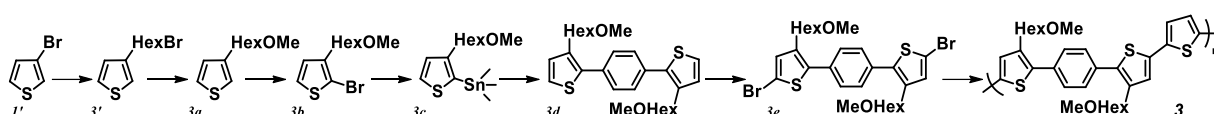
Scheme 3.5. Synthesis of Polymer **3**.

3-(6-bromohexyl)thiophene (3') → The product was synthesized according to reference [294].

3-(6-methoxyhexyl)thiophene (3a) → Sodium cubes (1,5 mmol) were dissolved in anhydrous methanol (≈ 10^{-1} M) at 0°C and under N$_2$ atmosphere. To this mixture **3'** (1 mmol) was added dropwise and the resulting solution was stirred 24 hours. The reaction was quenched with HCl aqueous solution (3N) and extracted with CH$_2$Cl$_2$/H$_2$O. The organic phases were combined and evaporated under reduced pressure. The residue was purified by flash chromatography (Cyclohexane 100 %). Colorless oil. Yield: 85%. EI-MS *m/z* 198(M$^+$). ^{1}H NMR (400 MHz, CDCl$_3$, TMS/ppm): δ 7.44–7.22 (m, 1H), 6.95–6.92 (m, 2H), 3.39 (t, 2H), 3.34 (s, 3H), 2.64 (t, 2H), 1.68–1.57 (m, 4H), 1.42–1.37 (m, 4H). ^{13}C NMR (100 MHz, CDCl$_3$, TMS/ppm): δ 143.1, 128.2, 125.1, 119.8, 72.8, 58.5, 30.5, 30.2, 29.6, 29.1, 25.9.

2-bromo-3-(6-methoxyhexyl)thiophene (3b) → The compound was prepared following the general procedure for bromination starting from **3a** (1 mmol) using 1 mmol of NBS. The residue was isolated by flash chromatography (Cyclohexane). Colorless oil. Yield: 90%. EI-MS *m/z* 276(M$^+$). ^{1}H NMR (400 MHz, CDCl$_3$, TMS/ppm): δ 7.15 (d, ^3J =4.0, 1H), 6.78 (d, ^3J =4.0, 1H), 3.36 (t, 2H), 3.32 (s, 3H), 2.56 (t, 2H), 1.62–1.54 (m, 4H), 1.42–1.35 (m, 4H). ^{13}C NMR (100 MHz, CDCl$_3$, TMS/ppm): δ 141.8, 128.2, 125.2, 108.8, 72.8, 58.5, 29.9, 29.6, 29.3, 29.0, 25.9.

3-(6-methoxyhexyl)thiophen-2-yl)trimethylstannane (3c) → The compound was prepared following the general procedure for stannylation starting from **3b**. The crude product was used without further purifications. Brown oil. Yield: 75%. EI-MS *m/z* 362(M$^+$). ^{1}H NMR (400 MHz, CDCl$_3$, TMS/ppm): δ 7.53 (d, ^3J =4.8, 1H), 7.08 (d, ^3J =4.8, 1H), 3.36 (t, 2H), 3.32 (s, 3H),

2.63 (t, 2H), 1.61–1.56 (m, 4H), 1.37–1.34 (m, 4H), 0.35 (s, 9H). ^{13}C NMR (100 MHz, CDCl$_3$, TMS/ppm): δ 150.7, 131.3, 130.5, 129.3, 72.8, 58.5, 32.5, 32.1, 29.6, 29.4, 26.1.

1,4-bis(3-(6-methoxyhexyl)thiophen-2-yl)benzene) (3d) → The compound was prepared following the general procedure for Stille Cross-coupling starting from **3c** and 1,4-dibromobenzene. The residue was isolated by flash chromatography (Cyclohexane/CH$_2$Cl$_2$, 90:10). Pale yellow solid. Yield: 65%. EI-MS *m/z* 470(M$^+$). ^{1}H NMR (400 MHz, CDCl$_3$, TMS/ppm): δ 7.48 (s, 4H), 7.25 (d, ^3J =5.2, 2H), 7.00 (d, ^3J =5.2, 2H), 3.35 (t, 4), 3.33 (s, 6H), 2.72 (t, 4H), 1.69–1.55 (m, 10H), 1.38–1.35 (m, 6H). ^{13}C NMR (100 MHz, CDCl$_3$, TMS/ppm): δ 138.7, 137.4, 133.7, 129.7, 129.6, 129.3, 123.8, 72.8, 58.5, 30.9, 29.6, 29.3, 28.7, 25.9.

1,4-bis(5-bromo-3-(6-methoxyhexyl)thiophen-2-yl)benzene (3e) → The compound was prepared following the general procedure for bromination starting from **3d**. The residue was isolated by flash chromatography (Cyclohexane/CH$_2$Cl$_2$, 95:5). Dark yellow semi-solid. Yield: 95%. EI-MS *m/z* 628(M$^+$). ^{1}H NMR (400 MHz, CDCl$_3$, TMS/ppm): δ 7.38 (s, 4H), 6.93 (s, 2H), 3.32 (t, 4H), 3.31 (s, 6H), 2.62 (t, 4H), 1.62–1.52 (m, 10H), 1.35–1.31 (m, 6H). ^{13}C NMR (100 MHz, CDCl$_3$, TMS/ppm): δ 139.5, 138.7, 133.0, 132.2, 129.7, 129.3, 110.6, 72.8, 58.5, 30.7, 29.5, 29.2, 28.5, 25.9.

Polymer 3 → The compound was prepared following the general procedure for Stille Cross-coupling starting from **3e** and 2,5-bis(tributylstannyl)thiophene. The crude product was filtered, suspended in MeOH and centrifuged three times. Yellow Solid. Yield: 50%. ^{1}H NMR (400 MHz, CDCl$_3$, TMS/ppm): δ 7.52–7.44 (m), 7.10–7.05 (m), 3.40–3.28 (m), 2.74–2.65 (m), 1.80–1.52 (m), 1.44–1.31 (m). Mw=4100, Mn=2200, PD=1.90.
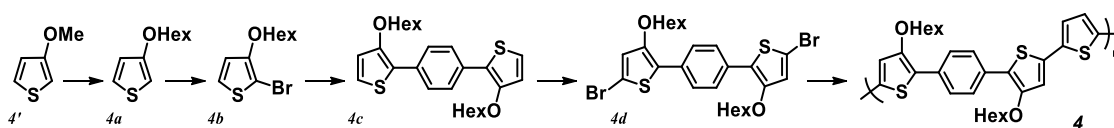
Scheme 3.6. Synthesis of Polymer **4**.

3-Hexyloxythiophene (4a) → To a solution of **4'** (1mmol) in anhydrous toluene (≈ 10^{-1} M) 1-hexanol (2 mmol) and *p*-toluenesulfonic acid monohydrate (0,1 mmol) were added under N$_2$ atmosphere. The reaction mixture was refluxed overnight. The resulting crude product was extracted with CH$_2$Cl$_2$/H$_2$O, the organic phases were combined and concentrated under reduce pressure. The residue was purified by flash chromatography (Cyclohexane/CH2Cl$_2$, 95/5). Colorless oil. Yield: 80%. EI-MS *m/z* 184(M$^+$). ^{1}H NMR (400 MHz, CDCl$_3$, TMS/ppm): δ 7.17 (dd, ^3J =5.6, ^4J =3.2, 1H), 6.76 (d, ^3J =5.6, 1H), 6.23 (d, ^3J =3.2, 1H), 3.95 (t, 2H), 1.81–1.76 (m, 2H), 1.51–

1.34 (m, 6H), 0.94 (t, 3H).). ^{13}C NMR (100 MHz, CDCl$_3$, TMS/ppm): δ 158.1, 124.5, 119.5, 96.9, 70.3, 31.6, 29.3, 25.7, 22.6, 14.0.

2-bromo-3-Hexyloxythiophene (4b) → The compound was prepared following the general procedure for bromination starting from **4a** (1 mmol) using 1 mmol of NBS. The residue was isolated by flash chromatography (Cyclohexane). Colorless oil. Yield: 95%. EI-MS *m/z* 264(M$^+$). ^{1}H NMR (400 MHz, CDCl$_3$, TMS/ppm): δ 7.17 (d, ^3J =5.6, 1H), 6.74 (d, ^3J =5.6, 1H), 4.04 (t, 2H), 1.81–1.73 (m, 2H), 1.53–1.43 (m, 2H), 1.39–1.32 (m, 4H), 0.94 (t, 3H). ^{13}C NMR (100 MHz, CDCl$_3$, TMS/ppm): 154.6, 124.1, 117.5, 91.5, 72.2, 31.6, 29.5, 25.5, 22.6, 14.0.

1,4-bis(3-(hexyloxy)thiophen-2-yl)benzene (4c) → The compound was prepared following the general procedure for Suzuki Cross-coupling starting from **4b** (2 mmol) and 1,4-benzenediboronic acid dipinacol ester (1 mmol). The residue isolated by flash chromatography (Cyclohexane/CH$_2$Cl$_2$, 95:5) was not completely pure (40% of impurity). Yellow solid. Yield: 55%. EI-MS *m/z* 442(M$^+$). ^{1}H NMR (400 MHz, CDCl$_3$, TMS/ppm): δ 7.77 (s, 4H), 7.11 (d, ^3J =5.2, 1H), 6.90 (d, ^3J =5.2, 1H), 4.12–4.05 (m, 4H), 1.87–1.79 (m, 4H), 1.56–1.48 (m, 4H), 1.44–1.33 (m, 8H), 0.92 (t, 6H).

1,4-bis(5-bromo-3-(hexyloxy)thiophen-2-yl)benzene (4d) → The compound was prepared following the general procedure for bromination starting from **4c**. The residue was isolated by flash chromatography (Cyclohexane/CH$_2$Cl$_2$, 95:5). Yellow semi-solid. Yield: 95%. EI-MS *m/z* 600(M$^+$). ^{1}H NMR (400 MHz, CDCl$_3$, TMS/ppm): δ 7.63 (s, 4H), 6.90 (s, 2H), 4.01 (t, 4H), 1.80–1.72 (m, 4H), 1.48–1.24 (m, 4H), 1.35–1.31 (m, 8H), 1.90 (t, 6H). ^{13}C NMR (100 MHz, CDCl$_3$, TMS/ppm): δ 152.1, 130.9, 126.5, 122.1, 121.6, 109.3, 72.1, 31.5, 29.5, 25.6, 22.6, 14.0.

Polymer 4 → The compound was prepared following the general procedure for Stille Cross-coupling starting from **7** and 2,5-bis(tributylstannyl)thiophene. The crude product was filtered, suspended in MeOH and centrifuged three times. Dark red solid. Yield: 60%. ^{1}H NMR (400 MHz, CDCl$_3$, TMS/ppm): δ 7.80–7.67 (m), 7.15–6.87 (m), 4.15–3.88 (m), 1.90–1.72 (m), 1.69–1.55 (m), 1.54–1.43 (m), 1.41–1.24 (m), 0.98–0.82 (m). Mw=5500, Mn=2800, PD=1.90.
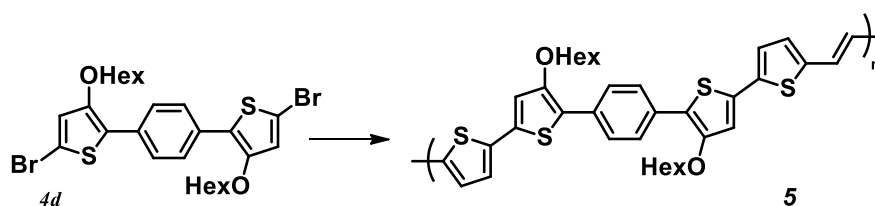
Scheme 3.7. Synthesis of Polymer **5**.

Polymer 5 → The compound was prepared following the general procedure for Stille Cross-coupling starting from **4d** and 1,2-bis(5-(trimethylstannyl)thiophen-2-yl)ethene. The crude product was filtered, suspended in MeOH and centrifuged three times. Deep red solid. Yield: 65%. ^{1}H NMR (400 MHz, CDCl$_3$, TMS/ppm): δ 7.87–7.31 (m), 7.09–6.67 (m), 4.16–3.99 (m), 1.89–1.73 (m), 1.58–1.43 (m), 1.42–1.28 (m), 0.99–0.86 (m). Mw=9100, Mn=4800, PD=1.90.
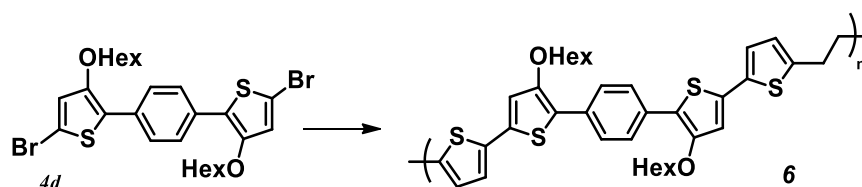
Scheme 3.8. Synthesis of Polymer **6**.

Polymer 6 → The compound was prepared following the general procedure for Stille Cross-coupling starting from **4d** and 1,2-bis(5-(trimethylstannyl)thiophen-2-yl)ethane. The crude product was filtered, suspended in MeOH and centrifuged three times. Yellow solid. Yield: 50%. ^{1}H NMR (400 MHz, CDCl$_3$, TMS/ppm): δ 7.578–7.73 (m), 7.02–6.97 (m), 6.94–6.89 (m), 6.73–6.66 (m), 4.15–4.00 (m), 3.22–3.08 (m), 1.89–1.73 (m), 1.56–1.23 (m), 0.99–0.83 (m). Mw=6200, Mn=3100, PD=2.00.
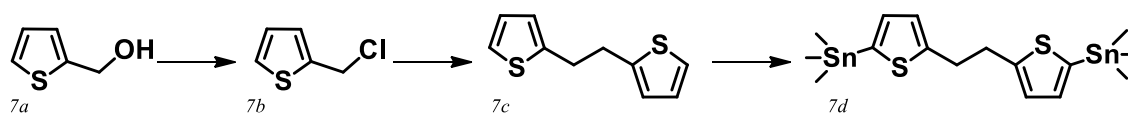
Scheme 3.9. Synthesis of the single-bond linker (**7d**).

2-(chloromethyl)thiophene (7b) → To thiophen-2-ylmethanol (1 mmol) thienyl chloride (1,5 mmol) was added dropwise at 0°C. The resulting mixture was heated to 80 °C for 5 hours. The reaction was quenched whit cold water and the mixture was extracted with CH$_2$Cl$_2$/H$_2$O, the organic phases were combined and the solvent removed by rotary evaporation. The residue was used without further purification. Brown oil. Yield: 95%. EI-MS *m/z* 132(M$^+$). ^{1}H NMR (400

MHz, CDCl$_3$, TMS/ppm): δ 7.31 (d, ^3J =5.2, 1H), 7.09 (d, ^3J =3.6, 1H), 6.97 (dd, ^3J=5.2, ^4J=3.6, 1H), 4.80 (s, 2H). ^{13}C NMR (100 MHz, CDCl$_3$, TMS/ppm): δ 140.1, 127.7, 126.92, 126.90, 40.3.

1,2-di(thiophen-2-yl)ethane (7c) → To a suspension of magnesium turnings (3 mmol) in anhydrous diethyl ether (≈ 4 M), 2-(chloromethyl)thiophene (1 mmol) was added dropwise under vigorous stirring. The reaction mixture started to reflux spontaneously and a white precipitate formed. The mixture was stirred 2 hours at room temperature. The reaction was quenched with aqueous HCl (≈ 8 N), the organic layers were combined and concentrated under reduced pressure. The residue was isolated by flash chromatography (Cyclohexane 100%). White crystals. Yield: 75%. EI-MS m/z 194(M$^+$). ^{1}H NMR (400 MHz, CDCl$_3$, TMS/ppm): δ 7.17 (d, ^3J =4.8, 1H), 7.00 (dd, ^3J=4.8, ^4J =3.2, 1H), 6.86 (d, ^3J =3.2, 1H), 3.26 (s, 4H). ^{13}C NMR (100 MHz, CDCl$_3$, TMS/ppm): δ 143.7, 126.8, 124.7, 123.4, 32.2.

1,2-bis(5-(trimethylstannyl)thiophen-2-yl)ethane (7d) → To a stirring solution of diisopropylamine (2,2 mmol) in THF$_{(dry)}$ (≈ 10^{-1} M) at -78°C, nBuli (2,2 mmol) was added dropwise under nitrogen atmosphere. The resulting mixture was stirred for 30 min and transferred dropwise by a syringe to a solution of 1,2-di(thiophen-2-yl)ethane (1 mmol) in THF$_{(dry)}$ (≈ 10^{-1} M) at -78°C and under N$_2$ atmosphere. The resulting mixture was stirred for 1 hour, quenched with Sn(Me)$_3$Cl (2,2 mmol) and then stirred overnight. The reaction mixture was extracted with CH$_2$Cl$_2$/H$_2$O, the organic phases were combined and evaporated under reduced pressure. The crude product was used without further purifications. Pale brown oil. Yield: 95%. EI-MS m/z 520(M$^+$). ^{1}H NMR (400 MHz, CDCl$_3$, TMS/ppm): δ 7.09 (d, ^3J=3.2, 2H), 7.01 (d, ^3J=3.2, 2H), 3.31 (s, 4H), 0.42 (s, 18H). ^{13}C NMR (100 MHz, CDCl$_3$, TMS/ppm): δ 149.9, 135.4, 135.1, 125.9, 32.6.
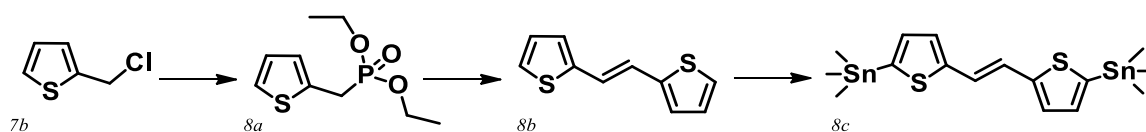
Scheme 3.10. Synthesis of the double-bond linker (**8c**).

diethyl (thiophen-2-ylmethyl)phosphonate (8a) → 2-(chloromethyl)thiophene and triethyl phosphite were refluxed at 160°C overnight under N$_2$ atmosphere. The resulting crude product was purified under vacuum distillation at 120°C for 1 hour. Colorless oil. Yield: 80%. EI-MS m/z 234(M$^+$). ^{1}H NMR (400 MHz, CDCl$_3$, TMS/ppm): δ 7.07 (d, ^3J =4.4, 1H), 6.88–6.83 (m, 2H), 4.02–3.92 (m, 4H), 3.26 (d, J=20.5, 2H), 1.25–1.15 (m, 6H). ^{13}C NMR (100 MHz, CDCl$_3$, TMS/ppm): δ 132.3, 127.3, 126.9, 124.7, 62.3, 28.6, 16.3.

1,2-di(thiophen-2-yl)ethene (8b) → To a solution of diethyl (thiophen-2-ylmethyl)phospho-nate (1 mmol) and NaH (1 mmol) in toluene ($\approx 10^{-1}$ M) thiophene-2-carbaldehyde (1 mmol) was added dropwise at 10°C. The mixture was refluxed at 110 °C for 4 hours and then poured into H_2O. The resulting aqueous mixture was extracted with CH_2Cl_2/H_2O, the organic phases were combined and evaporated under reduced pressure. The residue was isolated by flash chromatography (Cyclohexane 100%). Yellow powder. Yield: 90%. EI-MS m/z 192(M$^+$). ^{1}H NMR (400 MHz, CDCl$_3$, TMS/ppm): δ 7.21 (d, ^3J =5.2, 2H), 7.01 (s, 2H), 7.07 (d, ^3J =3.2, 2H), 7.02 (d, ^3J =5.2, ^4J =3.2, 2H).^{13}C NMR (100 MHz, CDCl$_3$, TMS/ppm): δ 142.4, 127.7, 126.1, 124.3, 121.5.

1,2-bis(5-(trimethylstannyl)thiophen-2-yl)ethane (8c)→ To a stirring solution of diisopropyl-amine (2,2 mmol) in THF$_{(dry)}$ ($\approx 10^{-1}$ M) at -78°C, nBuli (2,2 mmol) was added dropwise under nitrogen atmosphere. The resulting mixture was stirred for 30 min and transferred dropwise by a syringe to a solution of 1,2-di(thiophen-2-yl)ethene (1 mmol) in THF$_{(dry)}$ ($\approx 10^{-1}$ M) at -78°C and under N_2 atmosphere. The resulting mixture was stirred for 1 hour, quenched with Sn(Me)$_3$Cl (2,2 mmol) and then stirred overnight. The reaction mixture was extracted with CH_2Cl_2/H_2O, the organic phases were combined and evaporated under reduced pressure. The crude product was used without further purifications. Dark yellow powder. Yield: 90%. EI-MS m/z 518(M$^+$). ^{1}H NMR (400 MHz, CDCl$_3$, TMS/ppm): δ 7.16 (d, ^3J =3.2, 2H), 7.15 (s, 2H), 7.12 (d, ^3J =3.2, 2H), 0.49 (s, 18H). ^{13}C NMR (100 MHz, CDCl$_3$, TMS/ppm): δ 148.3, 137.5, 135.8, 127.1, 121.3.

3.3.2 Synthesis of NPs

Colloidal solutions of polymer **4-6** were prepared by the reprecipitation method, as already described for polymer P3HT,[285,286] using a THF solution of the polymer added dropwise to mi-liQ water under stirring. DLS and SEM were performed in order to characterize the size of the NPs (see appendix B).

3.3.3 Fluorescence Quantum Yields (φ$_f$)

Emission quantum yields (*QY*) were measured by the comparative method using the equation below:

$$QY\,(\phi_f) = QY_{ref}\,\frac{\eta^2}{\eta_{ref}^2}\,\frac{I}{A}\,\frac{A_{ref}}{I_{ref}}$$

Where the refractive index of the solvents is defined by η, I define intensity while A represents the absorbance value. For yellow colored polymers 7-Diethylamino-4-methylcoumarin was used as reference (ϕf=0.73, 25ºC, ethanol)[295] while red colored polymers quantum yields were calculated using Rhodamine 6G as reference (ϕf=0.95, 25ºC, ethanol).[296]

3.3.4 Polymer and NPs Deposition

The polymers as well as the corresponding NPs were deposited on the PET-ITO electrodes by the spray-casting method. The PET-ITO substrates were placed over a heating plate at 60 °C (for polymers dissolved in $CHCl_3$) or 90 °C (for NPs dispersed in miliQ water). The solutions or dispersions were then spray cast on the electrodes and dried in the heating plate for 1 minute between each layer. The polymeric printed solutions had a 5mg/ml concentration, in chloroform, while the NPs dispersions had a concentration of 3mg/ml (each batch), in miliQ water. For comparison purposes, the color of the final depositions was controlled by *in-situ* absorbance spectra.

3.3.5 Cyclic Voltammetry Measurements

The cyclic voltammetry (CV) was performed using an Autolab PGSTAT 100N potentiostat. The polymers spray-coated on PET-ITO substrates were used as working-electrode; the counter electrode a platinum wire; Ag/AgCl as a reference electrode and an electrolytic solution of $LiClO_4$ (0.1M) in acetonitrile. Additionally, the CV measurements were performed using a scan rate of 20mV/s.

3.3.6 SEM Measurements

SEM analyses were performed on a Zeiss LEO 1530 FE-SEM, operated at 5kV. The samples were spray-casted on a Si/SiO_2 wafer and observed with an In-lens SE detector.

3.3.7 Assembly of ECDs

The produced electrochromic devices (ECD) were assembled using the following structure: PET-ITO / Polymer or NPs / Electrolyte / Polymer or NPs / ITO-PET. The assembly of these electrochromic devices was performed by producing the two substrates of PET-ITO with the material deposited and then closing them together face-to-face using a double-taped adhesive in order to avoid short-circuits between the two PET-ITO substrates with an active area of $1cm^2$ on the working electrode. The electrolyte was deposited by hand filling the "pool" using

the amount calculated accordingly to the volume needed to fill the final ECD. The electrolyte used was a Li^{+} based UV curable electrolyte denominated *Ynv.El.®* property of *Ynvisible®* with the patent nº 20140361211. The absorption spectra of the ECD's (at different potentials) were acquired in a Cary 5000 UV-Vis-NIR spectrophotometer coupled to an Autolab PGSTAT 100N potentiostat. The range of potentials used varied from -1.5V (reduction) and 1.5V (oxidation) for most of the devices. Switching time measurement involves a pre-treatment of 15 cycles with 5 seconds at each potential, followed by 3 cycles with 60 seconds for oxidation and reduction while the charge consumed by the ECD's was calculated from the current (in Amperes) developed during the switching time of the experiment. The charge consumed is used to calculate the coloration efficiency (CE) accordingly to the change of color (in absorbance) using the CE equation.

3.3.8 DFT Calculations

All calculations have been performed with the TURBOMOLE program[297,298] using the PBE0-1/3 functional[299] and a def2-SV(P)[300] basis set. The COSMO solvation model[301,302] has been used to include the effects of a polarizable environment.

<div style="text-align: right;">**4**</div>

HYBRID BLENDS BASED ON A PYRENE-APPENDED POLYMER WITH CARBON NANOTUBES FOR FAST-SWITCHING AND LONG-LASTING ELECTROCHROMIC DEVICES

This chapter is based on a manuscript under submission, to this date. The author contributed to the planning and execution of all the experiments presented in this chapter, including synthesis of the polymers, preparation of the hybrid blends, assembly of solid-state electrochromic displays and their characterization. The author contributed to the interpretation and discussion of all the results, as well as the preparation of the manuscript.

Increasing the performance of solid-state electrochromic devices (ECDs) has attracted a lot of attention recently, due to their applications for commercial products. Among those are the well-known smart windows,[27,28] mirrors,[303] solar cells,[304] and organic light-emitting diodes (OLEDs).[305] Electrochromic displays were also recently developed for smart consumer goods or environmental areas including smart labels, cars, design, lifestyle, wearables and security, promising an ubiquitous presence of such displays as non-intrusive forms of displaying valuable information for human users.[1–9] ECDs are advantageous to these types of applications due to their flexibility, low power consumption and the innumerous possible solutions for an intelligent environment.

Since the market of electrochromic applications is emerging, also urges the necessity to turn the production of ECDs more cost-effective to allow a greater awareness of what this technology can offer. Therefore, the replacement of expensive components embedded in the structure of common electrochromic displays becomes a target in research *e.g.,* indium-tin-oxide (ITO), which is the most widely used material to produce transparent and conductive electrodes, due to its excellent conductivity and optical transparency in the visible region. However, ITO's hard processability and low availability of indium turns ITO as electrode a very expensive material to produce electrochromic devices in a large scale. At the same time, with the increase in the number of possible electrochromic applications, also rises the necessity to have more stable and durable electrochromic materials, to increase product viability in the market.

Conjugated thiophene-based polymers are the most promising color-changing material for electrochromic applications as thin-films,[8,11,223] due to advantages such as extensive color palette, fast switching times in the range of seconds, high optical contrast ratios, mechanical flexibility and durability, accessible straightforward processing (*via* spray-coating, ink-jet etc.) and compatibility with industrial processes like roll-to-roll (R2R) deposition.[306] Among the reported polythiophene materials in solid-state ECDs, only poly(3,4-ethylenedioxythiophene) (PEDOT)-based ECDs are found commercially due to the outstanding performance of PEDOT:PSS composites.[115,307]

The electrochromic properties of conjugated thiophene-based polymers result from an extended conjugated π-electron system where the optical and redox properties of the polymers can be easily tuned by the choice of the monomeric units through synthetic modifications. The donor-acceptor approach, *i.e.* alternating electron-rich and electron-poor units along

the conjugated polymer backbone, is a very effective method to generate low bandgap polymers with tunable colored electrochromic properties.[11,308]

Polythiophene electrochromic materials show very good performances in liquid state[10,122], however these performances are suppressed when a solid-state electrochromic device is assembled. A major obstacle for solid-state devices is the high internal resistance for the ion transfer from the electrode to the solid-electrolyte interface, mainly in the Stern layer.[127] Thus, there has been a great effort to produce gel-based electrolytes for electrochromic applications[309] promoting the use of flexible substrates, while avoiding major loss of electrochromic performance when moving to solid-state ECDs. Indeed, the stability of solid-state ECDs is dependent on the mechanical, electrochemical, chemical and photochemical stress applied on the display.[310] Mechanical damages can occur from defects in the thin-films during manufacturing while non-uniform voltage can lead to electrochemical damages in the film producing aggregation.[225] For these reasons, there is a very short number of solid-state ECDs presenting high durability in the scientific literature, *e.g.*, ionic liquids and WO_3.[59,311]

Moreover, in organic conjugated polymers like polythiophenes, there are drawbacks that hamper their large-scale application in electrochromic systems. Low electric conductivity and poor long term electrochemical stability lead to irreversible degradation of the displays limiting their range of applications.[10,15,128]

It is reported in the current state-of-the-art the use of carbon nanotubes (CNTs) to enhance the electrochemical properties of polythiophene materials with improved stabilities and lower charge-transfer resistances.[150,170,171,312] This enhancement occurs due to their very low electrical percolation threshold,[153] high mechanical resistance[154] and their semiconducting characteristics,[155] due to a high density of delocalized electrons.

More specifically, the use of an external electron rich unit, as pyrene, promotes π-π stacking interactions with CNTs allowing stable dispersions, thus, a processable ink for electrochromic applications. This π-π interaction between an electron-donor rich unit like pyrene and CNTs has already been reported, through the production of hybrid materials with enhanced properties used in fluorescence microscopy,[162,163] biology,[164,165] catalysis,[166] sensors,[167,168] and opto-electronic devices,[169,170] including electrochromism.[171]

Thus, it was explored an approach to increase the stability of polythiophene electrochromic materials through the formation of supramolecular structures using MWCNTs, based on the strong interaction between pyrene and CNTs.

In this chapter, it is reported the increased stability of CNTs dispersions using a pyrene-appended polymer empowering the production of very homogenous thin-films from chloroform solutions, enhancing electrochromic performances. In detail, very stable hybrid dispersions were obtained using a newly synthesized polythiophene-based copolymer with a pyrene-appended unit (PTP) with different wt.% (0 to 10%) of MWCNTs, in chloroform:toluene (5:1) mixtures. The hybrid blends (PTP/MWCNTs) were spray-coated in PET-ITO substrates and high-performance ECDs were assembled. A systematic study of the ECDs performance was executed to evaluate color contrast (ΔAbs, Δ%T and ΔE), switching times (t_{90}), charge consumed (Q), coloration efficiency (CE) and cyclability. Consequently, hybrid solid-state ECDs containing 7.5 wt.% of MWCNTs, when compared with ECDs using only PTP, presented higher color contrast (ΔT=17.8% *vs* 12.9%) and significantly faster switching times for the reduction process (t_{90}^{Red}= 0.3s *vs* 3.6s). In terms of cyclability, the hybrid ECD showed a very high durability with a number of cycles >35000 *vs* the ≈7000 cycles performed by the ECD using the pristine PTP material.

4.1 Results and Discussion

The main goal of this study is to synthesize a polymer containing a pyrene-appended moiety capable of engaging in anchored π-π interactions with the MWCNTs for the possible production of ITO-free electrochromic devices (see Figure 4.1).
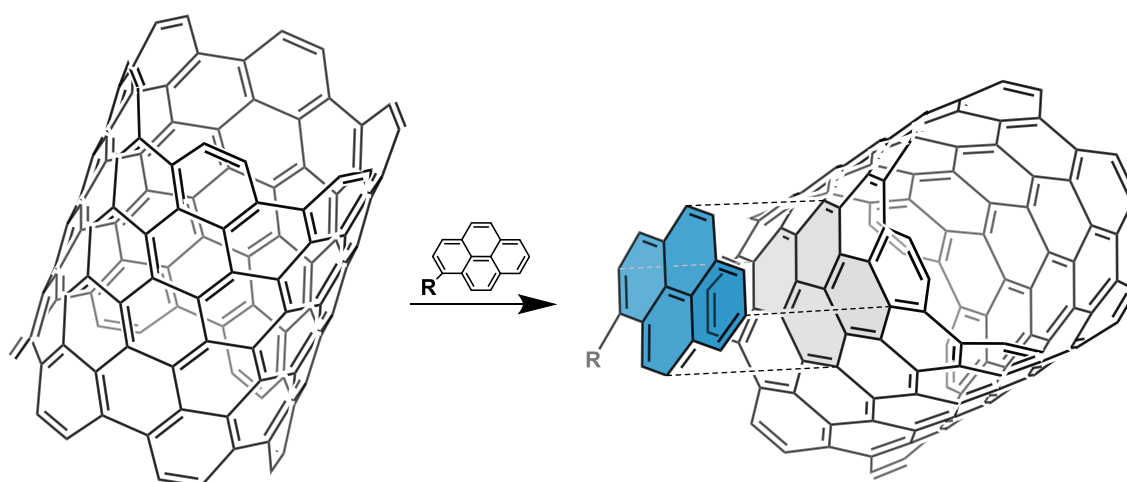

Figure 4.1. Concept of π-π stacking interactions between the outer
wall of MWCNTs CNTs and a pyrene unit.

This interaction[163,313–315] is expected to anchor the pyrene-appended copolymer with the CNT and produce a stable dispersion of the polymer-MWCNTs mixture to obtain a processable ink and fabricate ITO-free high-performance ECDs using PET substrates. Since PEDOT is known to have intrinsic electrical conductivity in its oxidized form (since it is a *p*-type semiconductor), has low redox potential required to observe color transitions (±1.5V), high color contrast and high coloration efficiencies,[307] the goal was to use a suspension of a PEDOT derivative based-polymer / MWCNTs directly on a transparent substrate (PET) avoiding the use of ITO, thus, producing a ITO-free high-performance ECDs. Following the motivation, a PEDOT derivative was synthesized with a pyrene-appended unit presented in Figure 4.2.
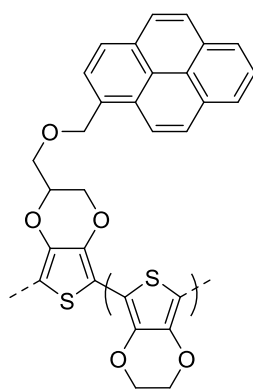

Figure 4.2. PEDOT derivative polymer (**9**) synthesized with a pyrene-appended unit.

The monomer containing the pyrene-appended moiety (**9a**) was synthesized and provided through a collaboration with the University of Vienna and the synthesis is described in the experimental section.

The synthesis of the PEDOT derivative (**9**) was achieved through a straightforward polymerization of monomers **9a** and 3,4-ethylenedioxithiophene (EDOT) using ferric chloride (FeCl3) *via* oxidative polymerization,[316] obtaining a black powder (see experimental section). In the synthesis of **9**, the equivalents of the monomer **9a** were adjusted (0.1eq – 10%) to gain sufficient interaction with the whole range of investigated CNTs loadings (0-10 wt.%) in order to provide stable and processable enough dispersions for electrochromics device integration.[315] However, the black powder obtained for polymer **9** is highly insoluble (no solubility was found on a high range of solvents), and the 1H-NMR characterization of this polymer could not be performed.

It was necessary to redesign the synthetic strategy to produce a polymer with acceptable solubility in common organic solvents, but still containing the pyrene-appended unit for the π-π anchoring of the aromatic unit with the wall of the CNT.

Dyer *et al.* published in 2010 the synthesis of a monomer that, within its structure, presents a di-alkyloxy chain attached directly to the thiophene unit (see Figure 4.3). The electron-donor effect of the two oxygens directly attached to the thiophene allows a lowering of the redox potential while the long alkyl chains induce solubility and steric distortion to the polymer.[11] These two features were suitable for its use on the synthesis of a new copolymer using this described monomer **10a**.
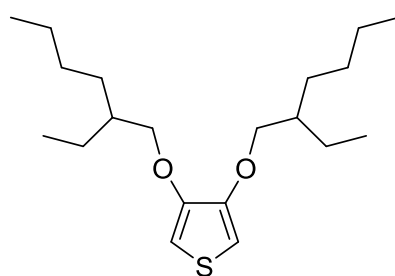
Figure 4.3. Monomer **10a** described by Dyer *et al.*[11]

Monomer **10a** was synthesized accordingly to the published procedure *via* a *p*-toluenosulfonic acid-catalyzed transetherification reaction between 3,4-dimethoxythiophene with 2-ethylhexanol.[11] Afterwards, monomer **9a** and **10a** were used to synthesize a new copolymer **10**, also with a 10% ratio of the pyrene-appended unit (see
Scheme 4.**1**). Homopolymer based on 10a was also synthesized (**11**) for comparison studies (see experimental section).
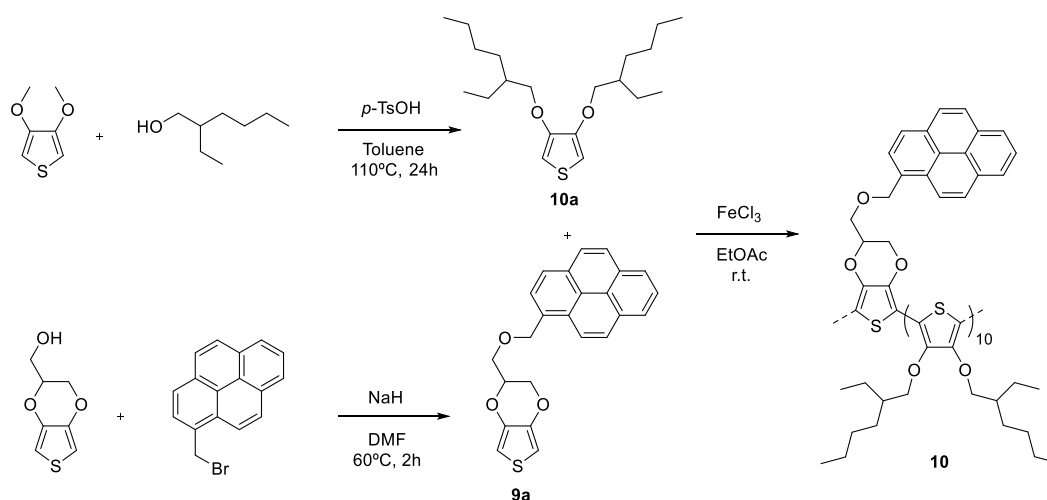
Scheme 4.1. Synthesis of monomers **9a**, **10a** and copolymer **10**.

The newly synthesized copolymer **10**, henceforth designated as <u>PTP</u>, presented a dark orange coloration and showed solubility in chloroform after a brief sonication (10min). The characterization of PTP was performed by ^{1}H-NMR spectroscopy (see appendix C.1.1.1-1.1.5), UV-Vis spectroscopy (see Figure 4.4) and its average chain length was determined with a combined electrospray deposition (ESD) and variable temperature Scanning Tunneling Microscopy (STM) analysis performed in ultrahigh vacuum conditions, enabling the determination of the polymeric strands with monomeric resolution (see Figure 4.5).[317] Due to the limited solubility of PTP, it was not possible to determine its molecular weight using gel permeation chromatography (GPC).

The presence of the pyrene moiety on PTP was confirmed with ^{1}H-NMR spectroscopy by the well-defined aromatic feature between 7 – 7.7 ppm assigned to the presence of the pyrene present on monomer **9a** (see figure C.1.1.5 in appendix). Additionally, UV-Vis spectroscopy of PTP in solution shows a broad absorbance band from 320 to 600nm with a peak located at 453nm (contribution from monomer **10a**), and a very distinctive spectroscopic fingerprint from the pyrene moiety appended on monomer **9a** at *ca.* 360nm (see Figure 4.4).
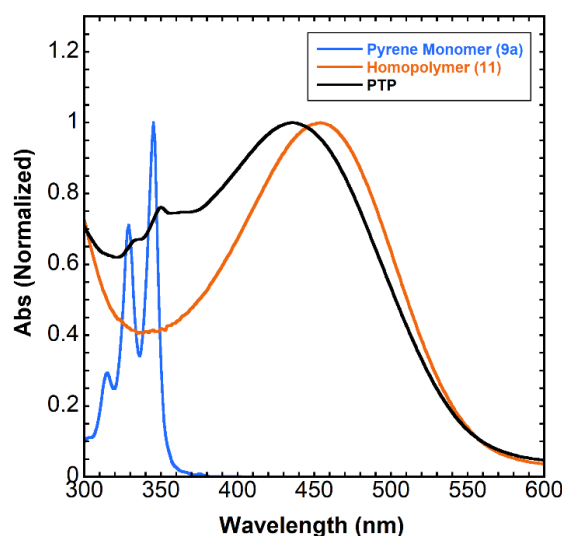
Figure 4.4. Absorption spectra, in chloroform solutions, of the pyrene monomer (blue), homopolymer **11** (orange) and PTP (black). Fingerprint of the pyrene unit can be observed at *ca.* 360nm in PTP.

From the STM characterization performed in collaboration with the University of Vienna, PTP was electrosprayed from a CHCl$_3$:MeOH (4:1 v/v) solution and deposited into a clean Au(111) mica substrate under vacuum. The STM characterization shows straight and extended

95

structures with sharp features attributed to the individual polymer strands. The average length of the polymer chains was evaluated with the majority length between the range of 10 – 30 monomers where a high regularity along the backbone of the polymer can be observed (see Figure 4.5).

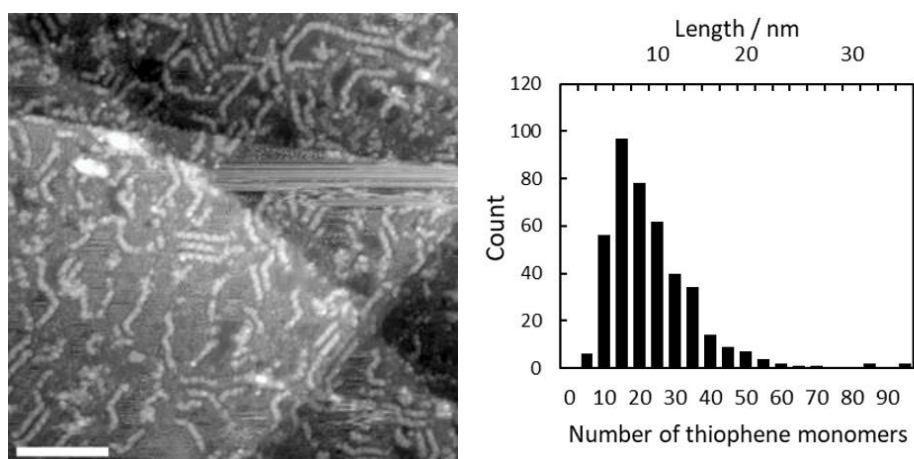
Figure 4.5. Length distribution of PTP obtained by STM analysis performed (scale bar 20nm). Credits to University of Vienna.

With the confirmed presence of the pyrene unit in the newly synthesized copolymer, a blend dispersion of MWCNTs with PTP was optimized. The optimization of this blend started by testing the contact angle of a selection of solvents on PET substrates considering the solubility of the polymer and boiling points (see experimental section and Figure C2.1). The importance on the choice of the solvent / solvent mixture is crucial to prevent coffee-stain effects upon deposition using solvents with different evaporation rates.[226] For deposition techniques like spray-casting or ink-jet, an ink formulation using low boiling point solvents is of great importance since a fast evaporation of the solvent or solvent mixture creates homogeneous films and reduces the exposure time of the material to higher temperatures.[318]

The solvent optimization led to a mixture of CHCl$_3$:toluene in a 5:1 ratio with a contact angle of 8° between the surface of the PET surface and a drop of the solvent mixture (liquid-solid interaction). The solvent mixtures were tested by drop casting in PET substrates at 60°C to evaluate the coffee-stain effect, which was absent when using the optimized solvent mixture with solubilized PTP (see Figure 4.6).
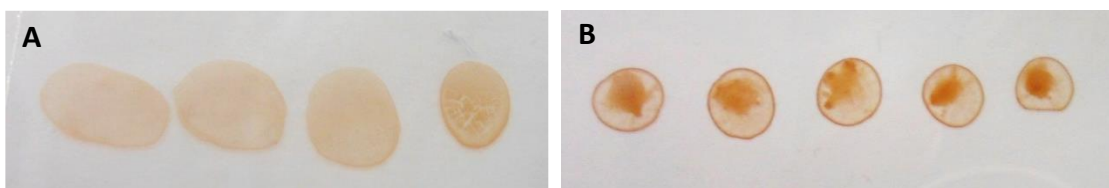
Figure 4.6. A - Drop-cast of PTP dissolved in CHCl₃:toluene in a 5:1 ratio; B - Drop-cast of PTP solubilized in CHCl₃. Replicas of the same dispersion in A and B.

Thus, blends containing different amounts of MWCNTs (0 – 10 wt. %) were prepared by sonicating 10mg of PTP in 10mL of CHCl₃ for 10 minutes at 40°C. The amounts of MWCNTs (0.25 – 1mg) were added to the solution and sonicated for additional 10 minutes before the addition of 2mL of toluene to achieve a CHCl₃:toluene (5:1 v/v) solvent ratio. The final mixture was again sonicated for 30 minutes at 40°C producing a homogeneous and stable dispersion of the MWCNTs (dispersions were stable for three days without sedimentation (see appendix C.3.1). For comparison, the same procedure was replicated using polymer 11 (non-pyrene-appended polymer) where, a homogeneous dispersion was not achieved despite the sonication for 6 hours at 40°C (see appendix C.3.2).

UV-Vis absorption measurements of the dispersions presents a decrease of light transmission with the increase of CNTs loading, observed by the constant increasing of the absorbance at *ca.* 750nm (see

Figure 4.**7**) assigned to the plasmonic absorbance of the CNTs. The absorbance band for the dark orange color of PTP is centered at 475nm and detectable until the loading of 7.5% of CNTs. At 10% of CNTs the dispersion significantly darkens, causing it to become unnoticeable the color of PTP.
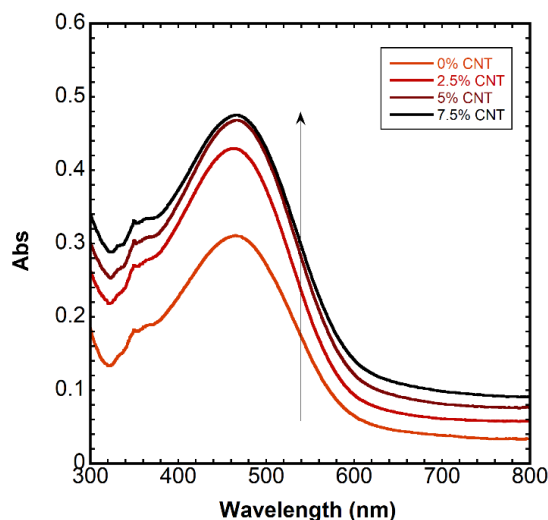

Figure 4.7. UV-Vis absorption spectra of the dispersions using PTP + 0 to 7.5% MWCNTs of 150µl from the optimized blend diluted to 5mL of CHCl₃:toluene (5:1 v/v).

The blends using different amounts of MWCNTs (0 – 10 wt. %) were coated in PET substrates and measured their electric resistivity. Using 0% of MWCNTs the film was nonconductive while the addition of 2.5 – 10% of MWCNTs resulted in resistivity values that varied from 130 to 20MΩ. The resistivity values obtained are far from resistivity values of commercially available PET-ITO (typically from 60 to 400 Ωsq)[319] and therefore insufficient to promote electrochromic activity in solid-state devices.

Nevertheless, the hybrid blends were spray-coated in PET substrates and cyclic voltammetry was performed to the films in solution, using an electrolytic solution of LiClO$_4$ (0.1M) in acetonitrile (see details in the experimental section). The CV measurements of the spray-coated films using 7.5 and posteriorly 15 wt. % of CNTs, did not present any electrochemical signal or color transition from PTP or PTP/MWCNTs hybrid material (see Figure 4.8).
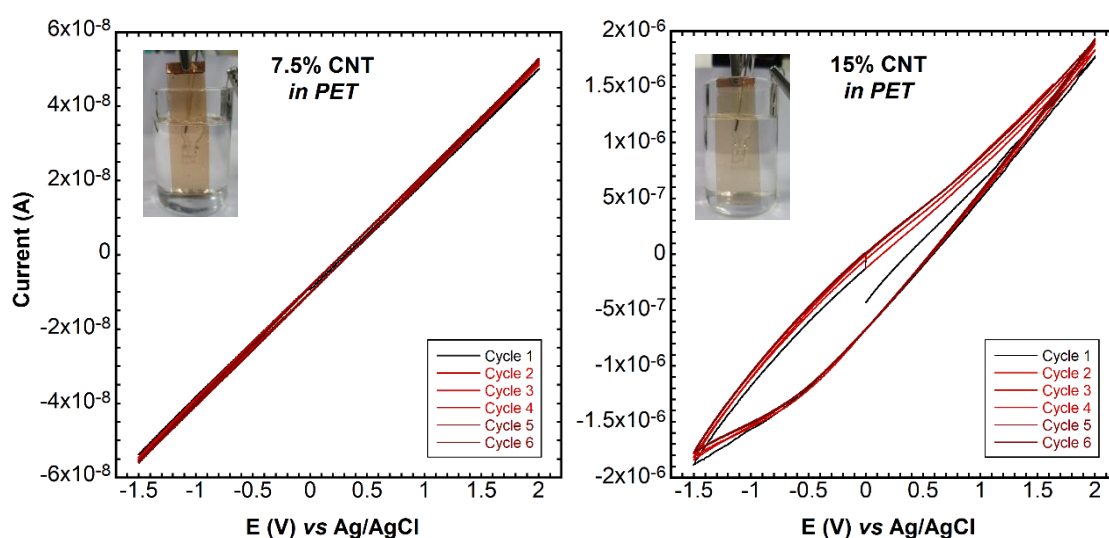

Figure 4.8. Cyclic voltammetry measurements to the blends spray-coated in PET substrates using 7.5 and 15% of MWCNTs. CV performed from -1,5 to 2V at 20mV/s using an electrolytic solution of LiClO$_4$ (0.1M) in acetonitrile, reference electrode Ag/AgCl, counter-electrode a platinum wire and the working electro the PET substrate with the coated blend (see inset pictures).

Despite the absence of electrochromic activity using the optimized blends spray-coated in PET substrates, there was still a huge motivation to take one step further with the developed blend, since the synthesis of an electrochromic pyrene-appended copolymer was achieved (PTP), and a very stable dispersion of the CNTs was obtained. Even if a further increase of %CNTs could improve the electrochemical signal, the production of ITO-free ECDs, at this point, was difficult to achieve since the addition of an increased amount of CNTs (in %) greatly reduces light transmission making the films black preventing to observe any electrochromic transition.

The study evolved to the assessment of eventual π-π interaction between pyrene-appended copolymer and different amounts of CNTs which could improve the performance of standard ECDs using PET-ITO substrates.

Hybrid films coated in PET-ITO substrates were produced using the spray-casting technique. The spray-casting technique is a very versatile deposition method widely applied for its high throughput and compatibility with large scale fabrication methods. Additionally, spray-casting allows the direct coating of a solution or dispersion without the addition of any binders/surfactants that could affect the electrochromic activity of the material.[318]

Thus, freshly preparer PTP / MWCNTs blends (0 – 7.5 wt. %) were manually sprayed in PET-ITO substrates using different number of sprayed layers (1, 3, 5, 7 and 9; see Figure 4.9). The spray-casting of the blends on the PET-ITO substrates was performed using an aerograph with a continuous applied pressure of 1 bar for each layer. To assure the homogeneity of the depositions, the aerograph with a 0.33mm opening was kept at a constant distance from the substrate (5cm) so that only the aerosol part of the sprayed mixture was deposited into the plastic substrate. Additionally, the spraying rate was kept constant for each layer and the PET-ITO substrate was placed on top of a heating plate at 60°C to promote fast evaporation of the solvent, to avoid coffee-stain effects in the deposited films.

The UV-Vis absorption spectra of the films presented, as expected, a trend of increase in absorption of the spray-coated PTP/MWCNTs films with the increase on number of layers (see appendix C.3.3). In figure 4.8 the maximum of absorbance of the copolymer at 475nm interestingly becomes more perceptible, especially in the films using 9 layers. This occurs due to an increased regioregularity observed by STM in the PTP/MWCNTs thin-films, originated from the π-π stacking of the pyrene units with the CNT surface. A possible surface plasmon enhanced absorption may occur in these blends contributing to the observed absorption features.[320]
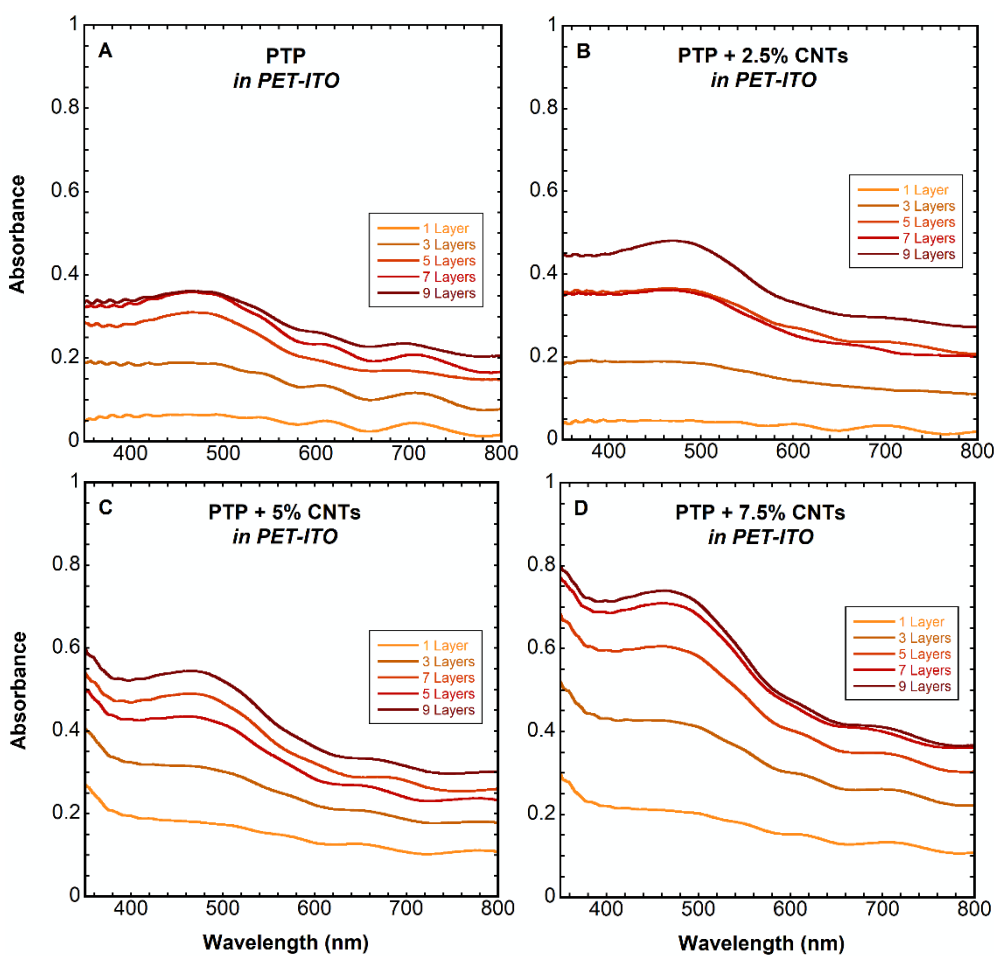
Figure 4.9. UV-Vis absorption spectra PET-ITO substrates spray-coated with the optimized blends using 1, 3, 5, 7 and 9 layers. (**A -** PTP; **B -** PTP + 2.5% CNTs; **C -** PTP + 5% CNTs and **D -** PTP + 7.5% CNTs).

Additionally, the morphological characterization of the hybrid films by scanning electron (SEM) and atomic force microscopy (AFM) was also performed. The top-view SEM images of deposited PTP and the hybrid blend using 7.5% of MWCNTs show a very different morphology of the films when the copolymer is deposited alone, or as a hybrid. Specifically, films of PTP present polymeric aggregates within the 200 – 300nm range. These aggregates do not form continuous films which develop several voids throughout the whole sample. On the other hand, the hybrid PTP/MWCNTs forms a much more continuous and homogeneous film. These observations are consistent with what was observed during the AFM measurements (see Figure 4.10).
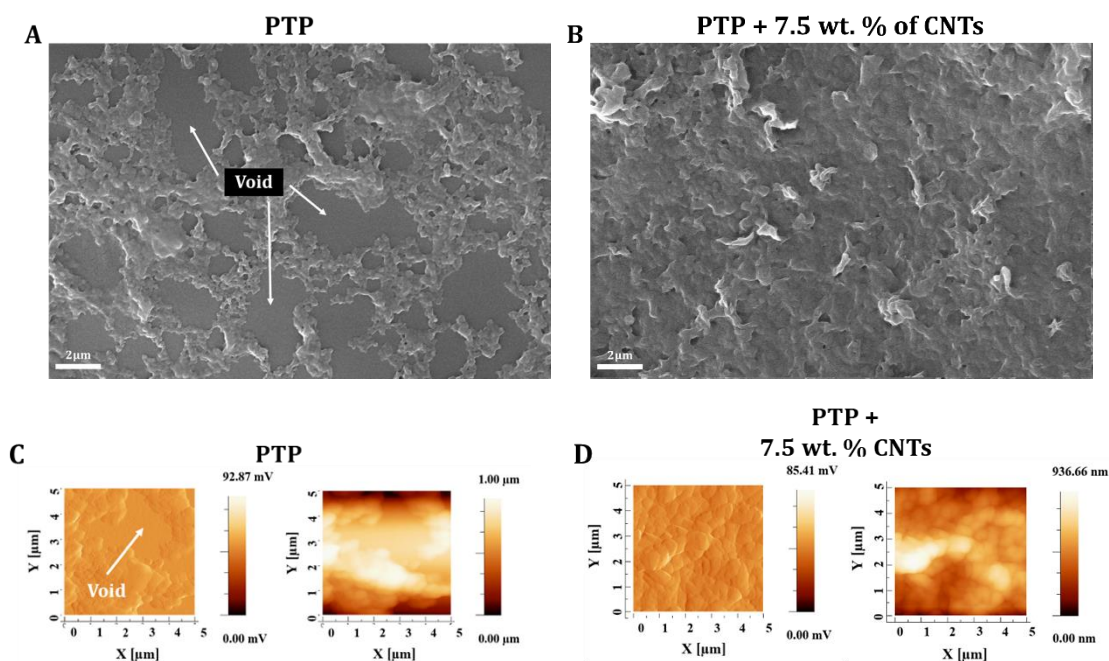
Figure 4.10. SEM (A + B) and AFM (C + D) images of PTP and the hybrid blend with PTP/MWCNTs (7.5 wt.%) spray-coated in a silicon substrate ate room temperature. Credits to University of Vienna.

The electrochromic behavior of the hybrid films with optimized blend of PTP/MWCNTs in PET-ITO substrates was evaluated by cyclic voltammetry measurements in solution. Due to the possible increased plasmonic effect and to maximize the electrochemical signal on the cyclic voltammetry, 9 layered films were used for the CV measurements. The coated films were dipped in an electrochemical cell with a three-electrode configuration using an electrolytic solution of $LiClO_4$ in acetonitrile (see experimental section for detailed description). As presented in Figure 4.11A - E, all the hybrid films using different % of CNTs showed electrochemical signal when voltage was applied, switching from dark orange color (reduced state) to sage green (oxidized state). The redox potential of the fully conjugated copolymer backbone was identified at 0.52/0.82V while, at 1.46V it is visible the oxidation peak of the pyrene-appended unit (see Figure 4.11A). Noticeably, the identified pyrene peak is quenched after the first cycle, probably due to the adsorption of the pyrene on the surface of the working electrode.

Figure 4.11F represents the cyclic voltammetry measurement of a spray-coated film of copolymer 12 (see experimental section), synthesized without the presence of the pyrene moiety. As expected, the CV measurement of copolymer 12 thin film did not present any pyrene signal at *ca.* 1.5V.
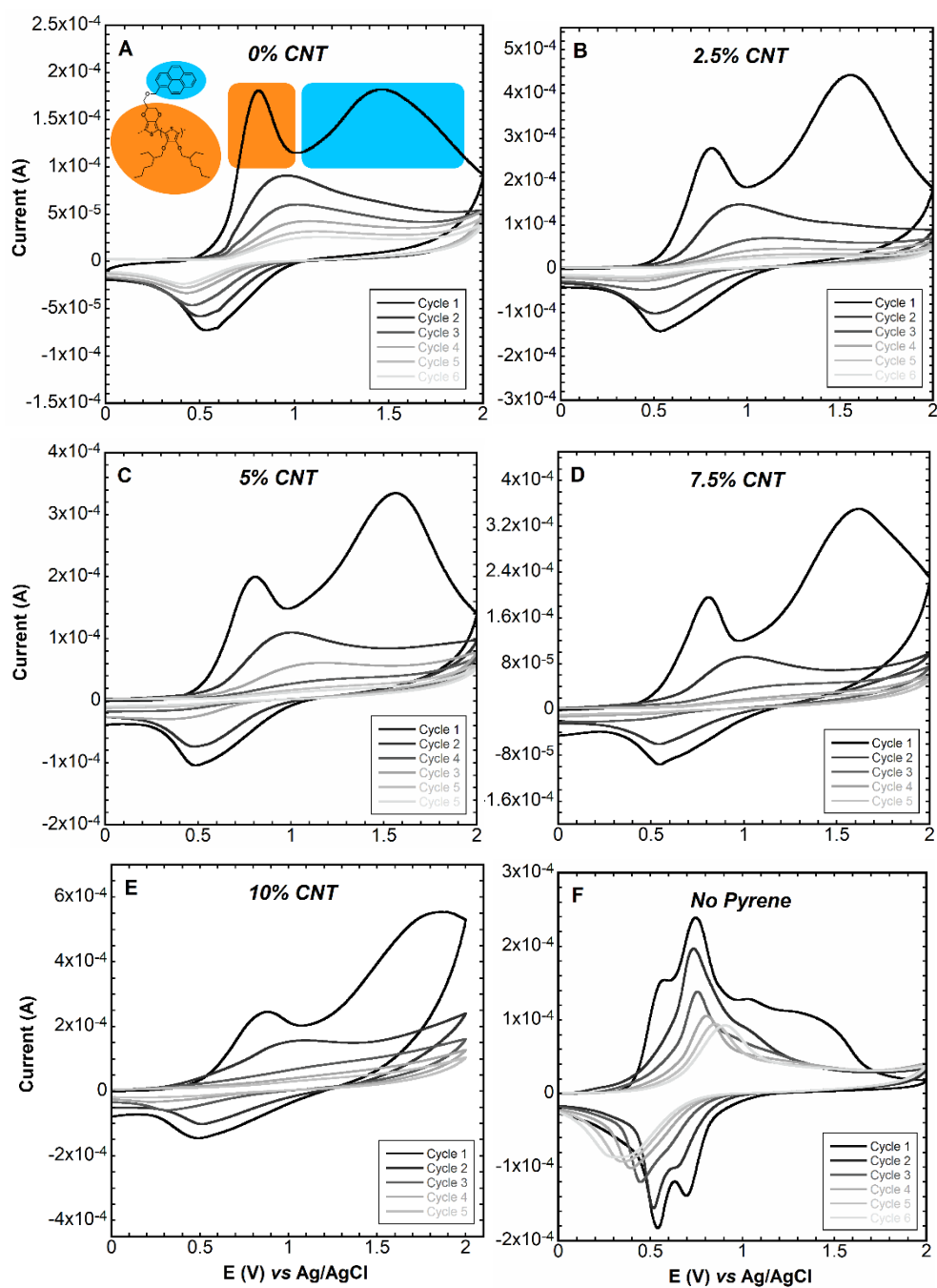
Figure 4.11. Cyclic voltammetry measurements performed to the hybrid films using an electrolytic solution of LiClO$_4$ (0.1M) in acetonitrile. CVs performed between 0 and 2V with a scan rate of 20mV/s. **A -** PTP; **B -** PTP + 2.5% CNTs; **C -** PTP + 5% CNTs; **D -** PTP + 7.5%; **E -** PTP + 10% CNTs and **F –** Copolymer with no pyrene unit.

Interestingly, the oxidation peaks from the conjugated polymer (0.82V) and the pyrene (1.46V) present their maximum electrical current value with a ratio very close to 1:1 (Figure 4.11A). Remarkably, along the increment of % CNT in the spray-coated blend (2.5 to 10 wt.%), the current ratio between the two identified peaks increases in an almost linear trend until a 1:2.5 ratio, since increasing the amount of CNTs also increases the number π-π interactions occurring between the pyrene-appended moieties and the CNTs (see Figure 4.12).

This result reveals a clear interaction of the hybrid blend in spray-coated films, due to the increase of charge transfer between the pyrene and the CNTs, resulting in an effective increase of current consumed during the CV. This effect explains the improved colloidal stability of the dispersions in CHCl$_3$:toluene mixtures that eases the formation of homogeneous films using the spray-casting technique for ECDs fabrication.
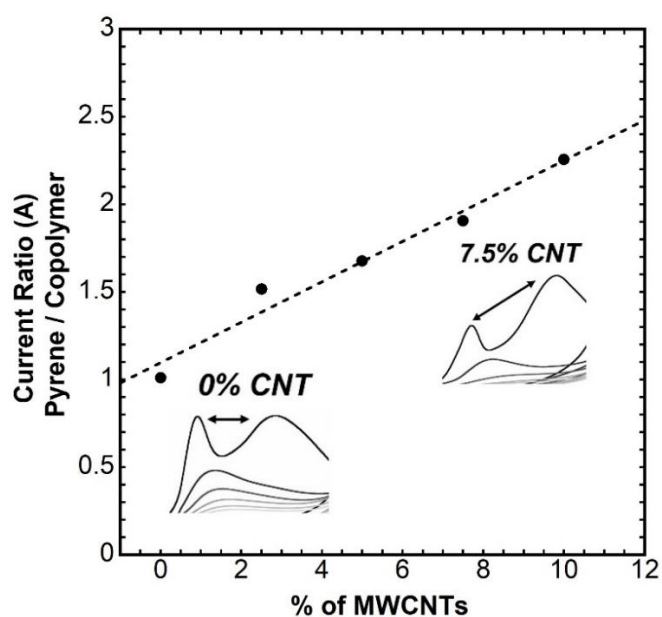

Figure 4.12. Current (in amperes) ratio between the PTP backbone oxidation peak and the peak attributed to the pyrene unit appended to PTP whilst the increase of %CNTs in the blend.

Solid-state ECDs were assembled with a vertical stack architecture using a UV curable Li^{+}-based gel electrolyte denominated *Ynv.El.®* property of Ynvisible® (patent n° 20140361211A1)[207] deposited between the previously spray-coated PET-ITO substrates using the optimized blends (see appendix C.4.1).

The performance of the assembled ECDs was evaluated through spectroelectrochemistry, switching time (ST), charge consumption (Q), optical contrast (in ΔAbs and Δ%T) and durability (cycling), as described in section 1.5.7. Figures of merit were calculated for all the assembled ECDs analyzing the influence of different % of CNTs in the blend (0 – 10 wt.%), application of different voltages (0.5 to 1.8V) and different number of layers of the blends spray-coated in PET-ITO substrates (3, 6, 9, 12 and 15), see Table 4.1, where:

The values calculated and presented in table 4.1 were obtained by performing *in* situ spectroelectrochemical measurements at a specific wavelength were the optical contrast of the films containing PTP/MWCNTs is maximum, namely 475nm. Qualitative characterization of the ECDs was measured both before and after the cycling measurements when the *optimum* conditions (highlighted in gray on Table 4.1) were found for this system (%CNTs= 7.5%, E(V)= 1.5V, number of layers=9). The cycling experiments were performed by recording color contrast upon application of 5s of reduction/oxidation cycles (-1.5/1.5V) where 1cycle=10s (see figures of merit in table 4.1), calculated using L*a*b* coordinates.

By the spectroscopic measurements performed to the assembled ECDs, upon application of potentials from 1.5 to -1.5V, all the devices exhibited dark orange (reduced state) – sage green (oxidized state) reversible color transitions (see appendix C.4.2). The maximum color contrast is located in the visible region of the UV-Vis spectrum at *ca.* 475nm, corresponding to a bleaching of the π,π^* transition of the neutral polymer. At the same time, electronic transitions at the red/NIR regions appear for the oxidized form of the polymer. As previously described by Heeger[321] and further mentioned by Reynolds,[14] this effect is due to an increase in the conjugation of the polymer backbone upon formation of bipolarons during the oxidation process which is responsible for the dramatic color change observed during the switch of the electrochromic device, through the combination of the disappearance of the π,π^* band at 475 and the appearance of a broad absorption band near the red/NIR region of the spectrum (see Figure 4.13).

Table 4.1. Figures of merit for color contrast (**ΔAbs** and **Δ%T**), switching times (**t_{90}^{Ox}**, **t_{90}^{Red}**), charge consumed (**Q_{Red}**, **Q_{ox}**) and coloration efficiency (**CE**) for all the produced electrochromic devices varying: % of MWCNTs added to the blend (**%CNT**), potential applied to the device for the color switch (**E(V)**) and the number of layers (**n**) added by spray-coating to the PET-ITO. All the values were calculated in a switching time experiment using 60s at each potential. The influence of the number of cycles on the performance using <u>7.5% of CNT, ±1.5V and 9 layers</u> *vs* <u>0% of CNT, ±1.5V and 9 layers</u> were 1 cycle = 10s. *Optimum* conditions for the hybrid ECDs highlighted in gray.

|							
Influence of %CNT (E=1.5 V, 9 layers)							
CNT (%)	ΔAbs	Δ%T	t_{90}^{Ox} (s)	t_{90}^{Red} (s)	Q_{red} (mC.cm^{-2})	Q_{ox} (mC.cm^{-2})	CE (C^{-1}.cm^2)
0	0.097	12.9	4.6	3.8	-0.89	1.13	71.5
2.5	0.107	14.5	4.9	0.5	-1.09	1.08	90.8
5.0	0.103	13.8	4.6	0.3	-1.22	1.16	80.0
7.5	0.148	17.8	3.6	0.3	-1.33	1.36	99.2
10.0	0.190	18.9	6.6	0.3	-1.82	1.62	98.9
Influence of E(V) (7.5% CNT, 9 layers)							
E (V)	ΔAbs	Δ%T	t_{90}^{Ox} (s)	t_{90}^{Red} (s)	Q_{red} (mC.cm^{-2})	Q_{ox} (mC.cm^{-2})	CE (C^{-1}.cm^2)
0.5	0.008	0.6	16.0	14.0	-0.05	0.05	84.8
1.0	0.060	6.4	11.0	0.9	-0.24	0.25	220.5
1.25	0.142	16.6	3.1	0.4	-0.65	0.71	189.5
1.5	0.148	17.8	3.6	0.3	-1.33	1.36	96.6
1.8	0.166	18.8	2.5	0.3	-2.26	2.64	58.0
Influence of number of layers (7.5% CNT, E=1.5 V)							
Layers (n)	ΔAbs	Δ%T	t_{90}^{Ox} (s)	t_{90}^{Red} (s)	Q_{red} (mC.cm^{-2})	Q_{ox} (mC.cm^{-2})	CE (C^{-1}.cm^2)
3	0.061	9.3	1.1	0.2	-0.47	0.58	106.8
6	0.078	10.5	2.3	0.2	-0.91	0.93	77.4
9	0.148	17.8	3.6	0.3	-1.33	1.36	99.2
12	0.172	18.1	7.1	0.4	-1.99	1.93	81.8
15	0.177	18.6	7.3	0.5	-2.10	2.10	79.4
Influence of the number of cycles (0% vs 7.5% CNT, E=1.5 V, 9 layers)							
cycles	ΔAbs	Δ%T	t_{90}^{Ox} (s)	t_{90}^{Red} (s)	Q_{red} (mC.cm^{-2})	Q_{ox} (mC.cm^{-2})	CE (C^{-1}.cm^2)
0% CNT							
0	0.120	13.8	2.6	1.0	-0.75	0.68	157.9
1600	0.085	10.5	2.7	3.2	-0.47	0.39	179.6
16000	0.000	0.1	—	—	—	—	—
7.5% CNT							
0	0.183	17.6	3.4	0.3	-1.24	1.08	150.8
1600	0.168	16.1	3.2	0.3	-0.98	0.93	167.5
16000	0.135	13.0	1.3	0.6	-0.56	0.62	212.8

All the values were calculated at 475nm.
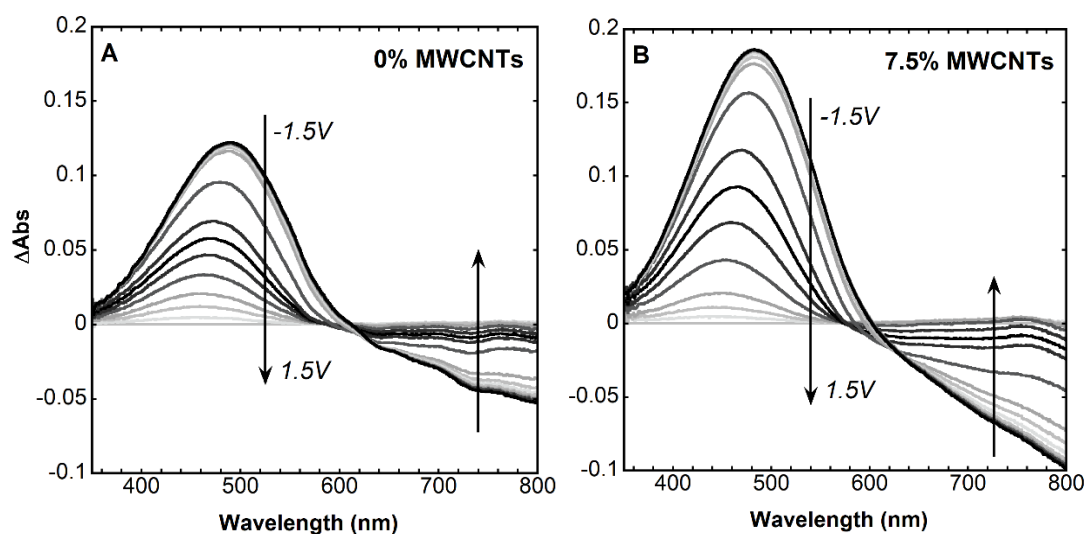
Figure 4.13. ∆Abs calculated from the UV-Vis spectroelectrochemistry measurements to the electrochromic devices using 0% and 7.5% of CNTs blend with PTP.

Throughout the characterization of the devices, it was varied the amount of CNTs, applied potential and number of coated layers, in order to understand what was the *optimum* set of parameters that maximizes the performance of these ECDs using PTP and MWCNTs (see appendix C.4.3).

Specifically, increasing the wt.% of MWCNTs in the composition of the hybrid blend reflected in a remarkable decrease of the reduction switching time of the ECDs, as well as an increase of color contrast when CNTs are present (see Table 4.1 and Figure 4.13). The best performance was registered for the devices containing 7.5% of MWCNTs (see Figure 4.14), for which the t_{90}^{Red} decreased from 3.6 s to 0.3 s, corresponding to a more than 10 times faster electrochromic device. The oxidation time (t_{90}^{Ox}) also decreased, (4.6 to 3.6s) but the decrease is much smaller. This is probably due to the fact that during the reduction process the CNTs act as very effective charge-balancing dopants.[157] Thus, the addition of CNTs and the promoted π-π stacking interaction with the polymer reduces the resistance of charge transfer, emerging enhanced electrochromic properties, including CE.

The use of 7.5 wt.% of CNTs while applying 1.5/-1.5V to films using 9 layers deposited by spray-casting presented the best compromise between color contrast, switching time and consequently coloration efficiency, wherein, additional layers increase film thickness promoting slower switching times. In detail, from Figure 4.15A, it is possible to observe during the reduction process a more abrupt increase of absorbance for the electrochromic device using 7.5% of CNTs.
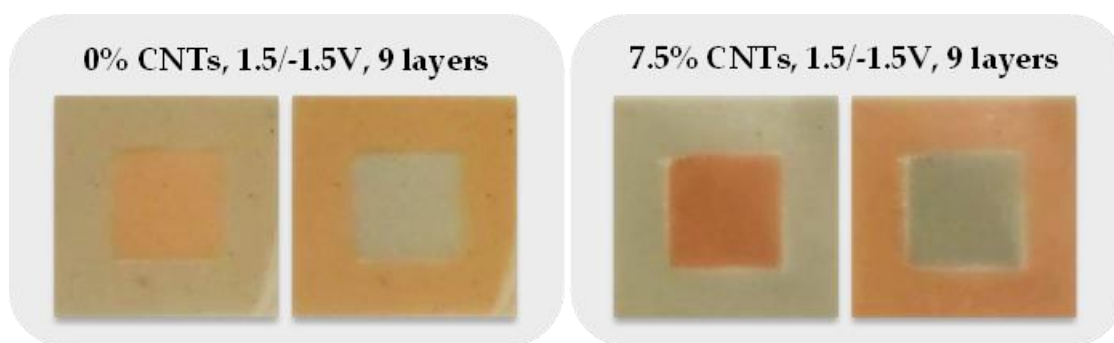
Figure 4.14. 9 layered-assembled electrochromic devices using 0% CNTs *vs* 7.5% CNTs while applying 1.5/-1.5V for 60 seconds in PET-ITO substrates.

Additionally, increasing the amount of CNTs in the optimized blend promotes a very significative improvement regarding durability. For the blend using 7.5 wt.% CNT, a qualitative characterization was performed before and after 16000 cycles where the device using the pristine PTP already does not shown any electrochromic switch, while a device containing 7.5 wt. % of CNTs switches with negligible degradation regarding switching time and color contrast (see Table 4.1 and Figure 4.15B). The same increase of performance (faster switching times and higher durability) was not observed to freshly prepared devices using the non-pyrene polymer **11** blended with 7.5 wt. % MWCNTs assembled following the previously optimized procedure (results in appendix, figures C.4.4 / C.4.5 and table C.4.1).
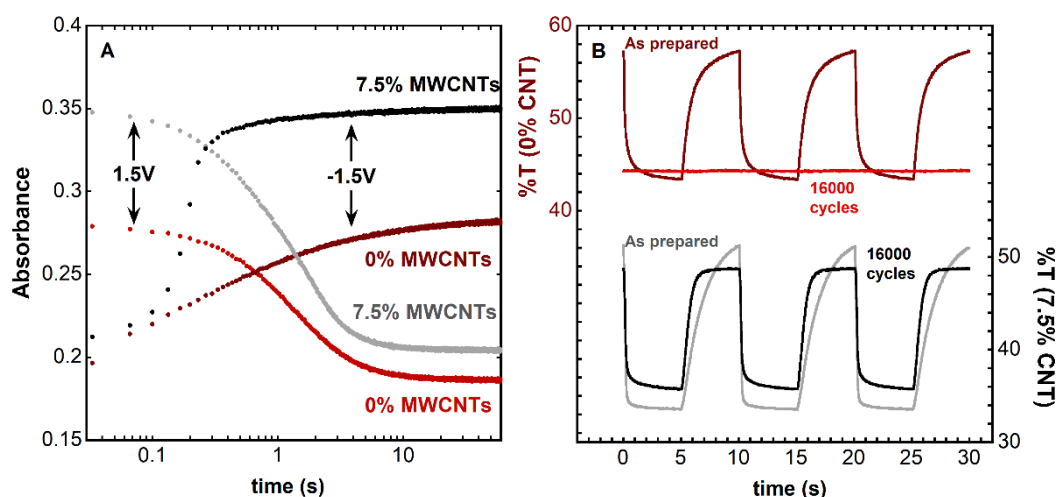

Figure 4.15. A - Variation of the absorbance during the switching time experiment for ECDs using 0 wt. % CNTs *vs* 7.5 wt. % CNTs; **B –** Comparison of color contrast between the ECDs using 0 wt. % CNTs *vs* 7.5 wt. % CNTs before and after the cycling measurement (16000 cycles).

This increase of performance regarding the switching time, occurs due to the formation of very homogeneous films when deposited in form of a hybrid blend. The presence of MWCNTs in

the blend induces regioregularity to the film, which generates higher electric mobility of the polymeric chains[322] (observed and discussed previously from STM results) and avoids the formation of polymer aggregates increasing the contact area between the conductive layer (ITO) and the deposited hybrid films (see SEM and AFM, Figure 4.10). This regioregularity and the higher number of contact points between the hybrid layer and the ITO also justifies the increase of color contrast (see Figure 4.13), since a larger number of PTP/CNT species are effectively available for electrochemical switch. This increased number of polymeric units performing electrochromic switch also generates a higher charge consumption as reported in Figure 4.16 using the values of Table 4.1.
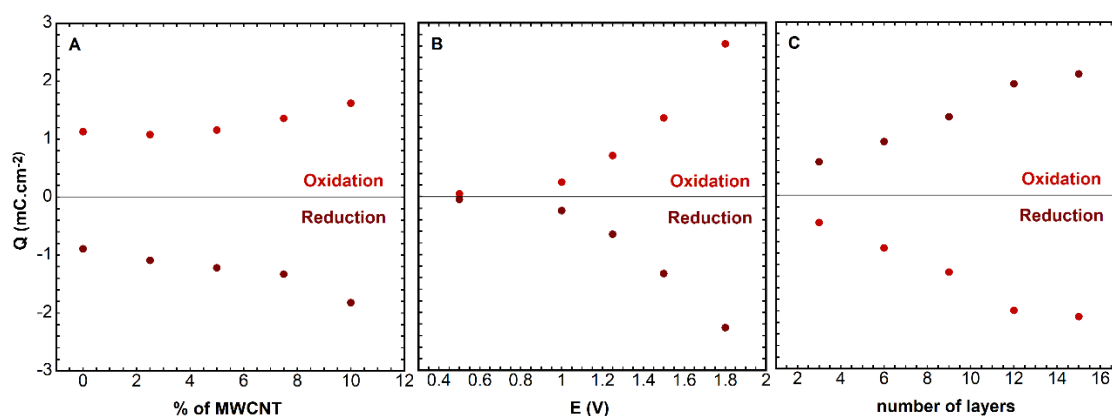

Figure 4.16. Charge consumed by the different electrochromic devices (values from Table 4.1) during redox varying: **A -** % of MWCNTs; **B -** Potential applied; **C -** number of layers spray-coated.

Furthermore , the simultaneous exposure of the electrochromic polymers (namely polythiophenes) to oxygen and UV light is known to cause a fast and irreversible degradation of the electrochromic performance of the polymer.[323] Previous studies prove that the degradation kinetics point to a radical-based degradation process in the solid state rather than a singlet oxygen-based mechanism as it is observed in liquid phase.[322] Here a remarkable enhancement in durability was observed when MWCNTs are present in the spray-coated films. This increase of durability comes from the ability of the CNTs to act as excited state quenchers and radical scavengers.[322] The presence of a unit with large electron density quickly quenches the presence of radicals, avoiding the formation of a random distribution of π-conjugated fragments which generates shorter conjugations. Even more drastic durability tests were carried out for freshly prepared ECDs using different wt. % of MWCNTs (0, 2.5, 5, 7.5 and 10%). Cycling measurements were performed to understand the effect of the CNTs in long term durability (see Figure 4.17).
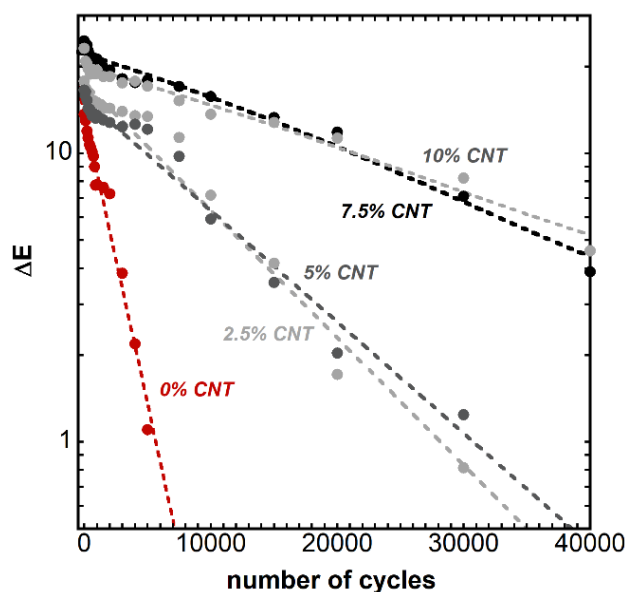
Figure 4.17. Cycling measurements performed in ECDs using PTP and different wt.% of CNTs (0, 2.5, 5, 7.5 and 10 wt.%). The results are presented in ΔE (calculated from L*a*b* coordinates calculated using a ColorChecker® as reference).

In Figure 4.17 are presented the cycling measurements (in ΔE, calculated using L*a*b* coordinates), showing a clear trend that increasing wt. % of CNTs present in the blend offers longer durabilities. Confirming previous results, the pristine PTP presents a fast degradation and the electrochromic device stopped switching around 7000 cycles. For blends using 2.5 and 5% this threshold was observed at 20000 cycles while blends using 7.5 and 10% presented long durability up to 35000 cycles.

These results widely exceed recent values reported on the current state-of-the-art for flexible ECDs based on organic materials and hybrids.[306,324–329] As benchmark, Wang *et al*. reported in 2021 a hybrid WO_3-Prussian Blue electrochromic device with a long-term stability of over 10000 cycles.[329] The same value of 10000 cycles was reported by Löbmann *et al.*, in 2020, with an organic roll-to-roll processable PEDOT-based polymer with switching times of around 10 seconds.[306]

4.2 Conclusions

In this chapter, high performance electrochromic devices were assembled using hybrid blends that include, a newly synthesized copolymer with a pyrene-appended unit (PTP) and multi-wall carbon nanotubes (MWCNTs).

A very stable dispersion bearing the pyrene-appended copolymer (PTP) and the CNTs was optimized and obtained by promoted π-π non-covalent interactions between the pyrene moiety and CNTs, in chloroform:toluene (5:1) solutions. Optimized blends containing different wt. % of MWCNTs (0, 2.5, 5, 7.5 and 10%) were spray-coated in PET-ITO substrates using the spray-casting technique and characterized morphologically by STM, SEM and AFM measurements, before the assembly of solid-state ECDs.

The characterization of the produced electrochromic devices using MWCNTs presented a dramatic increase of electrochromic performance regarding switching time transitions and durability. Specifically, ECDs containing 7.5 wt.% of CNTs in the hybrid blend granted switching times more than 10 times faster when compared with devices containing only PTP (3.8s to 0.3s). In terms of durability, the device holding 7.5 wt.% of CNTs showed a long-term durability of ≈35000 cycles with a 25% degradation (in color contrast) calculated from the qualitative characterization performed after 16000 cycles. On the other hand, the solid-state ECD using pristine PTP showed no electrochromic activity after 7000 cycles. This increase of performance occurs from the induced regioregularity of the produced films (observed by STM) and the formation of very homogeneous films of the hybrid blend, in contrast to the aggregated films of PTP (observed by SEM and AFM). Additionally, the remarkable enhancement in durability observed when MWCNTs are present comes from the ability of the CNTs to act as radical scavengers[322] and, therefore, avoids the formation of π-conjugated fragments with shorter conjugations that generates decreased electrochromic activity.

Thus, this unprecedent enhanced performance in switching time and durability of a thiophene-based polymer using a hybrid blend with CNTs promises new opportunities in electrochromism to expand the color pallet while development high performance ECDs for industrial applications.

# 4.3 Experimental Section

4.3.1 Synthesis
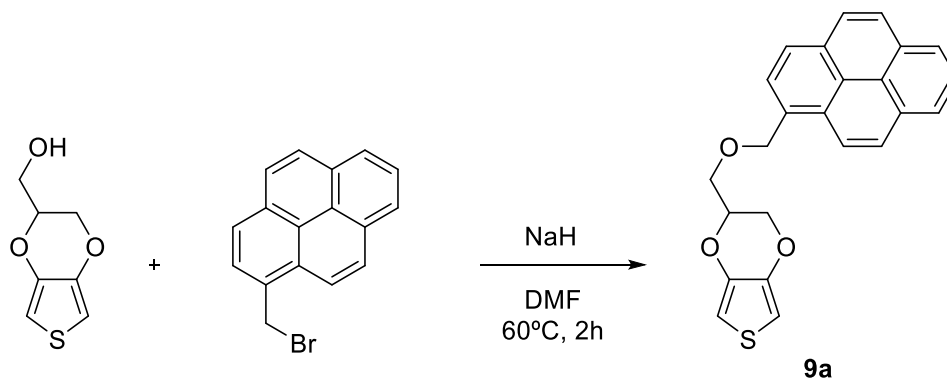
Scheme 4.2. Synthesis of monomer **9a.** Credits to the University of Vienna.

Synthesis of monomer 9a. A dispersion of NaH (60% in mineral oil, 390 mg, 9.75 mmol) and 2,3-dihydrothieno[3,4-b]-1,4-dioxin-2-methanol (961 mg, 5.58 mmol) in anhydrous DMF (20 mL) under argon was heated at 60 °C for 30 minutes, and 1-bromomethylpyrene (2.021 g, 6.85 mmol) was added, the mixture was stirred for 2 hours at 60 °C. Afterwards, the solvent was evaporated in vacuo and the crude was purified by silica gel column chromatography (eluent: n-hexane/AcOEt 8:1), affording an yellow powder. Finally, the powder was solubilized in CH$_2$Cl$_2$ and precipitated using MeOH affording the desired compound as a yellow-greenish powder (1.73 g, 80% yield).

^{1}H NMR (300 MHz, CDCl$_3$) δ (ppm) 8.37 (*d*, 1H, *J* = 9.2 Hz), 8.21-8.02 (*m*, 8H), 6.35 (*d*, 2H, *J* = 3.6 Hz), 6.32 (*d*, 2H, *J* = 3.6 Hz), 5.35 (*m*, 2H), 4.38-4.32 (*m*, 1H), 4.18 (*m*, 1H), 4.08-4.03 (*m*, 1H), 3.82-3.76 (*m*, 2H).

^{13}C NMR (75 MHz, CDCl$_3$) δ (ppm) 141.7, 141.6 131.7, 131.4, 130.9, 130.6, 129.6, 128.1, 127.8, 127.5, 127.4, 126.2, 125.5, 125.5, 125.1, 124.8, 124.6, 123.4, 99.9, 99.8, 72.8, 72.5, 68.3, 66.3.

HRMS (ESI$^+$): exact mass calculated for [M+H]$^+$ (C$_{24}$H$_{19}$SO$_3$$^+$) requires m/z 387.1055 found m/z 387.1055
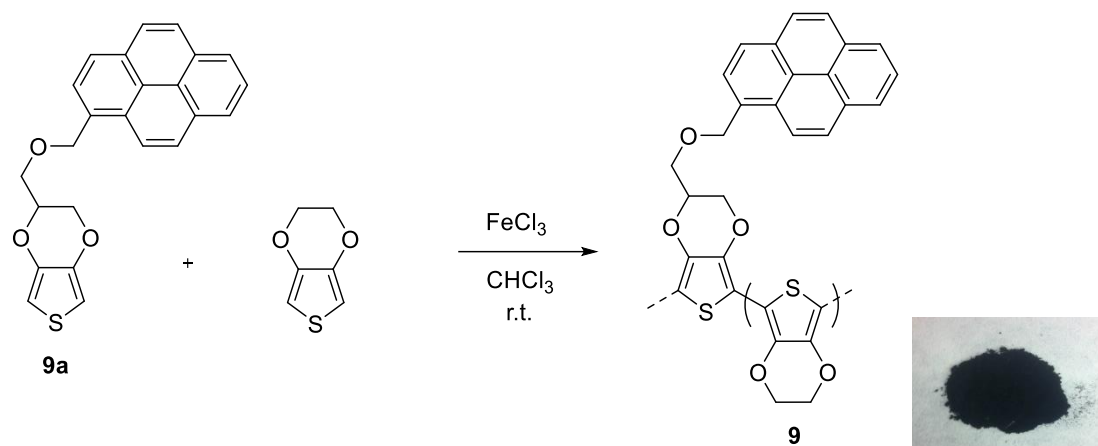
Scheme 4.3. Synthesis of polymer **9**.

Synthesis of polymer 9. To a solution of **9a** (50mg, 0.12mmol= in 60mL of chloroform was slowly added a solution of 3,4-ethylenedioxythiophene (EDOT) (16 4mg, 1.2mmol) in 3mL of chloroform. The solution was stirred for 5 minutes before the addition of FeCl$_3$ (1g, 6mmol) while stirring. The reaction was kept stirring at room temperature for 3 hours and the brown precipitate washed with chloroform and methanol. A very thin black powder was obtained and washed again with water and methanol under vacuum (192mg, 88.9% yield).
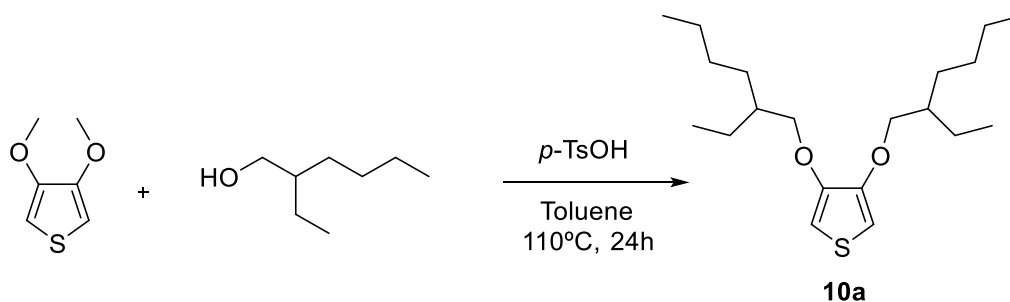
Scheme 4.4. Synthesis of monomer **10a**.

Synthesis of monomer 10a. A solution of 3,4-dimethoxythiophene (200 mg, 1.39 mmol), 2-ethylhexanol (0.92 mL, 5.88 mmol) and *p*-toluenesulfonyl acid (31 mg, 0.163 mmol) in dry toluene was stirred for 27 hours at 110 °C. During this time, the methanol formed during the reaction was regularly released from the flask through a needle. After cooling to rt, H$_2$O (10 mL) was added, and the phases were separated. The organic phase was washed by H$_2$O (2 x 10 mL), dried over Na$_2$SO$_4$, filtered and the solvent removed under reduced pressure. The crude material was purified by silica gel chromatography (Silica Gel 60, 0.04-0.06 mm; eluent: Hexane/DCM: 100/0 to 80/20) to yield the desired compound as a light-yellow oil (331 mg, 70 % yield).

¹H NMR (300 MHz, CDCl₃) δ (ppm) 6.17 (*s*, 2H), 3.85 (*d*, 4H, *J* = 5.9 Hz), 1.76 (*m*, 2H), 1.65-1.19 (*m*, 16H), 0.92 (*m*, 12H).

¹³C NMR (101 MHz, CDCl₃) δ (ppm) 148.2, 97.0, 73.3, 73.3, 39.4, 30.8, 29.2, 24.1, 23.2, 14.2, 11.3.
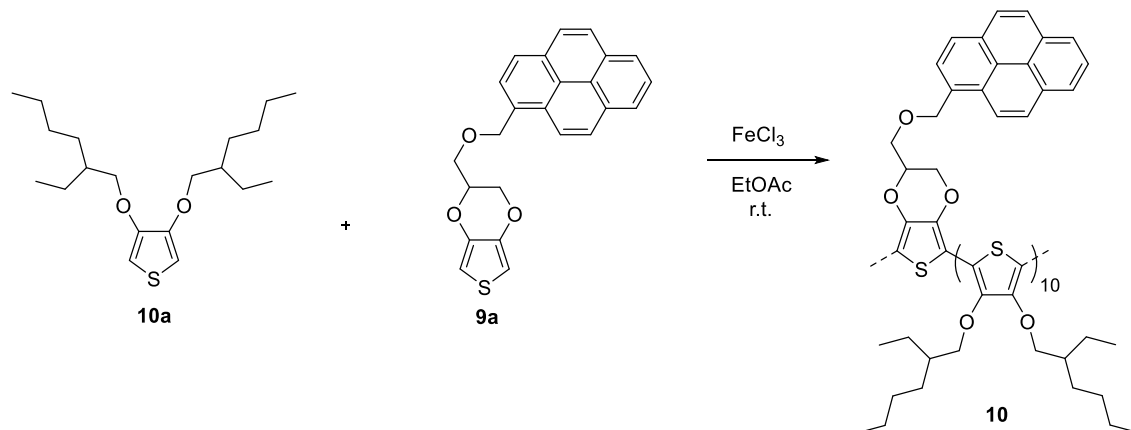
Scheme 4.5. Synthesis of polymer **10** (**PTP**).

Synthesis of polymer 10 (PTP). To a solution of **10a** (395 mg, 1.2 mmol) and **9a** (50 mg, 0.13 mmol) in ethyl acetate (10 mL) was added slowly a solution of iron chloride (1.2 g, 7.5 mmol) in ethyl acetate (10 mL). The reaction mixture was stirred for 24 h at room temperature. MeOH (50 mL) was then added to the mixture and the solution was filtered. The solid was dissolved in chloroform (100 mL) and hydrazine (2 mL) was added slowly to the mixture which was stirred for an additional 5 min. The mixture was concentrated until about 10mL. MeOH (100 mL) was added, and the solution was filtered. The solid was dissolved again in chloroform (20 mL), MeOH (150 mL) was added, and the solution was filtered. The solid is then dried to give the desired polymer as a reddish solid (188 mg, 42 % yield).

¹H NMR (400 MHz, CDCl₃, ppm) δ 7.73 – 7.02 (9H, Pyr.), 5.15 (2H, -OCH2-Pyr.), 4.24 – 3.32 (7H, -OCH2), 2.38 (2H, CH), 1.70 – 0.87 (28H, CH₂ + CH₃)
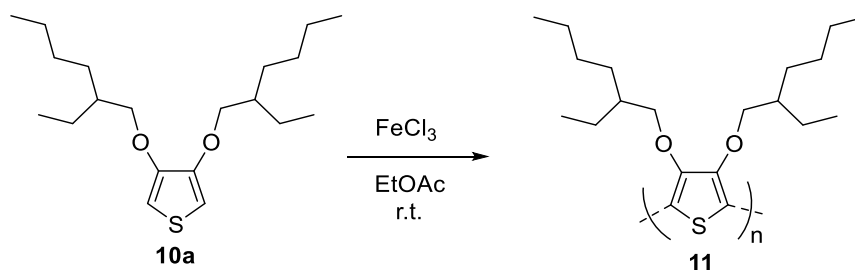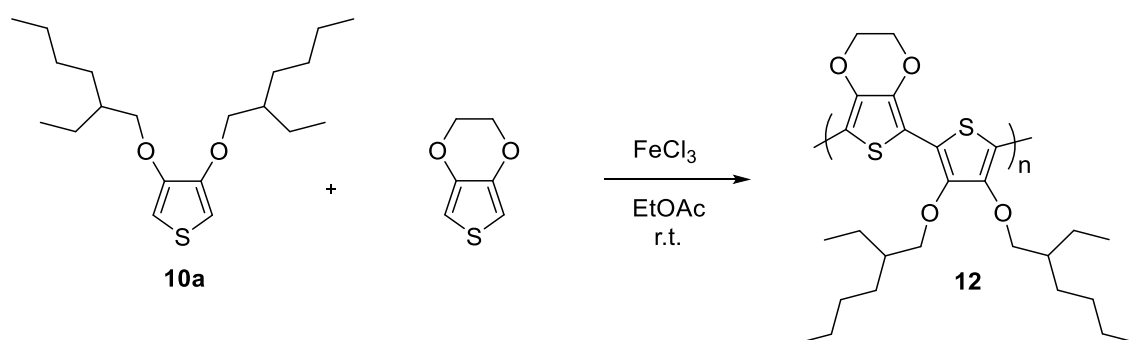

Scheme 4.6. Synthesis of polymer **11**.

Synthesis of polymer 11. To a solution of **10a** (100 mg, 0.29 mmol) in ethyl acetate (5 mL) was added slowly a solution of iron chloride (147 mg, 0.9 mmol) in ethyl acetate (5 mL). The reaction mixture was stirred for 24 h at room temperature. MeOH (50 mL) was then added to the mixture and the solution was filtered. The solid was dissolved in chloroform (10 mL) and hydrazine (1 mL) was added slowly to the mixture which was stirred for an additional 10 min. MeOH (50 mL) was added and the solution was filtered. The solid was dissolved again in chloroform (15 mL), MeOH (100 mL) was added, and the solution was filtered. The solid was extracted into a small flask and dried to give the desired polymer as a reddish viscous solid (31.1 mg, 31.1 % yield).

¹H NMR (400 MHz, CDCl₃, ppm) δ 3.95, 1.79, 1.30-1.55, 0.89

¹³C NMR (75 MHz, CDCl₃, ppm) δ 146, 115, 76, 40, 30, 29, 24, 23, 14, 11

Scheme 4.7. Synthesis of polymer **12**.

Synthesis of polymer 12. To a solution of **10a** (239 mg, 0.7 mmol) and 3,4-ethylenedioxythiophene (12 mg, 0.078 mmol) in ethyl acetate (10 mL) was added slowly a solution of iron chloride (729 mg, 4.5 mmol) in ethyl acetate (10 mL). The reaction mixture was stirred for 24 h at room temperature. MeOH (50 mL) was then added to the mixture and the solution was filtered. The solid was dissolved in chloroform (100 mL) and hydrazine (2 mL) was added slowly to the mixture which was stirred for an additional 5 min. The mixture was concentrated until about 10mL. MeOH (100 mL) was added, and the solution was filtered. The solid was dissolved again in chloroform (20 mL), MeOH (150 mL) was added, and the solution was kept in the fridge overnight and filtered. The solid reddish powder was dried and weighted. (29 mg, 11.3 % yield).

¹H NMR (400 MHz, CDCl₃, ppm) δ: 4.62-3.28 (m, 8H),1.79 (m,2H), 1.60 − 1.09 (m, 16H), 0.89 (m, 12H)

4.3.2 Contact Angle Measurements

Table 4.2. Contact angles of different solvents/solvent mixtures measured on PET substrates.

Solvent	Contact angle (°)
Toluene	14
DMF	16
Acetonitrile	30
THF	12
Ethyl Acetate	8.5
$CHCl_3$:toluene 1:1	11
$CHCl_3$:toluene 5:1	8

4.3.3 Cyclic Voltammetry Measurements

The cyclic voltammetry (CV) was performed using an Autolab PGSTAT 100N potentiostat. The polymers and blend mixtures with MWCNTs were spray-coated on PET/PET-ITO substrates and used as working-electrode; the counter electrode a platinum wire; Ag/AgCl as a reference electrode and an electrolytic solution of $LiClO_4$ (0.1M) in acetonitrile using a scan rate of 20mV/s.

4.3.4 Characterization of the Electrochromic Devices

The optical and electrochemical characterization of the ECDs was carried out using a Cary 5000 UV/Vis/NIR and an Autolab potentiostat PGSTAT204. The applied potentials varied from -1.5V for reduction (colored state) and 0V for the neutral state (bleached state).

The long-term cycling measurements of the devices were performed in a cycling box attached to a function generator capable of applying a squared function that generates color change to the devices, until the experiment is stopped. The cycling box incorporated camera takes pictures to the devices during the cycling measurement that, posteriorly, are processed in MATLAB to convert RGB into L*a*b* coordinates, with a ColorChecker® used as reference.

HYBRID COPPER-NANOWIRE-REDUCED-GRAPHENE-OXIDE COATINGS AS A GREEN SOLUTION TOWARDS ITO-FREE ELECTROCHROMIC DEVICES

This chapter is based on a manuscript under submission, to this date. The author was responsible for the execution, design and assembly of ITO-free electrochromic devices and their characterization while, the CuNWs-rGO electrodes were produced and provided from the University of Strasbourg, France. The author is the main responsible for the interpretation, discussion of all the results, and the preparation of the manuscript.

The development of highly conductive transparent electrodes is, nowadays, of great importance due to its applications in future optoelectronic technologies such as touchscreens, solar cells, LCD screens, organic light-emitting diodes (OLEDs) or wearable electronic devices.[327,330,331]

Indium-tin-oxide (ITO) is the most widely used material to produce transparent electrodes due to its excellent electrical conductivity, electrochemical stability and high transparency in the visible region of the spectra.[332] However, ITO electrodes are not cost-effective considering that they are mechanically fragile, hard to process in flexible supports and they are expensive due to the high preparation costs and scarcity of indium in earth. Therefore, the development of new, low-cost, stable and larged-area transparent electrodes is one of the major challenges in materials science in order to produce cost-effective conductive electrodes for optoelectronic applications including, electrochromic devices (ECDs).[177,178,192,193]

Recently, metallic copper nanowires (CuNWs) gained considerable attention due to their high electrical conductivity and optical transmittance comparable to ITO.[179] Additionally, CuNWs represent a cheap alternative and can be easily dispersed in solution and deposited in several substrates using spray-coating, that represents a great advantage for industrial applications due to easy processability and scale-up.[333]

However, as it was reported by Aliprandi et al.,[66] despite the growing interest in these types of nanomaterials, CuNWs show a limited chemical stability due to their susceptivity to oxidize and consequent loss of electrical conductivity. In order to remove the oxidized layer, several methods have been reported including, high temperature annealing in acidic conditions.[334] Additional efforts have been made to protect the pristine CuNWs from oxidation,[335,336] however, additional steps may turn the system non-cost-effective and turn the CuNWs no longer suitable as electrodes for optoelectronic applications.

Here, graphene can play a major role since graphene already has been reported as a very effective barrier for oxidation.[337,338] Despite the fact that, the processes to obtain graphene sheets are expensive and not suitable as low-cost electrodes, graphene oxide (GO) has been receiving a lot of recognition due to its low cost production and high dispersibility in polar solvents like ethanol or water. Graphene oxide is considered as an insulator that can be reduced thermally[339] or chemically,[340] restoring part of its original structure from graphene, still, with sheet resistances two orders of magnitude above graphene or ITO (1000 Ωsq), making graphene oxide not suitable for optoelectronic applications like electrochromism.[341]

Recently, Ruoff *et al.* reported the use of CuNWs covered with reduced graphene oxide (rGO) as transparent electrodes.[342] Ruoff *et al.* described the production of the CuNWs/rGO electrodes that involves the transfer of poly(methyl methacrylate) (PMMA) on top of the CuNWs, treatments with aggressive chemicals like hydrazine and thermal annealing under controlled atmospheres to reduce the final hybrid structure.

In this chapter it is reported a very simple method for the preparation of CuNWs/rGO films from the formation of CuNWs suspensions (based on the Maillard reaction concept[343]) and commercially available GO. The CuNWs and the GO were processed in thin films using PET substrates by three steps: *i)* spray coating of CuNWs suspended in ethanol; *ii)* spray coating of GO dispersed in ethanol and *iii)* chemical reduction of the GO using $NaBH_4$ as reducing agent. This method originated highly stable transparent electrodes suitable for flexible electronic devices using PET substrates. The produced CuNWs-rGO electrodes were used to assemble ITO-free solid-state ECDs with PEDOT as an electrochromic active material and as counter-electrode. The assembled ECDs were characterized using an active area of $1cm^2$. Posteriorly, it was tested the availability to produce large-area devices (A4 sheet size) in order to expand the possible pallet of industrial applications.

5.1 Results and Discussion

5.1.1 CuNWs-rGO Electrodes

The fabrication of the CuNWs-rGO electrodes was performed in collaboration with the University of Strasbourg, on the scope of the EU project DecoChrom (EU Horizon 2020 programme grant nº 760973), with the goal of fabricating ITO-free high-performance ECDs using PET substrates.[23]

The details for preparation of the CuNWs ink, deposition of graphene oxide and further reduction using $NaBH_4$ can be found in the experimental section of this chapter. The preparation of the CuNWs ink was focused on the Maillard reaction[343] approach since it is based on the use of "Green" reagents, suitable for industrial use and applications. The used copper source was $CuCl_2$ and the graphene oxide deposition was optimized from a commercially available GO suspension (see Scheme 5.1).
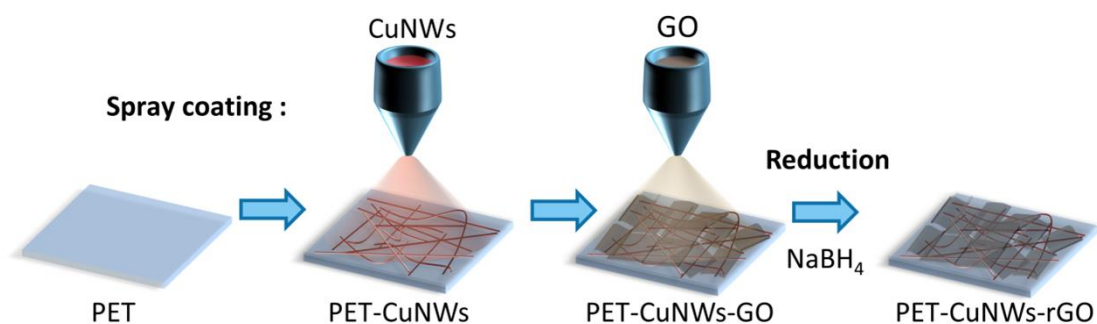
Scheme 5.1. Schematic representation for the production of transparent PET-CuNWs-rGO electrodes. Credits to the University of Strasbourg.

Furthermore, during optimization, the CuNWs ink deposited on PET substrates revealed very low electrical conductivity (≈50MΩsq) due to the presence of a thin layer of CuO on the NWs surface and, in parallel, the same low conductivity values were observed in the spray-coated GO films (≈0.4MΩsq). However, with GO, it was expected since GO is considered an insulator. In order to increase the conductivity of both CuNWs and the GO while maintaining high transparencies, it was found that a solution of $NaBH_4$ in water (0.1% w/w 14mM) was capable of reducing, simultaneously, the thin layer of cupric oxide on top of the CuNWs and the graphene oxide to rGO, only exhibiting a loss of about 10% of transmittance after the reduction with a sheet resistance of ≈30-40Ωsq, comparable with that of commercially available ITO. The reduction with $NaBH_4$ did not affect the morphology of the system CuNWs-rGO as presented on the SEM/Micrograph images on Figure 5.1.

Since the transmittance and sheet resistance of the electrodes are two key factors to produce electrochromic devices, it was evaluated and optimized the best compromise between their transparency and conductivity. The optimization enabled the production of electrodes with a transmittance of ≈70% (at 550nm) with a loss of ≈20 T% from the initial PET substrate to the final PET + CuNWs + rGO electrode (see Figure 5.2) while presenting a sheet resistance of 32 ± 2 Ωsq (measured with a 4-point probe).
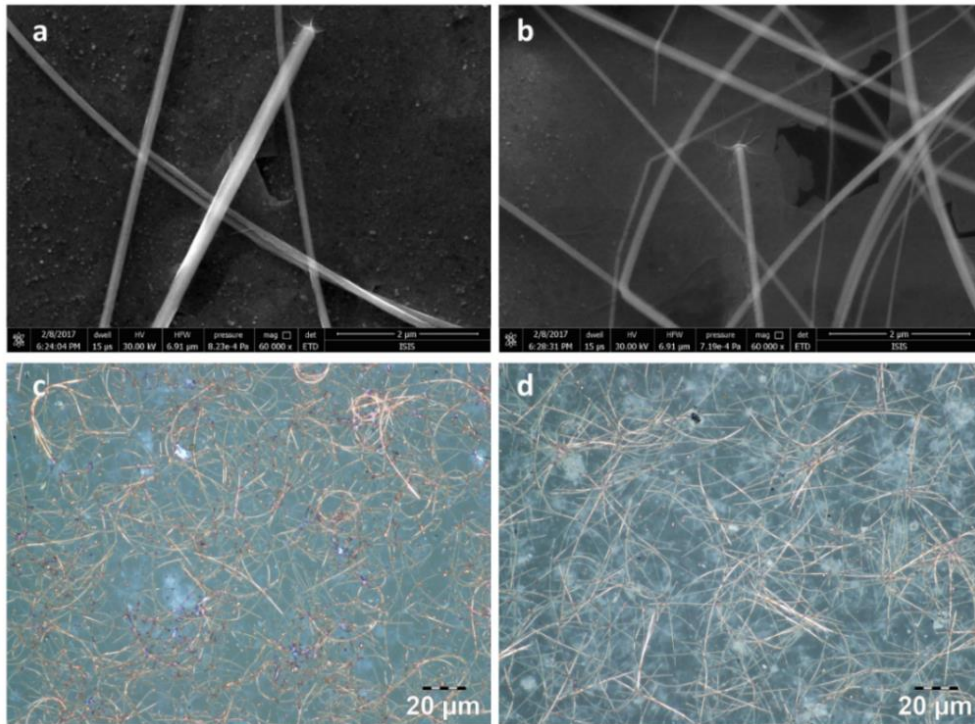
Figure 5.1. *Up:* SEM images of the hybrid CuNWs-rGO on Si+APTES before (a) and after (b) the reduction with NaBH₄; *Bottom:* Micrographs of the hybrid CuNWs-rGO on glass+APTES before (c) and after (d) the reduction with NaBH₄.
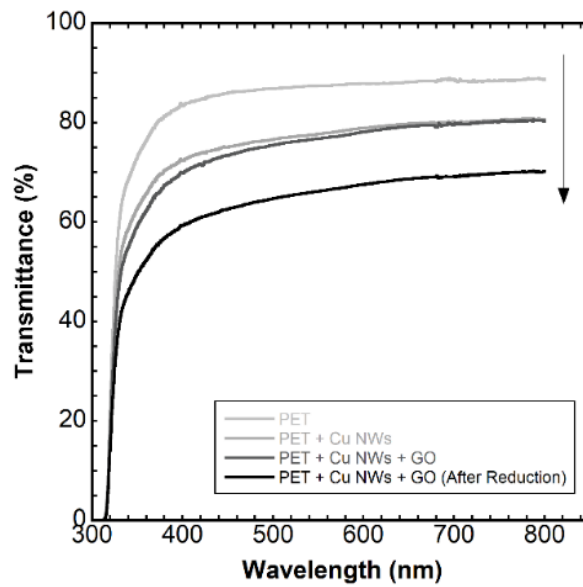

Figure 5.2. Transmittance spectra after each step for the production of the final PET + CuNWs + rGO electrodes.

The coating of the CuNWs ink onto the plastic substrates was previously optimized by spraying different number of layers (from 1 to 5) of the CuNWs dispersion in glass substrates and measured their transmittance / sheet resistance after each sprayed layer (see Figure 5.3).

It is perceptible that the sheet resistance does no decrease linearly with the addition of more sprayed CuNWs layers, presenting an exponential behavior, in agreement with existing literature.[344,345] At T=78% (ΔT=12%), the sheet resistance is *ca.* 30Ωsq, a value comparable with commercial glass-ITO films from Sigma-Aldrich.
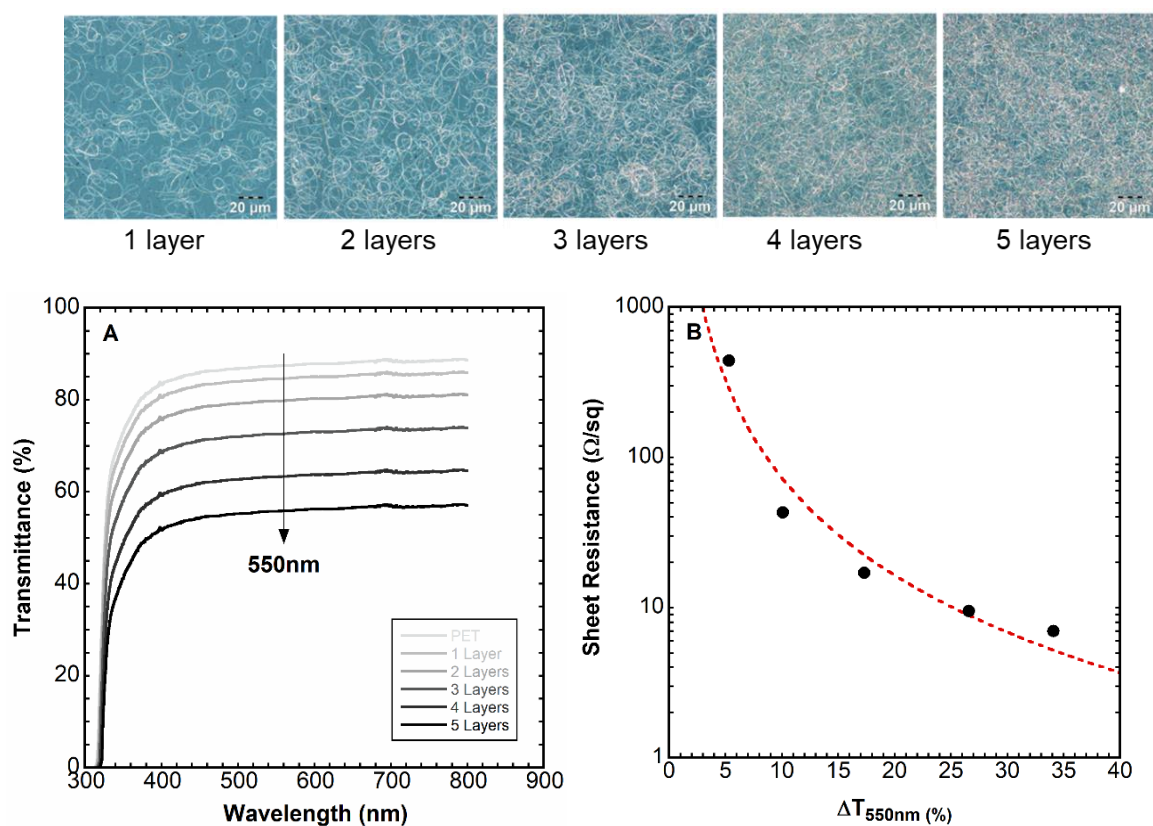
Figure 5.3. Transmittance and sheet resistance of the CuNWs films with different loadings of CuNWs layers in glass substrates; **A** – ΔT of the films with different layers of CuNWs (at 550nm); **B -** Sheet resistance of each electrode accordingly to the ΔT loss (at 550nm) after each added layer. Credits to the University of Strasbourg.

Additionally, the stability of the CuNWs/rGO film on PET substrates under bending both in static and dynamic configuration was assessed by measuring the variation of their electrical resistance. Figure 5.4A shows the sheet resistance of the film for different bending radius. The measurements shows that the sheet resistance is stable up to 5 mm of radius bending and then increases up to ~73 Ωsq for a radius of 1.5 mm. Furthermore, the stability under repeated

bending was tested (Figure 5.4B). Impressively, after 10000 bending cycles at a bending radius of 1cm the sheet resistance variation was less than 4%.
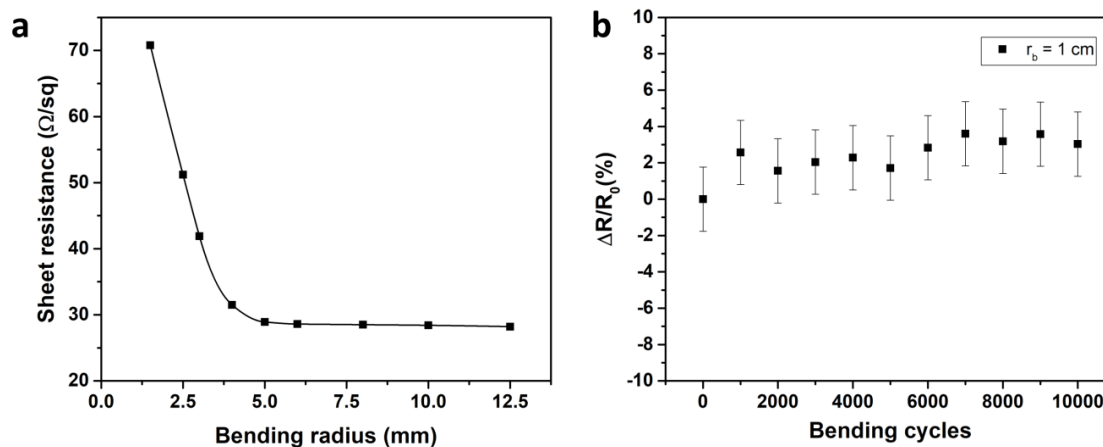

Figure 5.4. A - Sheet resistance of a hybrid CuNWs-rGO electrode in a PET substrate varying the bending radius; **B -** Variation of electrical resistance (in %) of the CuNWs-rGO electrode in function of the number of cycles using a bending radius of 1cm. Credits to the University of Strasbourg.

Cyclic Voltammetry measurements were also performed to the hybrid CuNWs-rGO electrodes (Figure 5.5). The cyclic voltammetry was performed to an electrode of the hybrid material spray-coated in a PET substrate, dipped in an electrolytic solution of $LiClO_4$ in acetonitrile. A scan rate of 20mV/s was used varying between 1.5 and -1.5V for complete 3 cycles.

From the CV measurement it is possible to observe an oxidation peak at 0.34V, corresponding to the oxidation of the CuNWs deposited on the PET substrate. This information is crucial to understand that the rGO layer is not capable of protecting the CuNWs from electrochemical oxidation. Therefore, further assembled ECDs using the hybrid CuNWs-rGO electrodes cannot be switched to oxidative potentials (1.5V in this case).

By AFM measurements, it was examined the topography of the hybrid films of CuNWs-rGO with a bare CuNWs film (see Figure 5.6). Particularly, it is possible to observe a decrease on the height of the film from 216 ± 22nm to 135 ± 5nm, originated by a decreased roughness after the coating of the films with rGO. Additionally, it is clear that rGO covers completely the CuNWs material and the substrate surface.
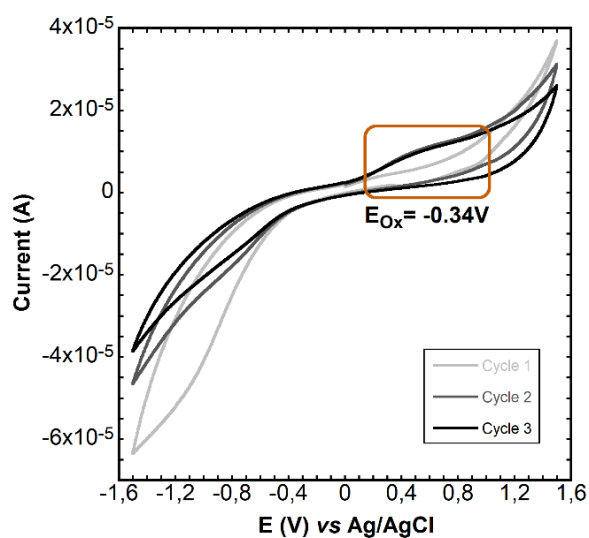
Figure 5.5. Cyclic voltammetry measurement of a hybrid PET + CuNWs + rGO electrode. In the CV was used a reference electrode of Ag/AgCl, platinum wire as counter-electrode and the hybrid PET + CuNWs + rGO electrode was used as working electrode. An electrolytic solution of LiClO$_4$ in acetonitrile was used with a scan rate of 20mV/s for 3 cycles.
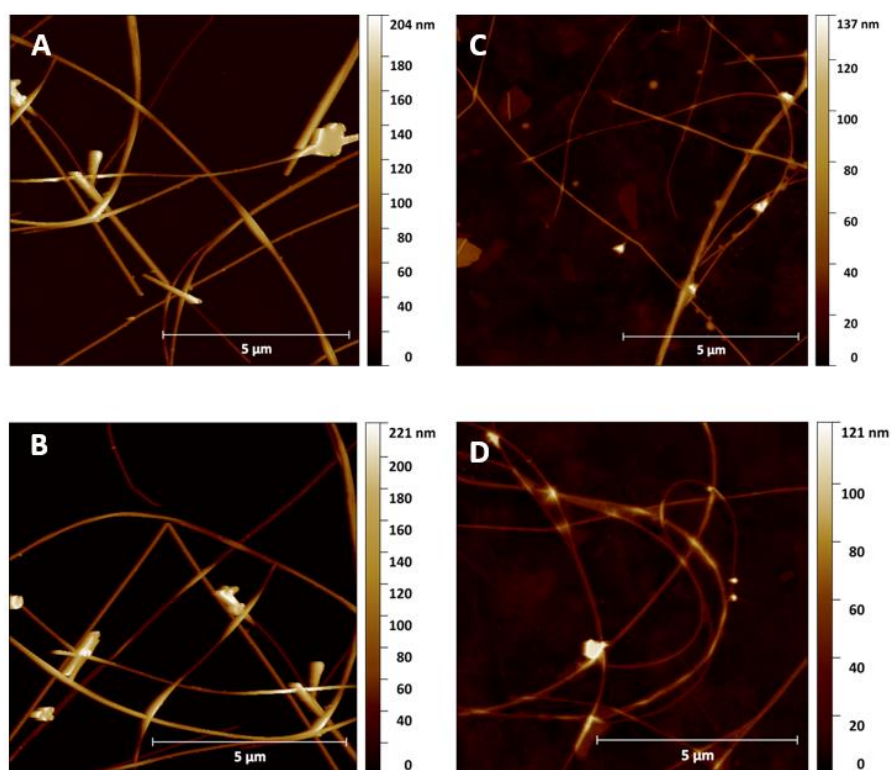

Figure 5.6. AFM images of (A, B) Cu NWs on Si/SiO$_2$ and (C, D) Cu NWs/rGO on Si/SiO$_2$. Credits to the University of Strasbourg.

124

5.1.2 ITO-free Electrochromic Devices

With the produced CuNWs-rGO electrodes by spray-coating in PET substrates, ITO-free electrochromic devices were assembled and characterized.

The electrochromic material selected to produce the desired devices was poly-(3,4-ethylenedioxythiophene) (PEDOT) due to its low redox potential required to observe color transition (±1.5V), high color contrast, high coloration efficiencies (CE)[233] and high processability using different deposition techniques (spray-coating, ink-jet, etc.) and already developed and commercially available ink formulations for different substrates.

The selected formulation was previously developed by *Ynvisible®* using PEDOT (see experimental section) and was deposited using the spray-casting technique. Subsequently, ITO-free ECDs were assembled according to the Scheme 5.2. The printing and assembly of the described ITO-free ECDs was specifically outlined for these type of electrodes where, the PET/CuNWs-rGO/PEDOT electrode acts as working electrode (E1) and PEDOT/PET was used as counter-electrode (E2) taking advantage of the fact that PEDOT can act, simultaneously, as electrochromic and conductive material,[307] allowing the fabrication of a completely ITO-free electrochromic device.
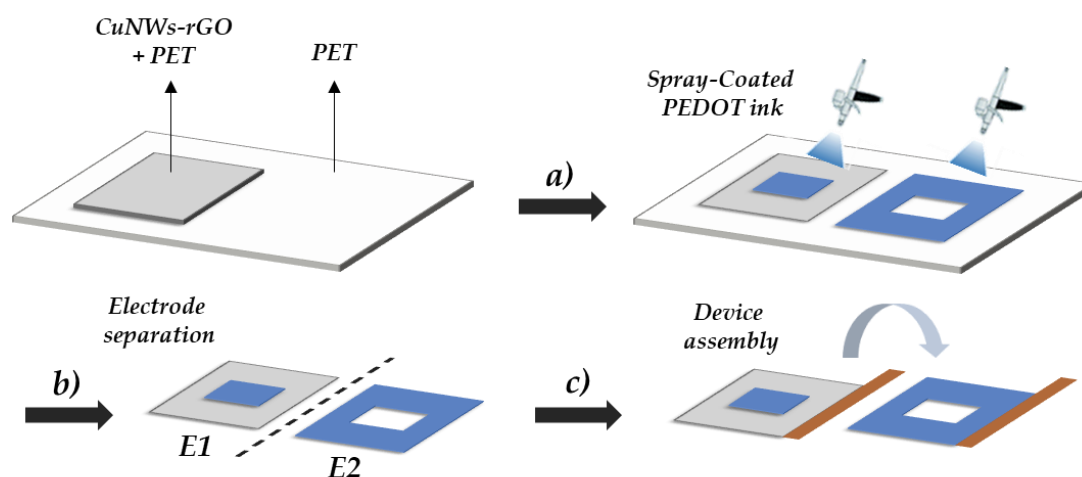
Scheme 5.2. Assembly of ITO-free electrochromic devices using PET/CuNWs-rGO/PEDOT (E1) vs PEDOT/PET (E2) electrodes. a) Deposition of PEDOT ink using adequate masks, b) Electrode separation and c) Device assembly using E1 and E2.

Regarding the deposition of the PEDOT on the electrode E1, an active area of 1cm² was spray-coated, while electrode E2 was fully spray-coated with the PEDOT ink, except the same 1cm² area in the center, avoiding the overlap with the active area in electrode E1, when stacked. The full coating of the PET (in E2) with PEDOT ensured that, during the assembly, the electrical

contact was extended for activation during the characterization (using conductive copper tape), as seen in scheme 5.2. The number of PEDOT layers spray-coated in each electrode was optimized until reaching an ideal ratio of 1:2 (2 layers for E1 *vs* 4 layers for E2). Between the two electrodes it was added a layer of UV-curable electrolyte denominated *Ynv.El.*® property of *Ynvisible*® with the patent nº 20140361211.[207] The assembled ITO-free electrochromic device can be found in Figure 5.7, switching between -1.5V and 0V. A clear color transition between the two states of the PEDOT from blue (-1.5V) to transparent (0V) can be observed. The potentials used to activate this ITO-free ECD were -1.5V (for reduction) to 0V (for oxidation), on the working electrode (E1). This means that electrode E1 is never switched to oxidative potentials (>0V), which causes a very fast oxidation of the CuNWs, as it was observed in the CV measurement presented in Figure 5.5. Nevertheless, an ITO-free electrochromic device was switched from 1.5/-1.5V and it was observed a loss of electrochromic activity after just a few cycles (see appendix figure D.1.1).

For a qualitative comparison, an electrochromic device using PET-ITO on E1 was also assembled and characterized using the same architecture that was used to assembly the ITO-free ECD presented in figure 5.3 (see appendix figure D.1.2).
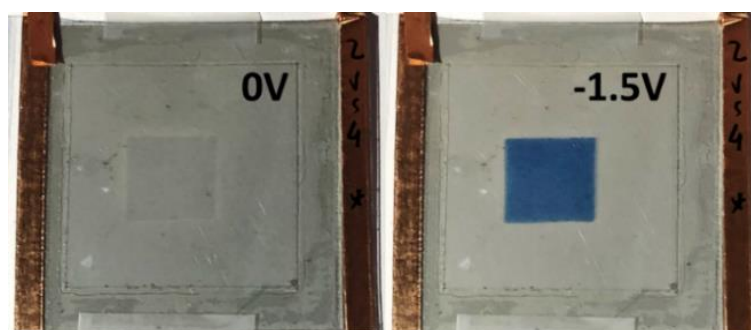
Figure 5.7. ITO-free ECD using PET/CuNWs-rGO/PEDOT vs PEDOT/PET switching from 0V to -1.5V.

The performance of the assembled ECDs was evaluated through spectroelectrochemistry, switching time (ST), charge consumption (Q), optical contrast (ΔT) and durability (Cycling), as described in section 1.5.7. Figures of merit were calculated for both assembled ECDs (ITO-free ECD vs PET-ITO ECD) for performance evaluation. The values calculated are presented in Table 5.1 and Figure 5.8, obtained for a specific wavelength were the optical contrast of PEDOT is maximum, namely 623nm and qualitative characterization of the ECDs was measured both before and after the cycling measurements. The cycling experiments were performed by recording the color contrast variation upon application of 5s of reduction/oxidation

cycles (-1.5/0V) where 1cycle=10s (see figures of merit in Table 5.1) and stopped when the ITO-free ECD reached 50% of its initial color contrast (ΔE), calculated using L*a*b* coordinates (Figure 5.8D).

Table 5.1. Transmittance (**ΔT**), switching time (**t_{70}** and **t_{90}** calculated for 70% and 90% of total color, respectively), charge consumption (**Q_{Red}**, **Q_{Ox}**) and coloration efficiency (**CE**) calculated for the active area of the ECDs (1cm2) on the ITO-free ECD and the ECD using PET-ITO instead of PET-CuNWs-rGO, with the same architecture. Values calculated after 30 and 30000 cycles where 1cycle=10s.

Nº of Cycles	ΔT (%)[a]	$T_{blank\ ECD}$ (%)[a]	t_{70}^{Red} (s)	t_{90}^{Red} (s)	t_{90}^{Ox} (s)	Q_{Red} (mC.cm^{-2})	Q_{Ox} (mC.cm^{-2})	CE (C^{-1}.cm^2)
				Using CuNWs-rGO				
				As prepared				
30	31.2	49.0	3.8	6.7	3.6	-1.82	1.03	234
				After 30000 cycles				
30000	18.9	49.0	13.2	21.7	14.3	-3.18	1.13	139
				Using PET-ITO				
				As prepared				
30	34.9	70.0	1.2	3.3	1.7	-1.78	0.78	452
				After 30000 cycles				
30000	27.6	70.0	10.3	15.0	6.7	-0.65	0.68	127

(a) λ_T = 623 nm

In terms of switching times, the ITO-free ECD presents values of 6.7 seconds for reduction (t_{90}^{Red}) and 3.6 seconds for oxidation (t_{90}^{Ox}) while the ECD using PET-ITO shows switching times of 3.3 and 1.7 seconds, respectively. In spite of the fact that the switching times are longer in the ITO-free devices, they are significantly shorter when compared with values reported in the literature with ITO-free devices using PEDOT as conductive electrode, where switching times of 20 seconds are reported.[115,177] Additionally, in the coloration step (reduction), if we consider the characterization performed after the cycling experiment, the switching time of the ITO-free ECD increased to 21.7 seconds (was 6.7, increment by a factor of 3.2) while the ECD using PET-ITO presented a switching time of 15 seconds (was 3.3, increment by a factor of 4.6).This means that the switching time values of the ITO-free ECD suffered a slower degradation during the 30000 cycles performed to both ECDs when compared with the ITO-based ECD.
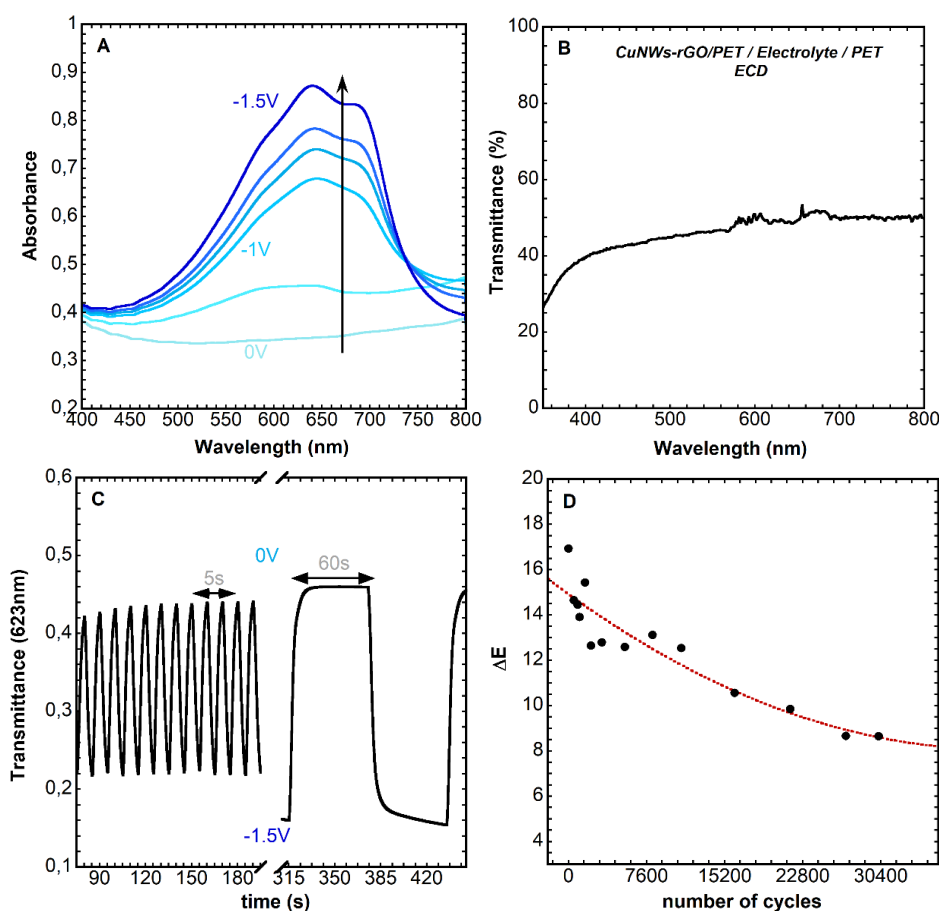
Figure 5.8. Characterization of the ITO-free electrochromic device. **A -** Spectroelectrochemistry of the device from 0V to -1.5V; **B -** Transmittance spectra of the blank device (with no electrochromic material); **C -** Switching time experiment of the device, in transmittance (at 623nm) and **D -** Cycling measurement performed on the ITO-free ECD, in L*a*b* coordinates. ΔE calculated using a ColorChecker® as reference.

Regarding the charge consumed for both devices in the oxidation step, the values are kept constant before and after the cycling experiment which was expected due to the application of 0V instead 1.5V, causing almost no electrochemical stress to the devices. Nevertheless, it is noticed that, in the reduction process, the device using CuNWs-rGO consumes -3.18mC/cm^2 after the cycling (applying -1.5V), which is almost the double of the value consumed before the cycling experiment (-1.82mC/cm^2). This increment on charge consumed during the reduction is not observed on the PET-ITO ECD, which indicates that this increase comes from the charge consumed by the reduced graphene oxide while it acts as a drain for the charge transfer provided to the ECD, avoiding additional electrochemical stress to the electrochromic material. This fact explains the slower degradation of the PEDOT using CuNWs-rGO instead of

128

PET-ITO that is, consequently, also observed in the CE values before and after the cycling measurements.

5.1.3 A4-Sized Electrochromic Device

After the successful fabrication of an ITO-free electrochromic device with a reasonable performance, the possibility to produce a large-area electrochromic device urged as a very interesting challenge. The necessity of ITO-free electrodes for large-area displays increases as the scarcity of indium rises its price and, consequently, the fabrication costs of this type of displays for, *e.g.*, electrochromic windows. Therefore, a similar strategy was designed to scale-up and produce an ITO-free electrochromic device using an A4 sized CuNWs-rGO electrode (210mm x 297mm), as shown in Scheme 5.3.
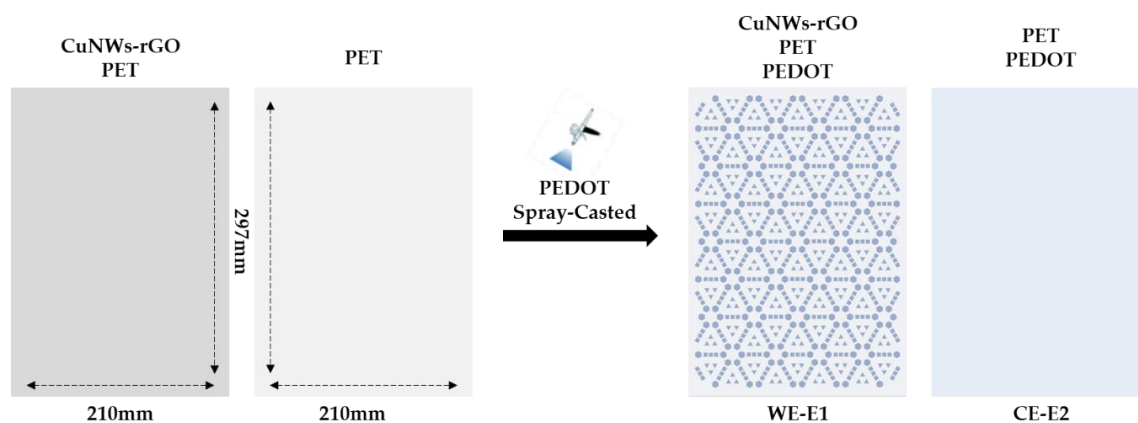
Scheme 5.3. Scheme for the fabrication of the A4 ITO-free electrochromic device using PEDOT/CuNWs-rGO/PET electrode (E1) vs PEDOT/PET electrode (E2).

The pattern selected to print the same PEDOT ink formulation on the WE-E1 involved a series of small areas of hexagons, squares, and triangles to act as electrochromic active area on the final A4 ECD (see Figure 5.9). These small areas were selected due to the slow activation switch of an active area of 12cm^2, tested on a previously A4 sized device (see appendix figure D.1.3). Additionally, having a costume designed pattern (different from a single big square) shows the versatility of the spray-coating technique and the diversity of possible applications by the production of different patterned electrochromic displays. In parallel to the previously reported ITO-free device, PET/PEDOT was used as conductive counter electrode (E2). The potential used to switch this A4 device was -2V/0V.

The produced A4 ITO-free ECD can be seen in Figure 5.9 as well as the absorbance spectra of both redox states, at -2V and 0V, acquired in one active area (0.3cm^2) printed on the

A4 ECD (Figure 5.9A). On Figure 5.9B is represented the color evolution of the A4 ECD with the application of -2V (for colored blue state) for 10 minutes and 0V (for the neutral bleached state) for 5 minutes. In spite of the fact that a functional A4-sized ITO-free ECD was achieved, the characterization of the A4 ECD clearly shows that the ECD is very slow with high charge consumption that leads to a poor CE, as presented in Table 5.2 (7.77$C^{-1}.cm^2$).
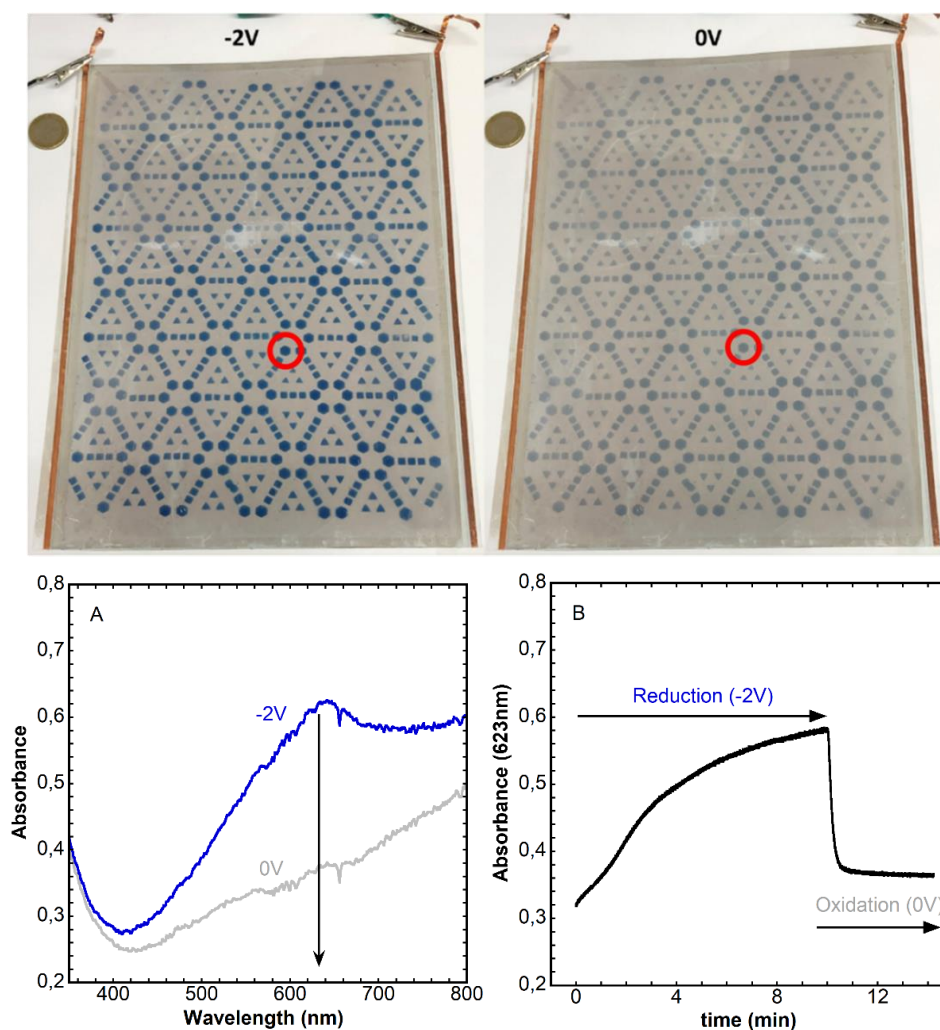

Figure 5.9. *Up:* Working A4 ITO-free electrochromic device switching from -2V (Reduced State) and 0V (Neutral State). 1 euro coin for size comparison; *Bottom:* **A -** Absorbance spectra of one active area (0.3cm^2) at -2V/0V (marked in red), **B -** Absorbance over time at 623nm applying -2V/0V for 10 and 5 minutes, respectively.

Table 5.2. Figures of merit for the A4 ITO-free ECD. t_{90}^{Red} and t_{90}^{Ox} calculated for 90% of total color after the application of -2V and 0V for 10 and 5 minutes, respectively. Q_{Red} and Q_{Ox} calculated after the 60s of application, of the selected active area with 0.3cm².

ΔAbs	ΔT (%)	$T_{blank\ ECD}$ (%)	t_{90}^{Red} (min)	t_{90}^{Ox} (min)	Q_{Red} (mC/cm²)	Q_{Ox} (mC/cm²)	CE (C^{-1}.cm²)
0.27	23.8	49.0	6.92	0.47	-34.7	9.1	7.77

In order to obtain a deeper understanding of the redox processes occurring on this A4 ITO-free ECD, electrical impedance spectroscopy (EIS) measurements were performed while switching to the reduced (-2V) and the oxidized state (0V). Figure 5.10 presents the Nyquist plots of the complex resistivity of the system. In impedance spectroscopy measurements, a frequency-dependent resistivity of the device is obtained that is described by equation 8:

$$Z^*(\omega) = Z'(\omega) - iZ''(\omega) \qquad \text{equation 8}$$

where,

    i)   ω is the applied frequency,

    ii)   Z' is the real part of the resistivity,

    iii)   Z'' is the imaginary part of the resistivity and,

    iv)   Z* is the total resistivity.

If there is no delay present in the system, the electric current and the voltage applied are in phase. Furthermore, a phase appears at a given frequency (or a delay) that is related to the imaginary part of equation (A). Z* can be further analyzed using the Cole-Cole equation 9:

$$Z^*(\omega) = Z_\infty + \frac{Z_0 - Z_\infty}{1 + (i\omega\tau)^{(1-\alpha)}} \qquad \text{equation 9}$$

The Cole-Cole equation is designed for a parallel Resistor (R) and Capacitor (C) circuit, where:

    i) Z_∞ is the resistance at infinite frequency,

    ii) Z_0 is at zero frequency,

    iii)   τ is the device relaxation time and,

    iv)   α is the deviation from an ideal Debye relaxation: α is zero if there is a single relaxation.

The experimental data was obtained during the application of -2V and 0V using 10mV of amplitude, fitted with equation 9 (see Figure 5.10), and the results are presented on Table 5.3.

Table 5.3. Fitted EIS of the A4 ITO-free ECD data using equation 9.

Voltage (V)	Z_∞ ($\Omega.sq$)	Z_0 ($\Omega.sq$)	τ (ms)	α
0	298	1015	12	0.52
-2	271	514	14	0.50
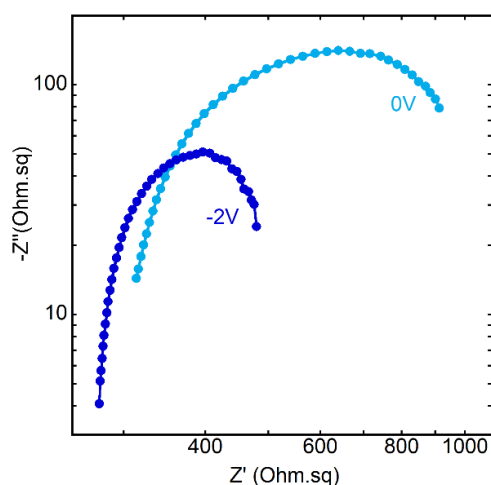
Figure 5.10. Nyquist plot of the EIS measurements performed on the A4 ITO-free ECD using -2V and 0V. Data points fitted using equation 9.

The Z_∞ vales obtained on this experiment are similar regardless of the applied voltage (-2 and 0V). This indicates that the value corresponds to the CuNWs-rGO electrode resistivity, of about 285 Ω.sq after the assembly of the device, which represents that no significant chemical reaction is happening on this electrode, during the switch. The Z_0 value, however, strongly decreases during the application of -2V, which suggests that this value corresponds to the resistivity of the PEDOT counter-electrode which is oxidized during the activation of the PEDOT on the CuNWs-rGO electrode. PEDOT is known to be a better electric conductor in its oxidized form since it is a *p*-type semiconductor.[307] The relaxation time calculated (13 ms) is attributed to the electrolyte diffusion and the α value indicates a distribution of relaxation times, probably because the working electrode (E1) and counter-electrode (E2) are different. Therefore, the IS data obtained supports that the Cu-NWs-rGO electrodes do not suffer electrochemical stress during their operation in the assembled A4-sized ITO-free electrochromic device.

In terms of cyclability, the A4 ITO-free device was not tested due to the slow switching between the reduced and neutral state.

5.1.4 Conclusions

In this chapter, highly conductive and transparent hybrid CuNWs-rGO electrodes were produced and successfully used as conductive electrode on the assembly of ITO-free electrochromic devices using PEDOT as electrochromic material.

The ITO-free electrochromic device was assembled and characterized presenting reasonable performances with good switching times, high durability (above 30000 cycles with color retention above 50%) and good modulated optical contrast ($\pm$63%), taking into account that the system PET/CuNWs / Electrolyte / PET presents T% of $\approx$50%, at 623nm.

The high performance of the produced ECDs promotes this PET/CuNWs-rGO electrodes as a good material for ITO replacement in ECDs and as well as other optoelectronic applications such as, organic light-emitting diodes and organic photovoltaic cells. Moreover, the CuNWs-rGO offers a cheap and viable alternative to these conductive materials like ITO and can be easily processed using printing methods like ink-jet or spray-coating. This simplified processability enables the preparation of large-area displays (such as the reported A4-sized ECD), for scale-up in different industrial applications, as shown in this chapter.

5.2 Experimental Section

5.2.1 Preparation of CuNWs Ink

CuNWs were prepared following a hydrothermal method. In particular, 380 mg of $CuCl_2·2H_2O$ and 2.6 g of octadecylamine were dissolved in 110 mL of deionized water. The suspension was sonicated until a light blue emulsion was obtained. Then 850 mg of glucose were added. The emulsion was stirred at 50 °C for 1 h to homogenize the emulsion. The emulsion was then transferred to a steel autoclave and heated to 115 °C for 8 hours. The resulting CuNWs were isolated from the reaction suspension by centrifuging firstly with water, then with ethanol/water mixture 1/1, and finally with pure ethanol (5000 rpm, 8 min). To separate the CuNWs from Cu nanoparticles, the mixture was first re-dispersed in water and then extracted with hexane; the water phase containing CuNPs was eliminated. Finally, the resulting pure CuNWs were centrifuged once more to remove hexane and dispersed into 40 mL of ethanol. The dispersion concentration was approximatively 1.2 mg/mL. Credits to the University of Strasbourg.

5.2.2 Production of CuNWs-rGO PET Electrodes

PET substrates were cleaned with ethanol and dried under a stream of air. Subsequently the ethanolic dispersion of CuNWs was diluted 15 times, homogenized by vortex and short sonication (1 min) and sprayed using a commercial airbrush onto the substrates. Then commercial graphene oxide dispersion in water (4mg/ mL, Graphenea©) was diluted with ethanol 60 times and sonicated 30 min. The clear yellow dispersion was then sprayed onto the top of CuNWs. Finally, the substrate was dipped into a fresh aqueous solution of $NaBH_4$ (0.1% w/w) for 2.5 hours. Then the substrates were washed with water and ethanol and dried with nitrogen in order to produce the final CuNWs-rGO electrodes. Credits to the University of Strasbourg.

5.2.3 Deposition of PEDOT Ink

The PEDOT was deposited on the CuNWs/rGO and PET electrodes by the method of spray-casting. The electrodes were placed over a heating plate at 80°C for 1 minute between each layer.

The PEDOT ink used for spray-casting contains PEDOT:PSS (PH1000) from Clevios®, DMSO, MiliQ water and surfactant Brij 30® from Sigma-Aldrich. This formulation is property of *Ynvisible®*, all the chemicals were used as purchased with no further purification.

5.2.4 Assembly ITO-free Electrochromic Devices

The final ECDs were assembled using the PE/CuNWs-rGO/PEDOT (Working Electrode, E1) and PEDOT/PET (Counter-Electrode, E2) producing a completely ITO-free electrochromic device using PEDOT as electrochromic as well as conductive material, deposited by spray-casting. The spray-casting of the PEDOT on the PET/CuNWs-rGO and PET substrates was performed using an aerograph with a continuous applied pressure of 1 bar for each layer. Ensuring the homogeneity of the depositions, the aerograph with a 0.33mm opening was kept at a constant distance from the substrate (5cm) so that only the aerosol part of the sprayed mixture was deposited into the plastic substrate. Additionally, the spraying rate was kept constant for each layer and performed on PET placed on top of a heating plate kept at 100ºC to promote fast evaporation of the solvent, which is crucial to avoid coffee-stain effects in the films. Between the two electrodes is placed an Li$^+$ based UV curable electrolyte denominated *Ynv. El.*® property of Ynvisible® with the patent nº 20140361211.

5.2.5 Assembly of A4 ITO-free Electrochromic Device

The assembly of the A4 sized electrochromic device was performed using the same type of electrodes (PET/CuNWs-rGO/PEDOT vs PEDOT/PET) with a size of 210mm *vs* 297mm.

Since this is a large area electrochromic device, a pattern was developed using small areas (hexagons, squares and triangles) to decrease the switching time required for color change to occur (see Scheme 5.3). The final assembled ITO-free A4 ECD is shown in the figure 5.9. The device was switched between the reduced state (-2V) and neutral state (0V).

5.2.6 Characterization of the Electrochromic Devices

The optical and electrochemical characterization of the ECDs was carried out using an AutoLab spectrophotometer kit UV/VIS and an Autolab potentiostat PGSTAT204. The applied potentials varied from -1.5V for reduction (colored state) and 0V for the neutral state (bleached state).

The long-term cycling measurements of the devices were performed in a cycling box attached to a function generator capable of applying a squared function that generates color change to the devices, until the experiment is stopped. The cycling box incorporated camera takes pictures to the devices during the cycling measurement that, posteriorly, are processed in MATLAB to convert RGB into L*a*b* coordinates, with a ColorChecker® used as reference.

GENERAL CONCLUSIONS AND
FUTURE PERSPECTIVES

Polythiophenes are semiconductor organic polymers with remarkable electrochromic properties in terms of color palette, color contrast and easily tunable opto-electronic properties through simple synthetic modifications. However, their implementation in a larger scale for electrochromic applications is still restricted by processability, scale-up, and stability issues. In this work, new polythiophene nanostructured materials were designed, synthesized, characterized, and used as electrochromic materials in solid-state electrochromic devices aiming for the enhancement of their electrochromic properties.

To achieve the proposed goal, polythiophene nanoparticles dispersed in water-based solutions were synthesized. Initially, a classic well-known polythiophene (P3HT) was used and then the approach was extended to a newly synthesized class of thiophene-based polymers using a repeated linear backbone of thienyl-phenyl-thienyl-thienyl units, aiming for a yellow-colored polymer. In both cases, the use of toxic organic solvents (*e.g.*, chloroform) during the coating of the electrochromic layer is avoided, increasing the health safety of the user while reducing the environmental impact, which are crucial features for the development of ECDs in industrial applications. Additionally, it was observed that solid-state ECDs using polythiophene nanoparticle films present enhanced electrochromic properties, including faster switching times, higher color contrasts and durabilities.

For the case of P3HT-NPs ECDs, a significant decrease of the reduction switching time was achieved when compared with ECDs using pristine P3HT (4.4s *vs* 13.4s). A facilitated full oxidation of the films bearing nanoparticles, by reducing the π-π* band, generates faster

displays and higher color contrasts, with an increase of almost 50% in transmittance, after 1000 cycles. For the case of the yellow-colored polymer, designed and straightforward synthetic structural modifications by the introduction of alkyl and alkyloxy chains directly bonded to the thiophene, which allowed the decrease of their redox potential, and the addition of single or double C-C bonds as linkers, modulating their conjugation thus rising different electrochromic colors, using the same core linear structure. The designed strategy allowed the synthesis of polymers **1**-**6**, where all polymers are capable of forming nanoparticles in water-based solutions. Specifically, the aim to synthesize a yellow-colored polymer (**6**) presenting low redox potentials was achieved, and the formation of nanoparticles from polymer **6** significantly improved their electrochromic performance, when compared ECDs using the pristine polymer **6**. Moreover, ECDs using **6**-NPs presented faster switching times (1.7s *vs* 11s) for the double of the color contrast (in transmittance), after 1000 cycles.

On a different approach, highly stable hybrid dispersions of a newly synthesized pyrene-appended polythiophene (PTP) and multi-walled carbon nanotubes (MWCNTs) were developed and optimized, taking advantage of the π-π non-covalent interactions between the pyrene unit and the CNTs. Solid-state ECDs were assembled using hybrid spray-coated films with an optimized amount of MWCNTs (from 0 to 10% w/w) in respect to the newly synthesized PTP. The characterization of the assembled ECDs presented a remarkable increase of electrochromic performance regarding switching times and durability when hybrid films were employed. In detail, electrochromic devices bearing 7.5 wt.% of MWCNTs presented reduction switching times 10 times faster, when compared with ECDs containing pristine PTP (0.3s *vs* 3.8s) and 5 times more durable (35000 cycles *vs* 7000 cycles) upon continuous electrochromic switching between -1.5 and 1.5V. This enhancement in electrochromic performance occurs due to an increased regioregularity and homogeneity of the hybrid films observed by STM, SEM and AFM, in contrast with aggregated films of PTP, generating faster switching times. Additionally, the striking increase in durability is generated from the ability of the MWCNTs to act as radical scavengers, avoiding the formation of π-conjugated fragments, with lower electrochromic activity, during the cycling measurement.

The original goal was to use these hybrid dispersions to obtain, simultaneously, an electrochromic and conductive layer by spray-coating them in a non-conductive substrate like PET, profiting from the high conductivities of the carbon material and thus, producing ITO-free ECDs. However, using a range from 2.5 to 10% of CNTs (in wt.%) spray-coated in PET substrates, the hybrid films presented high resistivities (from 130 to 20MΩ), which are not

suitable for electrochromic applications. Additionally, using a higher amount of CNTs would suppress the optic electrochromic color switch. Following that motivation, a different material was explored for the assembly of ITO-free ECDs, namely, a hybrid coating of copper-nanowires and reduced graphene oxide (CuNWs-rGO). Therefore, highly conductive, and transparent hybrid CuNWs-rGO electrodes were produced and used as conductive electrodes for the assembly of ITO-free ECDs using PEDOT as electrochromic material. The assembled ITO-free ECDs presented reasonable performances with switching times within the 5 second range (comparable with ITO), a good optical contrast and high durabilities (>30000 cycles).

Overall, the presented work contributes significantly to take one step further on the design and synthesis of new polythiophene materials, avoiding non-toxic solvents and the use of newly synthesized materials for the assembly of ECDs with enhanced performances. Furthermore, the approach of using polythiophene nanoparticles from water-based solutions can stimulate a new breakthrough in the industry where, simple synthetic modifications and nanostructured polythiophene materials using green solvents, can offer a larger choice of user-oriented materials and explore new enhanced properties for different organic devices such as electrochromic devices, solar cells, or LEDs. Additionally, the design, synthesis, and employment of hybrid materials for optoelectronic applications such as ECDs, can also promote an increased scientific interest in this area, expanding the color palette while achieving enhanced properties, with a possible scale-up for industrial applications.

<div style="text-align: right">

7

</div>

WORK DISSEMINATION

7.1 Publications Contributing to the Dissertation

Moreira,T., Laia, C.A.T., Zangoli, M., Antunes, M., Di Maria, F., De Monte, S., Liscio, F., Parola, A.J., Barbarella, G., Semicrystalline Polythiophene-Based Nanoparticles Deposited from Water on Flexible PET/ITO Substrates as a Sustainable Approach towards Long-Lasting Solid-State Electrochromic Devices, *ACS Appl. Polym. Mater.* (2020), **2**, 8, 3301-3309.
https://doi.org/10.1021/acsapm.0c00440

Moreira, T., Di Maria, F., Zangoli, M., Fabiano, E., Manet, I., Mazzaro, R., Morandi, V., Marinelli, M., Gigli, G., Parola, A.J., Laia, C.A.T., Barbarella, G., Processable Thiophene-Based Polymers with Tailored Electronic Properties and their Application in Solid-State Electrochromic Devices using Nanoparticle Films, *Adv. Electron. Mater.* (2021),**7**, 2100166.
https://doi.org/10.1002/aelm.202100166

T. Moreira, M. Maia, A. J. Parola, M. Zangoli, F. Di Maria and C. A. T. Laia, Ink-jet-printed semiconductor electrochromic nanoparticles: Development and applications in electrochromism (Chapter 12), in *Chemical Solution Synthesis for Materials Design and Thin Film Device Applications*, Elsevier, 2021, pp. 407–437.
https://doi.org/10.1016/B978-0-12-819718-9.00021-2

7.2 Communications

7.2.1 In National and International Scientific Meetings

XXVI Encontro Nacional da Sociedade Portuguesa de Química (SPQ), Porto, Portugal

T. Moreira, A. Aliprandi, C. Pinheiro, C. Laia, P. Samori, " Highly Transparent, Conductive and Flexible Electrodes for Electrochromic Devices using a "Green" Hybrid Copper-Nanowires-reduced-Graphene-Oxide Coating", XXVI Encontro Nacional da SPQ, 24-26th July 2019, Porto, Portugal, Poster Communication CPN7.

7th Portuguese Young Chemists Meeting, Online

T. Moreira, F. Di Maria, M. Zangoli, A.J. Parola, G. Barbarella, C.A.T. Laia, "Enhanced Electrochromic Performances using Water-Dispersible Poly-3-Hexylthiophene (P3HT) Nanoparticles", 7th Portuguese Young Chemists Meeting, 19-21st May 2021, Online, Oral Communication. OC4.

4th International Caparica Christmas Conference on Translational Chemistry (IC3TC 2021), Caparica, Portugal

T. Moreira, C.A.T. Laia, A.J. Parola, F. Di Maria, M. Zangoli, A. Stopin, D. Bonifazi, "Nanostructured Polythiophene Materials for Electrochromic Applications", IC3TC 2021, 6-8th December 2021, Caparica, Portugal, Oral Communication SG18.

4th International Caparica Christmas Conference on Translational Chemistry (IC3TC 2021), Caparica, Portugal

T. Moreira, C.A.T. Laia, A.J. Parola, F. Di Maria, M. Zangoli, A. Stopin, D. Bonifazi, "Nanostructured Polythiophene Materials for Electrochromic Applications", IC3TC 2021, 6-8th December 2021, Caparica, Portugal, Poster Communication PSG18.

28th PhotoIUPAC, Amsterdam, Netherlands

T. Moreira, C.A.T. Laia, A.J. Parola, F. Di Maria, M. Zangoli, A. Stopin, D. Bonifazi, "Nanostructured Polythiophene Materials for Electrochromic Applications", 28th PhotoIUPAC, 17-22nd July 2022, Amsterdam, Netherlands, Poster Communication, P53.

7.2.2 In Local Scientific Meetings

Coffee-Talk at CNR-ISOF, Bologna, Italy

T. Moreira, A. Aliprandi, C. Pinheiro, C.A.T. Laia, P. Samori, "Highly Transparent, Conductive and Flexible Electrodes for Electrochromic Devices using a "Green" Hybrid Copper-Nanowires-reduced-Graphene-Oxide Coating", Coffee-Talk at CNR-ISOF, November 27th, 2018, Bologna, Italy, Invited Oral Communication.

Webinar @DQ-NOVA School of Science and Technology, Online

T. Moreira, "Nanostructured Polythiophene Materials for Electrochromic Applications", Webinar Online@DQ-NOVA School of Science and Technology, June 9th, 2021, Online, Oral Communication.

BIBLIOGRAPHY

1   C. Yan, W. Kang, J. Wang, M. Cui, X. Wang, C. Y. Foo, K. J. Chee and P. S. Lee, *ACS Nano*, 2014, **8**, 316–322.

2   H. Müller, E. Napari, L. Hakala, A. Colley and J. Häkkilä, in *Proceedings of the 8th ACM International Symposium on Pervasive Displays*, ACM, New York, NY, USA, 2019, pp. 1–2.

3   W. Jensen, M. Löchtefeld and H. Knoche, in *Extended Abstracts of the 2019 CHI Conference on Human Factors in Computing Systems*, ACM, New York, NY, USA, New York, USA, 2019, pp. 1–6.

4   A. Colley, Ö. Raudanjoki, K. Mikkonen and J. Häkkilä, in *Proceedings of the 18th International Conference on Mobile and Ubiquitous Multimedia*, ACM, New York, NY, USA, 2019, pp. 1–5.

5   N. I. Jaksic and C. Salahifar, *Sol. Energy Mater. Sol. Cells*, 2003, **79**, 409–423.

6   A. Colley, J. Häkkilä, M.-T. Forsman, B. Pfleging and F. Alt, in *Proceedings of the 7th ACM International Symposium on Pervasive Displays*, ACM, New York, NY, USA, 2018, vol. 6, pp. 1–8.

7   H. Müller, A. Colley, J. Häkkilä, W. Jensen and M. Löchtefeld, in *Adjunct Proceedings of the 2019 ACM International Joint Conference on Pervasive and Ubiquitous Computing and Proceedings of the 2019 ACM International Symposium on Wearable Computers*, ACM, New York, NY, USA, 2019, pp. 1075–1078.

8   A. M. Österholm, D. E. Shen, J. A. Kerszulis, R. H. Bulloch, M. Kuepfert, A. L. Dyer and J. R. Reynolds, *ACS Appl. Mater. Interfaces*, 2015, **7**, 1413–1421.

9   Ynvisible Applications, https://www.ynvisible.com/solutions, (accessed 10 August 2022).

10   P. M. Beaujuge and J. R. Reynolds, *Chem. Rev.*, 2010, **110**, 268–320.

11   A. L. Dyer, M. R. Craig, J. E. Babiarz, K. Kiyak and J. R. Reynolds, *Macromolecules*, 2010, **43**, 4460–4467.

12   D. T. Christiansen, A. L. Tomlinson and J. R. Reynolds, *J. Am. Chem. Soc.*, 2019, **141**, 3859–3862.

13   K. Cao, D. E. Shen, A. M. Österholm, J. A. Kerszulis and J. R. Reynolds, *Macromolecules*, 2016, **49**, 8498–8507.

14   A. D. Child and J. R. Reynolds, *J. Chem. Soc. Chem. Commun.*, 1991, 1779–1781.

15   V. Rai, R. S. Singh, D. J. Blackwood and D. Zhili, *Adv. Eng. Mater.*, 2020, **22**, 1–23.

16   CHARM group at NOVA School of Science and Technology, https://laqv.requimte.pt/research/research-groups/112-cultural_heritage_and_responsive_materials, (accessed 14 September 2022).

17   Ynvisible, https://www.ynvisible.com/, (accessed 14 September 2022).

18   Mediteknology at CNR-ISOF, https://www.cnr.it/en/spinoff/14/mediteknology-s-r-l, (accessed 14 September 2022).

19   EU Project INFUSION Ref. 734834, https://cordis.europa.eu/project/id/734834, (accessed 14 September 2022).

20   M. Zangoli and F. Di Maria, *View*, 2021, **2**, 20200086.

21   Bonifazi Group at University of Vienna, https://bonifazi-group.univie.ac.at/, (accessed 14 September 2022).

22   Nanochemistry Laboratory at University of Strasbourg, http://www.nanochemistry.fr/, (accessed 14 September 2022).

23   EU Project DecoChrom Ref. 760973, https://decochrom.com/, (accessed 14 September 2022).

24   S. K. Deb, *Appl. Opt.*, 1969, **8**, 192.

25   J. S. E. M. Svensson and C. G. Granqvist, *Sol. Energy Mater.*, 1985, **12**, 391–402.

26   C. M. Lampert, *Sol. Energy Mater.*, 1984, **11**, 1–27.

27   Y. Wang, E. L. Runnerstrom and D. J. Milliron, *Annu. Rev. Chem. Biomol. Eng.*, 2016, **7**, 283–304.

28   M. Casini, *Renew. Energy*, 2018, **119**, 923–934.

29   D. Lötzsch, V. Eberhardt and C. Rabe, *Ullmann's Encycl. Ind. Chem.*, 2016, 1–26.

30   A. Ritter and Ritter Axel, *Smart Materials*, Birkhäuser Basel, Basel, Basel, 2007.

31   J. R. Platt, *J. Chem. Phys.*, 1961, **34**, 862–863.

32   F. G. K. Baucke, *Sol. Energy Mater.*, 1987, **16**, 67–77.

33   O. Glember and H. Saurr, *Zeitschrift für Anorg. Chemie*, 1943, **252**, 144–159.

34   O. Glemser and C. Naumann, *Zeitschrift für Anorg. und Allg. Chemie*, 1951, **265**, 288–302.

35   S. K. Deb, *Philos. Mag.*, 1973, **27**, 801–822.

36   S. K. Deb and H. Witzke, in *1975 International Electron Devices Meeting*, IRE, 1975, pp. 393–397.

37   E. L. Runnerstrom, A. Llordés, S. D. Lounis and D. J. Milliron, *Chem. Commun.*, 2014, **50**, 10555–10572.

38   A. Kraft, *ChemTexts*, 2019, **5**, 1.

39   P. Monk, R. Mortimer and D. Rosseinsky, in *Electrochromism and Electrochromic Devices*, Cambridge University Press, Cambridge, 2009, pp. 395–416.

40   F. G. K. G. K. Baucke, K. Bange and T. Gambke, *Displays*, 1988, **9**, 179–187.

41   K. Bange and T. Gambke, *Adv. Mater.*, 1990, **2**, 10–16.

42   F. G. K. Baucke, 2001, pp. 5–34.

43   *Byker, H. J. Electrochromic Devices with Bipyridinium Salt Solut. US5336448, 1994.*

44   C. J. Schoot, J. J. Ponjee, H. T. van Dam, R. A. van Doorn and P. T. Bolwijn, *Appl. Phys. Lett.*, 1973, **23**, 64–65.

45   J. Bruinink, *J. Electrochem. Soc.*, 1977, **124**, 1854.

46   *Varaprasad, D. V.; Mccabe, I. A.; Habibi, H.; Lynam, N. R.; Zhao, M.; Dornan, C. A. Electrochromic Mirrors Devices. US5724187, 1998.*

47   K. W. Shah, S.-X. Wang, D. X. Y. Soo and J. Xu, *Polymers (Basel).*, 2019, **11**, 1839.

48   Gentex Corporation.

49   J. Qian, D. Ma, Z. Xu, D. Li and J. Wang, *Sol. Energy Mater. Sol. Cells*, 2018, **177**, 9–14.

50   C. G. Granqvist, *Thin Solid Films*, 2014, **564**, 1–38.

51   U. Posset, M. Harsch, A. Rougier, B. Herbig, G. Schottner and G. Sextl, *RSC Adv.*, 2012, **2**, 5990.

52   C. M. Lampert, *Mater. Today*, 2004, **7**, 28–35.

53   G. Cai, A. L.-S. Eh, L. Ji and P. S. Lee, *Adv. Sustain. Syst.*, 2017, **1**, 1700074.

54   Saint-Gobain, SageGlass, Resources. SageGlass for Hospitals, https://sageglass.com/sites/default/files/sageglass-healthcare-en.pdf, (accessed 10 August 2022).

55 R. J. Mortimer, D. R. Rosseinsky and P. M. S. S. Monk, *Electrochromic Materials and Devices*, Wiley-VCH Verlag GmbH & Co. KGaA, Weinheim, Germany, Germany, 2013.

56 P. M. S. Monk, D. R. Rosseinsky and R. J. Mortimer, in *Electrochromic Materials and Devices*, Wiley-VCH Verlag GmbH & Co. KGaA, 2015, pp. 57–90.

57 H. J. Byker, *Electrochim. Acta*, 2001, **46**, 2015–2022.

58 G. J. Stec, A. Lauchner, Y. Cui, P. Nordlander and N. J. Halas, *ACS Nano*, 2017, **11**, 3254–3261.

59 C. Costa, C. Pinheiro, I. Henriques and C. A. T. T. Laia, *ACS Appl. Mater. Interfaces*, 2012, **4**, 1330–1340.

60 S. K. Deb, *Sol. Energy Mater. Sol. Cells*, 1995, **39**, 191–201.

61 C. G. Granqvist, in *Kirk-Othmer Encyclopedia of Chemical Technology*, John Wiley & Sons, Inc., Hoboken, NJ, USA, NJ, USA, 2006, vol. 2003.

62 R.-T. Wen, C. G. Granqvist and G. A. Niklasson, *Nat. Mater.*, 2015, **14**, 996–1001.

63 A. Paolella, C. Faure, V. Timoshevskii, S. Marras, G. Bertoni, A. Guerfi, A. Vijh, M. Armand and K. Zaghib, *J. Mater. Chem. A*, 2017, **5**, 18919–18932.

64 M. Schott, H. Lorrmann, W. Szczerba, M. Beck and D. G. Kurth, *Sol. Energy Mater. Sol. Cells*, 2014, **126**, 68–73.

65 T.-T.-N. Nguyen, C.-Y. Chan and J.-L. He, *Thin Solid Films*, 2016, **603**, 276–282.

66 A. Aliprandi, T. Moreira, C. Anichini, M.-A. Stoeckel, M. Eredia, U. Sassi, M. Bruna, C. Pinheiro, C. A. T. Laia, S. Bonacchi and P. Samorì, *Adv. Mater.*, 2017, **29**, 1703225.

67 S. M. Fonseca, T. Moreira, A. J. Parola, C. Pinheiro and C. A. T. Laia, *Sol. Energy Mater. Sol. Cells*, 2017, **159**, 94–101.

68 A. J. Heeger, *Polym. J.*, 1985, **17**, 201–208.

69 A. O. Patil, A. J. Heeger and F. Wudl, *Chem. Rev.*, 1988, **88**, 183–200.

70 G. Heywang and F. Jonas, *Adv. Mater.*, 1992, **4**, 116–118.

71 H. Yamato, K. Kai, M. Ohwa, T. Asakura, T. Koshiba and W. Wernet, *Synth. Met.*, 1996, **83**, 125–130.

72 H. J. Ahonen, J. Kankare, J. Lukkari and P. Pasanen, *Synth. Met.*, 1997, **84**, 215–216.

73 L. Groenendaal, F. Jonas, D. Freitag, H. Pielartzik and J. R. Reynolds, *Adv. Mater.*, 2000, **12**, 481–494.

74 I. H. Sanders, S. Electrochromics, Fading Protection and SageGlass®Products, SAGE Electrochromics, *2014*.

75 H. J. Byker, in *Electrochromic Materials and Devices*, Wiley-VCH Verlag GmbH & Co. KGaA, Weinheim, Germany, 2015, pp. 399–418.

76 G. Cai, J. Wang and P. S. Lee, *Acc. Chem. Res.*, 2016, **49**, 1469–1476.

77 X. Li, K. Perera, J. He, A. Gumyusenge and J. Mei, *J. Mater. Chem. C*, 2019, **7**, 12761–12789.

78 T. Ito, H. Shirakawa and S. Ikeda, *J. Polym. Sci. Polym. Chem. Ed.*, 1974, **12**, 11–20.

79 C. K. Chiang, C. R. Fincher, Y. W. Park, A. J. Heeger, H. Shirakawa, E. J. Louis, S. C. Gau and A. G. MacDiarmid, *Phys. Rev. Lett.*, 1977, **39**, 1098–1101.

80 H. Shirakawa, E. J. Louis, A. G. MacDiarmid, C. K. Chiang and A. J. Heeger, *J. Chem. Soc. Chem. Commun.*, 1977, 578.

81 C. K. Chiang, M. A. Druy, S. C. Gau, A. J. Heeger, E. J. Louis, A. G. MacDiarmid, Y. W. Park and H. Shirakawa, *J. Am. Chem. Soc.*, 1978, **100**, 1013–1015.

82 N. Yi and M. R. Abidian, in *Biosynthetic Polymers for Medical Applications*, Elsevier, 2016, pp. 243–276.

83 T. Yamamoto, K. Sanechika and A. Yamamoto, *J. Polym. Sci. Polym. Lett. Ed.*, 1980, **18**, 9–12.

84 G. Koßmehl and G. Chatzitheodorou, *Die Makromol. Chemie, Rapid Commun.*, 1981, **2**,

551–555.

85   G. Wegner, *Angew. Chemie Int. Ed. English*, 1981, **20**, 361–381.

86   K. Kaneto, Y. Kohno, K. Yoshino and Y. Inuishi, *J. Chem. Soc. Chem. Commun.*, 1983, 382.

87   J. L. Brédas, R. L. Elsenbaumer, R. R. Chance and R. Silbey, *J. Chem. Phys.*, 1983, **78**, 5656–5662.

88   R. J. Waltman, J. Bargon and A. F. Diaz, *J. Phys. Chem.*, 1983, **87**, 1459–1463.

89   M. N. Gueye, A. Carella, J. Faure-Vincent, R. Demadrille and J.-P. Simonato, *Prog. Mater. Sci.*, 2020, **108**, 100616.

90   T. Beduk, E. Bihar, S. G. Surya, A. N. Castillo, S. Inal and K. N. Salama, *Sensors Actuators B Chem.*, 2020, **306**, 127539.

91   Y. Wen and J. Xu, *J. Polym. Sci. Part A Polym. Chem.*, 2017, **55**, 1121–1150.

92   G. Huseynova, Y. Hyun Kim, J.-H. Lee and J. Lee, *J. Inf. Disp.*, 2020, **21**, 71–91.

93   M. T. Ramesan and K. Suhailath, in *Micro and Nano Fibrillar Composites (MFCs and NFCs) from Polymer Blends*, Elsevier, 2017, pp. 301–326.

94   R. R. Smith, A. P. Smith, J. T. Stricker, B. E. Taylor and M. F. Durstock, *Macromolecules*, 2006, **39**, 6071–6074.

95   L. Beverina, G. A. Pagani and M. Sassi, *Chem. Commun.*, 2014, **50**, 5413–5430.

96   Y. Yin, W. Li, X. Zeng, P. Xu, I. Murtaza, Y. Guo, Y. Liu, T. Li, J. Cao, Y. He and H. Meng, *Macromolecules*, 2018, **51**, 7853–7862.

97   M. De Keersmaecker, A. W. Lang, A. M. Österholm and J. R. Reynolds, *ACS Appl. Mater. Interfaces*, 2018, **10**, 31568–31579.

98   *Dietrich, M.; Heywang, G.; Jonas, F.; Schmidtberg, W.; Heinze, J. Polythiophenes, Process Their Prep. Their Use. EP0339340, 1988.*

99   F. Jonas and W. Krafft, *Jonas, F.; Krafft, W. New Polythiophene Dispersions, Their Prep. Their Use. EP0440957, 1992.*

100   X. Fan, W. Nie, H. Tsai, N. Wang, H. Huang, Y. Cheng, R. Wen, L. Ma, F. Yan and Y. Xia, *Adv. Sci.*, 2019, **6**, 1900813.

101   L. Hu, J. Song, X. Yin, Z. Su and Z. Li, *Polymers (Basel).*, 2020, **12**, 145.

102   K. Nawa, K. Miyawaki, I. Imae, N. Noma and Y. Shirota, *J. Mater. Chem.*, 1993, **3**, 113.

103   M. Dietrich, J. Heinze, G. Heywang and F. Jonas, *J. Electroanal. Chem.*, 1994, **369**, 87–92.

104   J. C. Gustafsson, B. Liedberg, O. Inganas and O. Inganäs, *Solid State Ionics*, 1994, **69**, 145–152.

105   J. D. Stenger-Smith, *Prog. Polym. Sci.*, 1998, **23**, 57–79.

106   C. Duc, G. G. Malliaras, V. Senez and A. Vlandas, *Synth. Met.*, 2018, **238**, 14–21.

107   D. Levasseur, I. Mjejri, T. Rolland and A. Rougier, *Polymers (Basel).*, 2019, **11**, 179.

108   L. Groenendaal, G. Zotti, P. H. Aubert, S. M. Waybright and J. R. Reynolds, *Adv. Mater.*, 2003, **15**, 855–879.

109   R. H. Bulloch, J. A. Kerszulis, A. L. Dyer and J. R. Reynolds, *ACS Appl. Mater. Interfaces*, 2015, **7**, 1406–1412.

110   L. R. Savagian, A. M. Österholm, D. E. Shen, D. T. Christiansen, M. Kuepfert and J. R. Reynolds, *Adv. Opt. Mater.*, 2018, **6**, 1800594.

111   S. A. Sapp, G. A. Sotzing, J. L. Reddinger and J. R. Reynolds, *Adv. Mater.*, 1996, **8**, 808–811.

112   J. R. Reynolds, A. Kumar, J. L. Reddinger, B. Sankaran, S. A. Sapp and G. A. Sotzing, *Synth. Met.*, 1997, **85**, 1295–1298.

113   B. Sankaran and J. R. Reynolds, *Macromolecules*, 1997, **30**, 2582–2588.

114   D. M. Welsh, A. Kumar, E. W. Meijer and J. R. Reynolds, *Adv. Mater.*, 1999, **11**, 1379–1382.

115   A. A. Argun, A. Cirpan and J. R. Reynolds, *Adv. Mater.*, 2003, **15**, 1338–1341.

116   B. D. Reeves, C. R. G. Grenier, A. A. Argun, A. Cirpan, T. D. McCarley and J. R. Reynolds, *Macromolecules*, 2004, **37**, 7559–7569.

117   A. A. Argun, P.-H. Aubert, B. C. Thompson, I. Schwendeman, C. L. Gaupp, J. Hwang, N. J. Pinto, D. B. Tanner, A. G. MacDiarmid and J. R. Reynolds, *Chem. Mater.*, 2004, **16**, 4401–4412.

118   R. M. Walczak, J. S. Cowart, Jr., K. A. Abboud and J. R. Reynolds, *Chem. Commun.*, 2006, 1604.

119   R. M. Walczak and J. R. Reynolds, *Adv. Mater.*, 2006, **18**, 1121–1131.

120   R. Berridge, S. P. Wright, P. J. Skabara, A. Dyer, T. Steckler, A. A. Argun, J. R. Reynolds, R. W. Harrington and W. Clegg, *J. Mater. Chem.*, 2007, **17**, 225–231.

121   P. M. Beaujuge, S. Ellinger and J. R. Reynolds, *Nat. Mater.*, 2008, **7**, 795–799.

122   C. M. Amb, A. L. Dyer and J. R. Reynolds, *Chem. Mater.*, 2011, **23**, 397–415.

123   J. A. Kerszulis, K. E. Johnson, M. Kuepfert, D. Khoshabo, A. L. Dyer and J. R. Reynolds, *J. Mater. Chem. C*, 2015, **3**, 3211–3218.

124   A. M. Österholm, D. E. Shen, D. S. Gottfried and J. R. Reynolds, *Adv. Mater. Technol.*, 2016, **1**, 1600063.

125   I. F. Perepichka and D. F. Perepichka, *Handbook of Thiophene-Based Materials*, John Wiley & Sons, Ltd, Chichester, UK, 2009.

126   H.-H. Chou, A. Nguyen, A. Chortos, J. W. F. To, C. Lu, J. Mei, T. Kurosawa, W.-G. Bae, J. B.-H. Tok and Z. Bao, *Nat. Commun.*, 2015, **6**, 8011.

127   B.-A. Mei, O. Munteshari, J. Lau, B. Dunn and L. Pilon, *J. Phys. Chem. C*, 2018, **122**, 194–206.

128   R. Celiesiute, A. Ramanaviciene, M. Gicevicius and A. Ramanavicius, *Crit. Rev. Anal. Chem.*, 2019, **49**, 195–208.

129   K. Salikolimi, M. Kawamoto, P. He, T. Aigaki and Y. Ito, *Polym. J.*, 2017, **49**, 429–437.

130   C. J. Barile, D. J. Slotcavage and M. D. McGehee, *Chem. Mater.*, 2016, **28**, 1439–1445.

131   X. Xing, Q. Zeng, M. Vagin, M. Fahlman and F. Zhang, *Nano Energy*, 2018, **47**, 123–129.

132   Y. Y. Y. Kim, Y. Y. Y. Kim, S. Kim and E. Kim, *ACS Nano*, 2010, **4**, 5277–5284.

133   C. Costa, C. Pinheiro, I. Henriques and C. A. T. T. Laia, *ACS Appl. Mater. Interfaces*, 2012, **4**, 5266–5275.

134   J. E. Millstone, D. F. J. J. Kavulak, C. H. Woo, T. W. Holcombe, E. J. Westling, A. L. Briseno, M. F. Toney, J. M. J. Fréchet and J. M. J. Fréchet, *Langmuir*, 2010, **26**, 13056–13061.

135   M. Bag, T. S. Gehan, L. A. Renna, D. D. Algaier, P. M. Lahti and D. Venkataraman, *RSC Adv.*, 2014, **4**, 45325–45331.

136   M. Bag, T. S. Gehan, D. D. Algaier, F. Liu, G. Nagarjuna, P. M. Lahti, T. P. Russell and D. Venkataraman, *Adv. Mater.*, 2013, **25**, 6411–6415.

137   J. P. Rao and K. E. Geckeler, *Prog. Polym. Sci.*, 2011, **36**, 887–913.

138   H. Shimizu, M. Yamada, R. Wada and M. Okabe, *Polym. J.*, 2008, **40**, 33–36.

139   C. E. Mora-Huertas, H. Fessi and A. Elaissari, *Adv. Colloid Interface Sci.*, 2011, **163**, 90–122.

140   G. Nagarjuna, M. Baghgar, J. a Labastide, D. D. Algaier, M. D. Barnes and D. Venkataraman, *ACS Nano*, 2012, **6**, 10750–10758.

141   F. D. Fleischli, N. Ghasdian, T. K. Georgiou and N. Stingelin, *J. Mater. Chem. C*, 2015, **3**, 2065–2071.

142   J. D. Robertson, L. Rizzello, M. Avila-Olias, J. Gaitzsch, C. Contini, M. S. Magoń, S. A. Renshaw and G. Battaglia, *Sci. Rep.*, 2016, **6**, 27494.

143   E. Zucchetti, M. Zangoli, I. Bargigia, C. Bossio, F. Di Maria, G. Barbarella, C. D'Andrea, G. Lanzani and M. R. Antognazza, *J. Mater. Chem. B*, 2017, **5**, 565–574.

144   C. Gu, A. Jia, Y.-M. Zhang and S. X. Zhang, *Chem. Rev.*, , DOI:10.1021/acs.chemrev.1c01055.

145   J. Zhu, S. Wei, M. J. Alexander, T. D. Dang, T. C. Ho and Z. Guo, *Adv. Funct. Mater.*, 2010, **20**, 3076–3084.

146   L. Ma, Y. Li, X. Yu, Q. Yang and C.-H. Noh, *Sol. Energy Mater. Sol. Cells*, 2008, **92**, 1253–1259.

147   Y.-C. Nah, S.-S. Kim, J.-H. Park, H.-J. Park, J. Jo and D.-Y. Kim, *Electrochem. commun.*, 2007, **9**, 1542–1546.

148   M. A. G. Namboothiry, T. Zimmerman, F. M. Coldren, J. Liu, K. Kim and D. L. Carroll, *Synth. Met.*, 2007, **157**, 580–584.

149   B. N. Reddy, M. Deepa, A. G. Joshi and A. K. Srivastava, *J. Phys. Chem. C*, 2011, **115**, 18354–18365.

150   S. Bhandari, M. Deepa, A. K. Srivastava, A. G. Joshi and R. Kant, *J. Phys. Chem. B*, 2009, **113**, 9416–9428.

151   S. Bhandari, M. Deepa, A. K. Srivastava, C. Lal and R. Kant, *Macromol. Rapid Commun.*, 2008, **29**, 1959–1964.

152   S. Rathinavel, K. Priyadharshini and D. Panda, *Mater. Sci. Eng. B*, 2021, **268**, 115095.

153   K. Yoshino, H. Kajii, H. Araki, T. Sonoda, H. Take and S. Lee, *Fuller. Sci. Technol.*, 1999, **7**, 695–711.

154   M.-F. Yu, O. Lourie, M. J. Dyer, K. Moloni, T. F. Kelly and R. S. Ruoff, *Science (80-.).*, 2000, **287**, 637–640.

155   T. W. Ebbesen, H. J. Lezec, H. Hiura, J. W. Bennett, H. F. Ghaemi and T. Thio, *Nature*, 1996, **382**, 54–56.

156   E. M. Byrne, M. A. McCarthy, Z. Xia and W. A. Curtin, *Phys. Rev. Lett.*, 2009, **103**, 045502.

157   K.-Y. Shen, C.-W. Hu, L.-C. Chang and K.-C. Ho, *Sol. Energy Mater. Sol. Cells*, 2012, **98**, 294–299.

158   M. S. M. Zambri, M. M. Norani and C. F. Kait, *Adv. Mater. Res.*, 2011, **364**, 338–343.

159   M. S. Mohd Zambri, N. M. Mohamed and C. F. Kait, in *AIP Conference Proceedings*, 2012, vol. 1482, pp. 107–111.

160   E. Nossol and A. J. G. Zarbin, *Sol. Energy Mater. Sol. Cells*, 2013, **109**, 40–46.

161   M. Jo and H. Ahn, *Int. J. Energy Res.*, 2022, 1–14.

162   B. K. Billing, M. Mayank, P. K. Agnihotri and N. Singh, *Analyst*, 2018, **143**, 3343–3352.

163   L. Qu, R. B. Martin, W. Huang, K. Fu, D. Zweifel, Y. Lin, Y.-P. Sun, C. E. Bunker, B. A. Harruff, J. R. Gord and L. F. Allard, *J. Chem. Phys.*, 2002, **117**, 8089–8094.

164   E. J. Petersen, R. A. Pinto, P. F. Landrum and W. J. Weber, Jr., *Environ. Sci. Technol.*, 2009, **43**, 4181–4187.

165   C. Walgama, N. Means, N. F. Materer and S. Krishnan, *Phys. Chem. Chem. Phys.*, 2015, **17**, 4025–4028.

166   P. D. Tran, A. Le Goff, J. Heidkamp, B. Jousselme, N. Guillet, S. Palacin, H. Dau, M. Fontecave and V. Artero, *Angew. Chemie*, 2011, **123**, 1407–1410.

167   N. Nakashima, Y. Tomonari and H. Murakami, *Chem. Lett.*, 2002, **31**, 638–639.

168   A. Şenocak, C. Göl, T. V. Basova, E. Demirbaş, M. Durmuş, H. Al-Sagur, B. Kadem and A. Hassan, *Sensors Actuators B Chem.*, 2018, **256**, 853–860.

169   A. T. Haedler, H. Misslitz, C. Buehlmeyer, R. Q. Albuquerque, A. Köhler and H. W. Schmidt, *ChemPhysChem*, 2013, **14**, 1818–1829.

170   R. Ayranci, G. Başkaya, M. Güzel, S. Bozkurt, F. Şen and M. Ak, *ChemistrySelect*, 2017, **2**, 1548–1555.

171   M. R. Karim, C. J. Lee and M. S. Lee, *J. Polym. Sci. Part A Polym. Chem.*, 2006, **44**, 5283–5290.

172 K. Yanagi, R. Moriya, Y. Yomogida, T. Takenobu, Y. Naitoh, T. Ishida, H. Kataura, K. Matsuda and Y. Maniwa, *Adv. Mater.*, 2011, **23**, 2811–2814.

173 M. Costalin, I. Mjejri, N. Penin, O. Viraphong, V. Shanov and A. Rougier, *J. Phys. Chem. Solids*, 2021, **154**, 110035.

174 Y. Nishikitani, T. Asano, S. Uchida and T. Kubo, *Electrochim. Acta*, 1999, **44**, 3211–3217.

175 M. O. M. Edwards, G. Boschloo, T. Gruszecki, H. Pettersson, R. Sohlberg and A. Hagfeldt, *Electrochim. Acta*, 2001, **46**, 2187–2193.

176 J.-W. Kim, D.-K. Kwon and J.-M. Myoung, *Chem. Eng. J.*, 2020, **387**, 124145.

177 R. Singh, J. Tharion, S. Murugan and A. Kumar, *ACS Appl. Mater. Interfaces*, 2017, **9**, 19427–19435.

178 S. Sharma, S. Shriwastava, S. Kumar, K. Bhatt and C. C. Tripathi, *Opto-Electronics Rev.*, 2018, **26**, 223–235.

179 S. Ye, A. R. Rathmell, Z. Chen, I. E. Stewart and B. J. Wiley, *Adv. Mater.*, 2014, **26**, 6670–6687.

180 J. Scarminio, *Sol. Energy Mater. Sol. Cells*, 2003, **79**, 357–368.

181 P. Monk, R. Mortimer and D. Rosseinsky, *Electrochromism: Fundamentals and Applications, VCH*, 1995.

182 J. Liu and J. P. Coleman, *Mater. Sci. Eng. A*, 2000, **286**, 144–148.

183 R. Brooke, E. Mitraka, S. Sardar, M. Sandberg, A. Sawatdee, M. Berggren, X. Crispin and M. P. Jonsson, *J. Mater. Chem. C*, 2017, **5**, 5824–5830.

184 A. Malti, R. Brooke, X. Liu, D. Zhao, P. Andersson Ersman, M. Fahlman, M. P. Jonsson, M. Berggren and X. Crispin, *J. Mater. Chem. C*, 2016, **4**, 9680–9686.

185 A. W. Lang, A. M. Österholm and J. R. Reynolds, *Adv. Funct. Mater.*, 2019, **29**, 1903487.

186 Z. Xu, W. Li, J. Huang, Q. Liu, X. Guo, W. Guo and X. Liu, *J. Mater. Chem. A*, 2018, **6**, 19584–19589.

187 S. H. Park, S. M. Lee, E. H. Ko, T. H. Kim, Y. C. Nah, S. J. Lee, J. H. Lee and H. K. Kim, *Sci. Rep.*, 2016, **6**, 1–12.

188 T. H. Kim, S. H. Park, D. H. Kim, Y. C. Nah and H. K. Kim, *Sol. Energy Mater. Sol. Cells*, 2017, **160**, 203–210.

189 C. Guillén and J. Herrero, *Thin Solid Films*, 2005, **480–481**, 129–132.

190 K. Ellmer, *Nat. Photonics*, 2012, **6**, 809–817.

191 R. M. Pasquarelli, D. S. Ginley and R. O'Hayre, *Chem. Soc. Rev.*, 2011, **40**, 5406.

192 K. Parvez, R. Li, S. R. Puniredd, Y. Hernandez, F. Hinkel, S. Wang, X. Feng and K. Müllen, *ACS Nano*, 2013, **7**, 3598–3606.

193 S. Pang, Y. Hernandez, X. Feng and K. Müllen, *Adv. Mater.*, 2011, **23**, 2779–2795.

194 G. Liu and T. J. Richardson, *Sol. Energy Mater. Sol. Cells*, 2005, **86**, 113–121.

195 Z. Y. Tang, J. J. Xue, C. Y. Liu and X. G. Zhuang, *Acta Phys. - Chim. Sin.*, 2001, **17**, 388.

196 A. Branco, L. C. Branco and F. Pina, *Chem. Commun.*, 2011, **47**, 2300–2302.

197 N. Jordão, L. Cabrita, F. Pina and L. C. Branco, *Chem. - A Eur. J.*, 2014, **20**, 3982–3988.

198 N. Jordão, H. Cruz, F. Pina and L. C. Branco, *Electrochim. Acta*, 2018, **283**, 718–726.

199 M. Hajzeri, M. Čolović, A. S. Vuk, U. Posset and B. Orel, *Mater. Tehnol.*, 2011, **45**, 433–438.

200 G. Chidichimo, M. De Benedittis, J. Lanzo, B. C. De Simone, D. Imbardelli, B. Gabriele, L. Veltri and G. Salerno, *Chem. Mater.*, 2007, **19**, 353–358.

201 N. Kobayashi, S. Miura, M. Nishimura and Y. Goh, *Electrochim. Acta*, 2007, **53**, 1643–1647.

202 Y. Ding, M. A. Invernale, D. M. D. Mamangun, A. Kumar and G. A. Sotzing, *J. Mater. Chem.*, 2011, **21**, 11873–11878.

203 C. A. C. Sequeira and D. M. F. Santos, *J. Electrochem. Soc.*, 2010, **157**, J202.

204   V. K. Thakur, G. Ding, J. Ma, P. S. Lee and X. Lu, *Adv. Mater.*, 2012, **24**, 4071–4096.

205   V. Neburchilov, J. Martin, H. Wang and J. Zhang, *J. Power Sources*, 2007, **169**, 221–238.

206   M. Miller and A. Bazylak, *J. Power Sources*, 2011, **196**, 601–613.

207   J. Marques, Ana. Pinheiro, Carlos. Baptista, *Electrolyte Solut. Print. method thereof resulting solid electrolyte, US20140361211A1, 2014*.

208   S. W. Jessica Wade, Joseph Hollis, *Printed Electronics*, 2018.

209   J. Izdebska, in *Printing on Polymers*, Elsevier, 2016, pp. 371–388.

210   D. Lupo, W. Clemens, S. Breitung and K. Hecker, in *Applications of Organic and Printed Electronics*, ed. E. Cantatore, Springer US, Boston, MA, 2013, pp. 1–26.

211   S. M. F. Cruz, L. A. Rocha and J. C. Viana, in *Flexible Electronics*, InTech, 2018, vol. i, p. 13.

212   X. Cao, H. Chen, X. Gu, B. Liu, W. Wang, Y. Cao, F. Wu and C. Zhou, *ACS Nano*, 2014, **8**, 12769–12776.

213   J. Lin, in *Printed Electronics*, John Wiley & Sons Singapore Pte. Ltd, Singapore, 2016, pp. 106–144.

214   J. Jensen, M. Hösel, A. L. Dyer and F. C. Krebs, *Adv. Funct. Mater.*, 2015, **25**, 2073–2090.

215   P. Sundriyal and S. Bhattacharya, 2018, pp. 89–113.

216   N. Komuro, S. Takaki, K. Suzuki and D. Citterio, *Anal. Bioanal. Chem.*, 2013, **405**, 5785–5805.

217   M. Bale, J. C. Carter, C. J. Creighton, H. J. Gregory, P. H. Lyon, P. Ng, L. Webb and A. Wehrum, *J. Soc. Inf. Disp.*, 2006, **14**, 453.

218   M. A. Lopez, J. C. Sanchez and M. Estrada, in *2008 7th International Caribbean Conference on Devices, Circuits and Systems*, IEEE, 2008, pp. 1–4.

219   Z. Bao, J. A. Rogers and H. E. Katz, *J. Mater. Chem.*, 1999, **9**, 1895–1904.

220   Z. Bao, *Adv. Mater.*, 2000, **12**, 227–230.

221   G. Cai, P. Darmawan, M. Cui, J. Chen, X. Wang, A. L.-S. Eh, S. Magdassi and P. S. Lee, *Nanoscale*, 2016, **8**, 348–357.

222   B.-H. Chen, S.-Y. Kao, C.-W. Hu, M. Higuchi, K.-C. Ho and Y.-C. Liao, *ACS Appl. Mater. Interfaces*, 2015, **7**, 25069–25076.

223   E. L. Howard, A. M. Österholm, D. E. Shen, L. P. Panchumarti, C. Pinheiro and J. R. Reynolds, *ACS Appl. Mater. Interfaces*, 2021, **13**, 16732–16743.

224   A. L. Dyer, E. J. Thompson and J. R. Reynolds, *ACS Appl. Mater. Interfaces*, 2011, **3**, 1787–1795.

225   T. A. S. J. R. Reynolds, B. C. Thompson, *Handbook of Conducting Polymers, Fourth Edition - 2 Volume Set*, Taylor & Francis Group, London, 2019.

226   D. Mampallil and H. B. Eral, *Adv. Colloid Interface Sci.*, 2018, **252**, 38–54.

227   Y. Li, Q. Yang, M. Li and Y. Song, *Sci. Rep.*, 2016, **6**, 24628.

228   H. Jin, J. Qian, L. Zhou, J. Yuan, H. Huang, Y. Wang, W. M. Tang and H. L. W. Chan, *ACS Appl. Mater. Interfaces*, 2016, **8**, 9088–9096.

229   H. Yildirim Erbil, *Adv. Colloid Interface Sci.*, 2015, **222**, 275–290.

230   P. Li, Y. Li, Z. K. Zhou, S. Tang, X. F. Yu, S. Xiao, Z. Wu, Q. Xiao, Y. Zhao, H. Wang and P. K. Chu, *Adv. Mater.*, 2016, **28**, 2511–2517.

231   H. Hu and R. G. Larson, *J. Phys. Chem. B*, 2006, **110**, 7090–7094.

232   X. Zhong and F. Duan, *Eur. Phys. J. E*, 2016, **39**, 18.

233   P. Monk, R. Mortimer and D. Rosseinsky, *Electrochromism and Electrochromic Devices*, Cambridge University Press, Cambridge, 2007.

234   S. M. Cho, T.-Y. Kim, C. S. Ah, J. Song, S. H. Cheon, H. Ryu, J. Y. Kim, Y.-H. Kim and C.-S. Hwang, *Sol. Energy Mater. Sol. Cells*, 2018, **177**, 89–96.

235   C. G. Granqvist, in *Kirk-Othmer Encyclopedia of Chemical Technology*, John Wiley & Sons,

Inc., Hoboken, NJ, USA, NJ, USA, 2017, pp. 1–28.

236   J. Schanda, *Colorimetry - Understanding the CIE*, Wiley, 2007.

237   G. Sharma, *Digital color handbook*, CRC press, 2003.

238   A. H. Almarri, *Ionics (Kiel).*, 2022, **28**, 4435–4444.

239   S. Hassab, D. E. Shen, A. M. Österholm, M. Da Rocha, G. Song, Y. Alesanco, A. Viñuales, A. Rougier, J. R. Reynolds and J. Padilla, *Sol. Energy Mater. Sol. Cells*, 2018, **185**, 54–60.

240   D. R. Monk, P. M. S.; Mortimer, R. J.; Rosseinsky and R. J. M. & D. R. R. Paul M S Monk, in *Electrochromism*, Wiley-VCH Verlag GmbH & Co. KGaA, Weinheim, Germany, Germany, 1995, pp. 2–21.

241   Q. Pei, G. Zuccarello, M. Ahlskog and O. Inganäs, *Polymer (Guildf).*, 1994, **35**, 1347–1351.

242   A. Rudge, J. Davey, I. Raistrick, S. Gottesfeld and J. P. Ferraris, *J. Power Sources*, 1994, **47**, 89–107.

243   A. L.-S. S. Eh, A. W. M. Tan, X. Cheng, S. Magdassi and P. S. Lee, *Energy Technol.*, 2018, **6**, 33–45.

244   J.-H. Huang, C.-Y. Yang, C.-Y. Hsu, C.-L. Chen, L.-Y. Lin, R.-R. Wang, K.-C. Ho and C.-W. Chu, *ACS Appl. Mater. Interfaces*, 2009, **1**, 2821–2828.

245   T.-H. Kim, K.-I. Choi, H. Kim, S. H. Oh, J. Koo and Y.-C. Nah, *ACS Appl. Mater. Interfaces*, 2017, **9**, 20223–20230.

246   E. Orgiu, N. Crivillers, M. Herder, L. Grubert, M. Pätzel, J. Frisch, E. Pavlica, D. T. Duong, G. Bratina, A. Salleo, N. Koch, S. Hecht, P. Samorì, L. Grubert, G. Bratina, N. Koch, P. Samorì, E. Orgiu, M. Herder, N. Crivillers, A. Salleo, S. Hecht, D. T. Duong, M. Pätzel, J. Frisch, M. Herder, L. Grubert, M. Pätzel, J. Frisch, E. Pavlica, D. T. Duong, G. Bratina, A. Salleo, N. Koch, S. Hecht and P. Samorì, *Nat. Chem.*, 2012, **4**, 675–679.

247   P. J. Brown, D. S. Thomas, A. Köhler, J. S. Wilson, J.-S. Kim, C. M. Ramsdale, H. Sirringhaus and R. H. Friend, *Phys. Rev. B*, 2003, **67**, 064203.

248   N. Banerji, S. Cowan, E. Vauthey and A. J. Heeger, *J. Phys. Chem. C*, 2011, **115**, 9726–9739.

249   N. J. Hestand and F. C. Spano, *Chem. Rev.*, 2018, **118**, 7069–7163.

250   B. E. Warren, *X-ray Diffraction*, Courier Corporation, 1990.

251   D.-M. M. Smilgies, *J. Appl. Crystallogr.*, 2009, **42**, 1030–1034.

252   S. Cook, A. Furube and R. Katoh, *Energy Environ. Sci.*, 2008, **1**, 294.

253   L. Gomes, A. Marques, A. Branco, J. Araújo, M. Simões, S. Cardoso, F. Silva, I. Henriques, C. A. T. Laia and C. Costa, *Displays*, 2013, **34**, 326–333.

254   F. Di Maria, A. Zanelli, A. Liscio, A. Kovtun, E. Salatelli, R. Mazzaro, V. Morandi, G. Bergamini, A. Shaffer and S. Rozen, *ACS Nano*, 2017, **11**, 1991–1999.

255   J. Gasiorowski, A. I. Mardare, N. S. Sariciftci and A. W. Hassel, *J. Electroanal. Chem.*, 2013, **691**, 77–82.

256   P. C. Mahakul and P. Mahanandia, *IOP Conf. Ser. Mater. Sci. Eng.*, 2017, **178**, 012024.

257   H. Müller and S. Morais, , DOI:10.18420/ecscw2019_ws2.

258   A. Colley, P. W. Woźniak, F. Kiss and J. Häkkilä, in *Proceedings of the 10th Nordic Conference on Human-Computer Interaction*, ACM, New York, NY, USA, New York, USA, 2018, pp. 39–46.

259   A. Colley, L. Hakala, E. Harjuniemi, P. Jarusriboonchai, H. Müller and J. Häkkilä, in *Proceedings of the 8th ACM International Symposium on Pervasive Displays*, ACM, New York, NY, USA, New York, USA, 2019, pp. 1–2.

260   T. Kololuoma, C. Pinheiro, I. Kaisto, A. Colley, K. Ronka, M. Keranen, T. Kurkela, T. Happonen, M. Korkalainen, M. Kehusmaa, L. Gomes, A. Branco and S. Ihme, *IEEE J. Electron Devices Soc.*, 2019, **7**, 761–768.

261   M. Löchtefeld, W. Jensen, H. Müller and A. Colley, in *Extended Abstracts of the 2019 CHI*

Conference on Human Factors in Computing Systems, ACM, New York, NY, USA, New York, USA, 2019, pp. 1–4.

262 T. P. Kaloni, P. K. Giesbrecht, G. Schreckenbach and M. S. Freund, *Chem. Mater.*, 2017, **29**, 10248–10283.

263 H. Iino and J. Hanna, *Polym. J.*, 2017, **49**, 23–30.

264 W. Xie, B. Li, X. Cai, M. Li, Z. Qiao, X. Tang, K. Liu, C. Gu, Y. Ma and S.-J. Su, *Front. Chem.*, 2019, **7**, 1–8.

265 Y. Wu, C. An, L. Shi, L. Yang, Y. Qin, N. Liang, C. He, Z. Wang and J. Hou, *Angew. Chemie Int. Ed.*, 2018, **57**, 12911–12915.

266 E. Moulin, E. Busseron and N. Giuseppone, *Self-assembled supramolecular materials in organic electronics*, 2015, vol. 2015- Janua.

267 C.-G. Granqvist, in *Electrochromic Materials and Devices*, Wiley-VCH Verlag GmbH & Co. KGaA, Weinheim, Germany, Germany, 2015, pp. 1–40.

268 H.-S. Liu, B.-C. Pan, D.-C. Huang, Y.-R. Kung, C.-M. Leu and G.-S. Liou, *NPG Asia Mater.*, 2017, **9**, e388–e388.

269 W. T. Neo, Q. Ye, S.-J. Chua and J. Xu, *J. Mater. Chem. C*, 2016, **4**, 7364–7376.

270 Q. Zhang, C.-Y. Tsai, L.-J. Li and D.-J. Liaw, *Nat. Commun.*, 2019, **10**, 1239.

271 K. Takada, R. Sakamoto, S.-T. Yi, S. Katagiri, T. Kambe and H. Nishihara, *J. Am. Chem. Soc.*, 2015, **137**, 4681–4689.

272 L. Gonzalez, C. Liu, B. Dietrich, H. Su, S. Sproules, H. Cui, D. Honecker, D. J. Adams and E. R. Draper, *Commun. Chem.*, 2018, **1**, 77.

273 G. Yang, J. Ding, B. Yang, X. Wang, C. Gu, D. Guan, Y. Yu, Y.-M. Zhang and S. X.-A. Zhang, *J. Mater. Chem. C*, 2019, **7**, 9481–9486.

274 T. Xu, E. C. Walter, A. Agrawal, C. Bohn, J. Velmurugan, W. Zhu, H. J. Lezec and A. A. Talin, *Nat. Commun.*, 2016, **7**, 10479.

275 S. Zhang, S. Chen, F. Yang, F. Hu, Y. Zhao, B. Yan, H. Jiang and Y. Cao, *J. Mater. Sci. Mater. Electron.*, 2019, **30**, 3994–4005.

276 T. Jarosz, K. Gebka, A. Stolarczyk and W. Domagala, *Polymers (Basel).*, 2019, **11**, 273.

277 W. Wu, M. Wang, J. Ma, Y. Cao and Y. Deng, *Adv. Electron. Mater.*, 2018, **4**, 1–19.

278 X. Chen, W. Qiao and Z. Y. Wang, *RSC Adv.*, 2017, **7**, 15521–15526.

279 J. A. Kerszulis, R. H. Bulloch, N. B. Teran, R. M. W. Wolfe and J. R. Reynolds, *Macromolecules*, 2016, **49**, 6350–6359.

280 D. T. Christiansen, D. L. Wheeler, A. L. Tomlinson and J. R. Reynolds, *Polym. Chem.*, 2018, **9**, 3055–3066.

281 G. S. Collier, I. Pelse and J. R. Reynolds, *ACS Macro Lett.*, 2018, **7**, 1208–1214.

282 F. Di Maria, M. Zangoli, M. Gazzano, E. Fabiano, D. Gentili, A. Zanelli, A. Fermi, G. Bergamini, D. Bonifazi, A. Perinot, M. Caironi, R. Mazzaro, V. Morandi, G. Gigli, A. Liscio and G. Barbarella, *Adv. Funct. Mater.*, 2018, **28**, 1–15.

283 US20190218338A1, 2019, 1.

284 F. Di Maria, M. Zangoli, I. E. Palamá, E. Fabiano, A. Zanelli, M. Monari, A. Perinot, M. Caironi, V. Maiorano, A. Maggiore, M. Pugliese, E. Salatelli, G. Gigli, I. Viola and G. Barbarella, *Adv. Funct. Mater.*, 2016, **26**, 6970–6984.

285 T. Moreira, C. A. T. Laia, M. Zangoli, M. Antunes, F. Di Maria, S. De Monte, F. Liscio, A. J. Parola and G. Barbarella, *ACS Appl. Polym. Mater.*, 2020, **2**, 3301–3309.

286 S. D. S. Das, *Chemical Solution Synthesis for Materials Design and Thin Film Device Applications*, Elsevier, Amsterdam, 1st edn., 2021.

287 G. Barbarella, M. Zangoli and F. Di Maria, in *Advances in Heterocyclic Chemistry*, Elsevier Ltd, 2017, vol. 123, pp. 105–167.

288 F. DiMaria and G. Barbarella, *J. Sulfur Chem.*, 2013, **34**, 627–637.

289   S. C. Rasmussen, S. J. Evenson and C. B. McCausland, *Chem. Commun.*, 2015, **51**, 4528–4543.

290   M. Marinelli, M. Lanzi, A. Liscio, A. Zanelli, M. Zangoli, F. Di Maria and E. Salatelli, *J. Mater. Chem. C*, 2020, **8**, 4124–4132.

291   C. M. Cardona, W. Li, A. E. Kaifer, D. Stockdale and G. C. Bazan, *Adv. Mater.*, 2011, **23**, 2367–2371.

292   S. Macher, M. Rumpel, M. Schott, U. Posset, G. A. Giffin and P. Löbmann, *ACS Appl. Mater. Interfaces*, 2020, **12**, 36695–36705.

293   H. Peng, X. Sun, W. Weng and X. Fang, *Polymer Materials for Energy and Electronic Applications*, Elsevier, 2017.

294   M. Zangoli, F. Di Maria, E. Zucchetti, C. Bossio, M. R. Antognazza, G. Lanzani, R. Mazzaro, F. Corticelli, M. Baroncini and G. Barbarella, *Nanoscale*, 2017, **9**, 9202–9209.

295   G. Jones, W. R. Jackson, C. Y. Choi and W. R. Bergmark, *J. Phys. Chem.*, 1985, **89**, 294–300.

296   R. F. Kubin and A. N. Fletcher, *J. Lumin.*, 1982, **27**, 455–462.

297   TURBOMOLE Version 7.1. 2016, a development of University of karlsruhe and Forschungszentrum Karlsruhe GmbH. 1989-2007. TURBOMOLE GmbH, since2007, www.turbomole.com, (accessed 10 August 2022).

298   F. Furche, R. Ahlrichs, C. Hättig, W. Klopper, M. Sierka and F. Weigend, *WIREs Comput. Mol. Sci.*, 2014, **4**, 91–100.

299   F. Weigend, M. Häser, H. Patzelt and R. Ahlrichs, *Chem. Phys. Lett.*, 1998, **294**, 143–152.

300   C. A. Guido, E. Brémond, C. Adamo and P. Cortona, *J. Chem. Phys.*, 2013, **138**, 021104.

301   A. Klamt and G. Schüürmann, *J. Chem. Soc., Perkin Trans. 2*, 1993, 799–805.

302   A. Klamt, *J. Phys. Chem.*, 1996, **100**, 3349–3353.

303   K. Wang, K. Tao, R. Jiang, H. Zhang, L. Liang, J. Gao and H. Cao, *Materials (Basel).*, 2021, **14**, 2771.

304   Z. Liu, J. Yang, G. Leftheriotis, H. Huang, Y. Xia, Y. Gan, W. Zhang and J. Zhang, *Sustain. Mater. Technol.*, 2022, **31**, e00372.

305   X. Lu, G.-J. Liu, Y.-H. Li, Y.-Y. Ma, J. Fan and M.-K. Fung, *Phys. status solidi*, 2018, **215**, 1800102.

306   S. Macher, M. Schott, M. Sassi, I. Facchinetti, R. Ruffo, G. Patriarca, L. Beverina, U. Posset, G. A. Giffin and P. Löbmann, *Adv. Funct. Mater.*, 2020, **30**, 1906254.

307   A. Elschner, S. Kirchmeyer, W. Lovenich, U. Merker and K. Reuter, *PEDOT - Principles and Applications of an Intrinsically Conductive Polymer*, CRC Press, 2010.

308   B. He, W. T. Neo, T. L. Chen, L. M. Klivansky, H. Wang, T. Tan, S. J. Teat, J. Xu and Y. Liu, *ACS Sustain. Chem. Eng.*, 2016, **4**, 2797–2805.

309   Y. Alesanco, A. Viñuales, J. Rodriguez and R. Tena-Zaera, *Materials (Basel).*, 2018, **11**, 1–27.

310   R. D. Rauh, *Electrochim. Acta*, 1999, **44**, 3165–3176.

311   W. Lu, A. G. Fadeev, B. Qi and B. R. Mattes, *Synth. Met.*, 2003, **135–136**, 139–140.

312   S. Kandpal, T. Ghosh, M. Sharma, D. K. Pathak, M. Tanwar, C. Rani, R. Bhatia, I. Sameera, A. Chaudhary and R. Kumar, *Appl. Phys. Lett.*, 2021, **118**, 153301.

313   J. Yoo, H. Ozawa, T. Fujigaya and N. Nakashima, *Nanoscale*, 2011, **3**, 2517–2522.

314   G. Bottari, G. de la Torre, D. M. Guldi and T. Torres, *Chem. Rev.*, 2010, **110**, 6768–6816.

315   C. Ehli, G. M. A. Rahman, N. Jux, D. Balbinot, D. M. Guldi, F. Paolucci, M. Marcaccio, D. Paolucci, M. Melle-Franco, F. Zerbetto, S. Campidelli and M. Prato, *J. Am. Chem. Soc.*, 2006, **128**, 11222–11231.

316   M. A. Ochieng, J. F. Ponder and J. R. Reynolds, *Polym. Chem.*, 2020, **11**, 2173–2181.

317   D. A. Warr, L. M. A. Perdigão, H. Pinfold, J. Blohm, D. Stringer, A. Leventis, H.

Bronstein, A. Troisi and G. Costantini, *Sci. Adv.*, 2018, **4**, 0–6.

318　T. Moreira, M. Maia, A. J. Parola, M. Zangoli, F. Di Maria and C. A. T. Laia, in *Chemical Solution Synthesis for Materials Design and Thin Film Device Applications*, Elsevier, 2021, pp. 407–437.

319　M. H. Ahn, E. S. Cho and S. J. Kwon, *Vacuum*, 2014, **101**, 221–227.

320　H. Wang, H.-Y. Wang, B.-R. Gao, Y. Jiang, Z.-Y. Yang, Y.-W. Hao, Q.-D. Chen, X.-B. Du and H.-B. Sun, *Appl. Phys. Lett.*, 2011, **98**, 251501.

321　J. L. Brédas, F. Wudl and A. J. Heeger, *Solid State Commun.*, 1987, **63**, 577–580.

322　H. Hintz, H. J. Egelhaaf, L. Lüer, J. Hauch, H. Peisert and T. Chassé, *Chem. Mater.*, 2011, **23**, 145–154.

323　M. Manceau, S. Chambon, A. Rivaton, J.-L. Gardette, S. Guillerez and N. Lemaître, *Sol. Energy Mater. Sol. Cells*, 2010, **94**, 1572–1577.

324　T. F. Ko, P. W. Chen, K. M. Li, H. T. Young, C. Te Chang and S. C. Hsu, *Materials (Basel).*, 2021, **14**, 1–13.

325　T. S. Tung and K. C. Ho, *Sol. Energy Mater. Sol. Cells*, 2006, **90**, 521–537.

326　Y. Zhao, X. Zhang, X. Chen, W. Li, L. Wang, Z. Li, J. Zhao, F. Endres and Y. Li, *Electrochim. Acta*, 2021, **367**, 137457.

327　Q. Liu, Z. Xu, W. Qiu, C. Hou, Y. Wang, P. Yao, R. Yu, W. Guo and X. Y. Liu, *RSC Adv.*, 2018, **8**, 18690–18697.

328　S. Kandpal, T. Ghosh, C. Rani, M. Tanwar, M. Sharma, S. Rani, D. K. Pathak, R. Bhatia, I. Sameera, J. Jayabalan and R. Kumar, *ACS Mater. Au*, 2022, **2**, 293–300.

329　K. Wang, H. Zhang, G. Chen, T. Tian, K. Tao, L. Liang, J. Gao and H. Cao, *J. Alloys Compd.*, 2021, **861**, 158534.

330　A. C. Arias, J. D. MacKenzie, I. McCulloch, J. Rivnay and A. Salleo, *Chem. Rev.*, 2010, **110**, 3–24.

331　Z. Liu, K. Parvez, R. Li, R. Dong, X. Feng and K. Müllen, *Adv. Mater.*, 2015, **27**, 669–675.

332　M. A. Martínez, J. Herrero and M. T. Gutiérrez, *Electrochim. Acta*, 1992, **37**, 2565–2571.

333　A. R. Rathmell and B. J. Wiley, *Adv. Mater.*, 2011, **23**, 4798–4803.

334　Y. Won, A. Kim, D. Lee, W. Yang, K. Woo, S. Jeong and J. Moon, *NPG Asia Mater.*, 2014, **6**, e105–e105.

335　Z. Chen, S. Ye, I. E. Stewart and B. J. Wiley, *ACS Nano*, 2014, **8**, 9673–9679.

336　A. R. Rathmell, M. Nguyen, M. Chi and B. J. Wiley, *Nano Lett.*, 2012, **12**, 3193–3199.

337　S. Chen, L. Brown, M. Levendorf, W. Cai, S.-Y. Ju, J. Edgeworth, X. Li, C. W. Magnuson, A. Velamakanni, R. D. Piner, J. Kang, J. Park and R. S. Ruoff, *ACS Nano*, 2011, **5**, 1321–1327.

338　L. Shi, R. Wang, H. Zhai, Y. Liu, L. Gao and J. Sun, *Phys. Chem. Chem. Phys.*, 2015, **17**, 4231–4236.

339　I. Sengupta, S. Chakraborty, M. Talukdar, S. K. Pal and S. Chakraborty, *J. Mater. Res.*, 2018, **33**, 4113–4122.

340　C. K. Chua and M. Pumera, *Chem. Soc. Rev.*, 2014, **43**, 291–312.

341　S. Pei and H.-M. Cheng, *Carbon N. Y.*, 2012, **50**, 3210–3228.

342　I. N. Kholmanov, S. H. Domingues, H. Chou, X. Wang, C. Tan, J.-Y. Kim, H. Li, R. Piner, A. J. G. Zarbin and R. S. Ruoff, *ACS Nano*, 2013, **7**, 1811–1816.

343　M. Kevin, G. Y. R. Lim and G. W. Ho, *Green Chem.*, 2015, **17**, 1120–1126.

344　T. Sannicolo, M. Lagrange, A. Cabos, C. Celle, J.-P. Simonato and D. Bellet, *Small*, 2016, **12**, 6052–6075.

345　R. M. Mutiso, M. C. Sherrott, A. R. Rathmell, B. J. Wiley and K. I. Winey, *ACS Nano*, 2013, **7**, 7654–7663.

APPENDIX – CHAPTER 2

A.1 ¹H-NMR Spectra
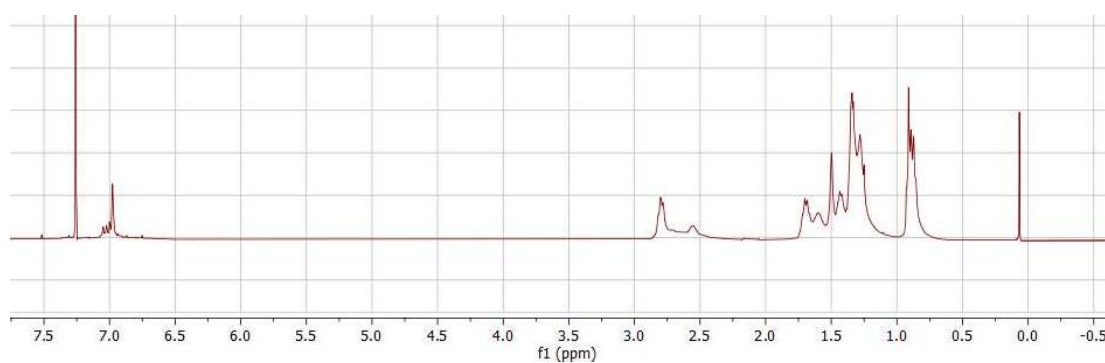
Figure A.1.1. ¹H-NMR spectrum in CDCl₃ of P3HT.

A.2 DLS Measurements

Table A.2.1. Dimensions of P3HT-NPs obtained by DLS.

	Size (nm)
	100±18
	116±20
P3HT-NPs	150±19
	200±22
	380±18
	400±20

A.3 X-ray Diffraction of a Thin film of P3HT cast from Chloroform and a Film of 100 nm NPs
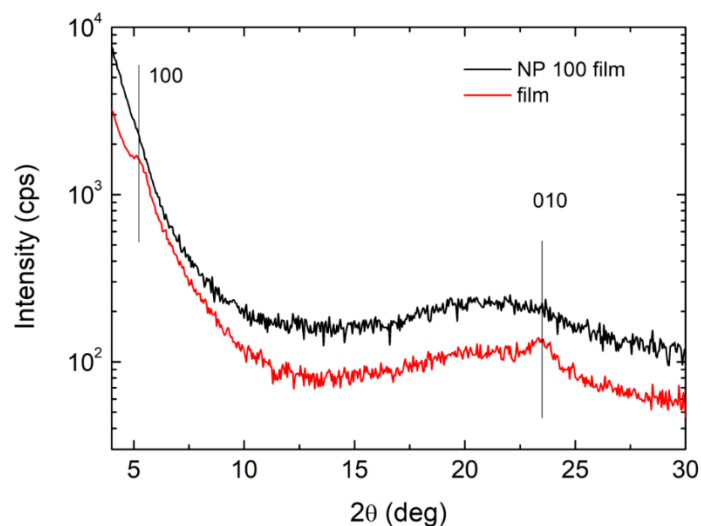
Figure A.3.1. Specular XRD scans of a thin film of P3HT spray-coated from chloroform (red line) and of a film of 100 nm nanoparticles (black line).

Figure A.3.1 shows the specular XRD scans of the continuous P3HT film and the film based on P3HT NPs with 100 nm size. They were obtained using a laboratory X-ray source which is characterized by a photon flux lower than the synchrotron radiation used for GIXRD measurements. This explains the absence of reflections in the film based by P3HT NPs.

A.4 Cyclic Voltammetry of P3HT and Different Sized P3HT NPs
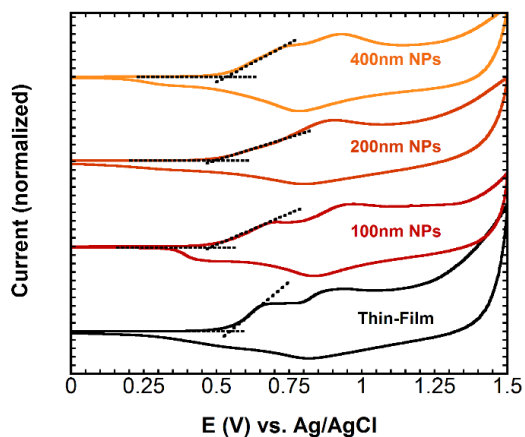
Figure A.4.1. Cyclic voltammograms of P3HT and different sized P3HT NPs spray-coated on PET-ITO substrates. The cyclic voltammograms were performed using Ag/AgCl as reference electrode, a platinum wire as counter-electrode, working electrode the PET-ITO substrate with the material deposited on top and an electrolytic solution of LiClO$_4$ (0.1M) in acetonitrile.

Appendix – Chapter 3

B.1 ¹H and ¹³C NMR Spectra of Polymers 1-6 and Intermediates
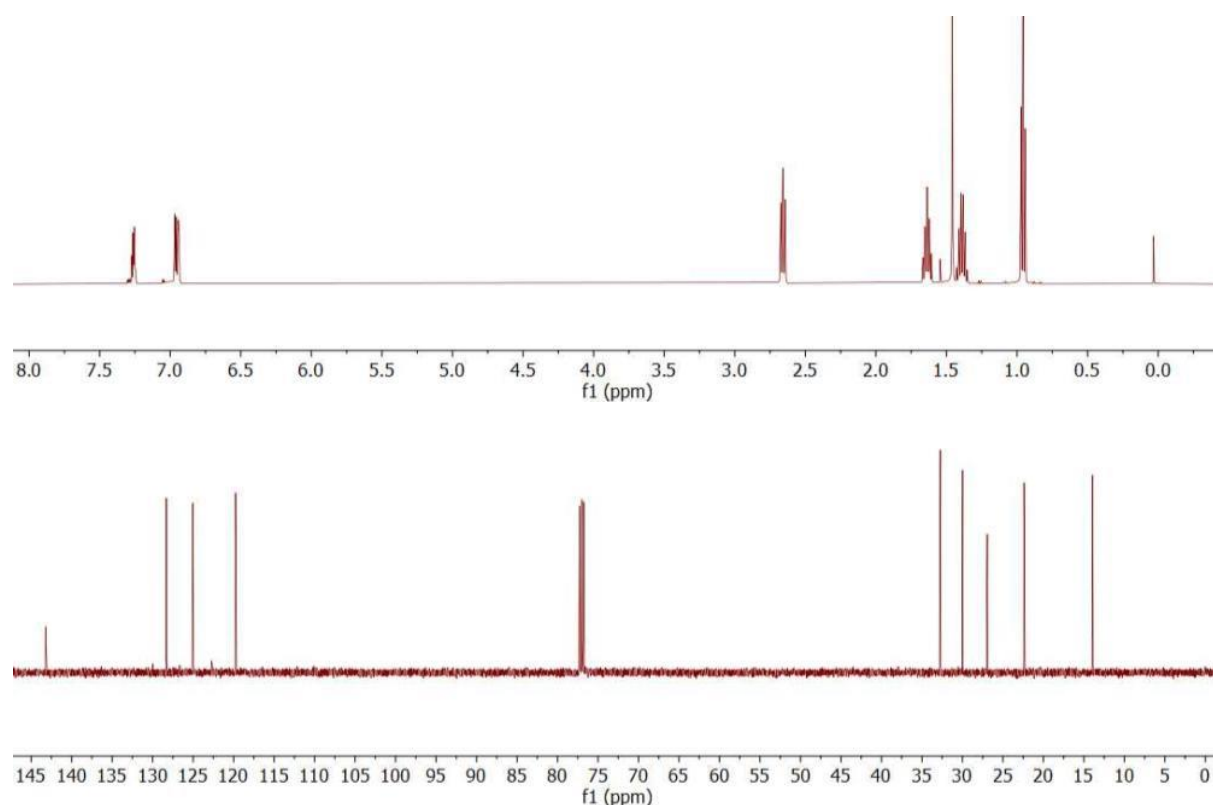
Figure B.1.1. ¹H and ¹³C NMR spectra of compound **1a**.
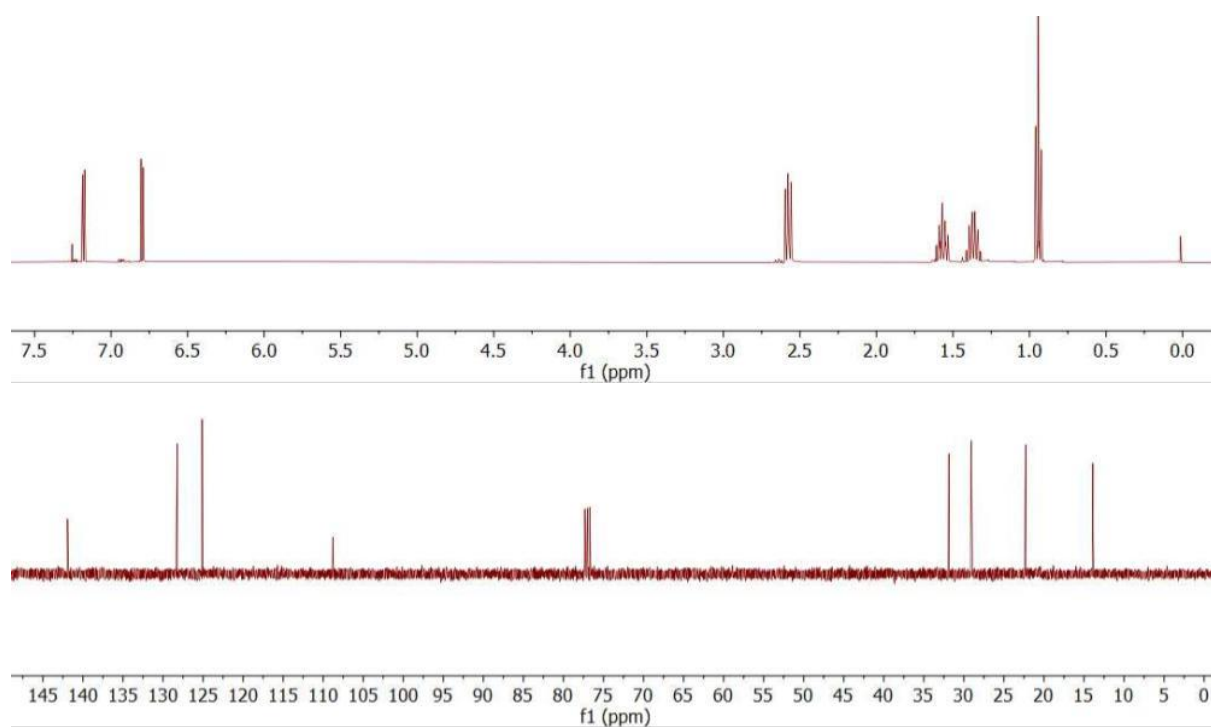
Figure B.1.2. ^{1}H and ^{13}C NMR spectra of compound **1b**.
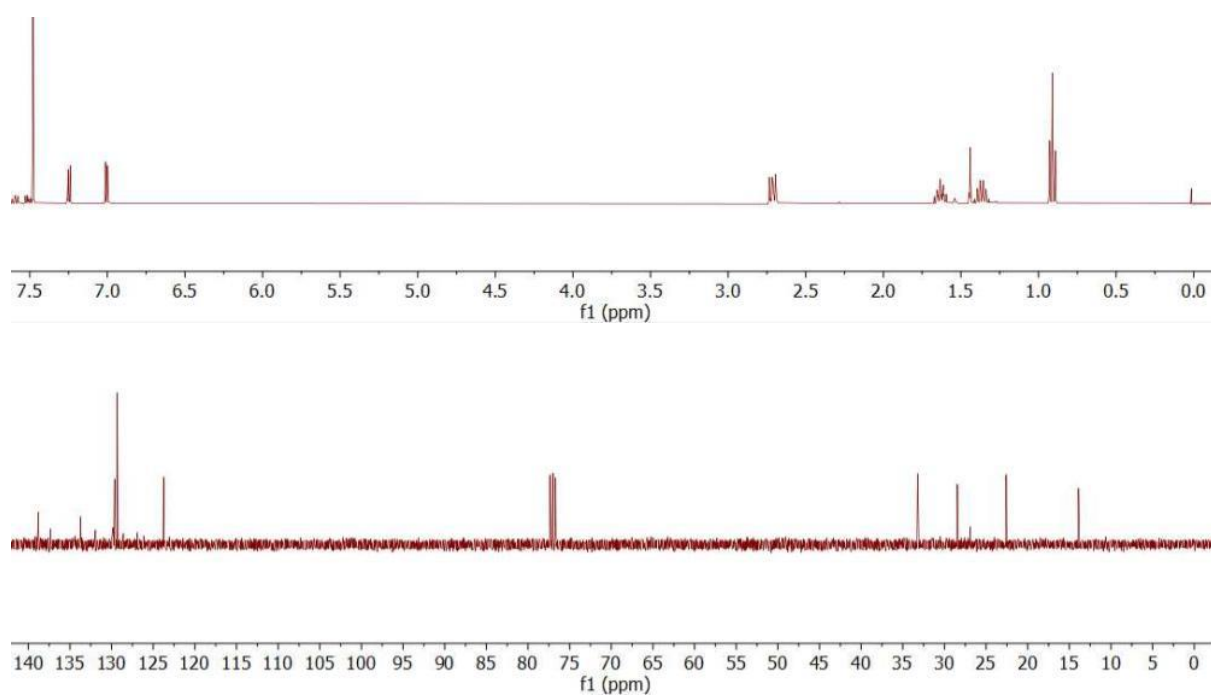
Figure B.1.3. ^{1}H and ^{13}C NMR spectra of compound **1c**.
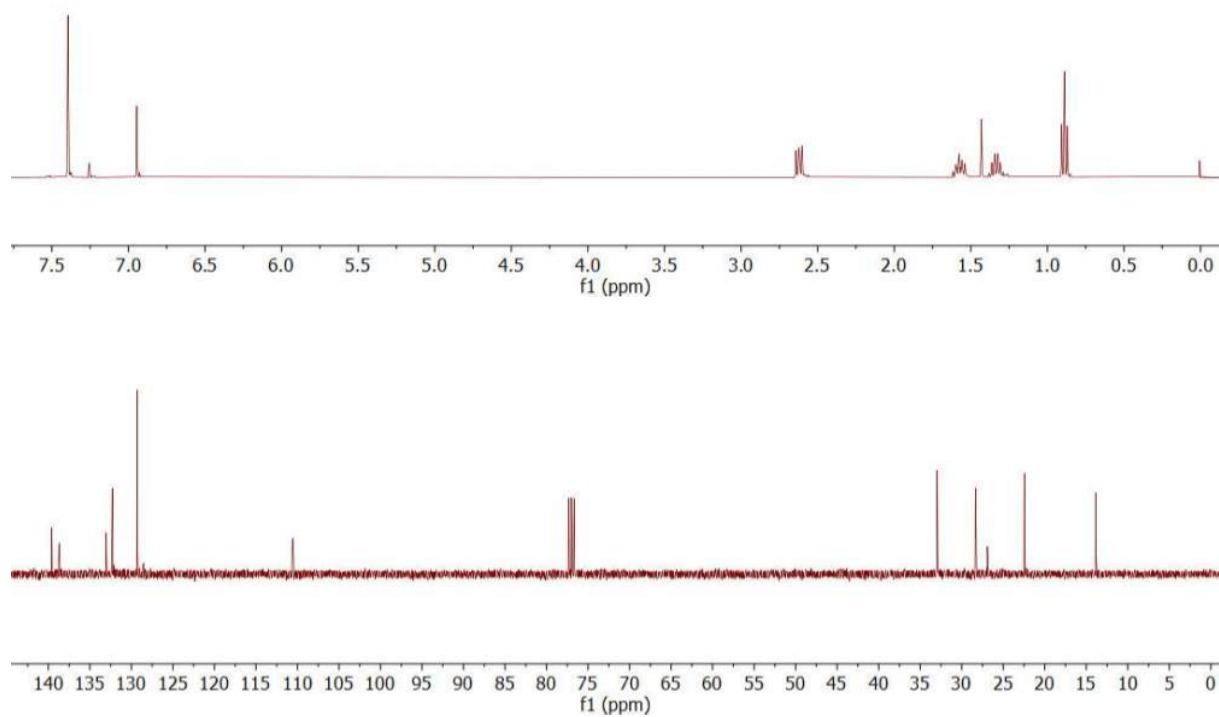
Figure B.1.4. ¹H and ¹³C NMR spectra of compound **1d**.
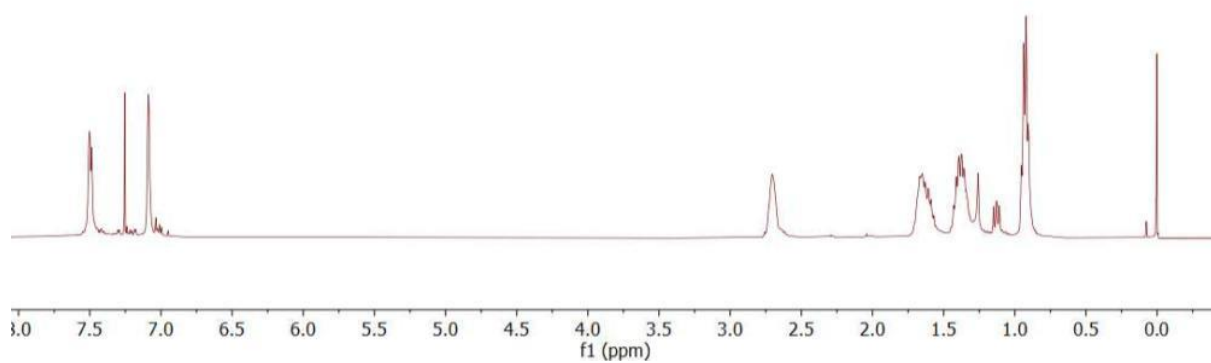
Figure B.1.5. ¹H NMR spectra of compound **polymer 1**.
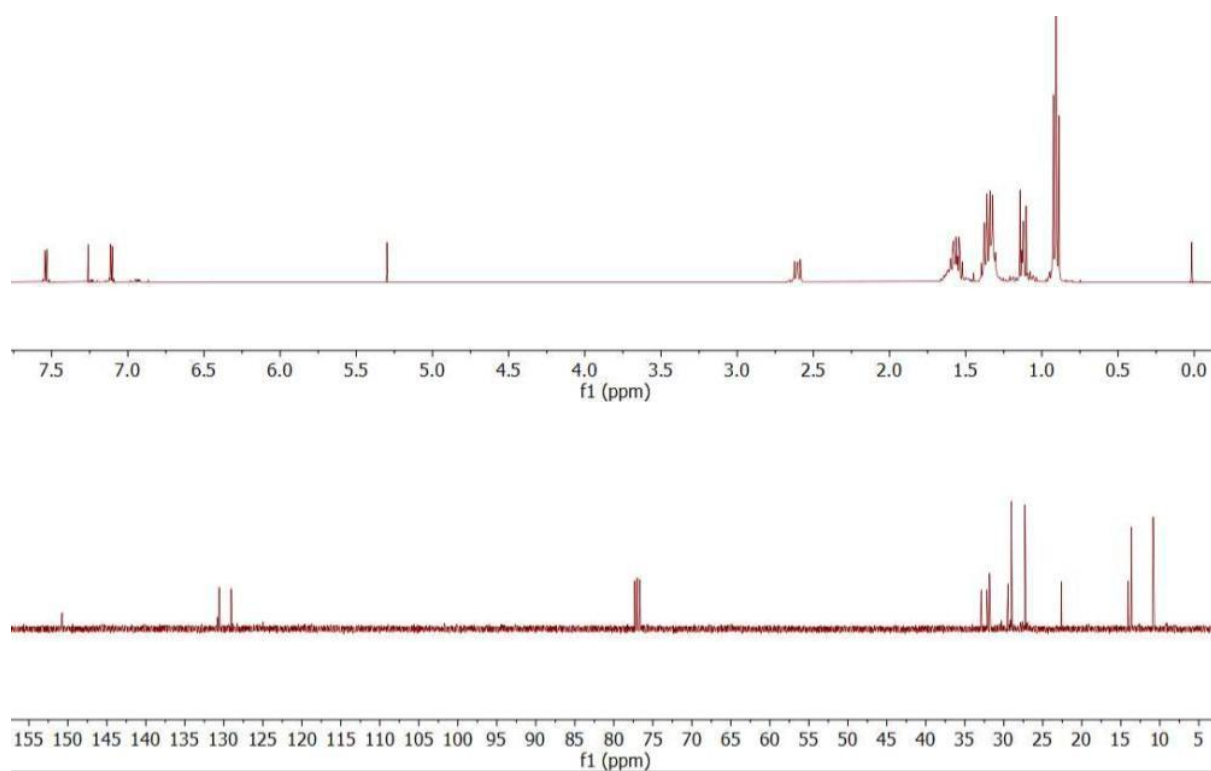
Figure B.1.6. ¹H and ¹³C NMR spectra of compound **2b**.
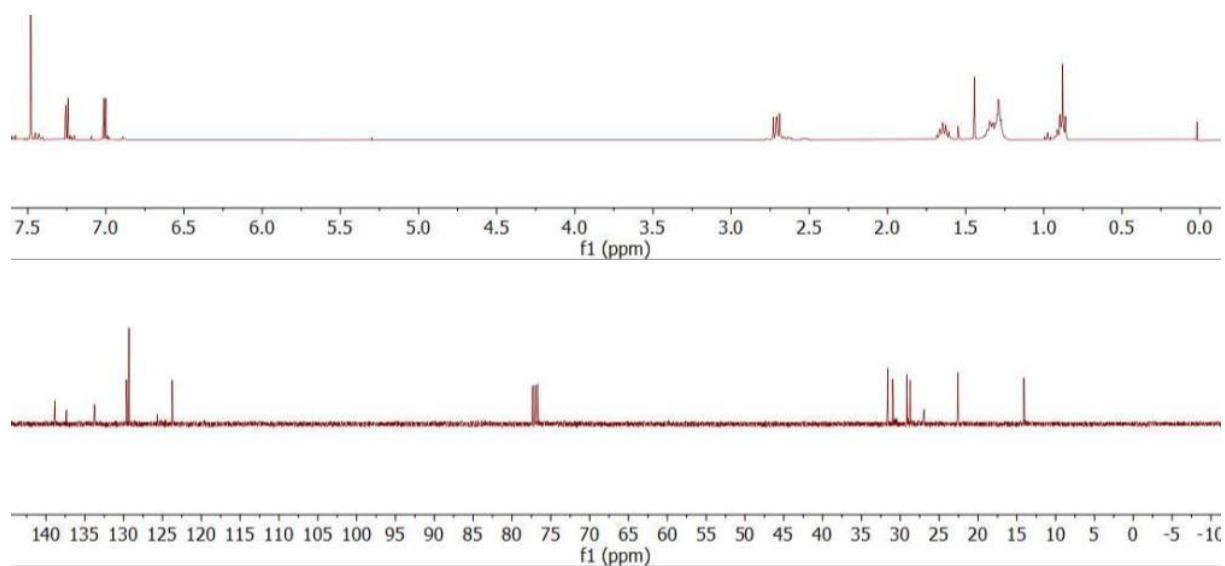
Figure B.1.7. ¹H and ¹³C NMR spectra of compound **2c**.
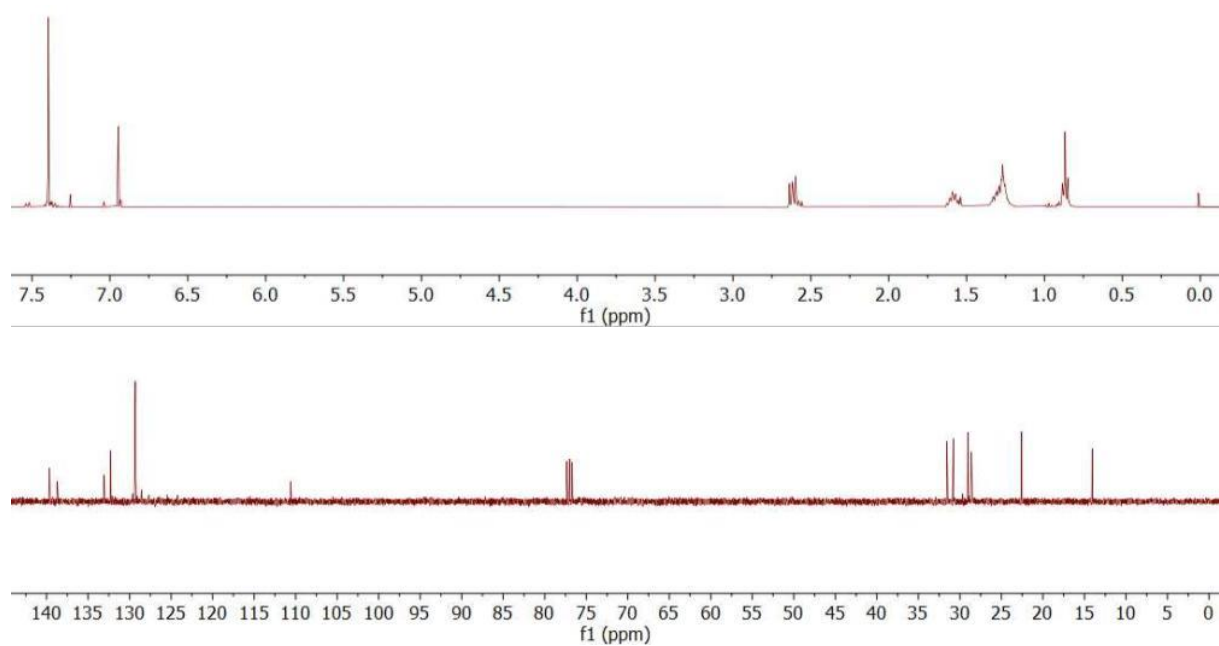
Figure B.1.8. ^{1}H and ^{13}C NMR spectra of compound **2d**.
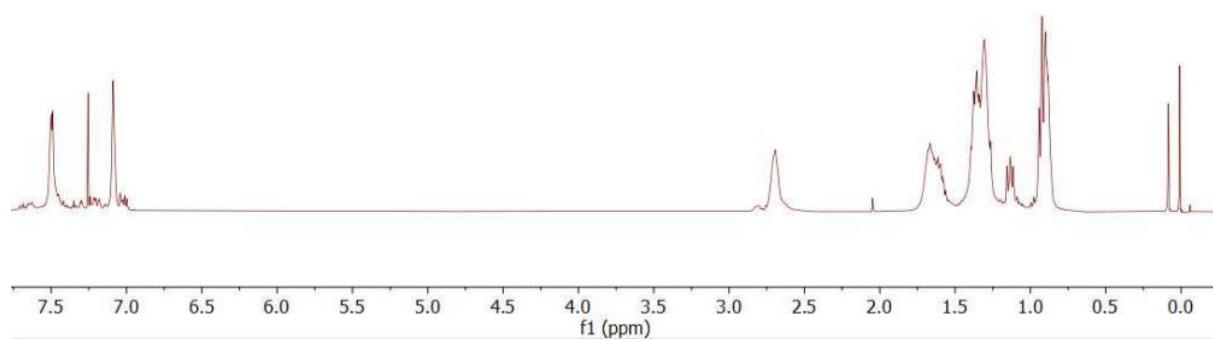
Figure B.1.9. ^{1}H NMR spectra of **polymer 2**
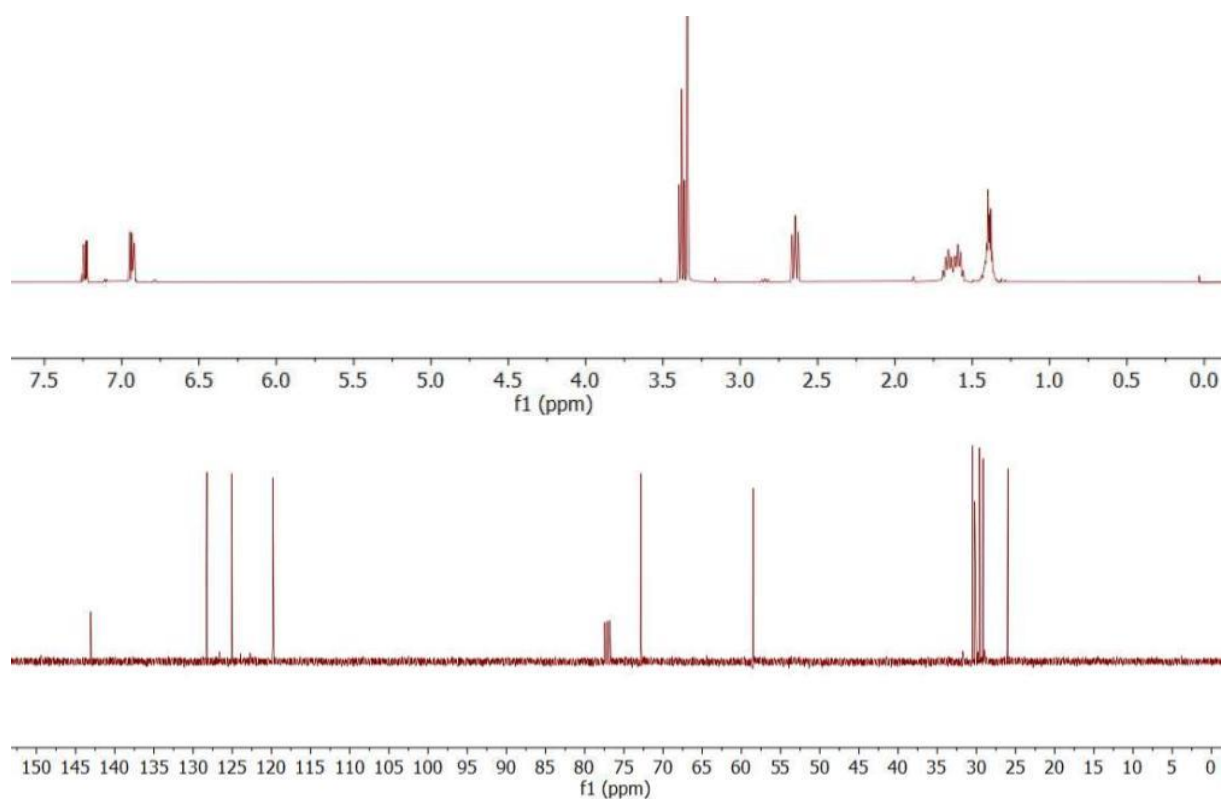
Figure B.1.10. ¹H and ¹³C NMR spectra of compound **3a**.
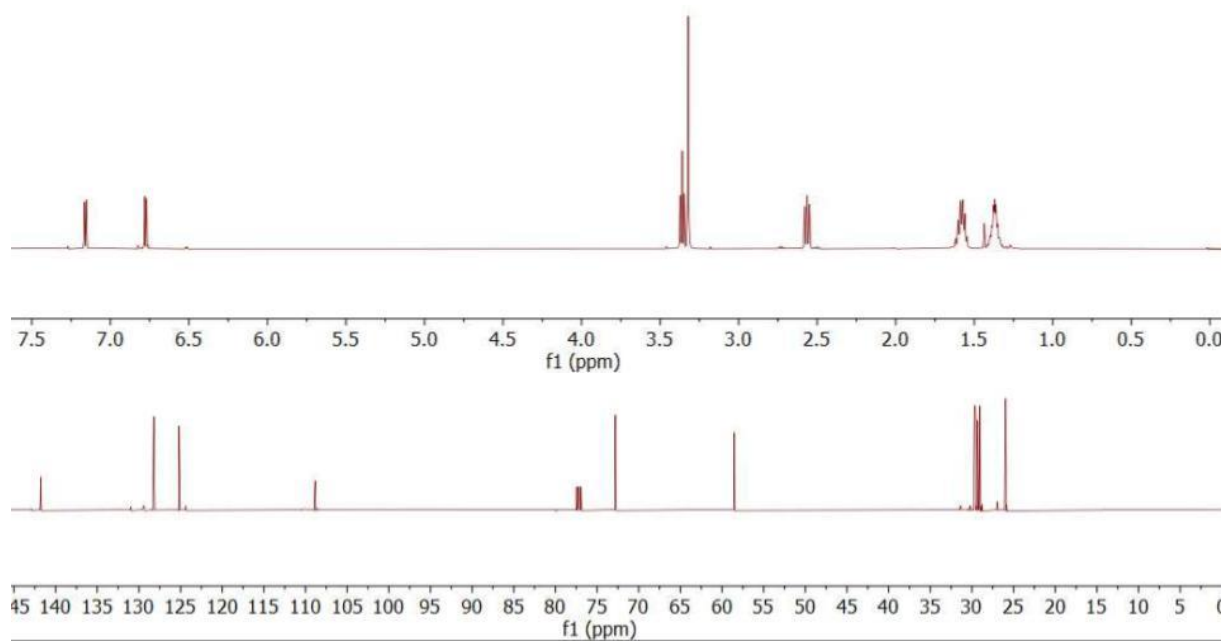
Figure B.1.11. ¹H and ¹³C NMR spectra of compound **3b**.
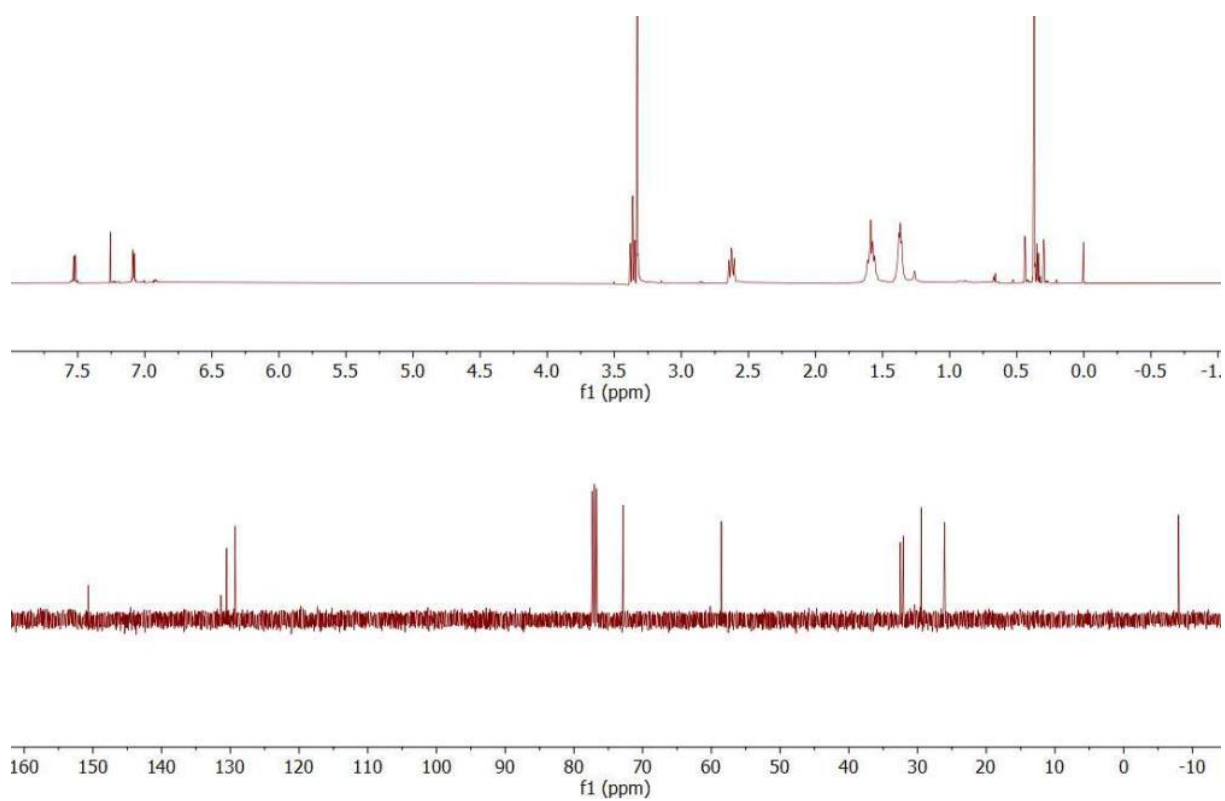
Figure B.1.12. ^{1}H and ^{13}C NMR spectra of compound **3c**.
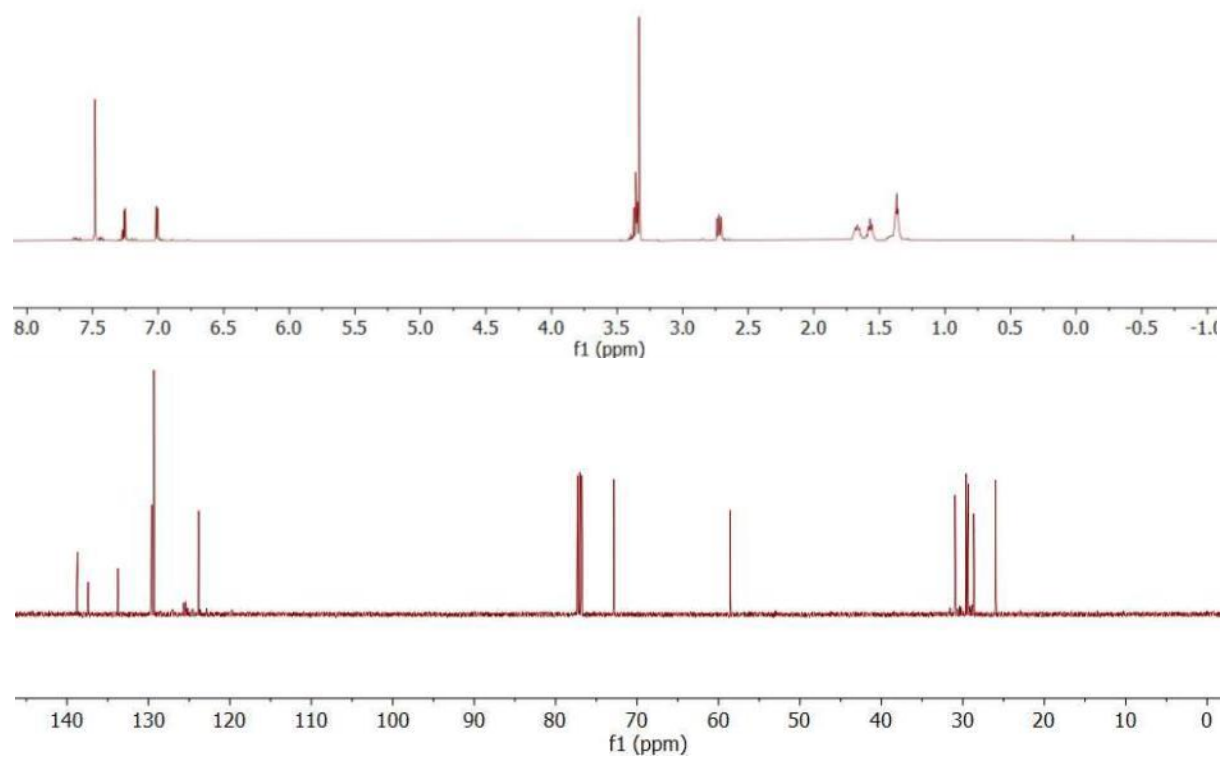
Figure B.1.13. ^{1}H and ^{13}C NMR spectra of compound **3d**.

167
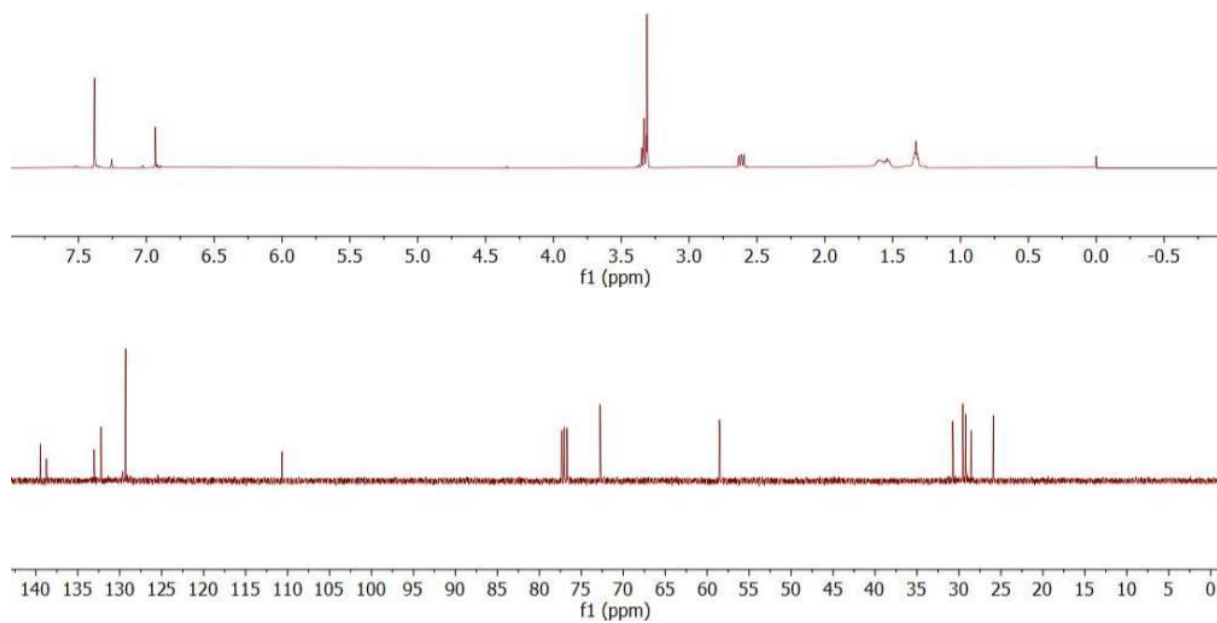
Figure B.1.14. ¹H and ¹³C NMR spectra of compound **3e**.
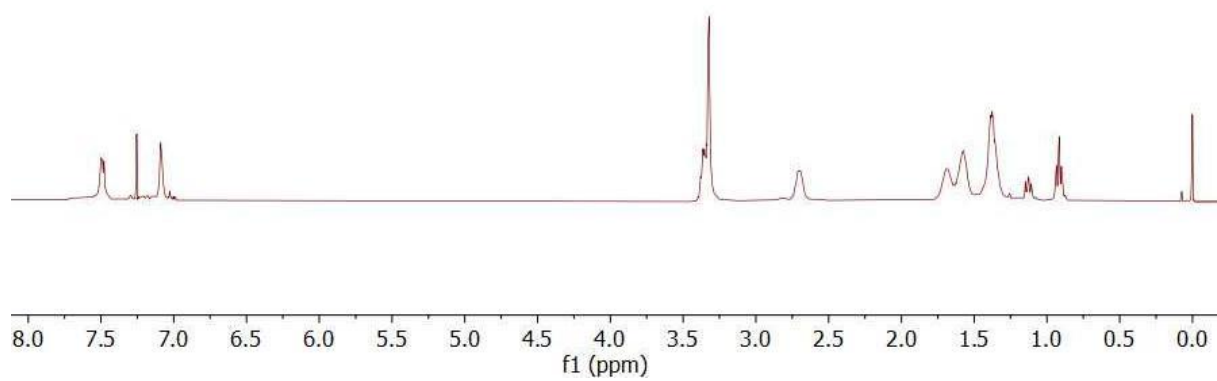
Figure B.1.15. ¹H NMR spectra of compound **polymer 3**.
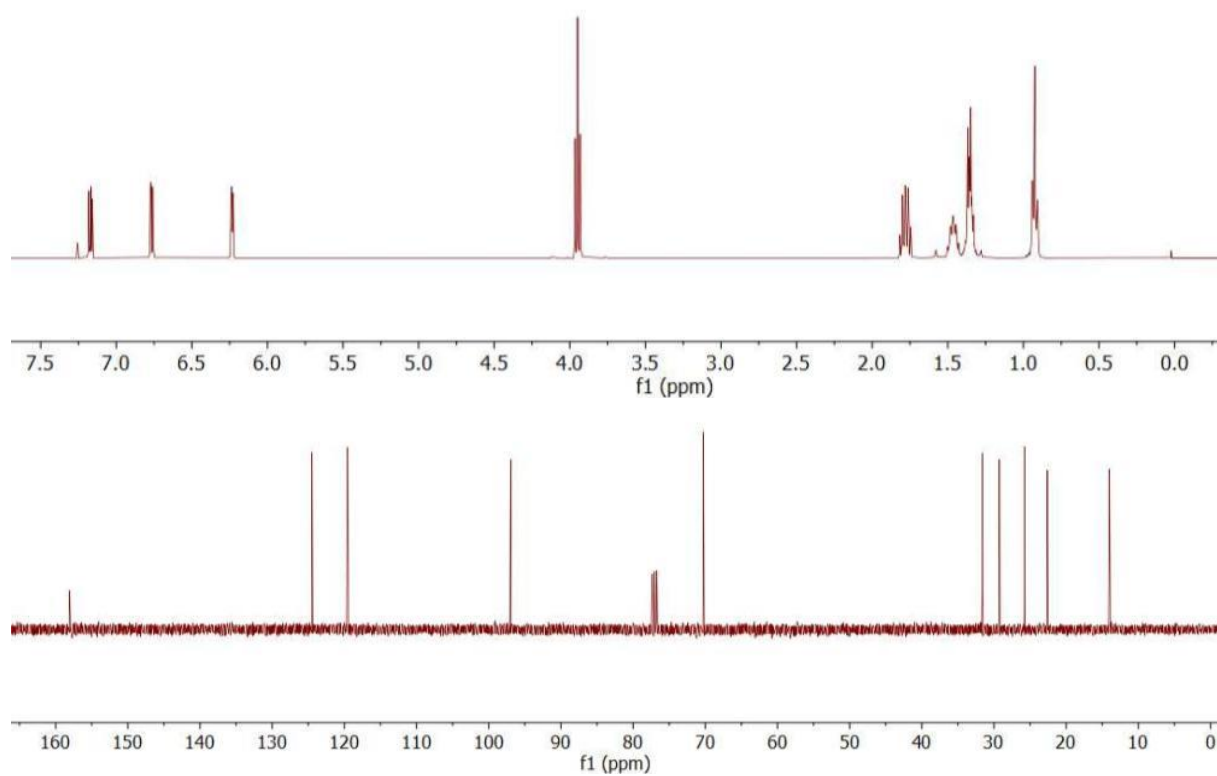
Figure B.1.16. ^{1}H and ^{13}C NMR spectra of compound **4a**.
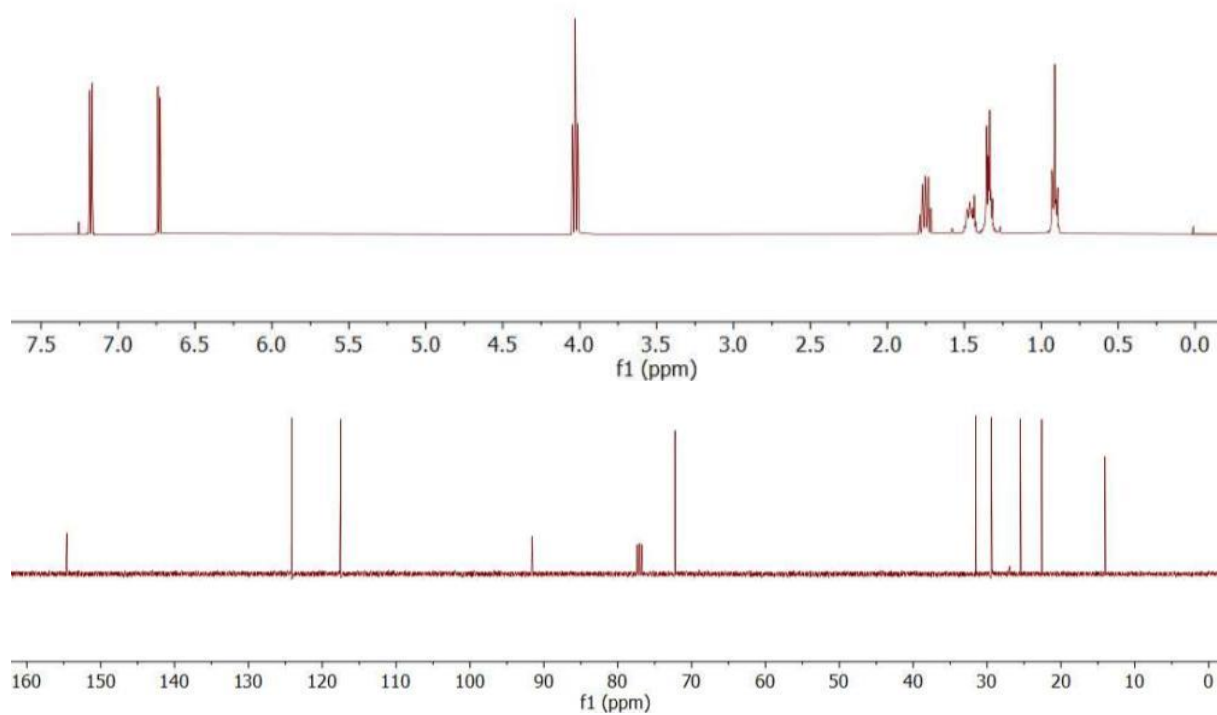
Figure B.1.17. ^{1}H and ^{13}C NMR spectra of compound **4b**.
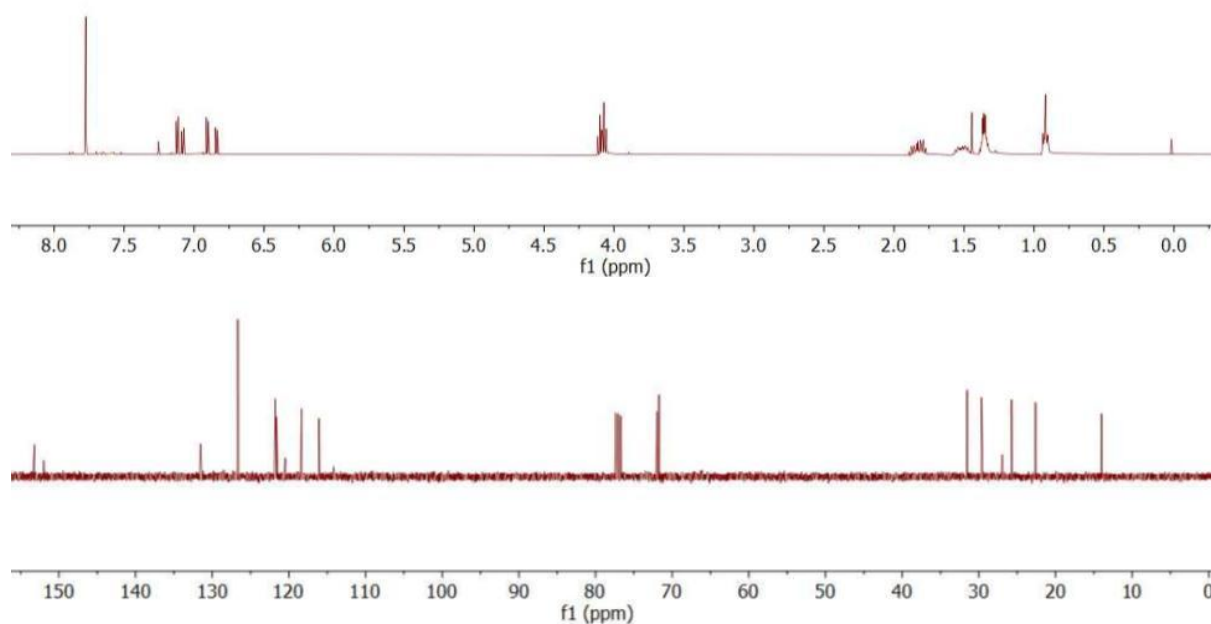
Figure B.1.18. ¹H and ¹³C NMR spectra of compound **4c**.
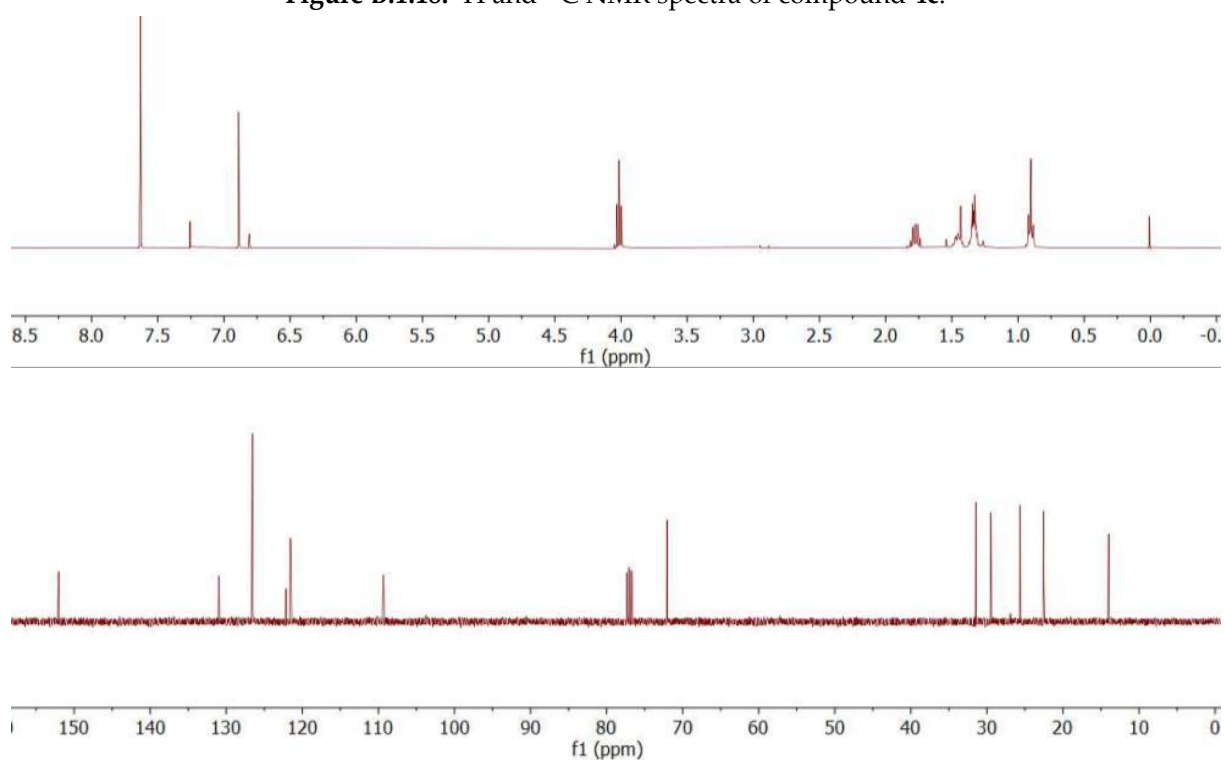
Figure B.1.19. ¹H and ¹³C NMR spectra of compound **4d**.
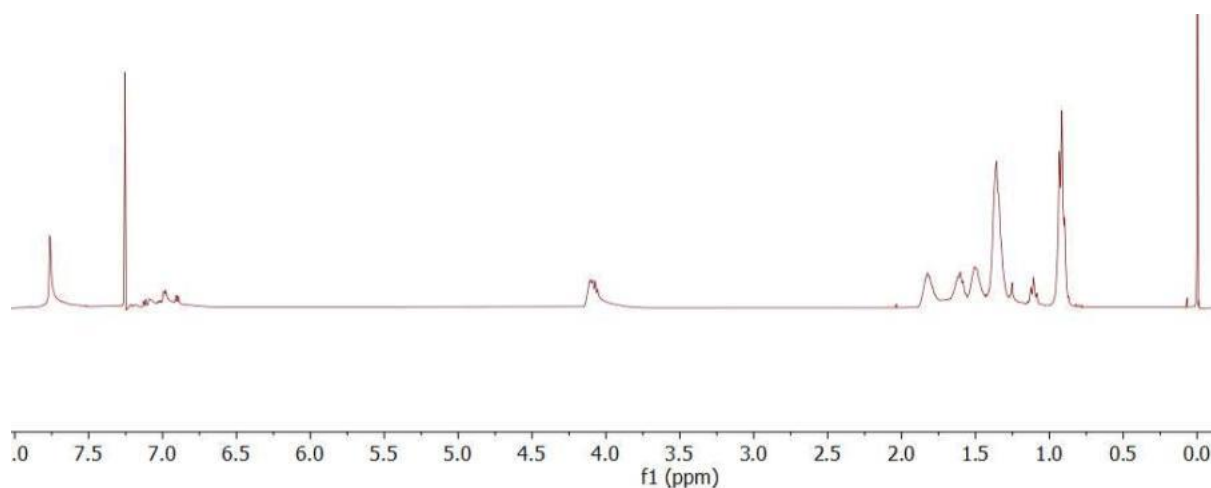
Figure B.1.20. ¹H NMR spectra of compound **polymer 4**.
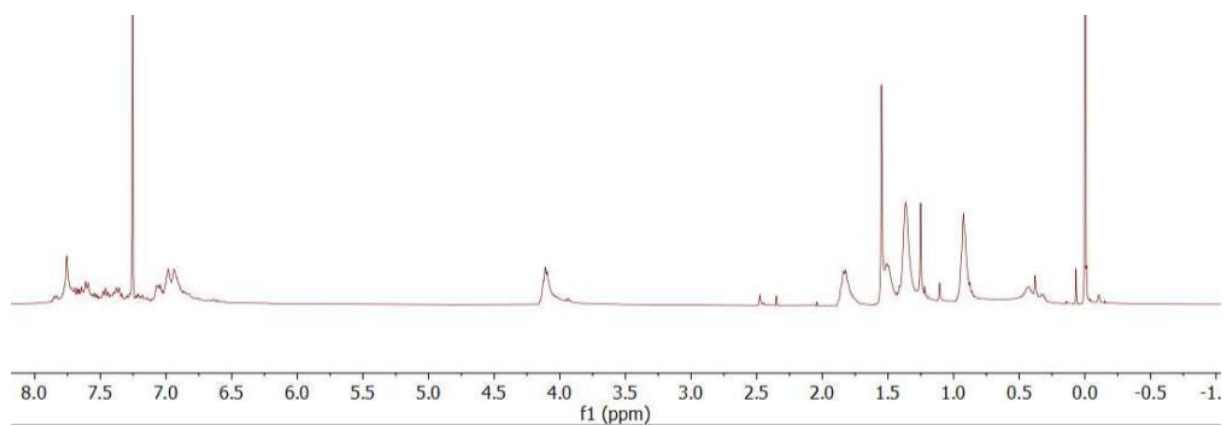
Figure B.1.21. ¹H NMR spectra of compound **polymer 5**
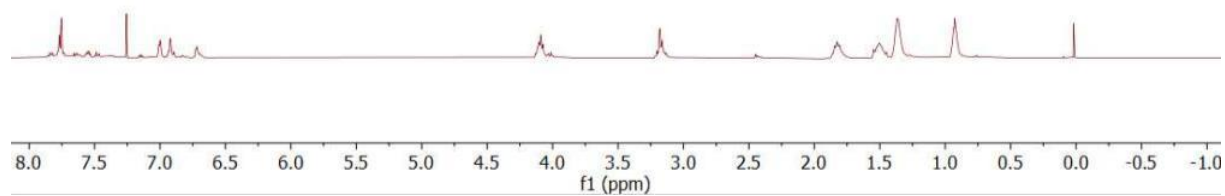
Figure B.1.22. ¹H NMR spectra of compound **polymer 6**.
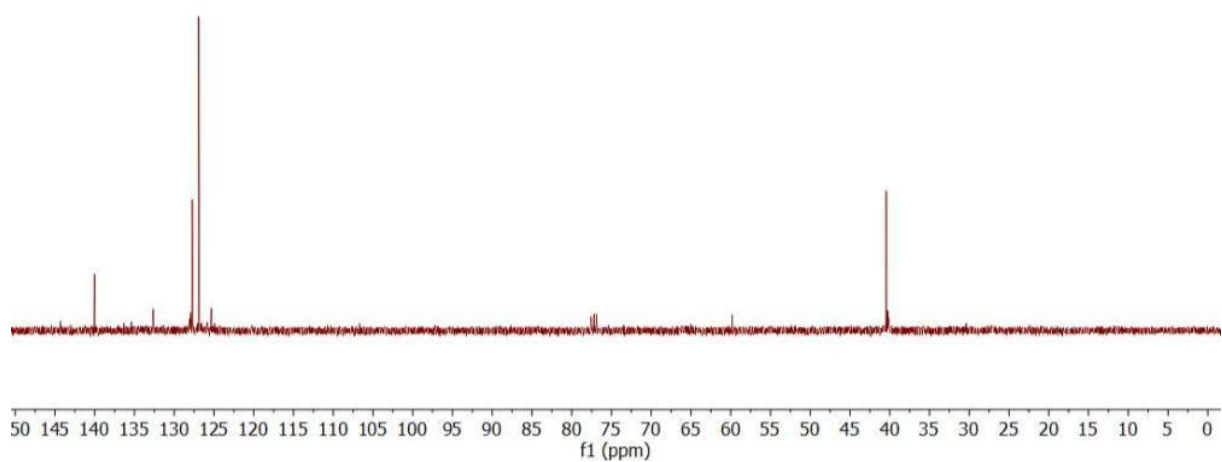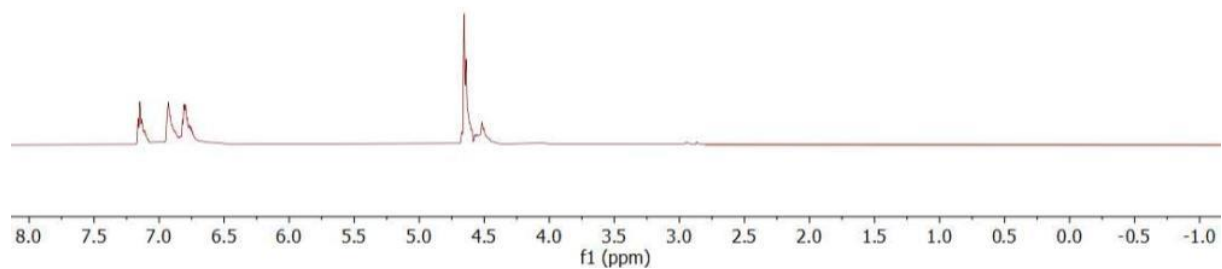
Figure B.1.23. ^{1}H and ^{13}C NMR spectra of compound **7b**.
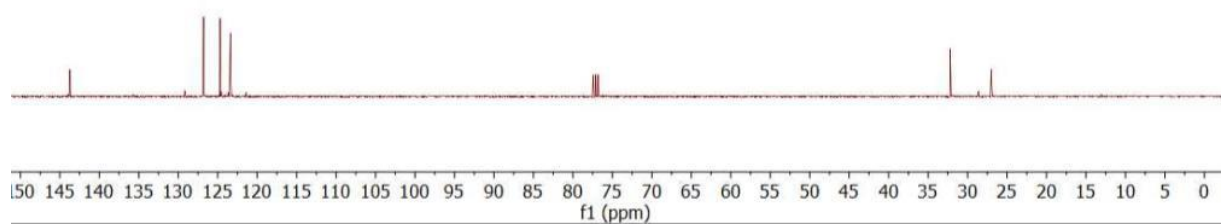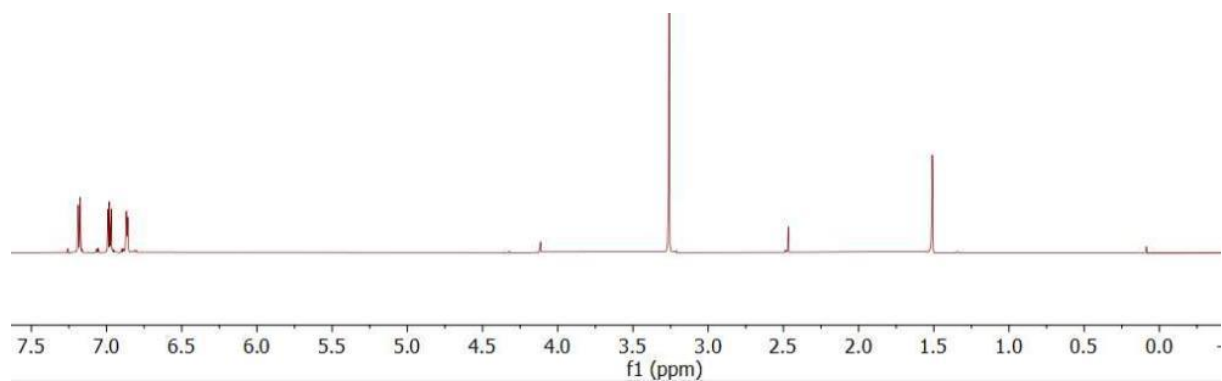
Figure B.1.24. ^{1}H and ^{13}C NMR spectra of compound **7c**.

172
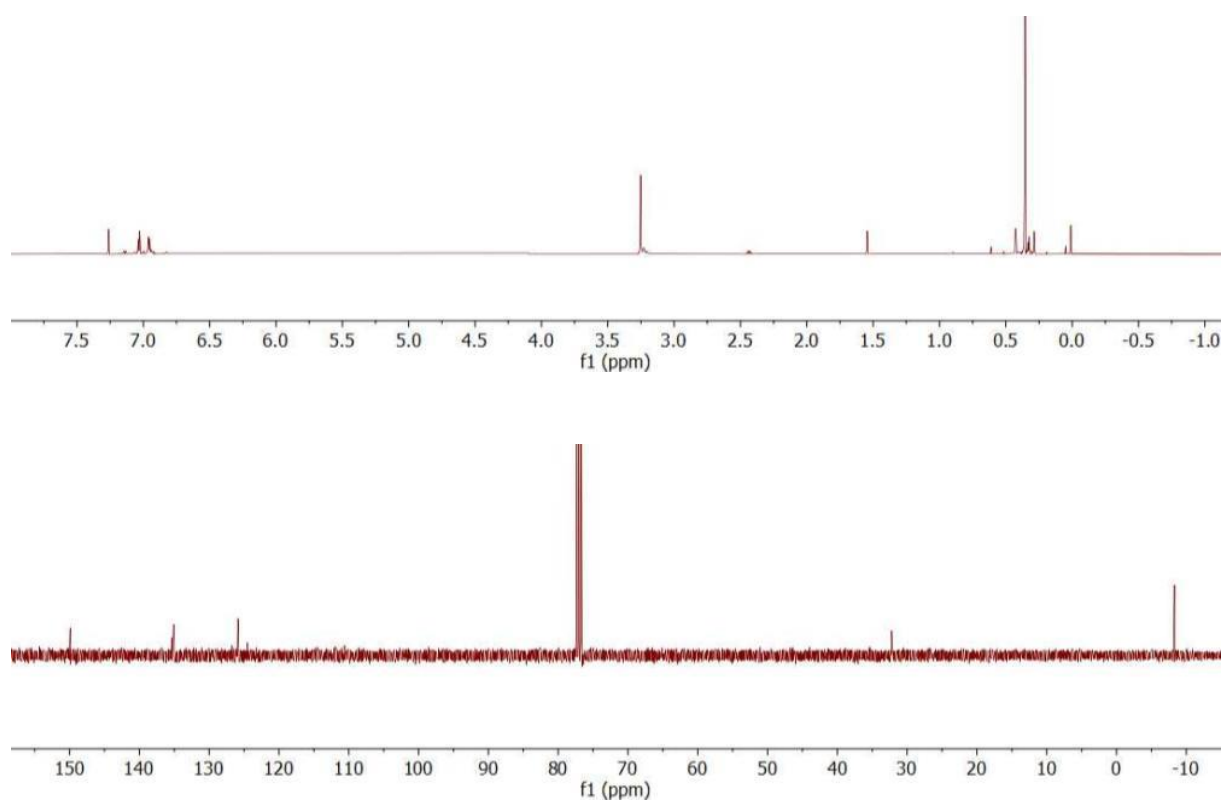
Figure B.1.25. ¹H and ¹³C NMR spectra of compound **7d**.
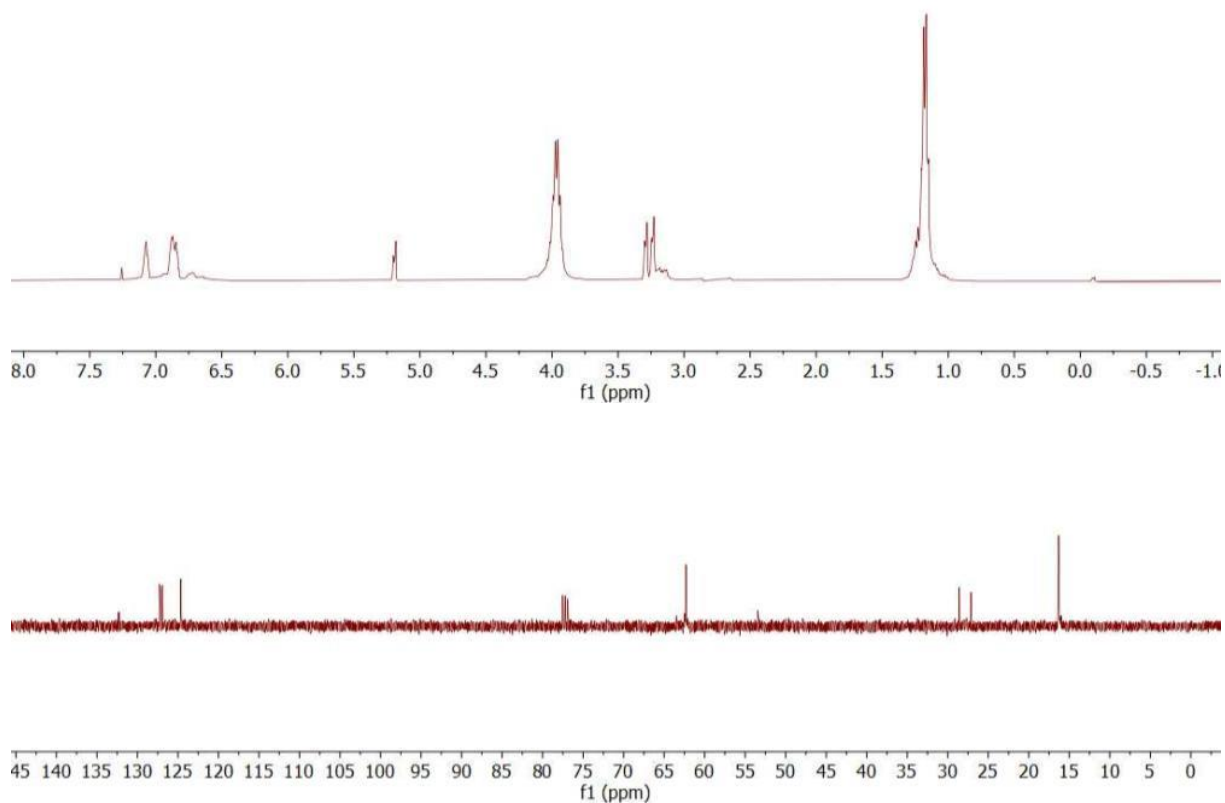
Figure B.1.26. ¹H and ¹³C NMR spectra of compound **8a**.

173
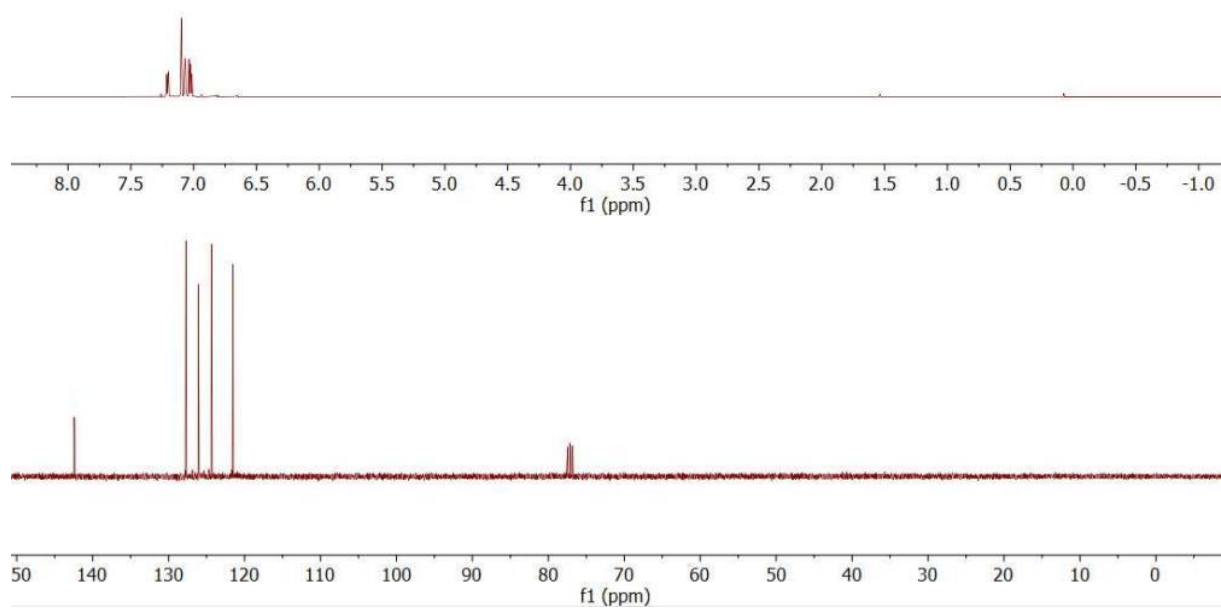
Figure B.1.27. ¹H and ¹³C NMR spectra of compound **8b**.
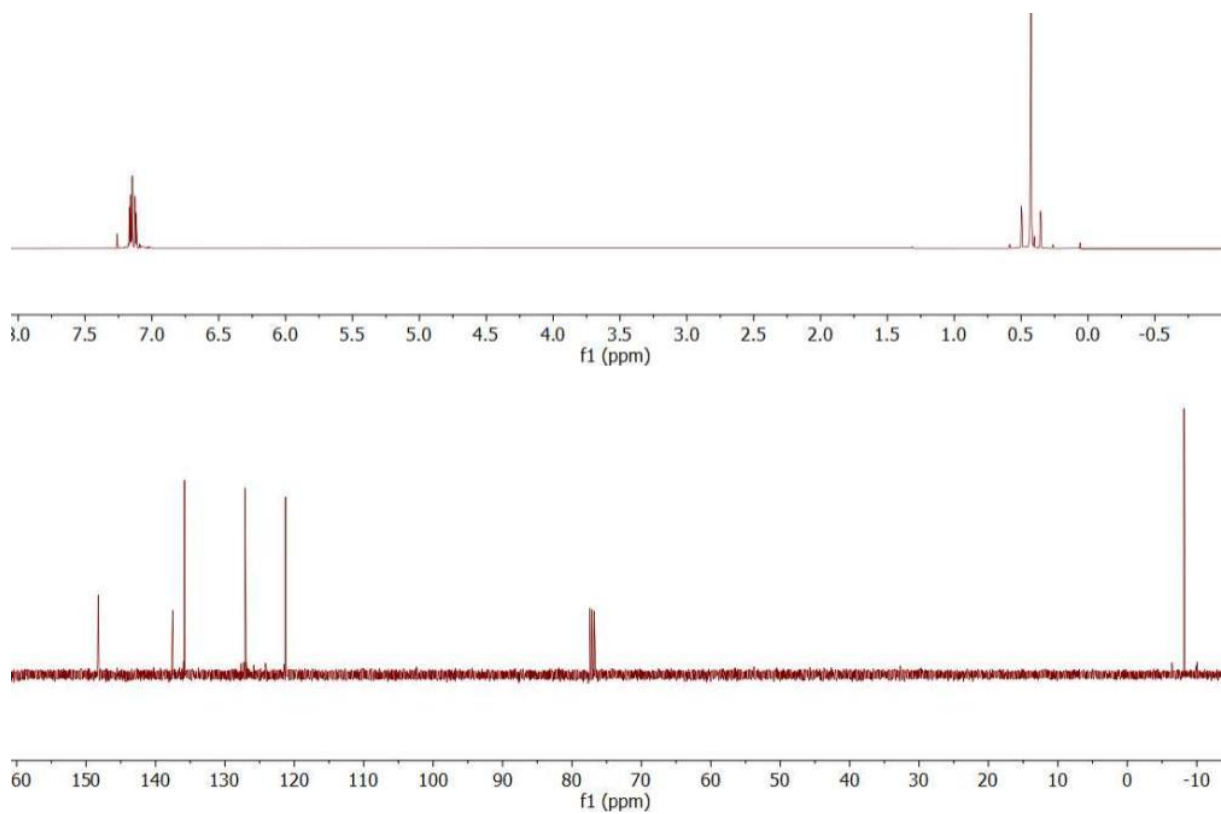
Figure B.1.28. ¹H and ¹³C NMR spectra of compound **8c**.

B.2   CIE LAB Coordinates of Polymers 1-6

Figure B.2.1. L*a*b* coordinates for reduced and oxidized states of all the synthesized polymers deposited on PET-ITO substrates.

One of the most used and efficient methods to define color of electrochromic materials is using CIE LAB (or L*a*b*) coordinates. LAB coordinates were defined in 1931 by the CIE (Commission Internationale de l'Éclairage) where color space is measured in a three-axis system X, Y and Z. The advantage of using this colorimetry system is that it replicates what the human eye can perceive, therefore, the LAB system consists in defining color using three parameters: *tone* - identification of color by spectral localization, *i.e.*, a wavelength associated to color; *saturation* – association between white and black levels; *brightness* - the brightness of the color offers the transparency information. Using this system, it is possible to define color, numerically. L*a*b* coordinates were measured for all the synthesized polymers when deposited on PET-ITO substrates. The color coordinates were calculated using a MATLAB algorithm developed by *Ynvisible*® for industrial applications, which uses an image taken with a small camera and converts, in the desired area, RGB into L*a*b* color coordinates using a ColorChecker® as reference.

B.3   HOMO-LUMO Bandgap Values of Polymers 1-6
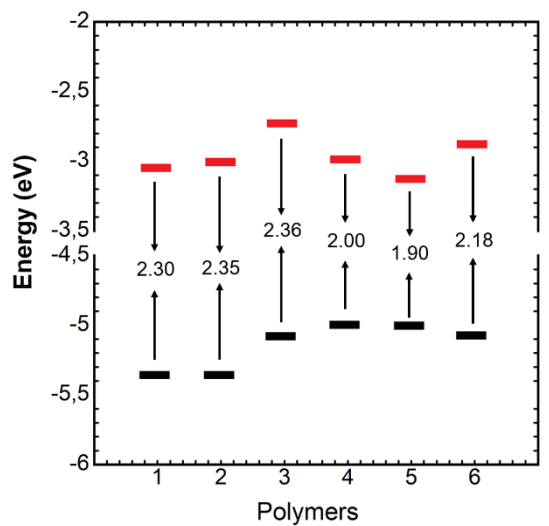
Figure B.3.1. HOMO, LUMO and energy gap levels calculated for all the synthesized polymers (**1-6**).

B.4   DFT Calculations Performed for Polymers 1-6
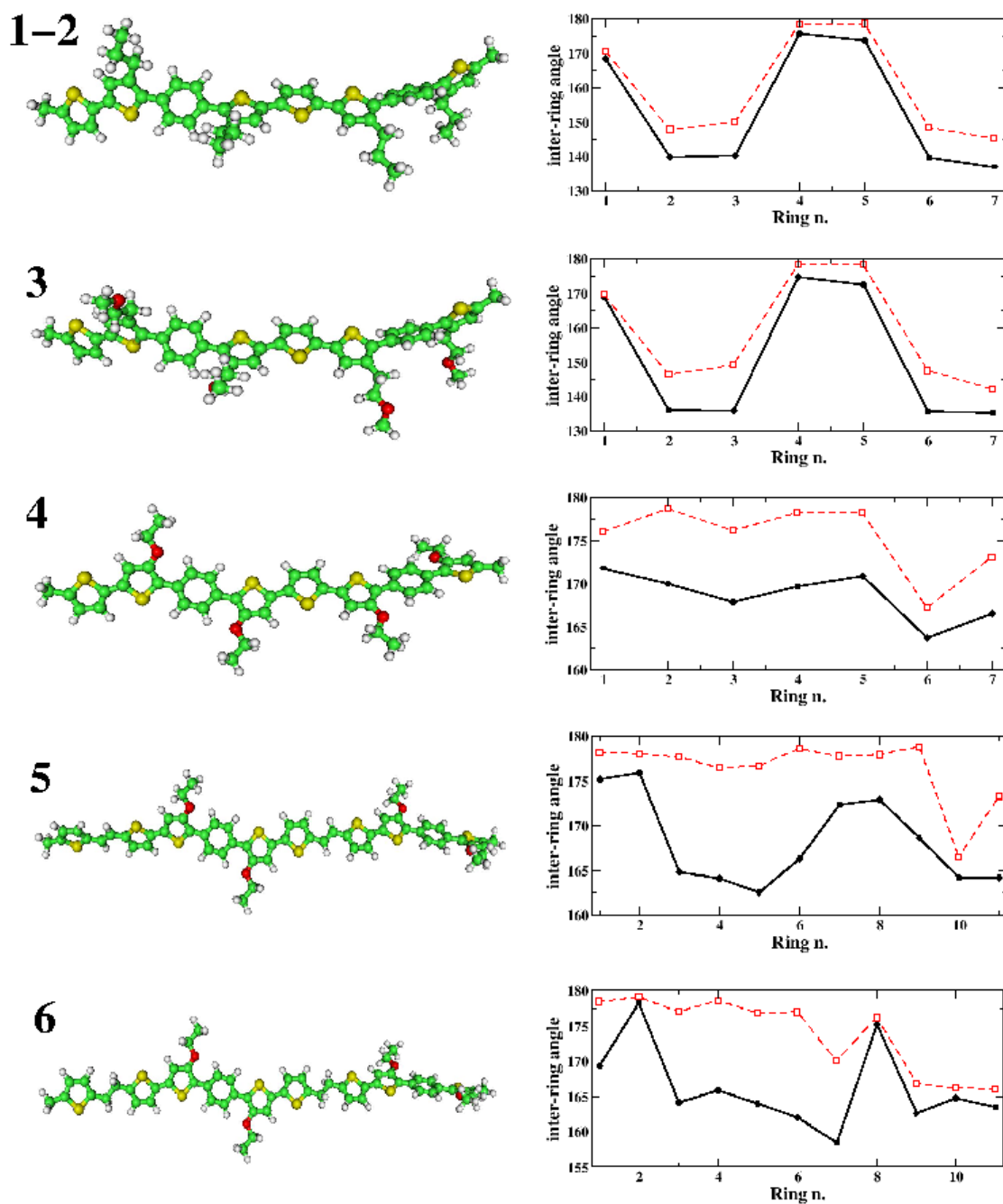
Figure B.4.1. Left: DFT calculated optimized structures of the dimers of the repeat units taken as models for polymers **1-6** in their neutral (reduced) forms. For simplicity –CH$_2$CH$_3$ has been used as a substituent for all compounds. Right: ring-ring dihedral (torsional) angles. In each panel, the solid line with filled circles indicates the neutral species, the dashed line with hollow squares indicates the oxidized species.

B.5　Scheme of NPs Formation and Deposition on PET-ITO
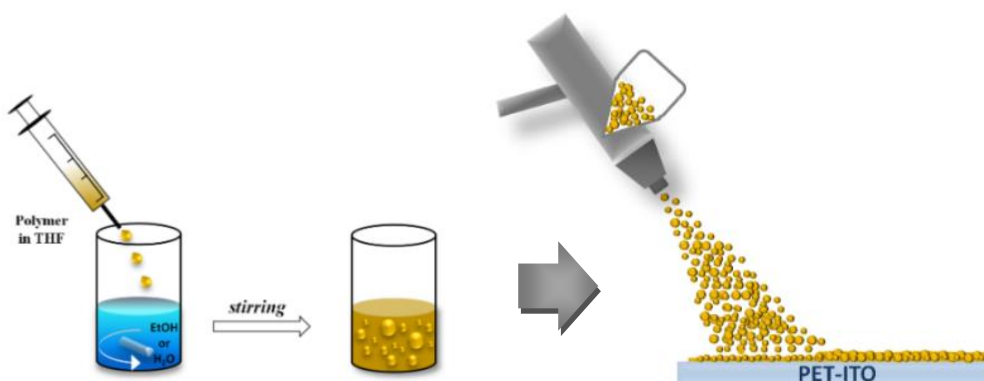
Figure B.5.1. Preparation of NPs in a water-based dispersion and spray-casting deposition of NPs in PET-ITO substrates for ECD assembly.

B.6　DLS and Optical Characterizations of NPs

Table B.6.1. NPs size obtained by DLS

NPs	Size (nm)	NPs	Size (nm)
1-NPs	384±14	**4-NPs**	204±8
2-NPs	364±12	**5-NPs**	210±7
3-NPs	430±12	**6-NPs**	158±5
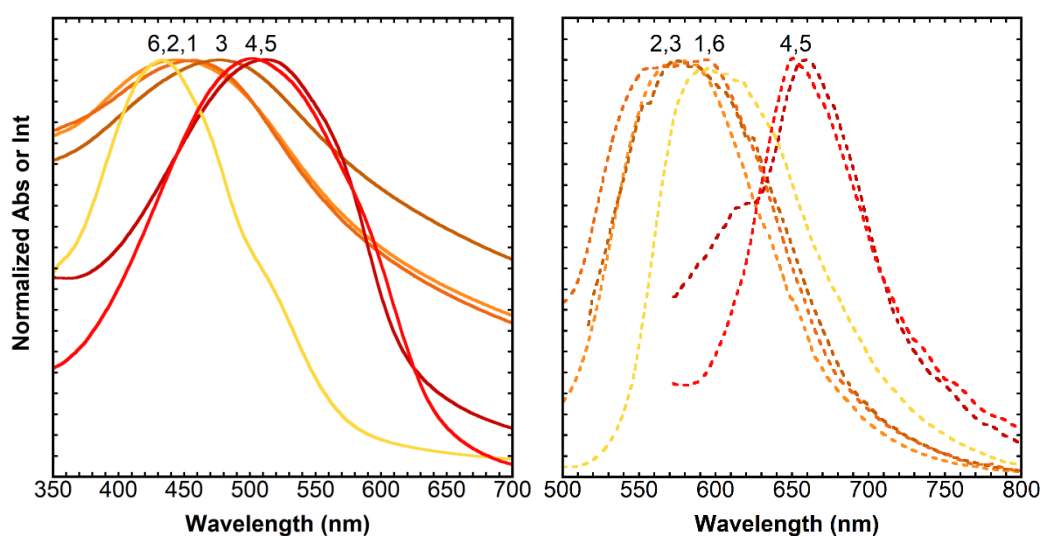
Figure B.6.1. Absorption and emission spectra of NPs.

Table B.6.2. Optical properties of NPs.

NPs	λ_{Abs}^{max} (nm)	λ_{em}^{max} (nm)	Stokes Shift (eV)
1-NPs	444	578	0.65
2-NPs	456	584	0.59
3-NPs	476	578	0.46
4-NPs	500	658	0.59
5-NPs	510	655	0.54
6-NPs	433	605	0.81

B.7   SEM of NPs 1-6
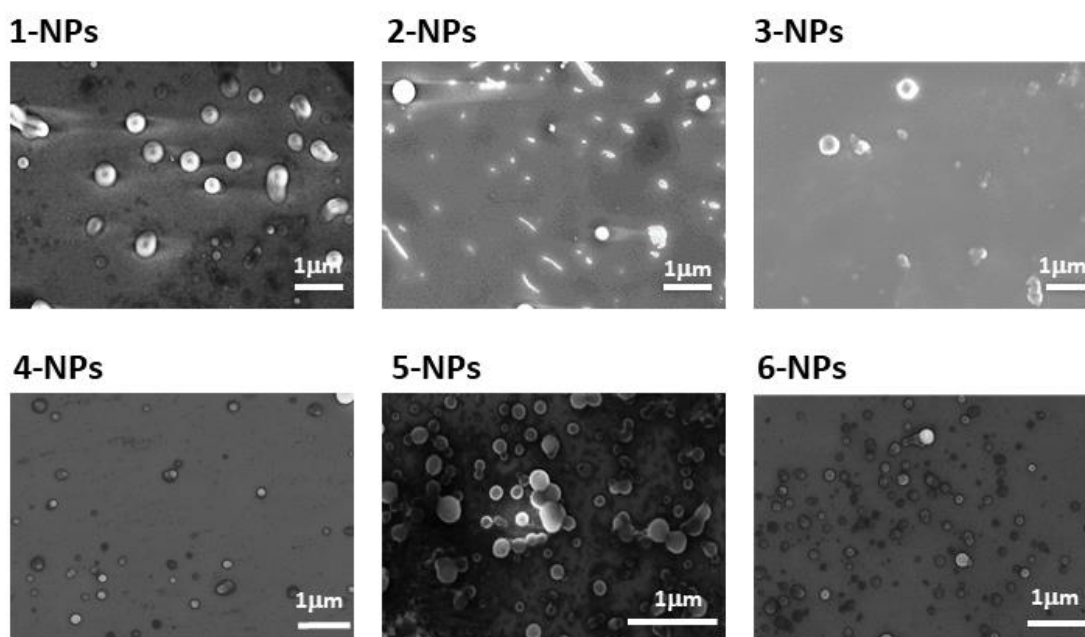
Figure B.7.1. SEM images of 1-6 NPs.
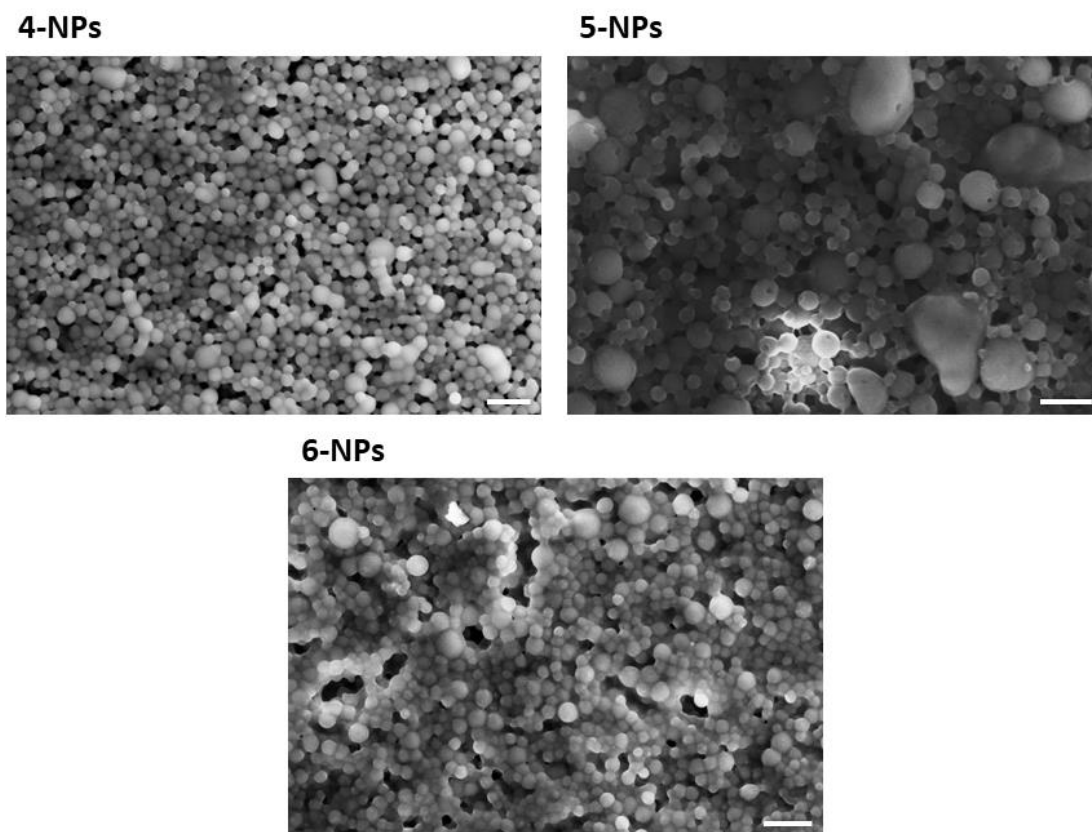
Figure B.7.2. SEM images of thin films of 4-6 NPs. *Scale bars* 500 nm.

B.8 Electrochromic Devices using NPs

Table B.8.1. ECDs of NPs (4-6) and respective colors in neutral, reduced (inner square) and oxidized (outside square) and the redox potentials employed in PET-ITO solid-state ECDs.

Polymer	Neutral	Active	Redox Potential
4-NPs			-1.5/1.5V
5-NPs			-1.5/1.5V
6-NPs			-1.5/1.5V

B.9 CV Measurements and Spectroelectrochemistry of NPs 1-6

Table B.9.1. Redox properties of the polymers deposited on PET/ITO substrates as NPs suspensions.

NPs	E^{onset}_{ox} (V) [a]	E_{HOMO} (eV)
4	0.55	4.95
5	0.56	4.96
6	0.60	5.00

(a) *vs.* Ag/AgCl, thin films measured using $LiClO_4$ (0.1M) in an ACN electrolytic solution.
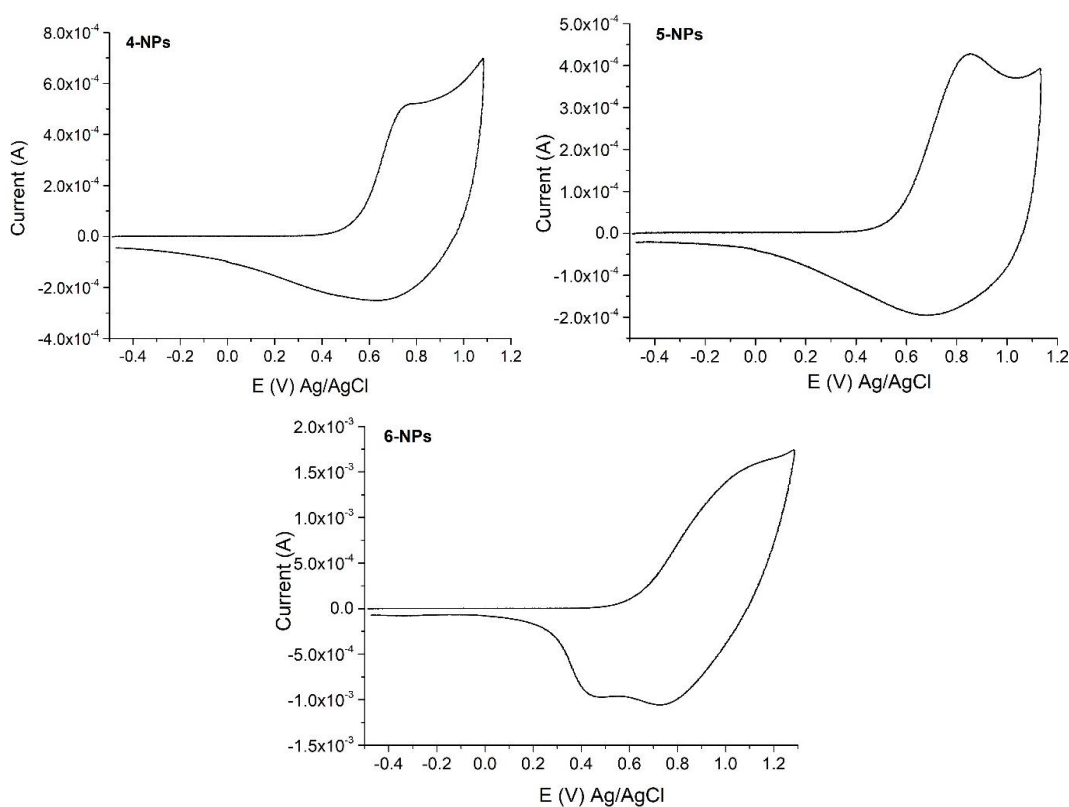
Figure B.9.1. Cyclic voltammograms of polymers 4-6 deposited on ITO as a suspension of NPs and used as the working electrode. An Ag/AgCl electrode was used as the reference, a platinum wire as counter-electrode, and an electrolytic solution of $LiClO_4$ (0.1M) in ACN. (Scan rate: 20mV/s).
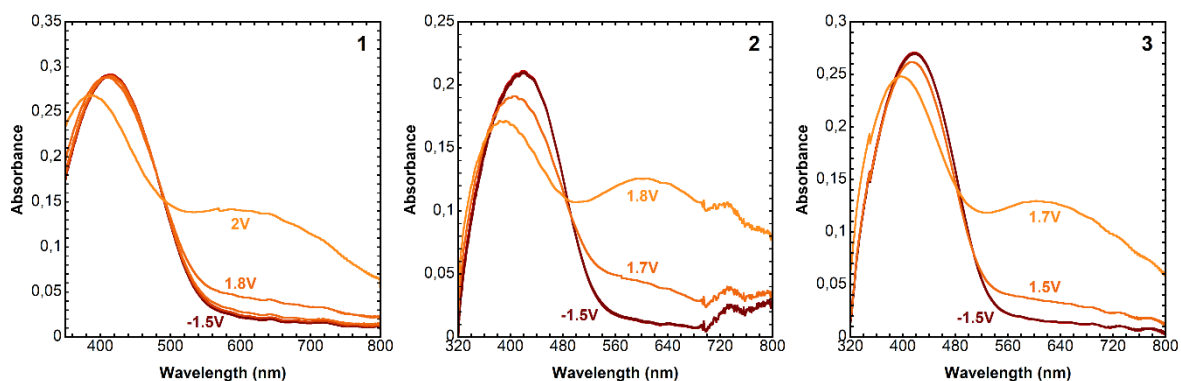
Figure B.9.2. Spectroelectrochemistry measurements of different ECD's assembled with the newly synthesized polymers (1,2,3). (Each spectrum was acquired after the application of the potential for 60 seconds).
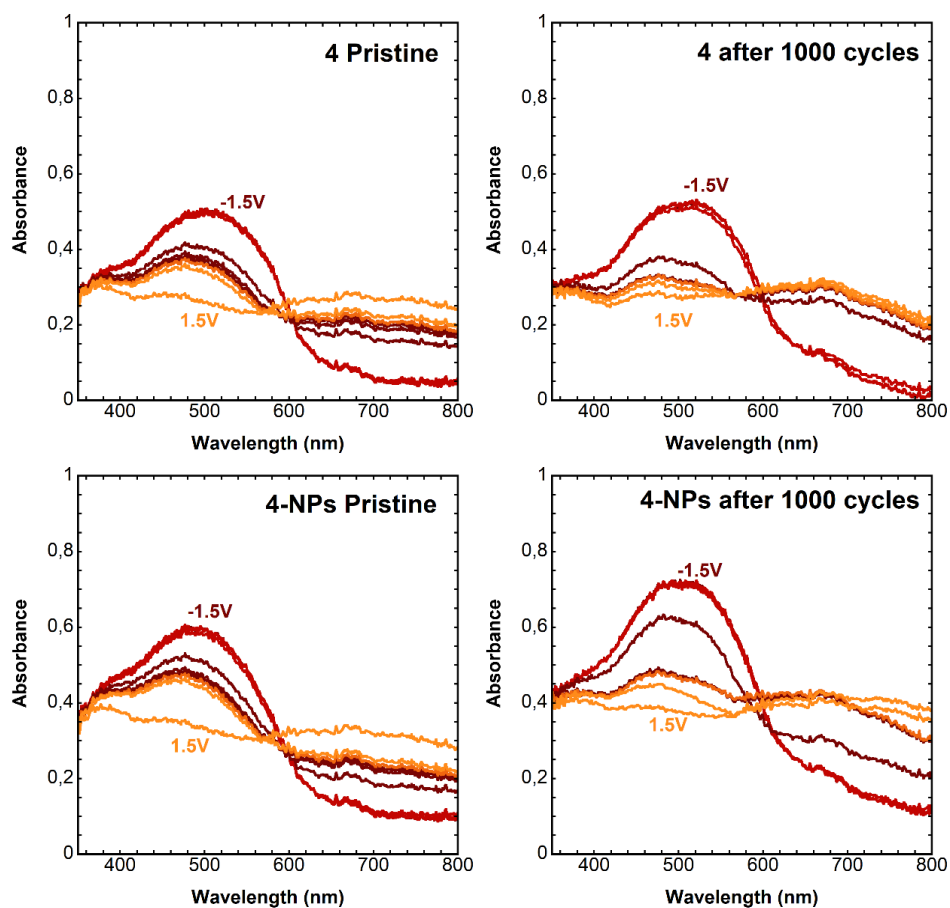
Figure B.9.3. Spectroelectrochemistry measurements for the ECDs using polymer 4 and 4-NPs before and after the 1000 cycles experiment. (Each spectrum was acquired after the application of the potential for 60seconds between 1.5 and -1.5V).
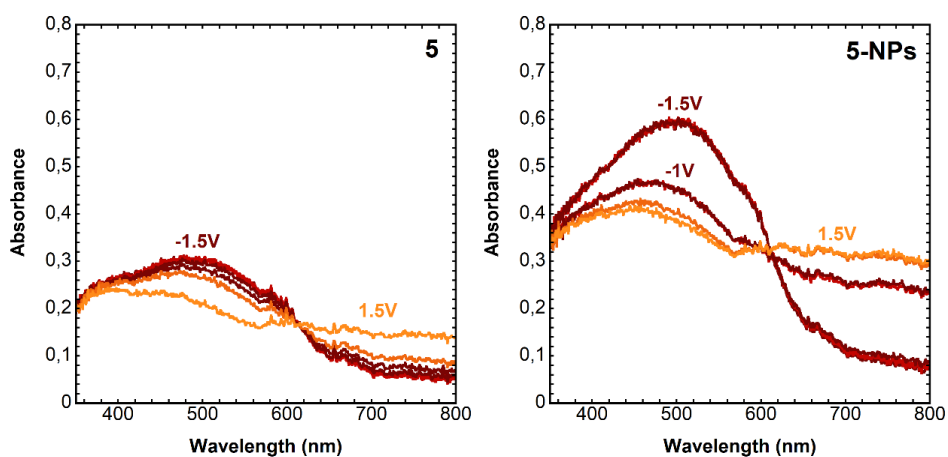
Figure B.9.4. Spectroelectrochemistry measurements of ECD's using polymer 5 (left) and 5-NPs (right). (Each spectrum was acquired after the application of the potential for 60seconds between 1.5 and -1.5V).
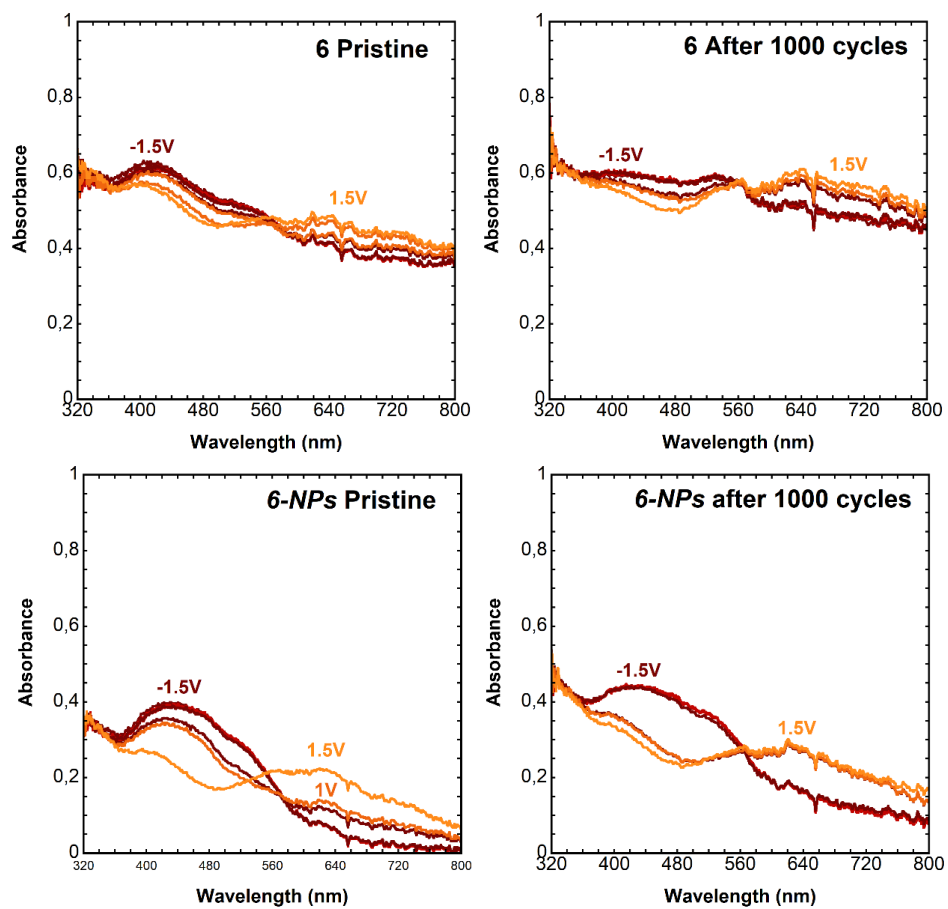
Figure B.9.5. Spectroelectrochemistry measurements for the ECDs using polymer 6 and 6-NPs before and after the 1000 cycles experiment. (Each spectrum was acquired after the application of the potential for 60seconds between 1.5 and -1.5V).

B.10 Switching of ECD's (Polymer 6 *vs* 6-NPs) after 1000cycles
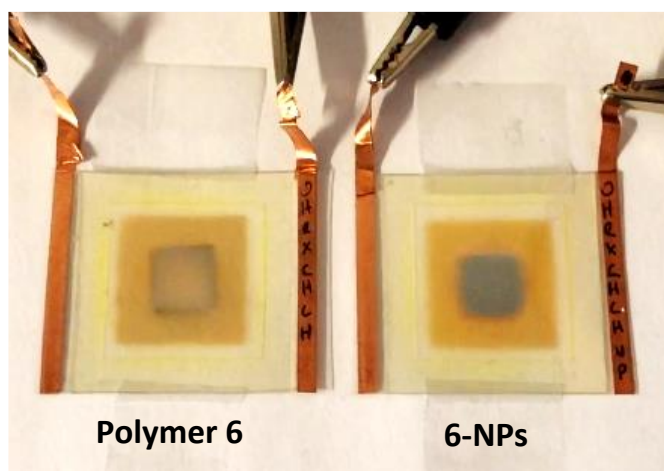
Figure B.10.1. Switch of assembled ECD's using polymer 6 and 6-NPs after 1000 cycles.

B.11 Flexibility of ECD using 6-NPs
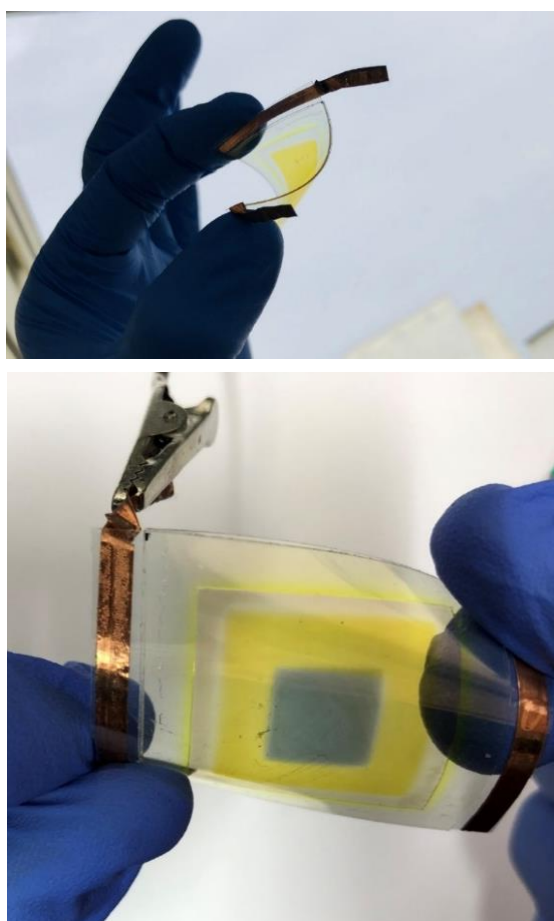
Figure B.11.1. Characterized flexible ECD while bending.

C

APPENDIX - CHAPTER 4

C.1 ¹H-NMR and ¹³C-NMR Spectra
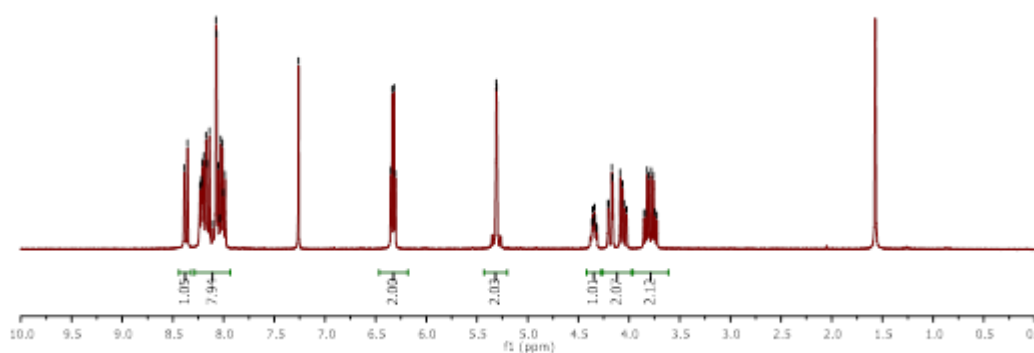
Figure C.1.1. ¹H NMR spectrum of **9a** in CDCl₃.
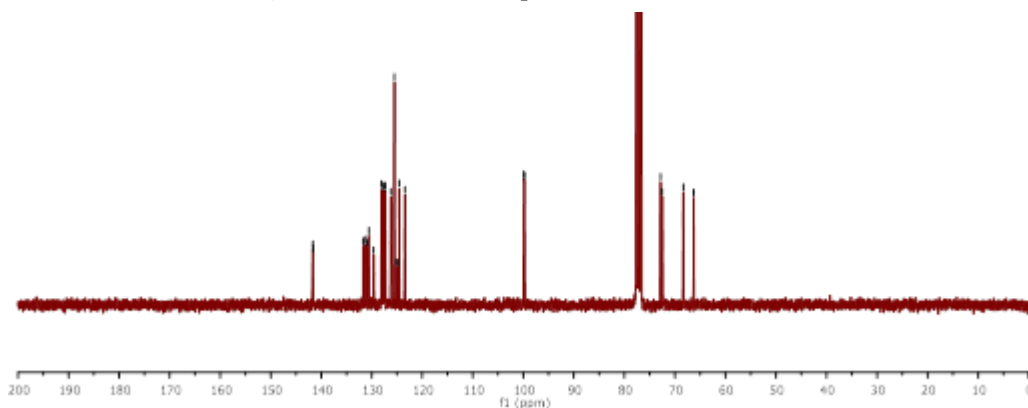
Figure C.1.2. ¹³C NMR spectrum of 9a in CDCl₃.
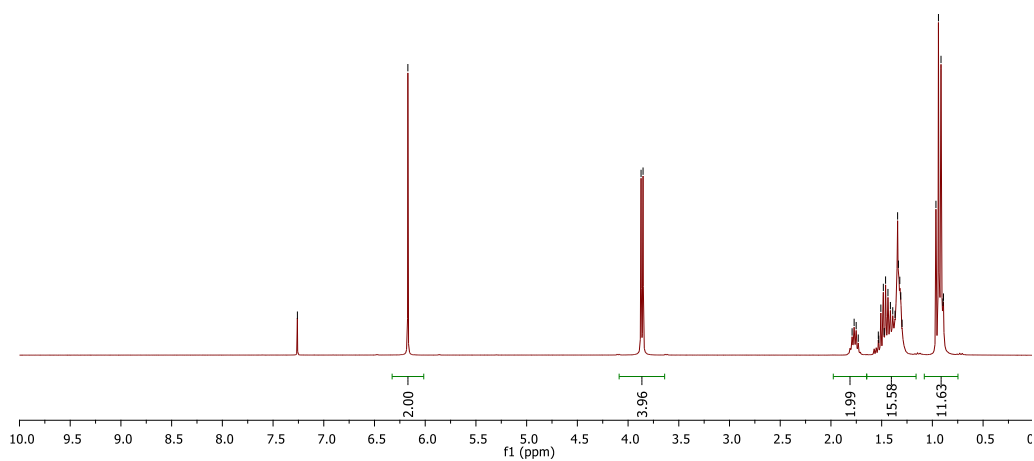
Figure C.1.3. ^{1}H NMR spectrum of **10a** in CDCl$_3$.
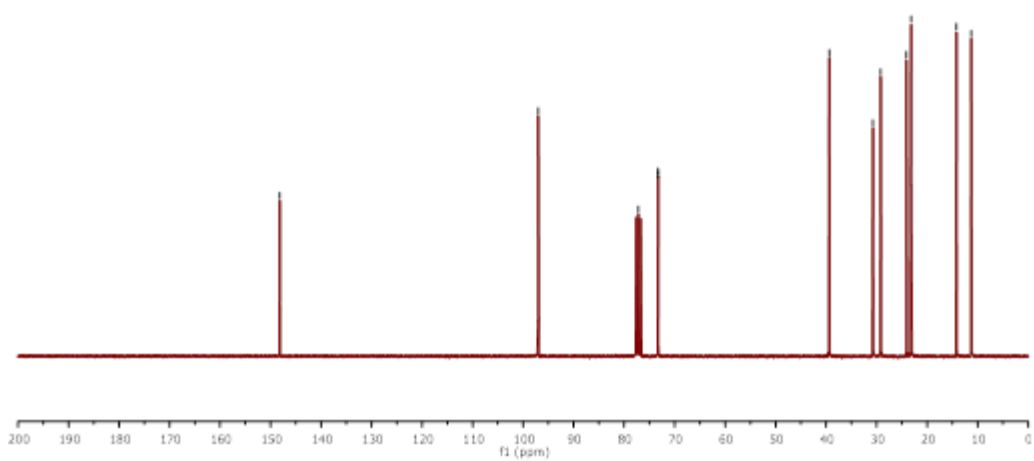
Figure C.1.4. ^{13}C NMR spectrum of 10a in CDCl$_3$.
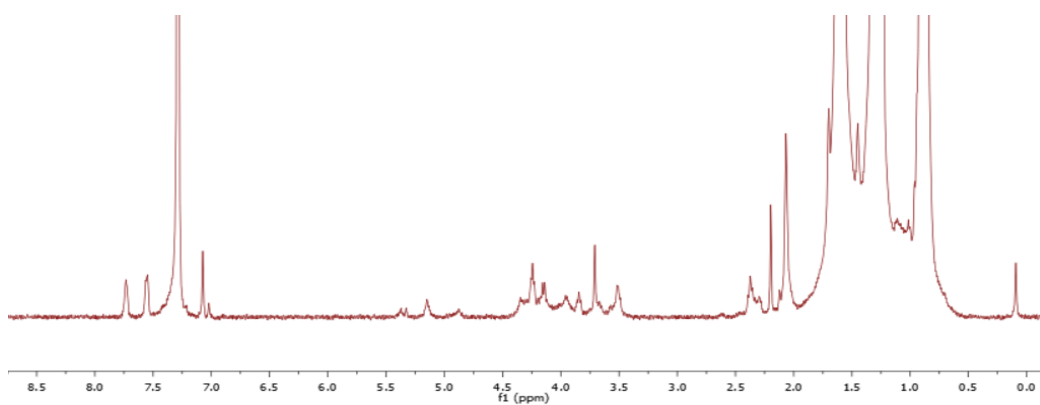
Figure C.1.5. ^{1}H NMR spectrum of **10 (PTP)** in CDCl$_3$.
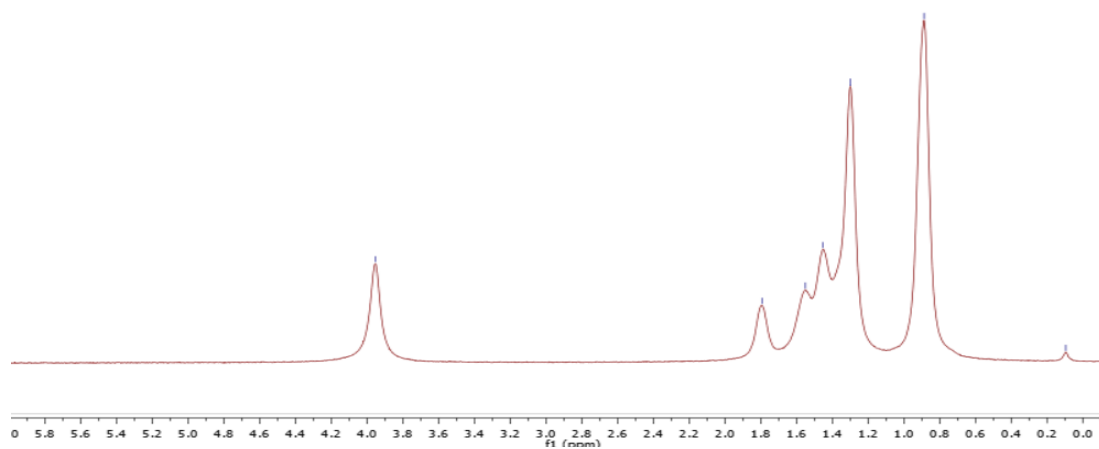
Figure C.1.6. ¹H NMR spectrum of **11** in CDCl₃.
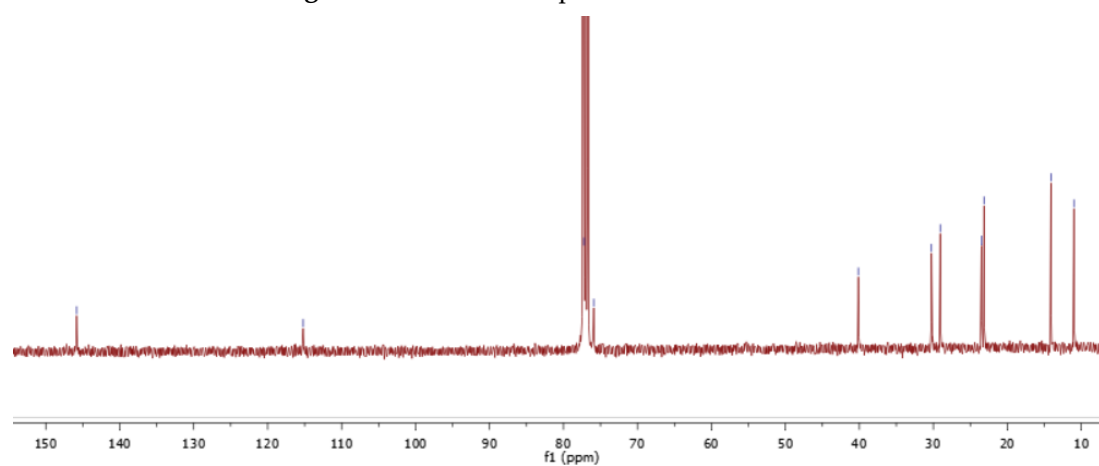
Figure C.1.7. ¹³C NMR spectrum of 11 in CDCl₃.
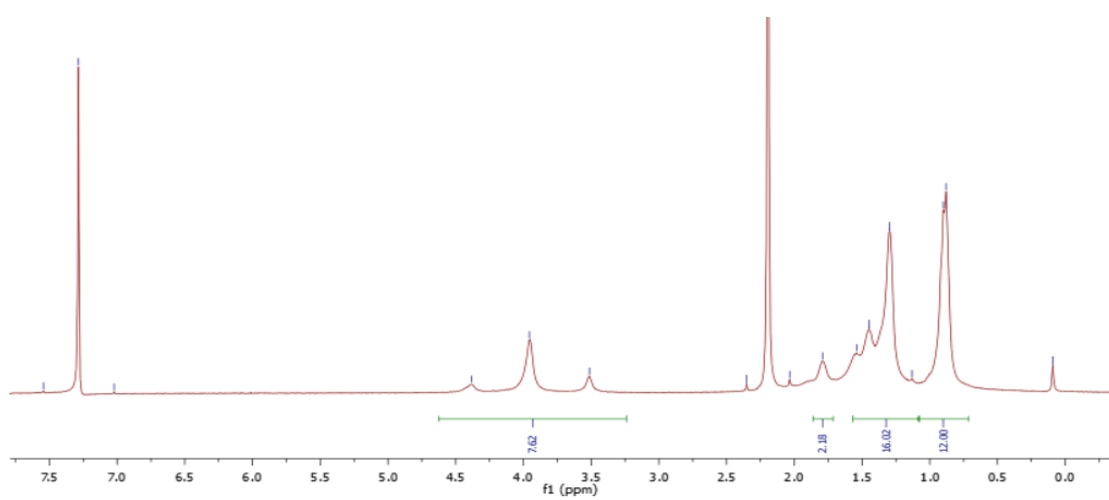
Figure C.1.8. ¹H NMR spectrum of **12** in CDCl₃.

C.2 Contact Angles
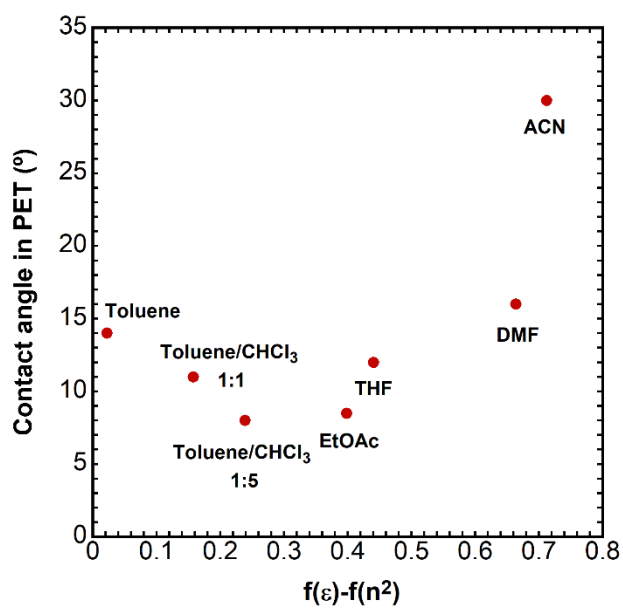
Figure C.2.1. Contact angle of the selected solvents /solvent mixtures in PET substrates.

C.3 Hybrid Dispersions
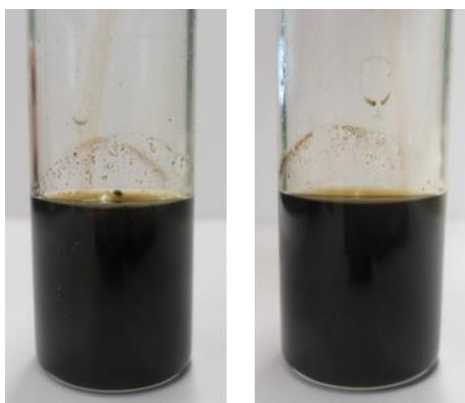
Figure C.3.1. Dispersion of PTP with 7.5% of MWCNTs in a solution of CHCl₃:toluene with a 5:1 ratio.

Left: Blend just after preparation; **Right:** Blend after 3 days.

Figure C.3.2. Dispersion of polymer 11 with 7.5% of MWCNTs in a solution of CHCl$_3$:toluene with a 5:1 ratio. **Left:** Blend just after preparation; **Right:** Blend after 6 hours of sonication at 40°C.
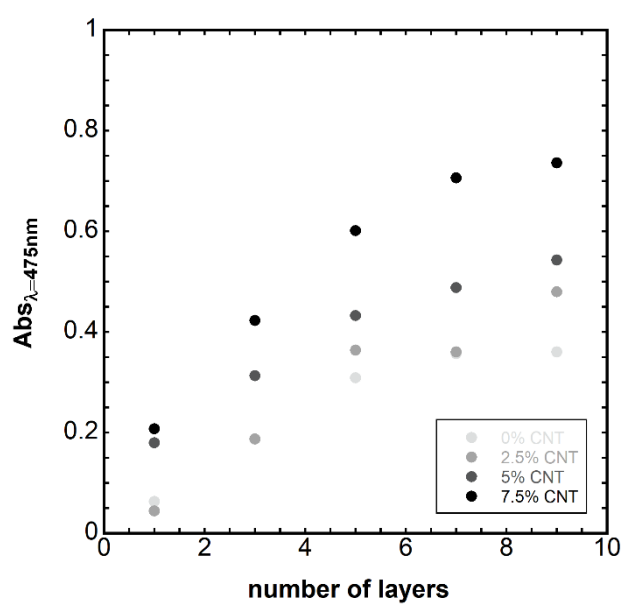
Figure C.3.3. Absorption, at 475nm of the spray-coated films with PTP + 0%, 2.5%, 5% and 7.5% of MWCNTs in PET-ITO substrates, using different layers.

C.4 Electrochromic Devices
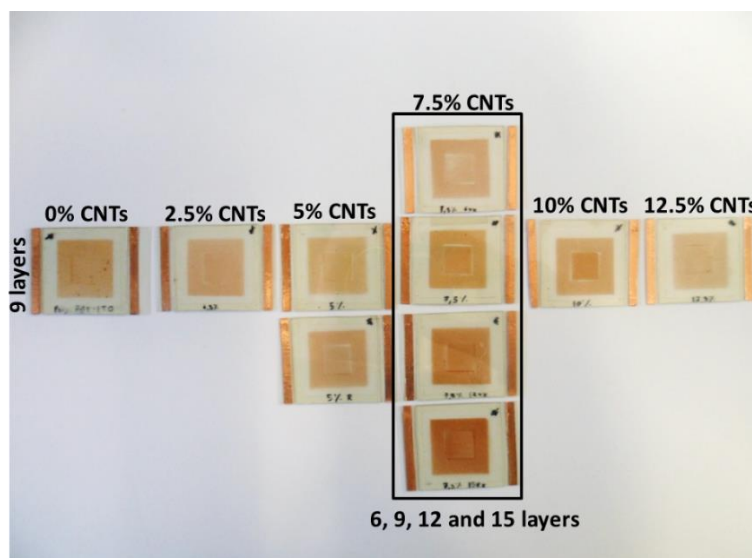
Figure C.4.1. Solid-state electrochromic devices assembled using the optimized blends (PTP/MWCNTs) varying the wt. % of CNTs and number of spray-coated layers.
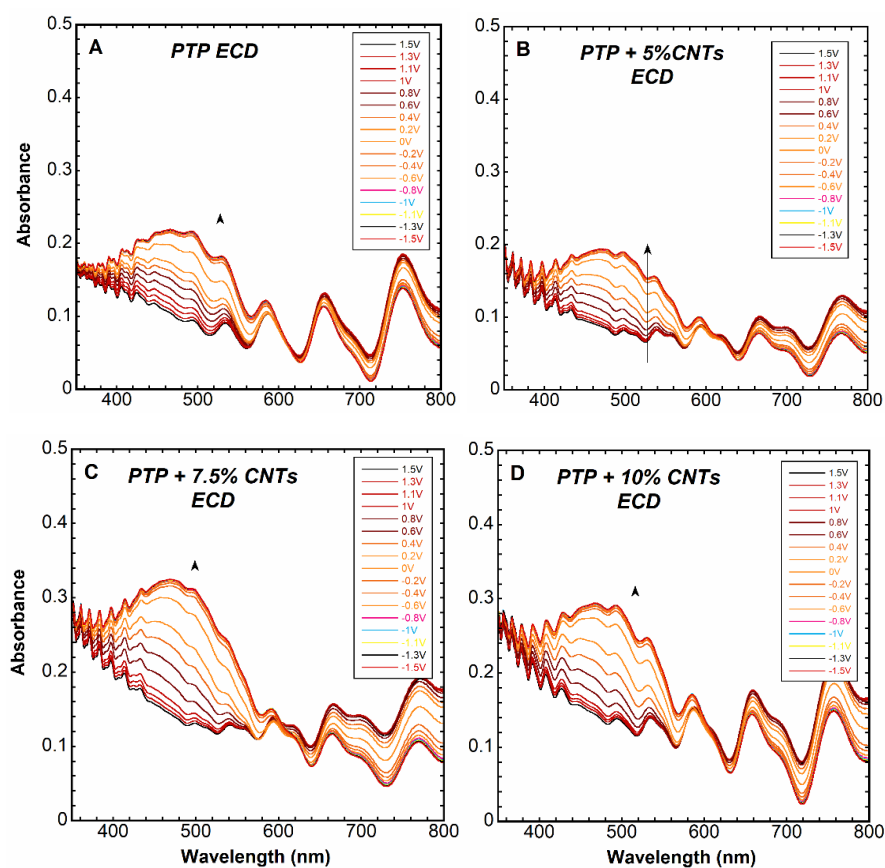
Figure C.4.2. Spectroelectrochemistry measurements performed to the solid-state devices with: **A -** PTP, B - PTP + 5%CNTs, C - PTP + 7.5%CNTs and D - PTP + 10%CNTs
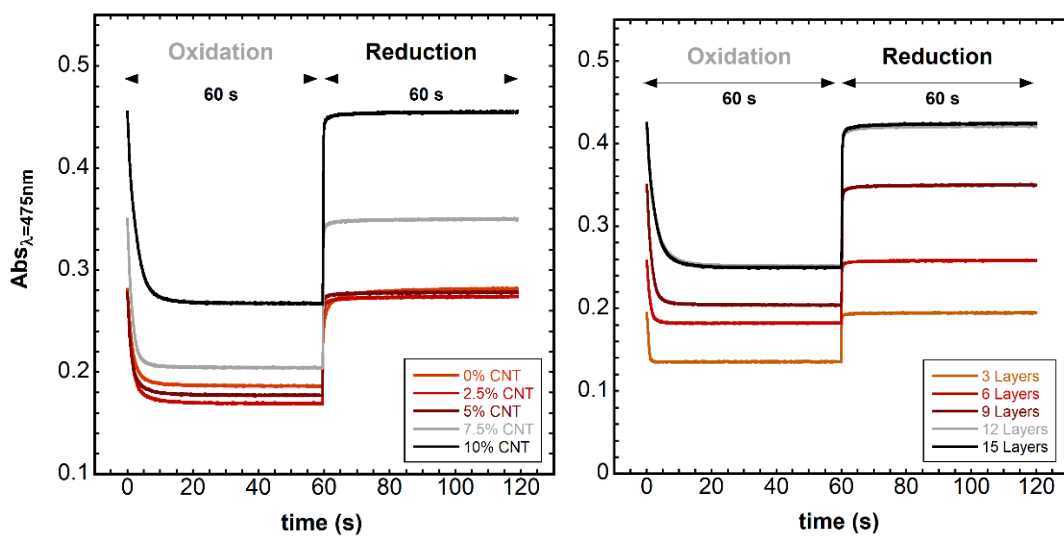
Figure C.4.3. Switching time measurements of assembled electrochromic devices varying: % of CNTs from 0 to 10%(Left) and number of layers spray-coated using 7.5% of CNTs (Right).
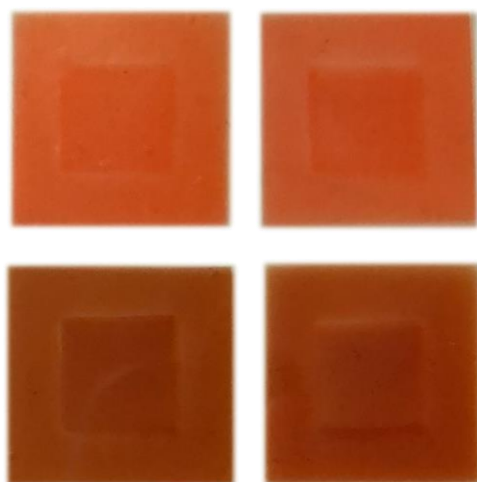

Figure C.4.4. Electrochromic devices using polymer 11. Up: 2 devices with spray-coated polymer 11, Down: 2 devices with spray-coated polymer 11 + 7.5% MWCNTs.

Table C.4.1. Figures of merit for color contrast (Δ**Abs**), Switching times (t_{90}^{Ox}, t_{90}^{Red}) and Coloration efficiency (**CE**) for the produced electrochromic devices using polymer 11 and a blend with polymer 11 + 7.5 wt.% of MWCNTs

% of MWCNT	ΔAbs	t_{90}^{Ox} (s)	t_{90}^{Red} (s)	CE (cm^2 C^{-1})
0	0.3	52.3	4.5	331
0	0.2	52.4	3.9	290
7.5	0.7	26.5	3.7	324
7.5	0.8	48.4	5.4	360
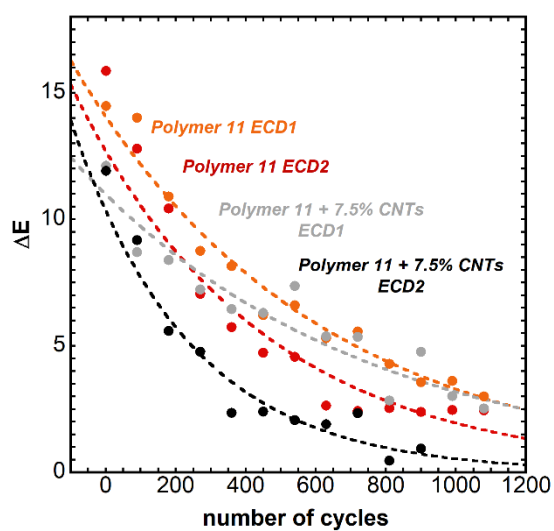
Figure C.4.5. Cycling measurements performed in 2 ECDs using polymer 11 and 2 ECDs using 7.5 wt.% of MWCNTs. The results are presented in ΔE (calculated from L*a*b* coordinates calculated using a ColorChecker® as reference).

APPENDIX - CHAPTER 5

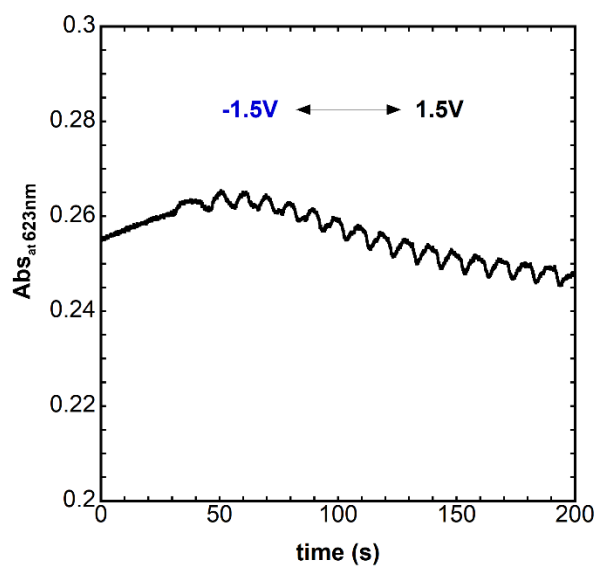## D.1 Electrochromic Devices

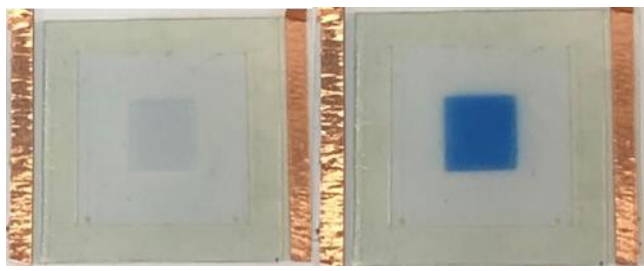**Figure D.1.1.** ITO-free ECD switching from -1.5V to 1.5V

Figure D.1.2. PET-ITO/PEDOT vs PEDOT/PET electrochromic device with an active

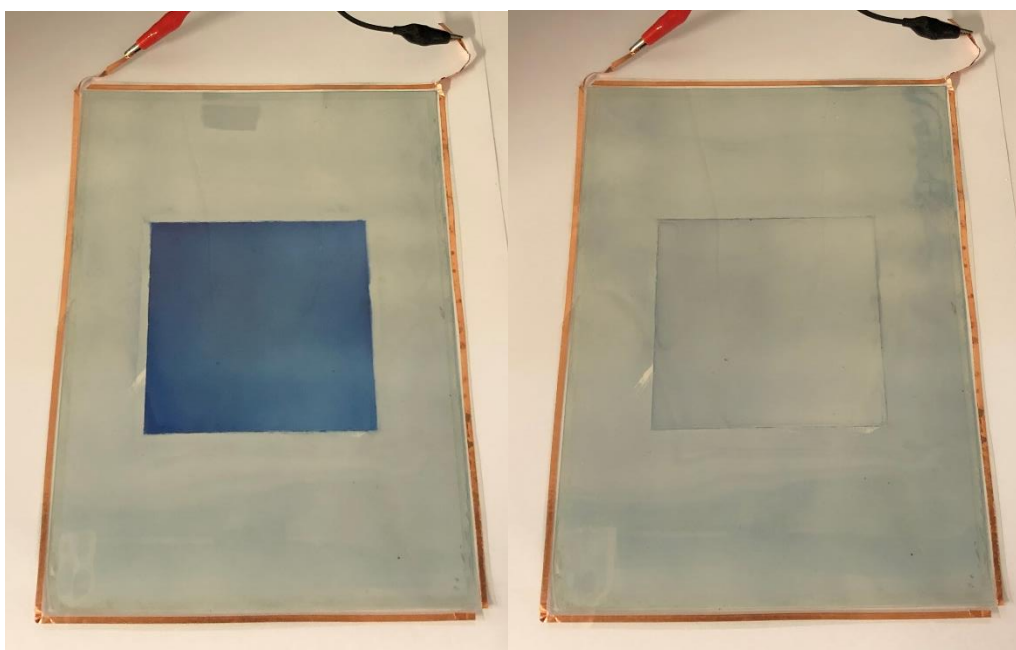area of 1cm² assembled and characterized for comparison with ITO-free ECD.

Figure D.1.3. A4-sized electrochromic device with a 12cm² of active area using PEDOT as electrochromic material.

NANOSTRUCTURED POLYTHIOPHENE MATERIALS FOR ELECTROCHROMIC APPLICATIONS

TIAGO ANDRÉ SEMEDO MOREIRA

2022